Swansea University

Development and application of a novel mass spectrometry ionization source for biological chemistry

Submitted to Swansea University in fulfilment of the requirements for the Degree of Doctor of Philosophy.

Rhodri N. Owen BSc, RSci, MRSC

2022

Abstract

Since its development, electrospray ionization (ESI) for the analysis of thermally labile, polar compounds and particularly biomolecules has been extremely useful. Not all compounds can be easily protonated and electron ionization (EI) is still a widely used ionization method for compounds like hydrocarbons. However, the low-pressure environment of the EI source requires complex and expensive vacuum systems and inlets. Therefore, a source which can ionises non-polar compounds while operating at atmospheric pressure would be highly advantageous. In this thesis I have undertaken development and characterisation of four prototype atmospheric pressure glow discharge ionization sources for the analysis of compounds not normally amiable to ionization by conventional atmospheric pressure ionization sources. A helium micro-glow discharge source ("Prototype V") operated using a direct current power supply was studied and its discharge characterised. Its current-voltage relationship increased linearly which is typical of the abnormal glow regime while thermal imaging showed it had a "cold" discharge. Prototype V was successfully interfaced with a Xevo G2-S time-of-flight and a Xevo TQ-S triple quadrupole (Waters Corp, Wilmslow, UK) and used with a range of sample introduction methods, initially a solids probe, but later APCI and ESI probes. These probes enabled prototype V to readily integrate with separation sciences; specifically liquid chromatography was demonstrated for complex mixture analysis. Prototype V exhibited high analytical sensitivity in the nanogram range in both positive and negative modes and could ionize a wide range of compound chemistries from polar to non-polar. In particular it showed sensitivity to non-polar compounds in negative-ion mode when compared to ESI. This gives the source the potential to operate in conjunction with a range of sample inlets and in combination with other ionization techniques as part of a multimodal platform to analyse the widest range of samples and a step towards a universal source.

Declarations and Statements

DECLARATION

This work has not previously been accepted in substance for any degree and is not being concurrently submitted in candidature for any degree.

Signed .....Rhodri N. Owen..... (candidate)

Date .....26/07/2022.....

STATEMENT 1

This thesis is the result of my own investigations, except where otherwise stated. Where correction services have been used, the extent and nature of the correction is clearly marked in a footnote(s).

Other sources are acknowledged by footnotes giving explicit references. A bibliography is appended.

Signed .....Rhodri N. Owen..... (candidate)

Date .....26/07/2022.....

STATEMENT 2

I hereby give consent for my thesis, if accepted, to be available for photocopying and for inter-library loan, and for the title and summary to be made available to outside organisations.

Signed .....Rhodri N. Owen..... (candidate)

Date .....26/07/2022.....

Contents

Acknowledgements

I would like to thank my fianceé Richard Jones who has been there for me and has supported me through this period.

I would like to thank my supervisors Prof Steven Kelly and Dr Jonathan Mullins for their advice and guidance during my research. Thank you to Prof Gareth Brenton for his vast knowledge of mass spectrometry, his supervision, mentoring, and friendship even during his retirement, he has been an inspiration and provided invaluable advice throughout the research - it has been a privilege to work with you.

Thank you the research staff at the former National Mass Spectrometry Facility in particular at Dr Ann Hunter for her invaluable knowledge of mass spectrometry, training, and keeping the instruments running both during my PhD and over the last 8 years we have worked together. I would like to thank the research staff at the Center for P450 Biodiversity particularly Dr Josie Parker and Dr Claire Price for their support, guidance, and advice. I'm very grateful to Mr Christopher Rushton in the Medical School Model Workshop for his skills in making component parts and adaptations. I would also like to thank Waters Corporation in particular, Dr William Johnson for donating an Universal Source Housing for the research, and Prof Michael Morris and Dr Stevan Bajic for their time and use of their Xevo TQ-S instrument for experimental work at the Waters's research laboratory in Wilmslow.

Finally, thank you to the Engineering and Physical Sciences Research Council for funding this research.

List of Figures

List of Tables

Abbreviations

ADI ambient desorption ionization.

APCI atmospheric pressure chemical ionization.

APGC atmospheric pressure gas chromatography.

APGD atmospheric pressure glow discharge.

API atmospheric pressure ionization.

APPI atmospheric pressure photoionization.

ASAP atmospheric-pressure solids analysis probe.

BPI base peak ion.

CI chemical ionization.

DART direct analysis in real time.

DBD dielectric barrier discharge.

DESI desorption electrospray ionization.

DL detection limit.

EI electron ionization.

ESI electrospray ionization.

FAMEs fatty acid methyl esters.

FAPA flowing atmospheric pressure afterglow.

FT-ICR Fourier-transform ion cyclotron resonance.

GC gas chromatography.

HPLC high performance liquid chromatography.

ICP inductively coupled plasma.

IE first ionization energies.

IUPAC International Union of Pure and Applied Chemistry.

KMD Kendrick mass defect.

LC liquid chromatography.

LTP low temperature plasma probe.

MALDI matrix-assisted laser desorption/ionization.

MRM multiple reaction monitoring.

MTBE methyl-*tert*-butyl ether.

PA proton affinity.

PAH poly-aromatic hydrocarbons.

PEEK polyether ether ketone.

PTFE polytetrafluoroethylene.

RSD residual standard deviation.

SEM standard error of the mean.

TIC total ion chromatogram.

TOF time-of-flight.

UHPLC ultra high performance liquid chromatography.

XIC extracted ion chromatogram.

Chapter 1

Thesis introduction and overview

1.1 Context of the study

In 2022 the anniversaries of two notable milestones in mass spectrometry will be celebrated. The first is the centenary of F.W. Aston's Nobel Prize in chemistry for his discovery of isotopes by means of mass spectrograph in 1922. The second is the 2002 Nobel Prize in chemistry won by J.B. Fenn for his work on electrospray ionization (ESI) and K. Tanaka for his work developing laser desorption ionization. Both developments were and continue to be significant in their own right. As a technique mass spectrometry offers exceptional sensitivity and detection limits (zeptomole range) for the analysis of molecules and biomolecules.

Mass spectrometers measure gas-phase ions which historically meant that only molecules with high vapour pressures and high thermal stability could be readily ionised limiting the range of molecules which could be studied. Vacuum based electron ionization (EI) sources was the predominant method for ionization

until the 1960s [1]. Various methods such as chemical ionization (CI) [2] and atmospheric pressure chemical ionization (APCI) [3] amongst other methods were developed to address the limitations of EI in the analysis of biomolecules (table 1.1). However, it was not until the development of new ionization sources specifically ESI and matrix-assisted laser desorption/ionization (MALDI) in the 1980s that truly allowed samples in the liquid and solid phases to be vapourised and ionised simultaneously allowing much larger thermally labile biomolecules to be studied for the first time. At the start of the current century, atmospheric pressure photoionization (APPI) [4] was developed to complement existing atmospheric pressure ionization (API) techniques and the development of ambient desorption ionization (ADI) sources [5, 6] began a further evolution in mass spectrometry with a focus on the *in situ* analysis of samples requiring minimal sample perpetration. The pairing of an ionization source and molecule can be key to generating useful analytical results. In general, EI and CI still tend to be favoured for low molecular mass non-polar molecules, while ESI and MALDI are preferred for polar molecules with high molecular mass.

Table 1.1: List of ionization sources based on electrical plasmas. The year of publication/widespread adoption, along with typical application areas and operating conditions are listed for comparison. †Glow discharge sources have existed since at least the 1870s [7] but the Grimm type lamp popularised its use. ⋆The low temperature plasma probe (LTP) is based on the principles of a dielectric barrier discharge which was first described by Siemens in 1857 [8].

Name	Year	Typical Applications	Operating Conditions
Chemical ionization [2]	1966	Molecular analysis	3 kV
Glow discharge [9]	1968†	Elemental analysis	3 kV d.c., 2 A
Atmospheric-pressure chemical ionization [3]	1974	Molecular analysis	$2kV$, $10^{-6}A$
Inductively couple plasma [10]	1980	Elemental analysis	R.F. 1-2 kW
Direct analysis in real-time [6]	2005	Ambient desorption	1-5 kV d.c
Low temperature plasma [11]	2008⋆	Ambient desorption	2-5 kHz, 2.5-5 kV a.c.
Flowing atmospheric-pressure afterglow [12]	2008	Ambient desorption	-500-700 V d.c.

1.2 Research problem

ESI is a powerful technique for the analysis of polar and semi-polar compounds including biopolymers [13]. The primary mechanism for the formation of positive ions by ESI is protonation based on Brønsted acid–base chemical reactions. However, not all compounds can readily be protonated, such as hydrocarbons, and EI proves to be a preferred high-sensitivity ionization technique as ions are formed by electron ejection. The use of EI is not without its own disadvantages such as a complex and costly sample inlet and vacuum systems. Therefore an ionization method that can bridge these techniques would be highly advantageous particularly in an open-source laboratory such as a university or the speciality and fine chemicals industry which handle a variety of sample chemistries. A universal ionization source which can analyse chemistries that are not normally amenable to ionization by existing atmospheric-pressure techniques would be useful in providing complementary data. Would an atmospheric pressure glow discharge (APGD) ionization source be suitable, as these sources potentially have several pathways to form ions [14]?

1.3 Introduction to mass spectrometry

A mass spectrum is a representation of a gas-phase ion's abundance as a function of its mass-to-charge ratio (m/z). A traditional mass spectrometer is formed from five principal component parts, (i) sample inlet, (ii) ionization source, (iii) mass analyzer, (iv) detector, and (v) the output, as shown in figure 1.1. A critical step in the process of producing a mass spectrum is transferring a molecule from a

solid, liquid or solute phase into the gas-phase and the ionization of the molecule, prior to sorting of the ion by its m/z in a mass analyser and its detection.

Figure 1.1: Schematic showing the five components of a typical mass spectrometer, (i) sample inlet, (ii) ionization source, (iii) mass analyzer, (iv) detector, and (v) the output.

Mass spectrometers are primarily used for measurement but they can also be used for separation of compounds. Its most infamous use might be in the refinement of uranium for the Manhattan Project and the development of the first atomic bombs [15], which used a Calutron mass spectrometer developed by E.O.Lawrence who won the Nobel Prize in Physics in 1939 for its invention.

Mass analysers measure the mass-to-charge ratio (m/z) can therefore mass-resolve based on the difference in an ion's momentum, velocity or kinetic energy and each design will make use of one or more of these properties. Many designs exist including Orbitrap (Kingdon trap [16]), quadrupole, ion trap, Fourier-transform ion cyclotron resonance (FT-ICR) (Penning trap [17]), magnetic sector, and time-of-flight (TOF) [18]. The quadrupole ion trap or Paul ion trap was developed by W. Paul and H.G. Dehmelt and allowed ions to be trapped in three-dimensions for the first time using fast switching radio frequencies overcoming the restrictions of Earnshaw's theorem earning them one half of the Nobel Prize in Physics in 1989. Mass analysers mass-resolve and focus the ions towards a single focal point on a detector.

1.4 An ideal ionization source

At the 1986 Asilomar Conference Curt Brunneé invited the audience to consider whether the ideal mass analyzer is fact or fiction [19, 20]. A similar question has been asked for ionization sources. What would a universal ionization source look like? An overview and comparison of some important performance characteristics of EI and ESI are shown in table 1.2. As can be seen there is a large contrast between the two ionization sources. This is maybe better illustrated in figure 1.2 where the approximate extent of the ionization capabilities of both sources is plotted against a theoretical analyte's polarity and molecular mass.

Table 1.2: High level overview of some of the characteristics of an EI and ESI source, some values taken from [21, 22]. †Cost comparison on source only, would vary greatly when taking into account mass spectrometer and chromatography instrument.

Characteristic	EI Performance	ESI Performance
Mass range	Low	High
Polarity	Non-polar	Polar / Semi-polar
Stability & reproducibility	High	Medium (influenced by electrolytes)
High ionization efficiency	1 in 10^3	1 in 10^5
Typical ions	Fragment ions	Protonated molecules
Gas consumption	none	High
Power consumption	High	Medium
Ease of Operation	Low	Medium
Cost†	High	Low
Sample introduction phase	Gas or solid	Liquid

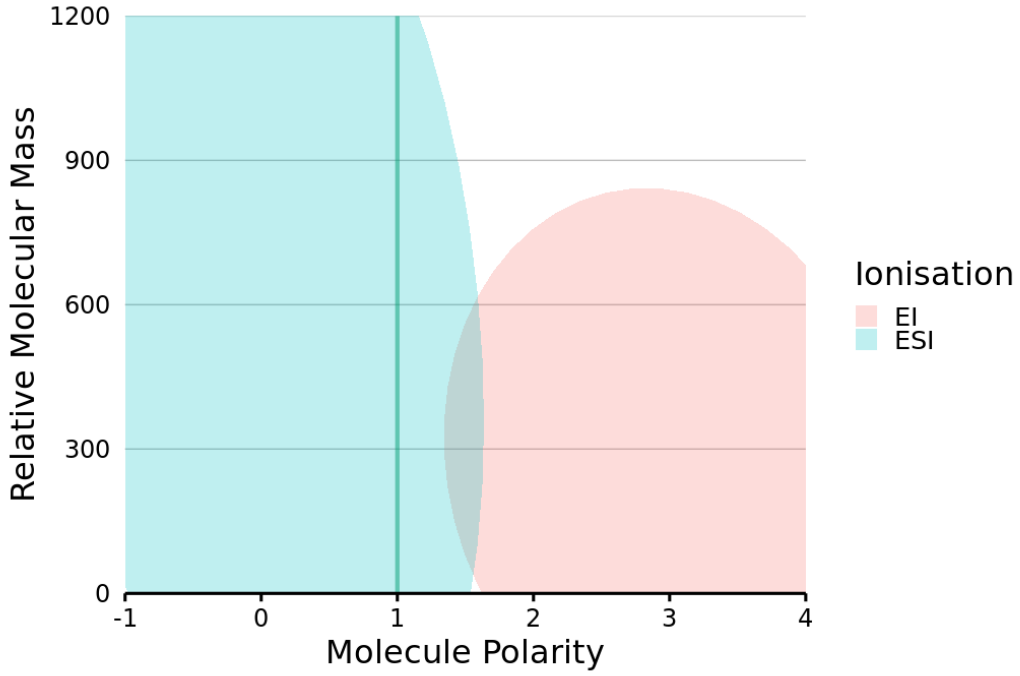

Figure 1.2: Map of the mass spectrometry ionization. Plot of the primary ionization method as a function of a molecule's molecular mass and polarity (decreasing from left to right).

With the information from table 1.2 and figure 1.2 it is possible to potentially begin to identify a solution to the question. An idealised source should be able to ionise the broadest possible mass range, from single atoms to the largest biomolecules [23]. This characteristic is also limited in part to the mass analyzer over a mass range, so the ability to multiply charge a high mass analyte is also desirable. It should be able to handle the widest range of molecule polarities, from ionic to polar to non-polar, in a varieties of phases i.e., solids (e.g. direct desorption), liquids (e.g. liquid chromatography (LC), supercritical fluid chromatography) and gases (e.g. gas chromatography (GC)).

In terms of operation an ideal source would be easy and cheap to construct, easy to operate, and have low gas and power consumption making it cheap to run. It should have high stability and reproducibility, for example ESI is noted to be affected by analyte concentration and can be overly affected by impurities and electrolytes at concentrations above 10^{-5} $mol\ L^{-1}$ which is undesirable [21]. The source should have high ionization efficiency which would allow achieving detection limit (DL) approaching the *zeptomole* range, and be able to provide both molecular and structural information on the analyte.

In answer to the question posed: it is most likely fiction to assume that a single source may achieve this goal. However, a multimodal solution may be the answer and several researchers have investigated combing two or more sources to broaden the types of analytes that can be ionised in a single analysis [24, 25, 26] suggesting a possible solution.

1.5 Ion formation

In mass spectrometry the process of ion formation can be classified as "hard" or "soft" ionization. Hard ionization occurs when molecules are ionised but have excess energy and are accompanied by extensive fragmentation and is classically associated with EI. On the other-hand soft ionization produces primarily protonated molecules and adduct molecules with limited or no fragmentation with ionization sources such as ESI, MALDI, APPI, and APCI.

1.5.1 Electron ejection

The process of electron ejection is typical of EI, developed by A.J. Dempster in 1918 [1]. Sample molecules are introduced at low-pressure into a stream of high energy electrons (70 eV) which causes ionization due to large fluctuations in the electric field around the molecules. For elements the maximum ionization energy, or first ionization energies (IE), required is 24.6 eV for the helium atom. However, it has been found that at these relatively low energy levels ionization is less efficient. At 70 eV the electrons de Broglie wavelength closely matches a molecules bond length (100-160 pm) allowing the most ionization efficiency at a rate of about one ion formed per 1,000 molecules. The high kinetic energy normally transfers into internal energy, which in turn causes the molecule to fragment.

$$M + e^- \longrightarrow M^{+\bullet} + 2e^- \tag{1.1}$$

1.5.2 Electron capture

Electron capture is a resonance process observed in negative ionization. In this process an electron emitted from the filament with low kinetic energy is incorporated into a molecule or atom's orbital. Negative molecular ions ($M^{-\bullet}$) tend to be formed when electrons have kinetic energy of 0-2 eV by associative resonance capture. Ions formed by electron capture tend to remain intact and produce strong molecular anion signals, unlike electron ejection.

$$M + e^- \longrightarrow M^{-\bullet} \tag{1.2}$$

1.5.3 Proton transfer

In proton transfer a protonated molecule is formed ($[M + H]^+$). This requires the presence of a reagent ion, which is a Brønsted acid (B), to transfer a proton to the analyte molecule. This forms the basis of ion formation of positive-ion ionization processes in CI, APCI, MALDI, and ESI, amongst other techniques.

$$M + [BH]^+ \longrightarrow [M + H]^+ + B \tag{1.3}$$

1.5.4 De-protonation

Both protonated molecules and de-protonated molecules are formed simultaneously but the relative proportions of the protonated verses de-protonated species will be greatly influenced by the structure and proton affinity (PA) of the molecule, it is however the polarity of the extraction voltage that influences which ions are detected. For acidic compounds, such as carboxylic

acids and phenolic alcohols, de-protonation will occur by disassociation.

$$M \longrightarrow [M-H]^- + H^+ \tag{1.4}$$

1.5.5 Hydride abstraction

Hydride abstraction, which is a subset of the anion abstraction process, can commonly occur for aliphatic alcohols and is sometimes the preferred mechanism over formation of protonated molecules depending on the sample chemistry.

$$M + X^+ \longrightarrow [M-H]^+ + XH \tag{1.5}$$

1.5.6 Adduct formation

Similar to the proton transfer process, adduct formation involves the whole reagent ion attaching by electrophilic addition to the analyte molecule. This is a common occurrence in ammonia CI with the formation of ammoniated molecules ($[M + NH_4]^+$). A similar phenomenon is observed in positive ESI when ammonium acetate is used as a modifier. Other common adducts in positive ionization are sodium and potassium, amongst others. While, negative ions will be formed in the presence of a Brønsted base (B), which acts as the reagent ion, as it will accept a proton from the analyte.

$$M + X^+ \longrightarrow [M+X]^+ \tag{1.6}$$

$$M + B \longrightarrow [M-H]^- + [BH]^+ \tag{1.7}$$

1.6 Glow discharge design

1.6.1 Low-pressure glow discharge

Low pressure glow discharge ionization sources have been favoured due to a combination of high excitation temperature and low kinetic temperature (figure 1.3) allowing both atomic and molecular analysis [27]. As a highly sensitive source (ppb levels for uranium) low pressure glow discharge mass spectrometry is a powerful technique for elemental analysis [28, 29]. The beginning of the main period of interest was in the late 1960s with the introduction of the "Grimm-type lamp" for use in glow discharge optical emission spectroscopy for the analysis of metals and alloys [27, 9].

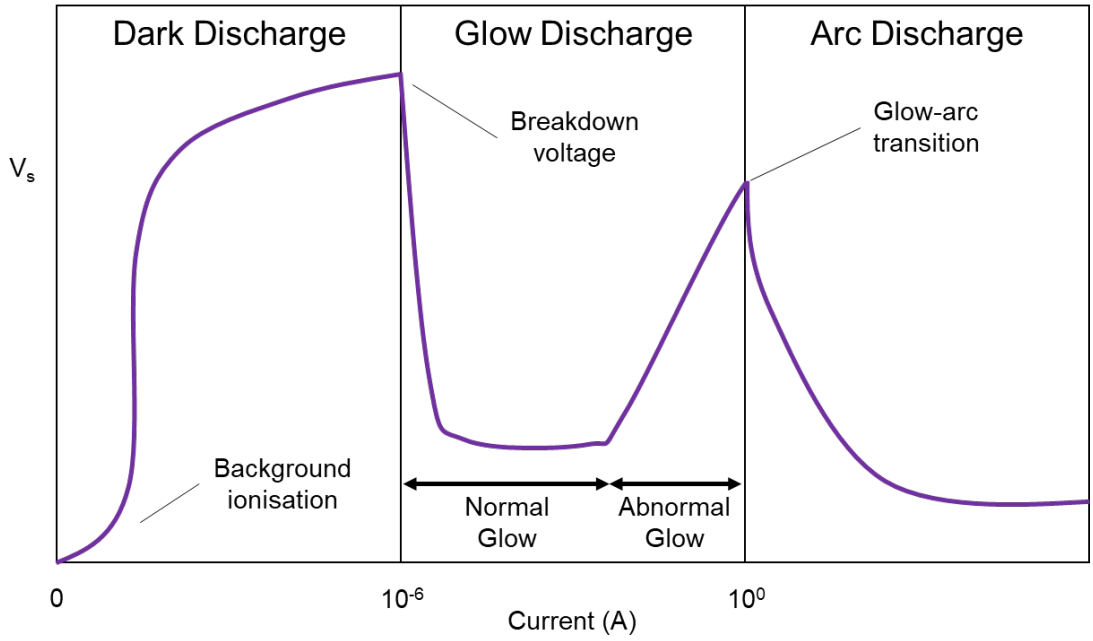

Figure 1.3: Plot of the voltage-current characteristics of a discharge. Highlighted are the three regions, dark discharge, glow discharge, and arc discharge.

1.6.2 Atmospheric pressure glow discharge

Atmospheric pressure ionization sources remove some of the complexity associated with the need for high vacuum systems and produces protonated molecules unlike the low-pressure counterparts. The atmospheric pressure glow discharge (APGD) design (figure 1.4) described by Kuwabara and Tsuchiya [30] used a needle electrode as a cathode and two counter electrodes, one acting as an anode and the other a wire grid with a retarding voltage for removing excess electrons with argon as the discharge gas (flow of 0.3 $L\ min^{-1}$). The use of a grid to remove electrons would suggest the primary ionization mechanism is via Penning ionization or alternatively via protonation through secondary reactions of the molecules with the solvent matrix (glycerol or nujol). An alternative ionization source design was described by Hiraoka *et al.* [31] which used a ring of ten tungsten needles as one electrode and a hollow capillary as the counter electrode a counterflow of argon was used as the discharge gas (4 $L\ min^{-1}$). Hiraoka *et al.* design allowed molecules in solution (or liquid molecules) to be continuously infused via the capillary into the discharge region which was not possible with Kuwabara and Tsuchiya's design which relied on the solution to be deposited on a fixed emitter.

1.6.3 Flowing atmospheric pressure afterglow

The flowing atmospheric pressure afterglow (FAPA) design isolated the glow discharge from the molecule sampling (termed the afterglow region, see figure 1.5) [32, 12]. The design incorporates a tungsten pin as the cathode and a plate with an orifice as the anode (10 mm diameter, 1 mm orifice), the design uses helium as the discharge gas (flow rate 0.5 – 2.0 $L\ min^{-1}$)). A further advancement was made to

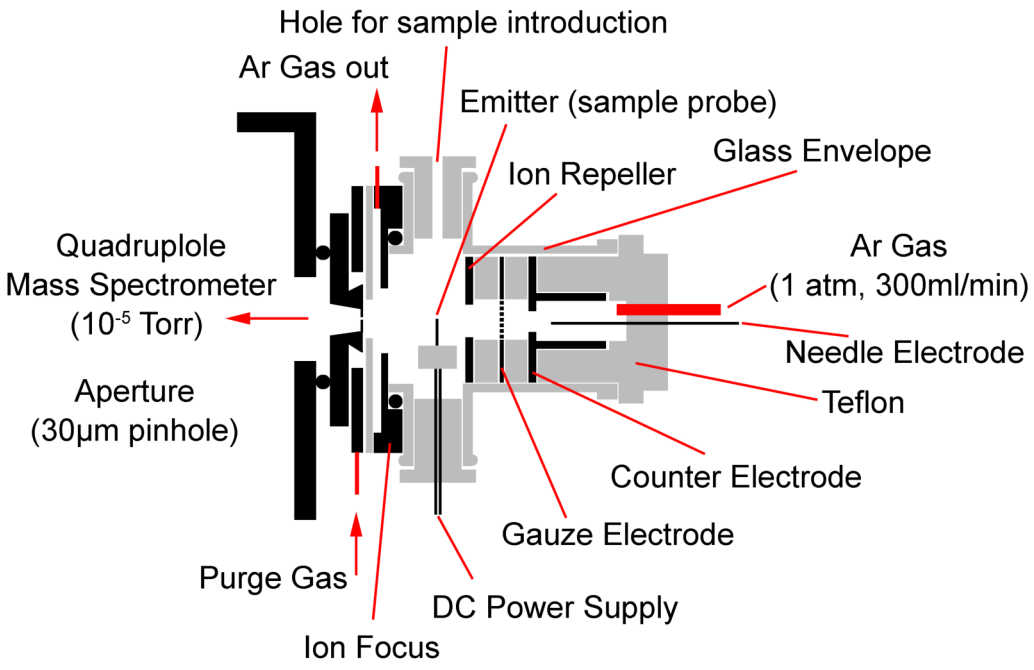

Figure 1.4: A schematic of an atmospheric pressure glow discharge. (Illustration by Rhodri N. Owen adapted from [30]. ©The Mass Spectrometry Society of Japan, 1982)

the design where the anode plate was replaced by a hollow capillary (1.6 mm o.d, 1.3 mm i.d, 25 mm long) which address significant oxidation of molecules seen in the original geometry [33]. The design makes the introduction of a sample easier and offers the possibility of surface analysis and mass spectrometry imaging. The FAPA benefits from high sensitivity (tens of pg for herbicides and pesticides) and low or no fragmentation making it ideal for trace analysis. However, the relative positing of sample surfaces, mass spectrometer and ionization source has led to questions about the design's reproducibility.

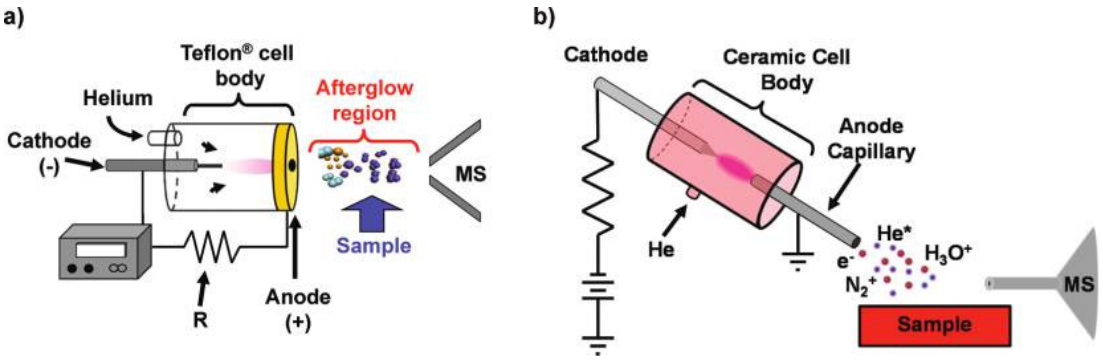

Figure 1.5: Two FAPA designs. The pin-to-plate geometry after Andrade *et al.* [32] (a). The pin-to-capillary geometry after Shelley *et al.* [33] (b). (Reproduced with permission from [33]. ©American Chemical Society, 2011)

1.6.4 Minaturisation of flowing atmospheric pressure afterglow

The miniaturisation of FAPA offers the possibility of higher electron and power densities that can result in greater sensitivity due to higher operating temperatures and higher reagent ion yields. The micro-flowing atmospheric-pressure afterglow (μ-FAPA) described in 2017 with a miniaturised halo design (figure 1.6) reported that operating temperatures of the cathode may have reached 525-1,200 $^{\circ}C$ at currents above 25 mA and that it was able to ionise some high molecular mass compounds (>2,000 $g\ mol^{-1}$) which had not been reported for FAPA previously [34]. Another example of compact sources is the helium plasma ionization developed in the laboratory of Attygalle [35, 36, 37] which in some respects is similar to the μ-FAPA. In this design the ESI source is adapted by replacing the normal solvent flow with helium gas (0.03 $L\ min^{-1}$) in constant voltage mode (3 kV) with additional heating (150–300 $^{\circ}C$) of the discharge by the nebulizer. The source has been primarily used for low molecular mass "small molecules" (<500 $g\ mol^{-1}$) and has reported high

sensitivity (pg range 2,4,6-trinitrotoluene). A mini-flowing atmospheric-pressure afterglow (miniFAPA) design showed good stability and high sensitivity ($fmol$ range) but these features were not specifically related by the authors to its miniaturisation [38].

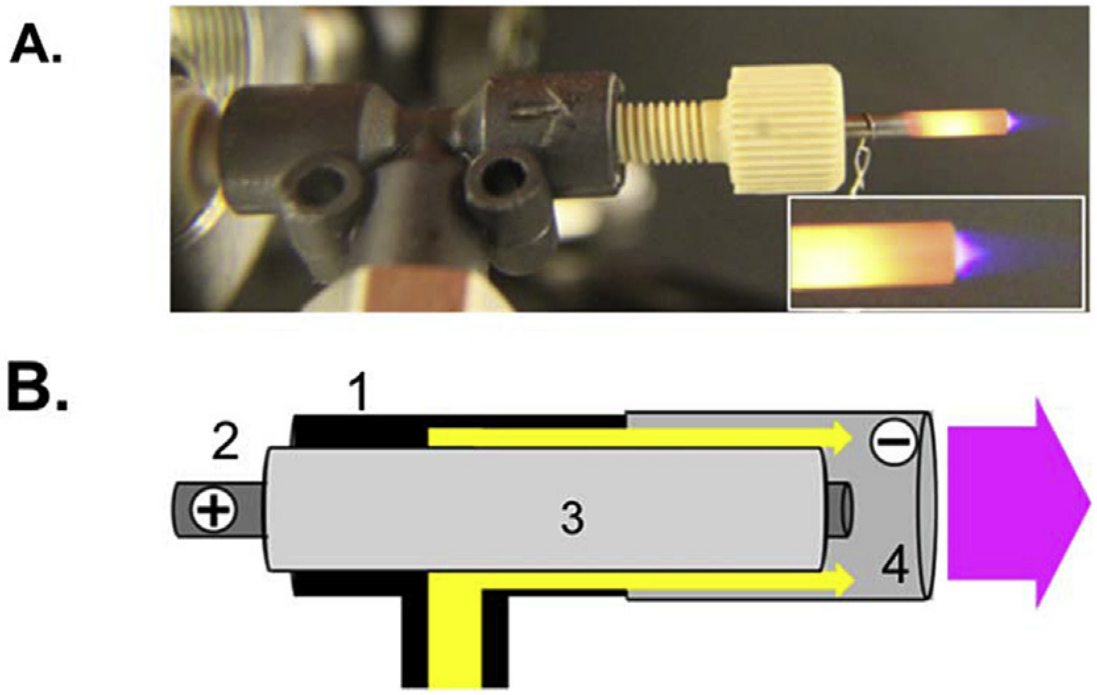

Figure 1.6: The microplasmaFAPA. The photograph shows the source in action with the electrodes glowing form heating and the faint purple glow of the halo shaped discharge (A). Schematic of the source showing the plastic body of the source (1), positive electrode (2), an insulator (3), and the negative electrode (4) (B). (Reproduced with permission from [34]. ©Elsevier, 2017)

1.6.5 Alternative discharge sources

There have been a variety of discharge source developed such as dielectric barrier discharge (DBD). A DBD is constructed of two electrodes one of which is covered by a dielectric material. A discharge is formed in-between the dielectric barrier

and the counter electrode when operated with an alternating voltage [39]. An early report of the DBD being used as an ionization source for ADI mass spectrometry was made by Na *et al.* [40]. They placed an analyte on the dielectric material, in this case a glass slide and the low-temperature plasma desorbed and ionised the analytes. The authors reported that the DBD benefited from a simple design and the lack of solvent needed to form desorbed ions. An advancement on dielectric barrier discharge ionization was reported by Harper *et al.* [11] who developed a compact 6.35 mm LTP. The LTP used a DBD but was different in that the plasma protruded from the probe and directly interacted with the sample. The benefit of which was to allow analysis of any type of a sample surface without the need to place it directly between the electrodes. A limitation of this approach is the molecular mass of compounds amiable to ionization is generally <400 $g\ mol^{-1}$ possibly due to the cool temperature (30 $^{\circ}C$) of the discharge which would limit its use to compounds with high vapour pressures.

1.7 Plasma modifiers and reagent ion systems

There are several ionization mechanisms available in glow discharge ionization sources which makes it attractive for the analysis of a wide variety of sample chemistries. Some may be more abundant in low pressure ionization sources while others may dominate in atmospheric conditions. The initial mechanism is that of EI which can either ionise the discharge gas or directly ionise a sample molecule (reaction 1.1). Electrons will also travel through and interact with the discharge gas and can form long lived metastable atoms, He^{*}, (reaction 1.8), $He_2^{+\bullet}$ ion, and the He_2^{*} excimer [41]. The metastable atoms can then go on to

collide and directly ionise sample molecules by Penning ionization (reaction 1.9) [42] which is favourable as the energy of metastable helium is 19.8 eV and it is very stable with lifetimes of hundreds of milliseconds. The presence of Rydberg atoms (He^{Rg}) formed from the recombination of slow electrons with helium ions has also been observed in glow discharge plasmas [43].

$$e^- + He \longrightarrow He^* + e^- \tag{1.8}$$

$$He^* + M \longrightarrow M^{+\bullet} + He + e^- \tag{1.9}$$

When molecules are introduced directly into the glow discharge these reactions are likely to dominate ionization of molecules. In the flowing afterglow APGD ionization source additional API *like* [44] ionization mechanisms exits. The first stage in positive mode is the production of $N_2^{+\bullet}$ and $N_4^{+\bullet}$ by Penning ionization, as electrons emanating from the discharge cell have insufficiently energy to ionise N_2 [32]. For $N_2^{+\bullet}$ the following sequence of reactions occur [45]:

$$N_2^{+\bullet} + 2N_2 \longrightarrow N_4^{+\bullet} + N_2 \tag{1.10}$$

$$N_4^{+\bullet} + H_2O \longrightarrow H_2O^{+\bullet} + 2N_2 \tag{1.11}$$

$$H_2O^{+\bullet} + H_2O \longrightarrow H_3O^+ + OH^\bullet \tag{1.12}$$

This leads to the formation of solvated protons $H^+(H_2O)n$ clusters, where n

is dependent on the partial pressure of water in the atmosphere. At atmospheric pressure, an important ionization mechanism for APGD is likely to be protonation by solvated protons. Molecules with higher proton affinity (PA) than the solvated proton clusters, which act as a Brønsted acids, will form ions by proton transfer (reaction 1.13).

$$H^+(H_2O)n + M \longrightarrow MH^+ + nH_2O \tag{1.13}$$

The reaction should proceed efficiently when PA($H^+(H_2O)n$) <PA(M) and should in practice mean that solvated proton clusters should readily protonate most organic molecules with a PA <697 $kJ\ mol^{-1}$ but will not be as amenable to protonate those molecules with PA >697 $kJ\ mol^{-1}$ such as small alkanes (table 1.3).

Table 1.3: Proton affinity of selected neutral molecules [21, 46, 47].

Neutral molecules	PA / $kJ\ mol^{-1}$
He	178
N_2	495
CH_4	552
C_2H_6	601
H_2O	697
CS_2	699
CH_2O	718
C_6H_6	759
CH_3OH	761
NH_3	854
CH_3NH_2	896

Ion formation by Brønsted acids (B) reaction can also occur via hydride abstraction (reaction 1.5) or via charge exchange (reaction 1.14).

$$BH^+ + M \longrightarrow M^{+\bullet} + BH^\bullet \tag{1.14}$$

Most organic molecules have IE of less than 10 eV so for charge exchange reactions to proceed the recombination energy (RE) of the Brønsted acids must be greater than the IE of the molecule. The RE of hydronium ion is about 6.4 eV and therefore can only charge exchange with molecules of low IE, which suggest this is not a particularly favourable pathway. Hydride abstraction will occur when the hydride ion affinity (HIA) of the Brønsted acids is high which in general is the reverse of the PA value of an ion. The $[M - H]^+$ ions are often observed in hydrogen and in methane CI mass spectra [2, 48].

Selection and control of the primary ionization mechanism [49] is desirable especially when analysing a broad range of sample chemistries. Changing the operating conditions of the flowing afterglow APGD has shown that reagent ion formation can be affected, at currents up to 25 mA $H^+(H_2O)n$, $O_2^{+\bullet}$ and NO^+ signals are observed. At elevated currents these signals drop sharply apart from NO^+ which continues to increase. In ambient conditions the prevalent ionization mechanism is subject to the changing composition of the atmospheric gasses in the laboratory or out in the field. Enclosed atmospheric, or sub-atmospheric, pressure housing offers the possibility of altering the reagent gas composition and consequently the favoured ionization mechanism. Removal of excess water moisture from the source using high purity nitrogen and drying lines will encourage charge transfer mechanisms by $N_2^{+\bullet}$ and $N_4^{+\bullet}$. Carbon disulfide is another reagent gas which has been used to promote charge transfer for analysis of aromatic hydrocarbons in low-pressure ionization sources [50]. The use of CS_2

as a solvent (sample concentration 1 $mg\ mL^{-1}$) has also been successful extended to a range of non-polar analytes using APCI [51].

1.8 Sample introduction and chromatography coupling

Ambient desorption ionization (ADI) is a relatively recent development in mass spectrometry allowing samples to be analysed *in situ* with no preparation or separation [52]. Molecules are desorbed directly from a sample surface by a stream of ions from a liquid (desorption electrospray ionization) [5], hot gas (direct analysis in real time) [6] or plasma (low-temperature plasma probe) [11]. The molecules are either simultaneously ionised as they desorb or are ionised quickly once they are in the gas-phase before being extracted into the high-vacuum mass spectrometer. The variation in sample surface and homogeneity of the molecules can give rise to issues with reproducibility and precision of measurements.

Solids probe

Probes allow solid or solvated samples to be vaporised in the ionization source. Vaporisation is kinetically favoured over decomposition when rapidly heated to high temperatures as described by the Arrhenius plot (where rate constant $k = A.exp^{(-E_a/RT)}$). An energy sudden probe is ideal for molecules with low thermal stability and low vapour pressure which many not otherwise be amenable to analysis by mass spectrometry [21]. The use of heating and nebulisation has also been used with some success with atmospheric pressure and ADI type ionization

sources [53, 54, 55, 56].

Liquid chromatography

High performance liquid chromatography (HPLC) involves the separation of a sample mixture in a liquid mobile phase passing through a column (2.1–4.6 mm diameter, 30–250 mm length). The components are separated as they move at different velocities based on their degree of interaction with the column's coating, or stationary phase, the time it takes for a component to elute from the column is called its retention time. HPLC allows the separation and analysis of very polar high molecular mass biopolymers which is not possible using gas chromatography [57]. Historically normal-phase HPLC was used to separate components in a sample involving a polar stationary phase such as silica or alumina and a non-polar mobile phase such as hexane or chloroform. The mechanism relies on polar interactions, such as dipole-dipole moment or hydrogen bonding, between the analytes and adsorptive surface of the stationary phase meaning more polar analytes are retained for longer while non-polar analytes are eluted sooner. In the 1970s reverse-phase HPLC was developed where the surface of the silica stationary phase was modified with C_{18} or C_8 straight chain alkyl groups making it non-polar. In reverse-phase the mobile phase is polar solvent such as water, more non-polar analytes are retained on the column by hydrophobic interactions. Changing the polarity of the mobile phase with methanol or acetonitrile increases the elution of the less polar analytes [57].

The coupling of liquid chromatography with mass spectrometry was not easy to achieve, the high flow rates of the liquid made maintaining the high vacuum of the mass spectrometer difficult. Several competing strategies were developed

including, (i) moving belt, (ii) particle beam, and (iii) direct introduction methods. ESI, APCI and APPI are currently the main interface for LC-MS and the use of sheath gas and counter-current gas along with heated transfer lines at the interface has become the main method of coupling the high flow rates of LC with the high vacuum of the mass spectrometer [58].

Gas chromatography

Gas chromatography uses a carrier gas typically helium (less commonly nitrogen and hydrogen) as a mobile phase and a capillary column (0.25-0.32 mm i.d., 1-30 m length) coated with a thin layer of stationary phase to separate volatile components in a sample mixture. The column is contained in an oven and typically a program is used to control a temperature ramp that assists in the elution of the analytes. Components with lower boiling points will generally elute before those components with higher boiling points [57, 59].

The interface of capillary column gas chromatography with mass spectrometry was relatively easy [60]. For traditional packed columns the use of jet separators or permselective membrane interface were developed. With the advent of capillary columns, they allowed direct interface into the ionization source without the need of any complex couplings due to the relatively low flow-rates of about 1-2 $mL\ min^{-1}$.

1.9 Application areas of analytical glow discharge sources in mass spectrometry

Application areas for analytical glow discharge sources in mass spectrometry are diverse, from atomic analysis and speciation [61, 43] through to molecular and biomolecular analysis [30, 62]. The focus in recent years with glow discharge sources for ADI has been on the analysis of small molecules, pharmaceuticals, drugs of abuse, pesticides, and explosives [63, 64, 65, 66].

1.9.1 Organic molecules

Organic compounds are made of a carbon backbone and are important as they form the basis for all known life forms. An APGD source was used to study a range of both straight chain and branched aliphatic hydrocarbons, cyclic hydrocarbons, halogen and aryl compounds. The Hiraoka group used both argon and helium and they reported that the former gave a more intense signal but for the latter the molecular ion formed the base peak [31, 67]. Initial studies with the FAPA pin-to-plate source focused on small ketones and aromatic compounds [32]. The use of plasma sources has also been uses for the analysis of synthetic polymers. The laboratory of McEwen reported the use PEG-400 as a mass calibrant using their atmospheric-pressure solids analysis probe (ASAP) probe [53].

1.9.2 Bio-analysis

Monitoring of biological systems can identify changes in health and the presence of diseases in populations and individuals. The use of a novel aerosol vacuum-assisted plasma ionization for the analysis of complex aerosol mixtures using a pin-to-plate FAPA source was reported as part of a study of prebiotic chemistry [68]. While the use of a glow discharge source for the study of phospholipids was reported, the technique was softer than others at the time [69]. The same group also reported on the investigation of amino acids and sugars [70]. While the use of APGD for the analysis of small peptides and nucleoside has also been reported [62], a DBD ionization source has also been used to analyse a range of amino acids from a glass slide [40], while the LTP probe has been used for the analysis of urine and stomach content [11].

1.10 Research objectives and hypothesis

The aim of this research thesis is to assess whether a APGD is an effective ionization source for chemistries not normally amiable to ionization by atmospheric-pressure techniques. In this study, I aim to design and characterise a prototype ionization source that can be easily retrofitted to existing mass spectrometers. A simplified and compact source will allow easier integration and portability between existing mass spectrometers. The study will compare a range of sample inlets and chromatography to measure the suitability of the prototype as a multimodal source. The ability to introduce samples in different states of matter, solid, liquid or gas, will allow flexibility in the analysis of compounds with different vapour pressures and thermal stability. Further, the

study will demonstrate the use of the prototype source in the analysis of non-polar compounds with a particular focus on lipids, pharmaceuticals and fine chemicals. A prototype APGD source with multimodal inlet will provide the ability to analyse a range of sample chemistries.

The development of the prototype source is limited to the Waters Xevo G2-S TOF mass analyser and Waters Xevo TQ-S triple quadrupole mass filter. A previous study has already examined the use of FAPA with a Thermo Orbitrap [71]. The design will however allow for future translation of the prototype to other manufacturers' instrumentation. The study will limit the comparison of sample inlets to ASAP probe, flow-infusion using a heated nebulizer (APCI IonSABER II probe), and liquid chromatography (HPLC and ultra high performance liquid chromatography (UHPLC)). The study will not examine all sample chemistries. Biopolymers such as proteins and carbohydrates are generally already well served by ESI, so the study will focus on those chemistries which are less amenable to ionization by such techniques in particular those with a non-polar component, although some polar compounds will also be examined to establish the extent of the sources capabilities.

1.11 Overview

This thesis contains seven further chapters. Chapter 2 deals with the materials, instruments, data collection and processing, and the research methods used in the study. Chapter 3 contains a review on the theory of glow discharges, with a comparison of FAPA and direct analysis in real time (DART). In Chapters 4, 5, 6, and 7 the results of data analysis are presented for the development of the

prototype ionization source, comparison of the sample inlets and application of the prototype ionization source to study compounds of interest. Finally, Chapter 8 includes a discussion of the key findings and conclusions of the current study.

Chapter 2

Experimental methods and materials

2.1 Instrumentation

2.1.1 Mass spectrometer

Waters Xevo G2-S time-of-flight mass spectrometer

Measurements in this thesis were undertaken using a Xevo G2-S TOF mass spectrometer (Waters Corp., Wilmslow, UK), which is an orthogonal accelerated TOF mass analyser, as shown in figure 2.1. The operating conditions are listed in table 2.1, unless otherwise stated. It operates on the same basic principles as the linear TOF first described by Stephens [18] where the m/z is directly proportional to time taken t for an ion to travel distance d using an acceleration voltage U as described in equation 2.1.

$$t = \frac{d}{\sqrt{2U}}\sqrt{\frac{m}{z}} \tag{2.1}$$

The linear TOF in principle has no upper mass range and benefits from high transmission efficiency giving them high sensitivity. However, a major limitation of the design was its low resolution owing to a number of factors principally kinetic energy, time, and space distributions which result in ions with the same m/z having different drift times. An improvement in resolution was described by Mamyrin in 1973 [72] of the electrostatic reflectron mirror which improved the resolution of TOF mass analyser from initial unit mass resolution to mass resolution of up to 3,500. While modern instruments typically have a resolution of 10^5. The reflectron consists of grid and ring electrodes which deflect ions back through the flight tube. It corrects the distribution of ions with the same m/z as ions with larger energies penetrate deeper into the reflectron and spend a greater time there compared to lower energy ions with the same m/z. The sensitivity and mass range are however limited at the cost of improved resolution. Another major step forwards in the development of the TOF was made by Dawson and Guilhaus [73] when they introduced 'orthogonal acceleration' (oa) of the ions. The ion beam from the source is accelerated orthogonally into the flight tube in packets by an electrostatic field operating at 10-100 *ns*. The ions gain a new velocity which is vectorially decoupled to the original ion beam velocity. The major benefit of the oa-TOF is that all the ions with the same m/z enter the drift free region with the same average velocity in the orthogonal direction. These advances combined with improved computing power allowed the commercial introduction of QTOF and QqTOF for routine mass spectrometry research and analysis [74].

Table 2.1: Operating conditions of the Waters Xevo G2-S time-of-flight mass spectrometer, unless otherwise stated.

Variable	Value
Cone	45 V
Source Offset	80 V
Source Temperature	120 $°C$
Probe Temp	450 $°C$
Cone Gas Flow	20 $L\ h^{-1}$
Desolvation Gas Flow	400 $L\ h^{-1}$

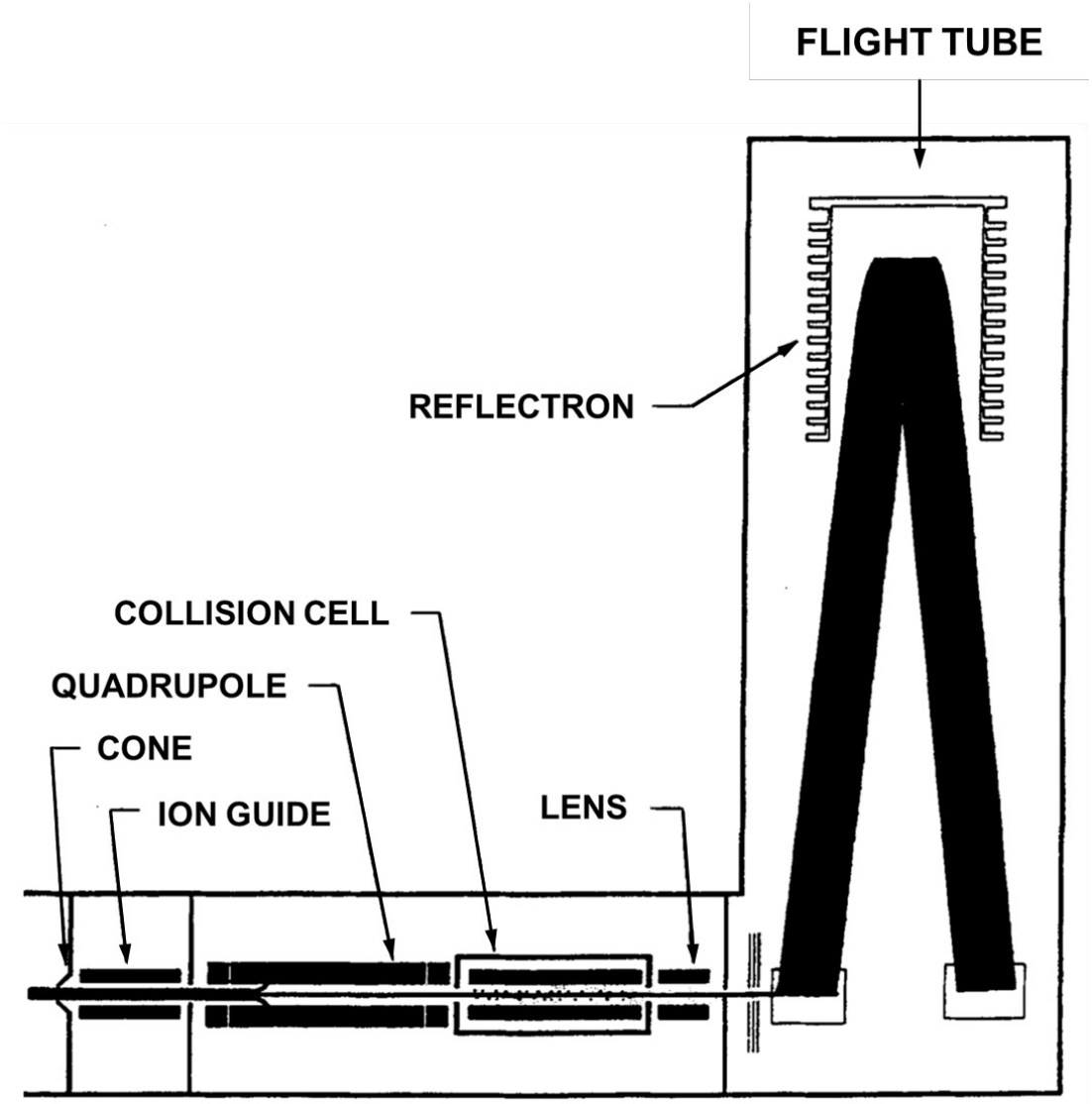

Figure 2.1: Schematic of a Waters Xevo G2-S mass spectrometer used to acquire measurements in this work. (Reproduced with permission from [74]. ©John Wiley and Sons, 1998)

Waters Xevo TQ-S triple quadrupole mass spectrometer

Measurements in chapter 7 of this thesis were undertaken using a Xevo TQ-S mass spectrometer (Waters Corp., Wilmslow, UK), which is a triple quadrupole mass filter, as shown in figure 2.2. The operating conditions are listed in 2.2, unless otherwise stated.

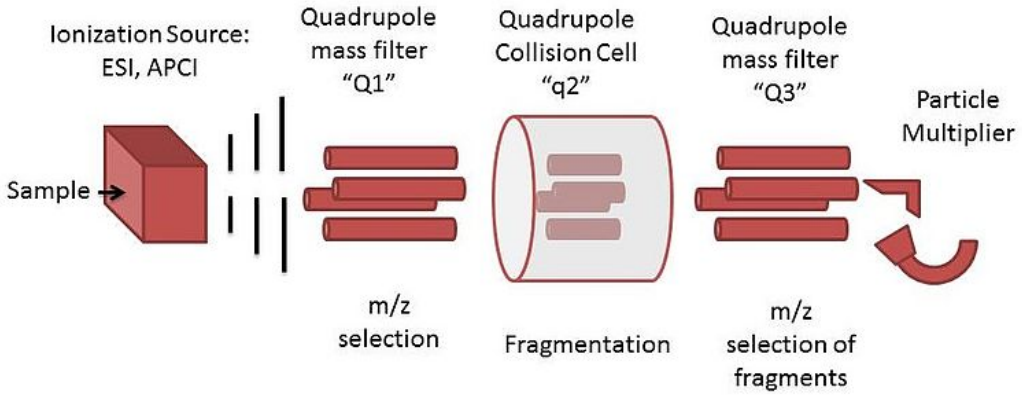

Figure 2.2: Schematic of a triple quadrupole mass spectrometer used to acquire measurements in this work. The collision cell 'q2' sits between the first quadrupole 'Q1', labelled as MS1, and the third quadrupole 'Q3', labelled MS2. A triple quadrupole was used for measurements in chapter 7. (Reproduced with permission from wikipedia.org. CC BY-SA 3.0 MiaJ601, 2015)

A simple linear quadrupole is made up of four cylindrical or hyperbolic rods in a square configuration, with pairs of opposite rods electrically connected to each other, one pair is held with a direct current component U and the other pair held with a radio frequency component V as described by Paul [76]. Ions enter the quadrupole along the z axis are subject to the total electric field causing the ions to oscillate in the x and y directions (equation 2.2 and 2.3). Ions of m/z subject to angular frequency ω with stable trajectories (derived from the Mathieu equation) where both the x and y components remain less than the rod spacing

r_0 will pass through the quadrupole. Those ions of m/z with unstable trajectories in either the x or y axis, i.e greater than r_0, will be lost to the rod assembly.

$$a_x = -a_y = \frac{8ezU}{mr_0^2\omega^2} \tag{2.2}$$

$$q_x = -q_y = \frac{4ezV}{mr_0^2\omega^2} \tag{2.3}$$

The quadrupole can routinely measure to m/z 2,000 [22] and theoretically has a maximum m/z range of up to 4,000 [57] and is generally considered to have low resolution, however, the resolution can be improved by adjusting a/q ratio to high values but this is at the cost of reduced ion transmission [21, 57]. Quadrupoles can be operated in two modes either scanning in which the electric field is quickly changed at rates of 16,000 m/z *per second* allowing the whole mass-to-charge range to be measured, or alternatively the quadrupole is "parked" on a selected m/z and the specific ion can then be monitored. Mass spectrometers can have an arrangement of three quadrupoles (QqQ), the first 'Q1' and third 'Q3' quadrupoles are used for m/z selection and the central or second quadrupole 'q2' (set in a RF-only mode to transmit ions of all masses) acts as a collision cell fragmenting the selected precursor ion. Fragmentation occurs when a precursor ion selected in Q1 enters q2 which is filled with an inert gas, the ion collides with the gas converting kinetic energy into internal potential energy. The high internal energy causes the ion to fragment producing fragment ions which pass into Q3. The triple quadrupole in general can be operated in three different scan modes, (i) *product ion scan* where a precursor ion with a specific m/z is chosen in Q1 and the fragment ions are all monitored in Q3, (ii) *precursor scan* the Q3 is set

to monitor a specific m/z fragment while ions are scanned in Q1 across the mass range, and (iii) *neutral loss scan* where Q1 and Q3 are scanned together but with a constant offset between the quadrupoles with Q3 monitoring for an $[m - a]$ fragment ion of the m precursor ion exiting Q1, where a is a neutral fragment of known mass.

Table 2.2: Operating conditions of the Waters Xevo TQ-S triple quadruple mass spectrometer, unless otherwise stated.

Variable	Value
Cone	30 V
Source Offset	50 V
Source Temperature	150 $°C$
Desolvation Gas Temperature	550 $°C$
Desolvation Gas Flow	400 $L\ h^{-1}$
Cone Gas	150 $L\ h^{-1}$
Collision Gas Flow	0.15 $mL\ min^{-1}$

2.1.2 Liquid chromatography

Agilent 1100 series high performance liquid chromatography

Measurements using a reversed-phase liquid chromatography hyphenated to the Waters Xevo G2-S time-of-flight mass spectrometer in this thesis were conducted using an 1100 series HPLC (Agilent, Stockport, UK), the operating conditions are listed in table 2.3. Typically this involves a non-polar stationary phase such as C_{18}, or n-octadecyl, bonded to 5 μm diameter silica particles and a polar mobile phase such as water, methanol or acetonitrile. In general the more polar analytes will elute more rapidly than non-polar analytes. The retention time t_R is the time taken for an analyte to elute from the column. The ability of the system to separate two analytes A and B is important and the resolution R can

be calculated using equation 2.4 where ω_A and ω_B are the peak widths.

$$R = \frac{t_{R(B)} - t_{R(A)}}{0.5(\omega_B + \omega_A)} \tag{2.4}$$

Table 2.3: Operating conditions of the Agilent 1100 series HPLC, unless otherwise stated.

Variable	Value
Solvent A	Water with 2 % acetonitrile and 0.2 % acetic acid
Solvent B	Acetonitrile with 0.2 % acetic acid
Flow rate	0.200 $mL\ min^{-1}$
High pressure limit	400 bar
Column Type	Fortis C_{18} 3 μm, 2.1 $\times$ 150 mm

Waters ACQUITY Class I UPLC

UHPLC is said to offer grater resolution, speed and sensitivity compared to conversional HPLC systems [77]. Measurements in chapter 7 are made using an ACQUITY Class I UPLC (Waters Corp., Wilmslow, UK) hyphenated with the Waters Xevo TQ-S triple quadrupole mass spectrometer with its operating conditions as listed in table 2.4.

Table 2.4: Operating conditions of the Waters ACQUITY Class I UPLC, unless otherwise stated.

Variable	Value
Solvent A	Water
Solvent B	Acetonitrile
Flow rate	0.500 $mL\ min^{-1}$
High pressure limit	15000 psi
Column Type	ACQUITY UPLC BEH C_{18} 1.7 μm, 2.1 $\times$ 50 mm

2.1.3 Infra-red thermography

Measurements of thermodynamic gas temperatures in this thesis was conducted using a Hti HT02 thermal imaging camera (Dongguan Xinatai Instruments, China). Th camera has a operating range of -20 to +300 $\pm 2\ ^{\circ}C$ and a resolution of 1024 pixels.

2.2 Materials

2.2.1 Flowing atmospheric-pressure afterglow sources

The materials used in the fabrication of the FAPA prototype sources are listed below (table 2.5).

The micro-glow discharge source ("Prototype V") was based on a micro cavity design. The design of the micro-glow discharge source was drawn using computer aided design (CAD) open-source software QCAD Community Edition (RibbonSoft, GmbH., version 3.22.0). The source was fabricated from off the shelf parts and was assembled and tested in our laboratory (Faculty of Medicine, Health, and Life Science, Swansea University). The micro-glow discharge source requires a high voltage DC power supply and helium gas flow. A positive voltage is applied to the hollow electrode. The power supply is operated in current controlled mode and can be set at 0-35 μA. Operating conditions of the micro-glow discharge source are listed below (table 2.6).

Table 2.5: Materials used for the fabrication of the FAPA prototype sources

Material	Manufacturer	Part Number
DC power supply (-1200 V, 0-50 mA)	Hertzinger GmbH, Germany	LCN1200-5
Tungsten pin	Huntingdon Fusion, UK	Multistrike ®
Ballast resistor (4.7 $k\Omega$)	Digital Paradise, Hong Kong	10W4K7J, NH515722
Stainless steel capillary (1/8" x 20 gauge (O.D. 3.18 mm, I.D. 1.35 mm))	Coopers Needleworks Ltd, UK	n/k
Quartz Glass Tube (O.D. 10 mm, I.D. 8 mm, Length 10 mm)	Quartz Silica Products Ltd, UK	n/k
Electrical Wire Terminals and T-Tap	Gasea, Guangdong, China	B01NCAZD6Q
Universal source enclosure	Waters, Wilmslow, UK	700004319
Ion chamber captive assembly	Waters, Wilmslow, UK	n/k
Stainless-steel probe tip assembly	Waters, Wilmslow, U K	M955615BC2
PEEK fingertight union	Upchurch	n/k
PEEK LC thumb nut	Upchurch	55067-U
Variable area flow meter	Key Instruments, Trevose, USA	MR3A12BVBN
Crimp ring terminal (6 mm)	RS Components	200-6947
PEEK tube (O.D. 1/16")	Upchurch	n/k
Ceramic Washer (M5)	RS Components Ltd	223-7406
Tubing PTFE (O.D. 1/8", length 3 m)	Thames Restek	JR-T-6800

A universal ESI source enclosure (Waters, Wilmslow, UK) was modified to allow the micro-glow discharge source to be inserted into the side of the housing (figures A.1 and A.2). Optimal settings were determined with the source axially to the mass spectrometer inlet. An ASAP probe, ESI or APCI IonSABER II probe was used to introduce samples into the source.

Table 2.6: Operating conditions of the micro-glow discharge source.

Variable	Value
Helium Flow	0.1 to 0.5 $mL\ min^{-1}$
Current	0 to 35 μA
DC Voltage	0 to 5,000 V

2.2.2 Chemicals and reagents

Analytes used in this work are from a variety of suppliers and are listed in tables 2.7, 2.8, and 2.9. Solvents dichloromethane(HPLC grade), methanol, water and acetonitrile (LC-MS grade) were all purchased from Fisher Scientific (Loughborough, UK). Yeast used in this work are listed in table 2.10.

Table 2.7: List of compounds used in this study. Physical and chemical data from PubChem [78].(*n/k- values not known)

Compound	Formula	Mono-isotopic mass ($g\ mol^{-1}$)	Melting point ($°C$)	Log P
Caffeine	$C_8H_{10}N_4O_2$	194.0804	235-237	-0.1
Chloramphenicol	$C_{11}H_{12}Cl_2N_2O_5$	322.0123	150.5	1.1
Cholesterol	$C_{27}H_{46}O$	386.3549	149	8.7
Cumarin	$C_9H_6O_2$	146.0368	71	1.4
2,5-Dihydroxybenzoic acid	$C_7H_6O_4$	154.0266	200-205	1.6
Ergosterol	$C_{28}H_{44}O$	396.3392	160	7.4
Estradiol	$C_{18}H_{24}O_2$	272.1776	173	4.0
Estrone	$C_{18}H_{22}O_2$	270.1620	255	3.1
4-Fluorobenzoic acid	$C_7H_5FO_2$	140.0274	184	2.1
4-Hydroxybenzyl alcohol	$C_7H_8O_2$	124.0524	124.5	0.2
1-Isoquinolinol	C_9H_7NO	145.0528	n/k*	1.3
Lactonic Sophorolipid (1',4"-Sophorolactone 6',6"-diacetate)	$C_{34}H_{56}O_{14}$	688.3670		3.4
4-Methoxybenzyl alcohol	$C_8H_{10}O_2$	138.0681	25	1.1
3-Nitrobenzoic acid	$C_7H_5NO_4$	167.0219	139-141	1.8
Palmitic acid	$C_{16}H_{32}O_2$	256.2402	62	6.4
Palmitoleic acid	$C_{16}H_{30}O_2$	254.2246	-0.1	6.4
Pentafluorobenzoic acid	$C_7HF_5O_2$	211.9897	100-102	2.0
Pentafluorocinnamic acid	$C_9H_2F_5O_2$	238.0053	154-156	2.4
Polyethylene glycol (PEG-400)	$(C_2H_4O_1)n$	44.05	-13	-1.4
Polyethylenimine (low-molecular weight)	$(C_2H_5N)n$	43.04	72-78	-0.4
Polypropylene glycol (PEG-725)	$(C_3H_6O)n$	58.04	-50	-0.7
Testosterone	$C_{19}H_{28}O_2$	288.2089	155	3.3

Table 2.8: List of oligopeptides used in this study

Name	Formula	Mass	Sequence	Log P
MFRA	$C_{23}H_{37}N_7O_5S$	523.2577	Met-Arg-Phe-Ala	-3.8
Leucine Enkephalin	$C_{28}H_{37}N_5O_7$	555.2693	Try-Gly-Gly-Phe-Leu	-2.3
Angiotensin I	$C_{62}H_{89}N_{17}O_{14}$	1295.6775	Asp-Arg-Val-Tyr-Ile-His-Pro-Phe-His-Leu	-1.1

Table 2.9: List of standards used in this study.

Compound	Part Number	Supplier
PAH calibration mix	CRM47940	Sigma
Biodiesel	ERM - EF001	Sigma
Mobil Jet Oil II	n/k	n/k
"Six-mix" standard	700008892-4	Waters Corp
Extractables & leachables screening standard	186008063	Waters Corp
APGC standard	700005254-6	Waters Corp

Table 2.10: List of yeast samples.

Yeast	Type	Supplier
S. cerevisiae ex-bayanus	EC-1118	Lalvin (Lallemand Inc.)
S. cerevisiae	WY938a	Wyeast Laboratories Inc.
S. cerevisiae	WLP925	White Labs
S. cerevisiae	Vermont	n/k

2.3 Experimental methods

2.3.1 Lipid extraction protocol

Lipids were extracted from biological matrices using modified version of the methyl-*tert*-butyl ether (MTBE) protocol [79]. The sample was mixed with 3 volumes of methanol and the tube was vortexed. Then, 10 volumes of MTBE was added and the solution was incubated for one-hour. To the sample 2.5 volumes of water was added. The solution consists of non-extractable residues in a MTBE/methanol/water mixture (10:3:2.5, *v/v/v*). Phase separation of the sample was achieved by centrifuging at 1,000 *g* for 10 *min.* The upper (organic) phase and the lower (aqueous) phase were collected.

2.4 Data processing

All data was acquired using MassLynx 4.1 (Waters Corp, Wilmslow, UK) in continuum mode in the range *m/z* 50 to 2,000. High resolution accurate mass data was acquired but nominal masses were reported, except where compound identification was required where accurate mass measurements were made using known background ions as reference lock-masses. Signal intensity was calculated by integrating the peak area using mean smoothing and automatic noise measurement.

The 'R' programming language [80] was used for statistical analysis and graphical representation of the data. Okabe and Ito colour universal design [81] was used for figures so that they are friendly to colour-blind people.

2.4.1 Analytical figures-of-merit

Analytical figures-of-merit are the performance characteristics of an analytical determination and in this instance is used to assess the performance of the APGD ionization sources and compared where available in the literature with other ionization techniques. Some of the most useful figures-of-merit are range of reliable response, the DL, and the sampling error.

Range of reliable response

The range of reliable response refers to the consistency of measure values in the data set. One such approach is to calculate the coefficient of determination (R^2) which is calculated using equation 2.5 which describes the variance between the predicted values of the model and the observed outcomes.

$$R^2 = 1 - \frac{\sum(y_i - f_i)^2}{\sum(y_i - \bar{y})^2} \tag{2.5}$$

Where, y_i is data set of the observed value of y for n values, f_i is the fitted values of y from the model, and $\bar{y}$ is the mean of the observed values of y. The coefficient of determination is in the range 0 to 1.

Detection limit

The detection limit can be described as is the lowest concentration of an analyte that can be distinguished from the background or blank signal [82]. The DL is inverse of the sensitivity of the technique in terms of the variation of the signal to the sample concentration, as represented by the slope s of the linear calibration curve [83]. The DL can be calculated based on the standard deviation σ of the

response and the slope s, as shown in equation 2.6 [84].

$$DL = \frac{3\sigma}{s} \tag{2.6}$$

Sampling error

Error can be calculated in a number of ways such as standard deviation of the sampling distribution, or standard error of the mean (SEM), using equation 2.7. From a calibration graph it is also possible to calculate the residual standard deviation (RSD) from the liner regression line [85].

$$\sigma_{\bar{x}} = \frac{\sigma}{\sqrt{n}} \tag{2.7}$$

Where, $\sigma_{\bar{x}}$ is the SEM, σ is the standard deviation, and n is the number of sampling points.

2.4.2 Kendrick mass analysis

It is common place to specify the mass and mass-to-charge ratio (m/z) using the definition of one mole as equal to 12 grams of the isotope Carbon-12 ($_{12}C$), or more correctly today exactly $6.02214076 \times 10^{23}$ elementary entities of a substance [86]. The complexity of organic mass spectra led Kendrick to proposed the use of CH_2 with a molecular mass of exactly 14.0000 as the base unit for his method [87]. Compounds separated by CH_2 repeating unit such as hydrocarbons and fatty acids would share the same mass defect and so the relationship between associated ions can be more easily deduced. Further it is claimed that this method reduces by a factor of about 30-times the amount of data that requires processing.

The Kendrick mass is calculated using equation 2.8.

$$Kendrick\ mass = observed\ m/z \times \frac{14.0000}{14.0157} \tag{2.8}$$

$$KMD = (nominal\ observed\ m/z - Kendrick\ mass) \tag{2.9}$$

For Kendrick mass analysis, the Kendrick mass defect (KMD), which can be calculated using equation 2.9, is plotted against the Kendrick mass. It can be inferred that ions on the same horizontal rows belong to the same compound class with the same repeating units, while those in the same vertical columns are compounds with the same base formula but different heteroatoms or degrees of saturation.

Chapter 3

Theory of glow discharges

3.1 Underlying theory of glow discharges at low, intermediate and high pressures

3.1.1 Low pressure (High vacuum to 10 kPa)

The classical glow discharge is observed at low pressure in an inert atmosphere. The principal design of the discharge cell involves two electrodes separated by a gas through which a current flows. Initially the gas acts as an insulator, but when an electrical current is applied electrons are emitted from the cathode, at a critical voltage applied to the discharge cell when it equals the static breakdown voltage V_s the gas becomes a conductor. Paschen's law (equation 3.1) describes the V_s that is required to start a discharge between two electrodes as a function of the product of pressure and distance *pd*.

$$V_s = f(pd) \tag{3.1}$$

The Townsend avalanche or discharge [88] initiates the release of electrons by ionization of the gas. In a uniform field they gain energy and a cascade effect allows further ionization and release of more electrons. Positive ions accelerated towards the cathode can also liberate ions from collision with the electrode surface. The voltage drops sharply from V_s as the current rises to the glow discharge voltage V_g which is required to maintain the discharge. The current then varies exponentially at a fixed voltage at different inter electrode distances. This relationship is described by Townsend in the following formula (equation 3.2), where I is the current in the discharge, I_0 is the current at the cathode surface, d is the inter electrode distance, α_n is the first Townsend ionization coefficient, and ϵ_i is the Townsend second ionization coefficient.

$$\frac{I}{I_0} = \frac{e^{\alpha_n d}}{1 - \epsilon_i(e^{\alpha_n d} - 1)} \tag{3.2}$$

The static breakdown voltage from calculations of the Paschen's law can be plotted for different gases (figure 3.1). At a constant inter electrode distance the reduction of the pressure reduces the static breakdown voltage required to initiate a discharge until it reaches a critical point $p_0.d_0$, the minimum, after which the voltage required to initiate a discharge rises rapidly [88].

At very low pressures, 0.01 *Pa*, electron-molecule interactions are reduced and initiation of the discharge is reliant on electrode surface phenomena. It is suggested that the magnetic field plays a part in increasing ionization and consequently increases the effective *pd* of the gas.

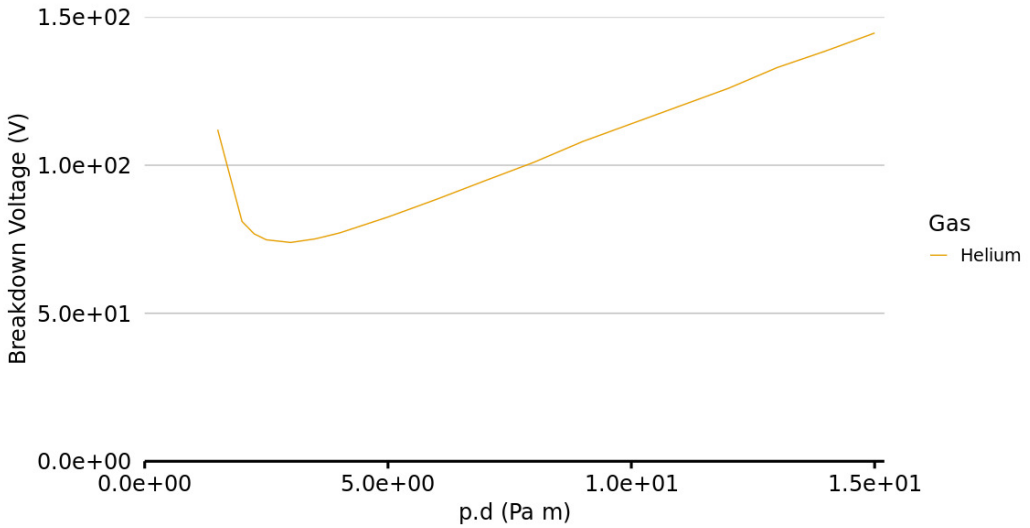

Figure 3.1: Plot of $p.d$ against breakdown voltage calculated from the Paschen law approximation for helium. Constants A and B are 2.25 $V\ Pa^{-1}\ m^{-1}$ and 25.50 $Pa^{-1}\ m^{-1}$ respectively.

3.1.2 Intermediate pressure (10 kPa to 200 kPa)

It was originally thought that only electrons emitted by the cathode could contribute to the glow discharge at intermediate pressures. In air at atmospheric pressure the formation of a discharge occurs rapidly in a gap of 1 cm usually in $\sim 10^{-7}$ s or less while secondary processes of positive ions moving towards the cathode, governed by the ϵ_i coefficient, happen at much slower rates of $\sim 10^{-5}$ s. At intermediate pressure narrow luminous tracks, known as streamers or *kanals*, are observed between the electrodes which is as a result of the reduction of lateral diffusion reducing the broadening of the discharge. However, early work had relied on rectified or smoothed alternating current to provide the electric field which fluctuated. Further work using power supplies with steady voltages ($\pm 0.1\%$) showed that at higher pressures the formation of the discharge follows the

Townsend equation and it will only occur when both primary electron ionization and secondary ionization processes are present [89].

3.1.3 High pressure (> 200 kPa)

Unusually, at high pressures the spark breakdown voltage is lower than would be expected at a particular value of *pd* given by the Paschen law. Experimental evidence also shows that there is 5-10 % spread in the V_s values and that these values also vary with both cathode material and surface finishes which differs to that at lower pressures [88]. It has been suggested that field emission of cold electrons occur at high pressure contributing to the deviation in Pacshen's law. At these pressures the electric field tends to be about two orders of magnitude higher at a constant *pd* values, and this phenomena has been exploited in the use of gases at high pressure as insulators for high voltage systems [88, 90].

3.2 Physical processes within the gas discharge cell

The optical processes within the glow discharge cell are easy to observe (figure 3.2). At the cathode, the Aston dark space *ADS* separates it from the first luminous layer called the cathode glow *CG* followed by a second dark space called the Crookes dark space *CDS* also referred to as the cathode fall. The *CDS* separates the *CG* from the negative glow *NG*. At the anode, the anode dark space ADS separates it from the luminous positive column *PC*. The *PC* is separated from the *NG* by the Faraday dark space *FDS*, sometimes there is a brighter region

at the anode end of the PC called the anode glow AG. These regions are typical of all glow discharges and little variation is observed between different apparatus.

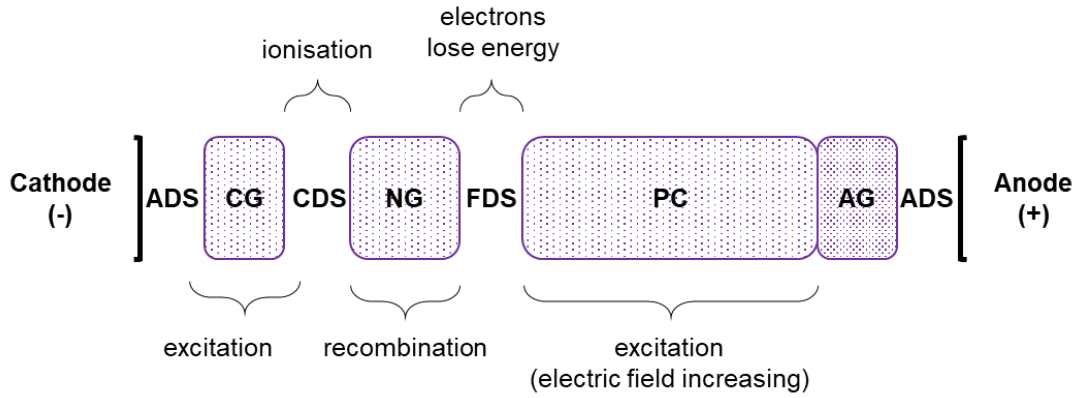

Figure 3.2: A discharge tube illustrating the different glowing regions that make up a glow discharge. Shaded: CG cathode glow, NG negative glow, PC positive column, AG anode glow; Unshaded: ADS Aston dark space, CDS Crookes dark space, FDS Faraday dark space, ADS anode dark space. (Illustration by Rhodri N. Owen)

These visual phenomena are an indication of what physio-chemical processes are occurring within the glow discharge. In the formation of the glow discharge the first process to occur is the emission of electrons from the cathode which ionise the neutral gas atoms. This happens by several processes which are illustrated in figure 3.3 for a low pressure helium discharge. The different ionization mechanisms that can occur in the plasma are described here.

Dark and light regions

The dark regions in the glow discharge are an indication of fast electrons with sufficient energy to ionise atoms, while the luminous regions occur as a result of slower electrons with only sufficient energy to excite atoms or recombine with ions and decaying to the ground state emitting a photon with wavelength in the

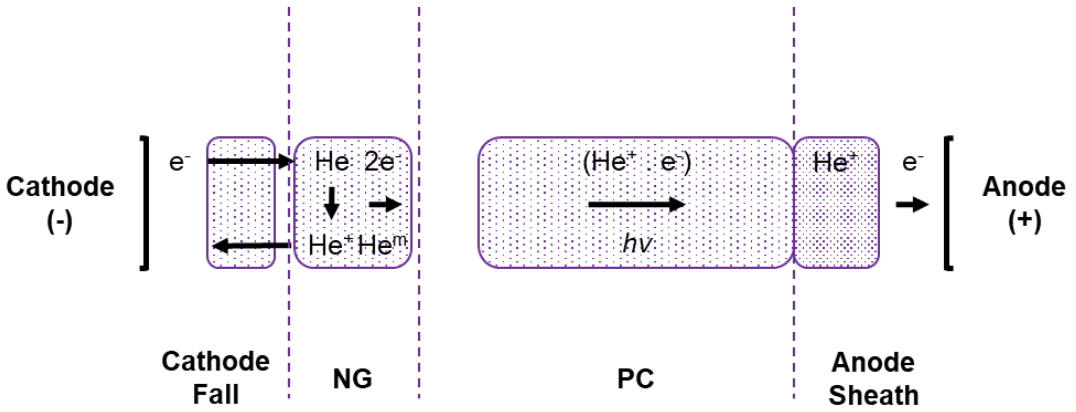

Figure 3.3: A representation of processes occurring within the different regions of the glow discharge. Electrons being released from the cathode, with ionization and excitation of the neutral helium plasma in the negative glow (*NG*), positive ions being accelerated towards the cathode and electrons moving towards the anode. (Illustration by Rhodri N. Owen adapted from [43]. ©American Physical Society, 2003)

visible range (λ 380 – 750 nm).

Direct ionization

The ionization of the neutral helium gas requires electrons to have sufficient energy greater than or equal to the IE of helium (24.6 eV or 2,372 $kJ\ mol^{-1}$). The rate of production of helium ions is dependent on the collision frequency Z and is given by equation 3.3.

$$Z = n_A n_B \sigma_{AB} \sqrt{\frac{8 k_B T}{\pi \mu_{AB}}} \tag{3.3}$$

Where μ is the reduced mass, σ is the reaction cross-section, n is the number density, T is the temperature in Kelvin, and k_B is the Boltzmann constant. Solving the equation for a helium APGD at the *cathode fall* gives a collision frequency of $4.6 \times 10^{21}\ m^{-3}\ s^{-1}$ ($k_B = 1.38 \times 10^{-21}\ J\ K^{-1}, T = 400\ K$, $\sigma_{AB} =$

$3.02 \times 10^{-21}\ m^2$, $\mu_{AB} = 9.10 \times 10^{-31}\ kg$, $n_A = 3.5 \times 10^{18}\ m^{-3}$, $n_B = 3.85 \times 10^{18}\ m^{-3}$).

Stepwise electron ionization

Stepwise electron ionization of excited species can occur and this process can be much faster than direct electron ionization. In this process the primary interaction of a neutral atom with a free plasma electron is only sufficient to excite the valence electron to an electronically excited state e.g., when a metastable helium species is formed which requires 19.8 eV of energy. In the second step, a second free plasma electron with much lower energy can then subsequently interact with the excited atom and raise the valence electron beyond its IE forming an ion.

Photo-ionization

Helium ions can also be generated by photo-ionization (equation 3.4), however this process is not highly favourable as there are few photons with the required wavelength of 50.4 nm, which is in the extreme ultraviolet range. Much of the electro-magnetic radiation in the discharge is emitted in the visible region ($\sim$ 380-750 nm, or 2.75-1.98 eV) such as the bright PC, meaning that photo-ionization is of limited importance in the formation of ions in discharge.

$$He + \lambda \longrightarrow He^+ + e^- \tag{3.4}$$

Particle-Particle ionization

Ionisation can also occur by collision of heavy particles, but ion-neutral collisions rarely produce an ionization event as the required energy of the ion must be 10-100 keV to be resonant which is much greater than the IE of neutral atoms and molecules [89]. On the other hand, Penning ionization is highly favourable as metastable atoms, such as He^* which has 19.8 eV of energy and the cross section is in the order of 10^{-15} cm^2. Metastable atoms can also undergo associative ionization (equation 3.5) with neutral molecules in the plasma, particularly when the molecular ion's electronic energy term crosses the electronic energy terms of the colliding atoms.

$$He^* + M \longrightarrow HeM^+ + e^- \tag{3.5}$$

Secondary electron emission

Emission of secondary electrons by surface ionization can occur through photo-electron emission, Penning mechanism involving metastable atoms, and electron-electron emission. This process is governed by the *work function* for the surface material derived from the Sommerfeld formula [91] and the secondary emission coefficient γ which is the electron yield per collision [89].

Gas phase reactions in the discharge

Once ions have been formed in the glow discharge they can then undergo chemical reactions. Ions have low activation energies and can have high kinetic energies which make their contribution to physical processes in the plasma significant.

The recombination of ions with electrons is highly exothermic. In atomic gases the recombination process involves three bodies (equation 3.6) the second free electron being able to absorb the excess kinetic energy.

$$He^+ + e^- + e^- \longrightarrow He^* + e^- \tag{3.6}$$

For ions of molecular gases one of two processes can occur, dissociative electron-ion recombination (equation 3.7) or an ion conversion process (equation 3.8).

$$AB^+ + e^- \longrightarrow AB^* \longrightarrow A + B^* \tag{3.7}$$

$$M^+ + 2M \longrightarrow M_2^+ + M \tag{3.8}$$

Additionally, radiative recombination can occur with the conversion of excess energy into a photon (equation 3.9), but this is a relatively slow process.

$$e^- + M \longrightarrow M^* \longrightarrow M + h\upsilon \tag{3.9}$$

The transfer of charge by ion-molecule conversion is described in equation 3.8, ions can also charge transfer to neutral atoms, this can be via resonant charge transfer where there is no defect in electronic energy (equation 3.10).

$$A^+ + B \longrightarrow A + B^+ \tag{3.10}$$

While non-resonant charge transfer can also occur where there is a deficiency

in energy required in the charge transfer, such as with nitrogen and oxygen (equation 3.11) where their first ionization energies are 14.5 eV and 13.6 eV, respectively.

$$N^+ + O \longrightarrow N + O^+,\ \Delta E = -0.9\ eV \tag{3.11}$$

Exothermic ion-molecule reactions have no activation energy and have high rate coefficients of reaction, in part as any molecule repulsion is offset by charge dipole attraction.

Information on the mechanisms of ion and excited species formation allows an understanding of the processes occurring in the glow discharge and afterglow of FAPA and other APGD sources.

3.3 Ionization mechanisms responsible for FAPA

3.3.1 Ionized and excited species present in the gas discharge cell

Generally FAPA is operated with helium gas, but its use has been reported with other gases. Electron ionisation is the primary method of ionising helium atoms in the gas to form ions. While electrons with insufficient energy can still interact with helium atoms and excite a valance electron, the excited valance electron will normally relax by radiative decay back to the ground state emitting a photon in the process. In some circumstances however the valance electron will be in an

excited level that is strongly forbidden from return to the ground state [92]. These excited helium atoms are described as being metastable and can exist for up to 7,870 s [93]. Helium ions can also be formed by *stepwise electron ionization* with low energy electrons ionising metastable helium atoms, as these atoms are already excited to 19.8 eV as they only require 4.8 eV of addition energy to liberate the valance electron to form an ion. Conversely, helium ions can recombine to with slow moving electrons to form excited species including metastable atoms [43].

Both helium atoms and ions can undergo processes to form diatomic helium ions ($He_2^{+\bullet}$) and diatomic metastable excitmers (He_2^*). The mechanism for the formation of $He_2^{+\bullet}$ (equation 3.12) was first described by Hornbeck and Molnar in 1951 [94]. A similar recombination of helium metastable with atoms can lead to the formation of He_2^*.

$$He^* + He \longrightarrow He_2^{+\bullet} + e^- \tag{3.12}$$

Even high purity helium contains trace amounts ($\sim$ 0.001 %) of impurities primarily nitrogen but also oxygen, hydrogen and moisture. The formation of nitrogen ions ($N_2^{+\bullet}$) by electron ionization requires 15.6 eV of energy. $N_2^{+\bullet}$ can also be generated in the plasma by Penning ionization from the metastable helium species He^* and He_2^*, or from charge transfer by $He_2^{+\bullet}$ as all these species carry sufficient energy to ionise nitrogen. It is also well established that nitrogen can form $N_4^{+\bullet}$ ions through the reaction of neutral nitrogen gas with $N_2^{+\bullet}$ [21]. The presence of NO^+ and $O_3^{+\bullet}$ have been reported in the FAPA plasma [32].

3.3.2 Species transported to and present in the afterglow region

Basic processes

Electrons have the highest density in the region of the *cathode fall* but their abundance and energy reduce rapidly in the bulk plasma of the *positive column*. A similar pattern is observed for helium ions and the helium metastable atoms. The $He_2^{+\bullet}$ and $N_2^{+\bullet}$ ions along with the He_2^* atom have highest densities in the *positive column*. The $N_4^{+\bullet}$ ion is present throughout the discharge but at lower densities than other species. The presence of nitrogen, and oxygen, species is as a result of trace impurities and diffusion of atmospheric gases into the discharge cell. In simulations [95] a second density maximum also appears near the anode for the majority of species particularly for electrons, $He_2^{+\bullet}$ and He_2^* but it was reported that this phenomena may be an artefact of the anode shape. The high density species present at the anode will have a greater probability of exiting through the anode orifice into the afterglow region than more defuse species. The neutral gas atoms will also be transported out of the discharge cell by combination of internal pressure of the system and by diffusion.

A theory of survivor species in the afterglow region

The survival of electrons, ions and metastables into the afterglow region will be affected by their ability to be penetrate into the atmospheric gas. This will be governed in part by the mean free path L of a particle before a collision event takes place, and is given by equation 3.13.

$$L = \frac{k_B T}{\sqrt{2} p \sigma} \tag{3.13}$$

Where k_B is the Boltzmann constant, T is the temperature, p is the pressure and σ is the collision cross-section. For an ion at atmospheric pressure the mean free path is 8.56 μm ($k_B = 1.38 \times 10^{-21}\ J\ K^{-1}, T = 400\ K, \sigma = 45 \times 10^{-20}\ m^2, p = 1.013 \times 10^5\ Pa$). In practice, the actual value of the mean free path of the reactive species exiting the anode may be greater as they are surrounded and "protected" by a sheath of helium gas. In any event, this would allow for the rapid formation of secondary ions in atmospheric gas, in particular $N_2^{+\bullet}$ due to the high concentration of nitrogen in air. Corona discharge in APCI is a well established process by which $N_2^{+\bullet}$ is produced by electron ejection, while Penning ionization (equation 3.14) and charge transfer (equation 3.15) have been established as further processes for ion formation in plasma discharges.

$$He^* + N_2 \longrightarrow He + N_2^{+\bullet} + e^- \tag{3.14}$$

$$He_2^{+\bullet} + N_2 \longrightarrow 2He + N_2^{+\bullet} \tag{3.15}$$

The presence of $N_2^{+\bullet}$ in the afterglow has been established by spectroscopic techniques [41], and the penetration of $N_2^{+\bullet}$ deeper into the afterglow with higher discharge gas flow rates (from 0.4 to 1.6 $L\ min^{-1}$) has been measured for the LTP [96]. It is unclear whether the presence of these $N_2^{+\bullet}$ ions in the afterglow is as a result of transportation from the plasma or primarily from rapid formation in the afterglow region, though the latter seems more probable due to the higher

concentration of $N_2^{+\bullet}$ in atmospheric gas compared to the plasma.

A complete understanding of which reactive species are transported into the afterglow is hindered in part as He^* decays at λ 62.6 nm outside the range of most UV spectrometers while the $He_2^{+\bullet}$ exists in a form that does not radiatively decay. It has been inferred by Chan *et al.* [96] from the measured rotational temperature profiles of the $N_2^{+\bullet}$ ions in the LTP probe that $He_2^{+\bullet}$ ions are present in afterglow as the rotational temperature exhibit unusually rapid increase at the tail of the afterglow. The reaction (equation 3.15) involving charge transfer between the helium dimer ion and nitrogen is consistent with elevated rotational temperatures of up to 900 K which have been observed in the afterglow of FAPA [41].

A proposal for the species responsible for FAPA

The major reagent ions expected to be present in the afterglow are likely to be API-*like* ions of $N_2^{+\bullet}$, $N_4^{+\bullet}$ and $n(H_2O)H^+$. The formation of these secondary reagent ions are however reliant on the reactive species of the plasma. The presence of He^* and He_2^* at densities of 2×10^{19} m^{-3} and 6×10^{18} m^{-3} respectively at the anode in a APGD model [95] would strongly support the probability that these species would be transported at high concentrations into the afterglow region especially given their long lifetimes. The evidence points to the $He_2^{+\bullet}$ ion as a key energy carrier and its presence in the afterglow is inferred from the measured rotational temperatures of $N_2^{+\bullet}$ ions [96]. Electron density of 3×10^{18} m^{-3} has been modelled at the anode [95] but they have less than 10 eV of energy at this point. The presence of electrons in the afterglow does not appear to have been measured to give any conclusive evidence, but with low energies it is unlikely that they contribute greatly to the direct ionization of any organic analytes and do

not possess the necessary energy to ionise atmospheric gases to produce reagent ions in the afterglow.

3.4 Comparison of Direct Analysis in Real Time and Flowing Atmospheric Pressure Afterglow

The DART source is another example of an APGD based ionization source but the design uses a somewhat different arrangement of electrodes and power regime to FAPA (table 3.1).

Table 3.1: Summary of typical operating conditions of DART [6] and FAPA [33].

Condition	DART	FAPA
Voltage	-5 kV	-400 V
Current	5 mA	25 mA
Gas flow rate	1 $L\ min^{-1}$	0.6 $L\ min^{-1}$
Ambient afterglow temperature	55 $°C$	235 $°C$

The arrangement of the DART source (figure 3.4) consists of three chambers. The first is the discharge chamber consisting of the electrode needle and counter electrode, the second chamber is bound by a second counter electrode that can be used to remove ions, and the third chamber can be used to heat the gas flow [6]. It is suggested that the use of the perforated disk counter electrodes removes ions from the gas flow, making Penning ionization or associative ionization the primary initiators for the production of the secondary reagent ions [97]. DART operates at voltages of up to -5 kV and current in the region of 2 mA with the current-voltage conditions characteristic of the corona-to-glow transition, while

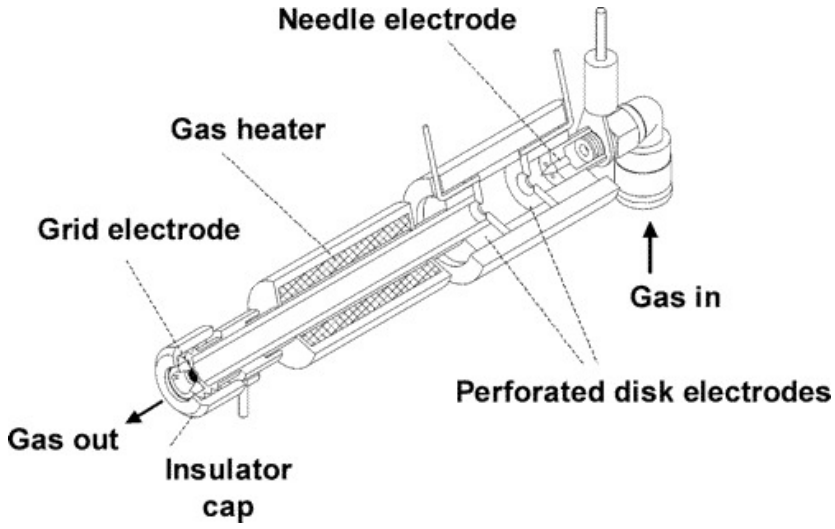

Figure 3.4: Schematic of DART source. (Reproduced with permission from [6]. ©American Chemical Society, 2005)

FAPA operates at a voltage in the region of -500 V and current of up to 50 mA more characteristic of the glow-to-arch transition. Characterisation of the respective discharges has shown that the major reagent ions in the afterglow region of DART are protonated water clusters but for FAPA in addition to protonated water clusters there were other ions $N_2^{+\bullet}$, NO^+, and $n(H_2O)H_3O^+$ and $O_2^{+\bullet}$ present suggesting that protonation is the main ionization mechanism of DART while both protonation and charge transfer is possible with FAPA [98]. This is in contrast to studies that show that adjustment of the relative position of DART can influence the intensity of $O_2^{+\bullet}$ ions and allows for the possibility of charge transfer [97].

The afterglow of FAPA has been measured by infra-red thermography reach a maximum 235 $°C$ compared to DART which reached 55 $°C$ [98] most probably as a result of higher current densities of the former and consequently increasing its desorption efficiency. DART overcomes the limitation in its desorption abilities

by having an integrated gas heater which can be set to 250 $°C$.

3.5 Discussion and Summary

Reactive species of helium from the plasma play an important part in the generation of organic analyte ions, whether through direct ionization or via secondary reagent ion generation (table 3.2). In addition to the traditional view of Penning ionization by metastable helium species being a major pathway there is evidence which strongly supports the idea that helium dimer ions ($He_2^{+\bullet}$) are a major contributor of at least 30 % to ionization in the afterglow region. The high concentration of nitrogen in atmospheric gases of the afterglow region allows for rapid ionization by the reactive helium species to $N_2^{+\bullet}$ and ultimately $N_4^{+\bullet}$ ions which must be the major contributors to charge transfer ionization pathways of analytes in the afterglow.

Table 3.2: Reactions occurring in the glow discharge and secondary reagent ions generated in the afterglow.

Plasma	Afterglow
$e^- + He^- \longrightarrow He^+ + 2e^-$	$He^* + N_2 \longrightarrow N_2^{+\bullet} + He + e^-$
$He^+ + 2e^- \longrightarrow He(or He^*) + e^-$	$He_2^* + N_2^{+\bullet} \longrightarrow 2He + N_2^+ + e^-$
$He^* + e^- \longrightarrow He^+ + 2e^-$	$He_2^{+\bullet} + N_2 \longrightarrow N_2 + He_2^*$
$e^- + He \longrightarrow He^* + e^-$	$N_2^{+\bullet} + 2N_2 \longrightarrow N_4^{+\bullet} + N_2$
$He^* + He^* \longrightarrow He_2^{+\bullet} + e^-$	$N_2^{+\bullet} + H_2O \longrightarrow N_2 + H_2O^+$
$He^* + 2He \longrightarrow He_2^* + He$	$H_2O^{+\bullet} + H_2O \longrightarrow H_3O^+ + OH$
$He_2^* + He_2^* \longrightarrow He_2^{+\bullet} + 2He + e^-$	$H_3O^+ + n(H_2O) \longrightarrow n(H_2O)H_3O^+$

This is supported by recent modelling from the Bogaerts laboratory, which also identified reactive NO and O_3 neutral species in the afterglow [99]. The production of protonated water clusters by nitrogen dimer ions is favourable due to the high dipole moment and low ionization potential of water despite the

water's low molar concentration in air. It is likely that there is limited or no ionization contribution from EI and photo-ionisations in the FAPA afterglow. In summary, it is expected that API-*like* ionization by protonation and charge transfer, as well as Penning ionization will all be major ionization processes in the afterglow.

Chapter 4

Development of prototype flowing atmospheric pressure afterglow ionization sources

4.1 Introduction

In Chapter 1 current APGD sources designs were reviewed, in this chapter the development and characterisation of three FAPA ionization source prototypes is made. These three prototype sources were designed in-house and were a sequence of incremental improvements to increase analytical performance (figure 4.1). A FAPA source decouples the generation of reagent ions in the glow discharge from the sampling region where the analytes are ionised. It was explored in chapter 3 that it is likely this class of APGD sources will provide API-*like* ionization producing protonated molecules $[M + H]^+$ and molecular ions $[M]^{+\bullet}$. Previous studies of FAPA on a LTQ Orbitrap XL mass spectrometer (Thermo Fisher

Scientific, Altrincham, UK) have shown this class of ionization sources to have high analytical sensitivity [71]. In the first section of this chapter the interfacing and operation of this pin-to-capillary FAPA source, which is referred to here as "prototype II", using a Xevo G2-S mass spectrometer (Waters Corp, Wilmslow, UK) is described. The second section of this chapter describes the design and fabrication of a more compact ionization source, referred to as "prototype III". The characterisation and operation of prototype III on the bench and its interfacing with the mass spectrometer is presented. A selection of low molecular mass polar and non-polar compounds were analysed to determine prototype III analytical capabilities. In the final section of this chapter a capillary-to-capillary design, referred to as "prototype IV" is described. The operating conditions and characterisation of this prototype is reported, along with an assessment of its analytical capabilities.

The data in this study were acquired using a Waters Xevo G2-S time-of-flight mass spectrometer operating in full scan mode. Samples were introduced via the ASAP probe or injected via a fine capillary. Data were processed using Waters MassLynx 4.1 and ions observed in negative and positive modes are discussed in the following sections.

Table 4.1: List of APGD prototypes developed, characterised, and optimised on the Waters Xevo G2-S mass spectrometer in this thesis. †Not described in this thesis.

Prototype	Description	Image
I	An early glass pin-to-capillary previously developed [71]†.	(Not Shown)
II	A pin-to-capillary FAPA designed in-house [71] and the component parts manufactured by a subcontract workshop (Angstrom Ltd, Staffordshire, UK).	
III	A compact FAPA designed and manufactured in-house, with a pin-to-capillary geometry but scaled down reducing the discharge cell volume by 95 % to allow positioning within the universal source housing.	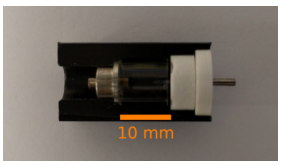
IV	A capillary-to-capillary geometry, where a stainless steel tube acts as the anode and second stainless steel tube acts as a cathode replacing the sharpened tungsten pin.	
V	A micro-glow discharge formed from a stainless-steel probe tip assembly o.d. 640 μm, which acts as the anode. The characterisation and optimisation of this prototype is discussed in chapter 5.	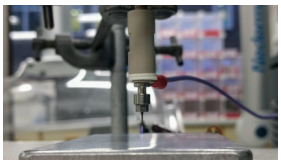

4.2 Pin-to-capillary FAPA ionization source (Prototype II)

The initial ionization source was designed in-house [71] and the component parts manufactured by a subcontract workshop (Angstrom Ltd, Staffordshire, UK). The design was based on the FAPA pin-to-capillary geometry and was intended to be used with the Imax™ housing on a Thermo Scientific LTQ Orbitrap XL mass spectrometer. It was previously established on that instrument that the ionization source could provide high analytical sensitivity with a DL in the low $pmol\ \mu L^{-1}$ range.

Briefly the design consisted of a discharge cell made of quartz tube (i.d. 16 mm, o.d. 19 mm, length 47 mm) containing a sharpened tungsten pin acting as the cathode and a stainless steel tube acting as the anode, as shown in figure 4.1. The helium discharge gas was connected via a gas-line and controlled by means of a pressure regulator set at 6 psi. A high voltage external power supply was connected via a ballast resistor (4.7 Ω, 10 W), which was housed inside the ionization source assembly, to the cathode.

Directly transferring prototype II from the LTQ Orbitrap XL to the Waters Xevo G2-S mass spectrometer was not straight forward. The Waters universal source enclosure is a much more compact source housing and the mass spectrometer inlet faces the right when the instrument is observed head on (with respects to the Thermo Scientific Imax housing). A loaned universal source enclosure (from Dr A. Ruth Godfrey, Swansea University) had the viewing window and nebulizer probe assembly removed which made access to the mass spectrometer inlet easier. The prototype II ionization source was positioned

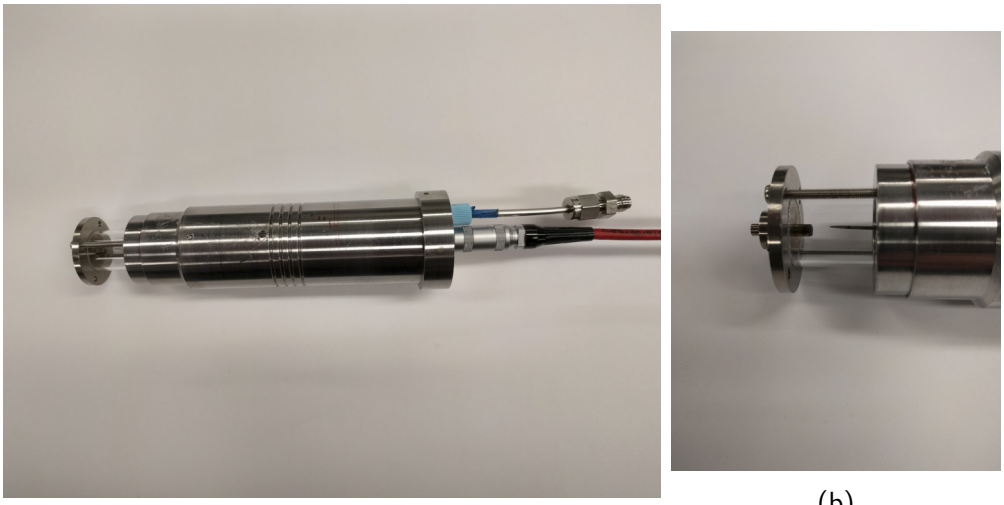

(a) (b)

Figure 4.1: Photograph of the prototype II FAPA ionization source. Prototype II is shown with the power connection (red lead) and gas inlet (blue PEEK nut) entering the source on the right hand side (panel (a)). A close up of the discharge cell can be seen (panel (b)) containing the sharpened tungsten pin protruding from the body of the ionization source and stainless steel on the left hand side which provides a counter electrode and means of transporting the glow discharge ions and excited species into the afterglow region.

using a laboratory bench clamp and could be placed axially (head-on) or radially (side-on) with respects to the mass spectrometer inlet. In atomic mass spectrometry the orientation of the inductively coupled plasma (ICP) torch can affect the resultant mass spectra, by having improved sensitivity in the axial position but has a poor reputation in terms of matrix effects while in the radial orientation it is said to provide better stability and precision [100, 101]. Waters instruments in general have the sample inlet orthogonally (or radially) to the mass spectrometer inlet which allow the charged ions to be extracted and enter the inlet, while the neutral molecules are swept past though to the exhaust reducing contamination.

In this a study examining the affect of altering the orientation of the FAPA

source with respects to the entrance of the mass spectrometer was undertaken. The compound octylamine ($C_8H_{19}N$, M_r 129) was selected as it has previously been studied using the prototype II source on the LTQ Orbitrap XL mass spectrometer. The sample was dissolved in acetonitrile:water (1:1 v/v) to a concentration of 1 $mg\ mL^{-1}$ and injected using a fine capillary into the afterglow of the prototype II source. The resulting spectra in both radial and axial positions was recorded (figure 4.2).

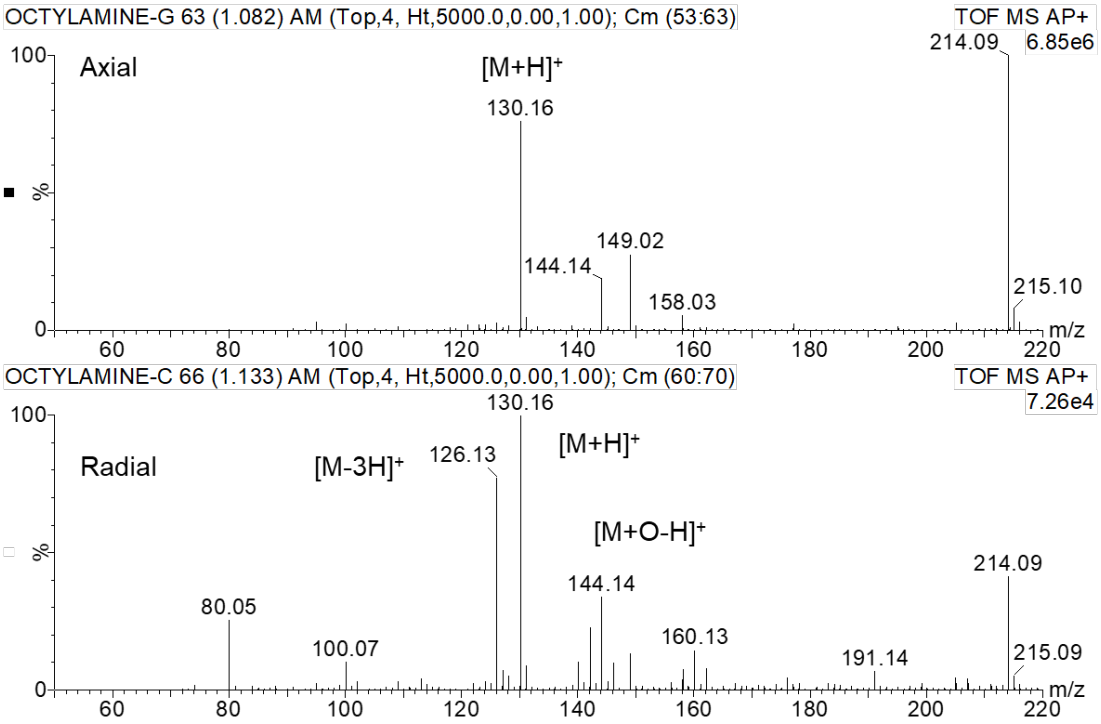

Figure 4.2: Mass spectrum of octylamine ($C_8H_{19}N$, M_r 129) using the prototype II FAPA ionization source. The ionization source is positioned axially in the mass spectrum (top panel) and radially (bottom panel), the ion at *m/z* 130.15 represents the protonated molecule. The observed *m/z* 144.14 which could be an oxygen adduct ion $[M-H+O]^+$ while ions observed at *m/z* 126.13 suggests that the ion with formula $C_8H_{16}N$ ($[M-3]^+$). The background ion at *m/z* 214 is n-butyl benzenesulfonamide. In the radial position signal intensity is two orders of magnitude lower than the axial position suggesting it is less sensitive.

The base peak of the mass spectrum of octylamine averaged over 10 scans is an ion at *m/z* 130, the protonated molecule ($[M+H]^+$). Also observed is an ion at *m/z* 144 which could be an oxygen adduct ion $[M-H+O]^+$. This phenomena has been previously reported for FAPA [33] and as the housing used with prototype II is open to the atmosphere then this can readily occur. Ions are also observed at *m/z* 126. The accurate mass measurement suggests that the ion with formula $C_8H_{16}N$ ($[M-3]^+$, observed *m/z* 126.1272 $\delta - 1.1$ *mDa*) and could tentatively suggest weak fragmentation and loss of three hydrogen atoms. In the radial position signal intensity is two orders of magnitude lower than the axial position which supports observations seen in ICP atomic spectroscopy. Reproducibility in both orientations was poor however as the position of the prototype II held by the bench clamp varied with respect to the mass spectrometer inlet, and the sample introduction was done manually introducing further uncertainty.

4.2.1 Background mass spectrum of prototype II

A mass spectrum of the background ions was acquired in positive ion mode on the Waters Xevo G2-S mass spectrometer using the source in the axial position with respects to the inlet is shown in figure 4.3. In the mass spectrum several protonated molecules ($[M+H]^+$) can be seen and readily identified, including *m/z* 149 phthalic anhydride, *m/z* 279 dibutylphthalate, *m/z* 391 diisooctyl phthalate, *m/z* 214 n-butyl benzenesulfonamide, and *m/z* 355, 462 and 536 polysiloxane, which are all common background ions.

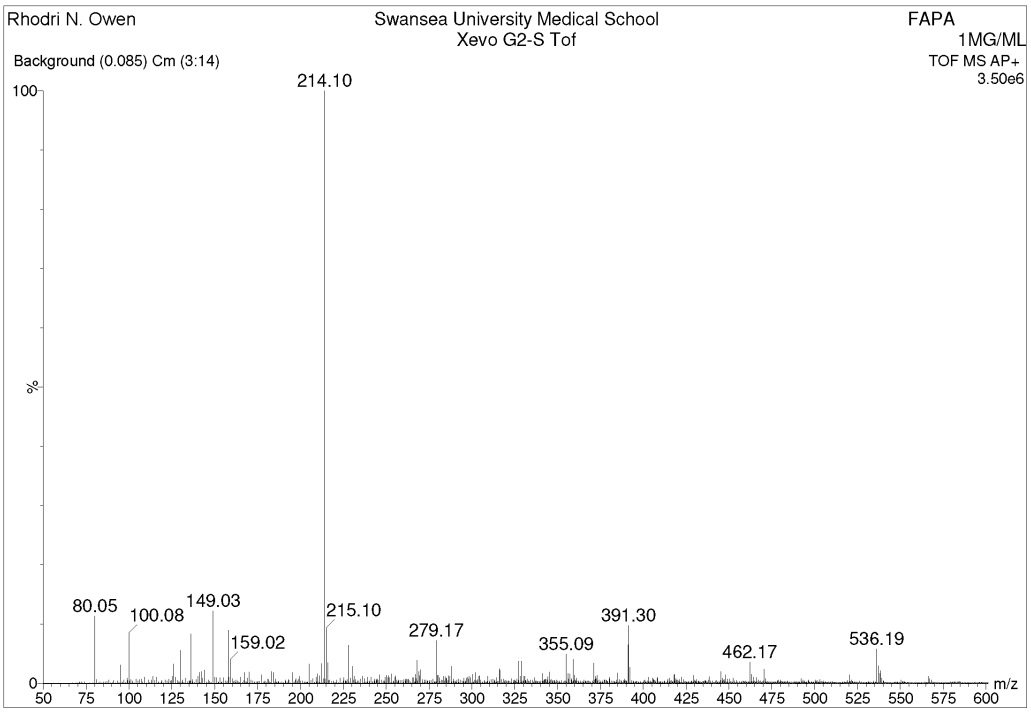

Figure 4.3: Mass spectra showing background ions acquired in positive ion mode using prototype II FAPA ionization source on the Waters Xevo G2-S mass spectrometer. Several protonated molecules ($[M+H]^+$) can be seen and readily identified, including *m/z* 149 phthalic anhydride, *m/z* 279 dibutylphthalate, *m/z* 391 diisooctyl phthalate, *m/z* 214 n-butyl benzenesulfonamide, and *m/z* 355, 462 and 536 polysiloxane, which are all common background ions.

4.2.2 Temperature measurements of prototype II

To characterise the thermodynamic gas temperature of the glow discharge, a study was made using an infrared thermal camera. The images in figure 4.4 show the ignited glow discharge of prototype II operating at 20 mA and +541 V with the overlaid infrared thermography showing the maximum thermodynamic gas temperature in the centre of the discharge being 46.3 $°C$ compared to the background laboratory temperature of 23.1 $°C$ after 25 minutes of operation.

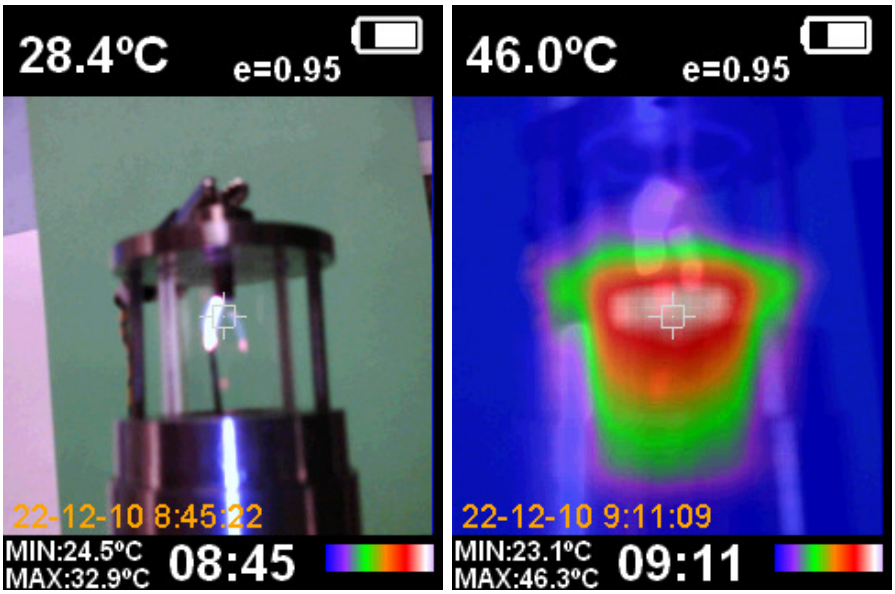

(a) (b)

Figure 4.4: Infrared thermography of prototype II. Image of the ignited glow discharge of prototype II can be seen between the pin-and-capillary (4.4a). Overlaid infrared thermography showing maximum thermodynamic gas temperature of 46.3 $°C$ at the centre of the discharge after 25 minutes operation at 20 mA (4.4b).

4.2.3 Sample Analysis

For comparison and based on the findings of studies undertaken using a Thermo Scientific LTQ Orbitrap XL mass spectrometer [71] compounds were selected for study with prototype II in combination with the Waters Xevo G2-S mass spectrometer namely, octylamine ($C_8H_{19}N$, M_r 129), nicotine ($C_{10}H_{14}N_2$, M_r 162), and adenosine ($C_{10}H_{13}N_5O_4$, M_r 267). Mass spectra of the compounds were acquired in positive ion mode. For octylamine the protonated molecule $[M+H]^+$ is the base peak observed at m/z 130, as shown in figure 4.5. Adenosine also produced an intense protonated molecule at m/z 268 (figure 4.6), while nicotine produced a m/z 163 protonated molecule as its base peak (Appendix A, figure A.3). Samples with low vapour pressure tended not to produce ions suggesting external heating to aid desorption and vaporisation of analyte samples is essential in combination with the FAPA ionization source, particularly for higher molecular mass compounds.

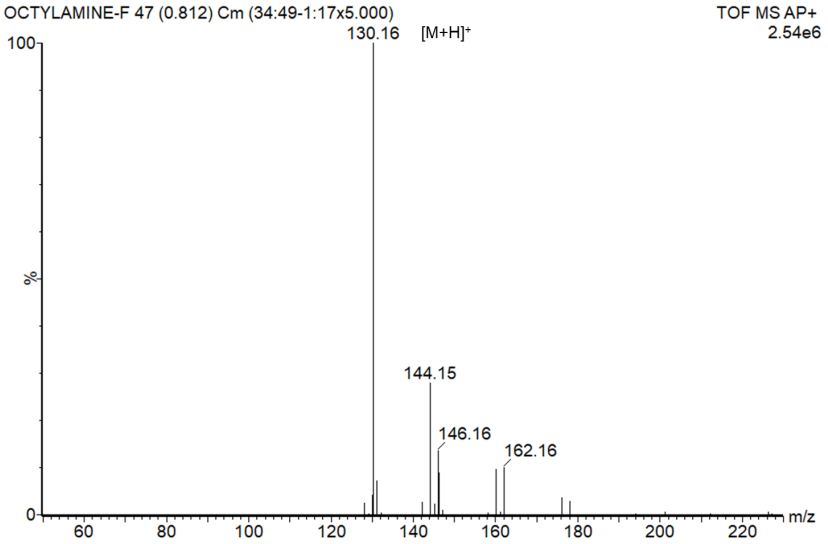

Figure 4.5: Mass spectra of octylamine acquired in positive ion mode using prototype II FAPA ionization source on the Waters Xevo G2-S mass spectrometer. Ion observed at *m/z* 130.15 is the protonated molecule $[M+H]^+$ which is the base peak for octylamine ($C_8H_{19}N$, M_r 129).

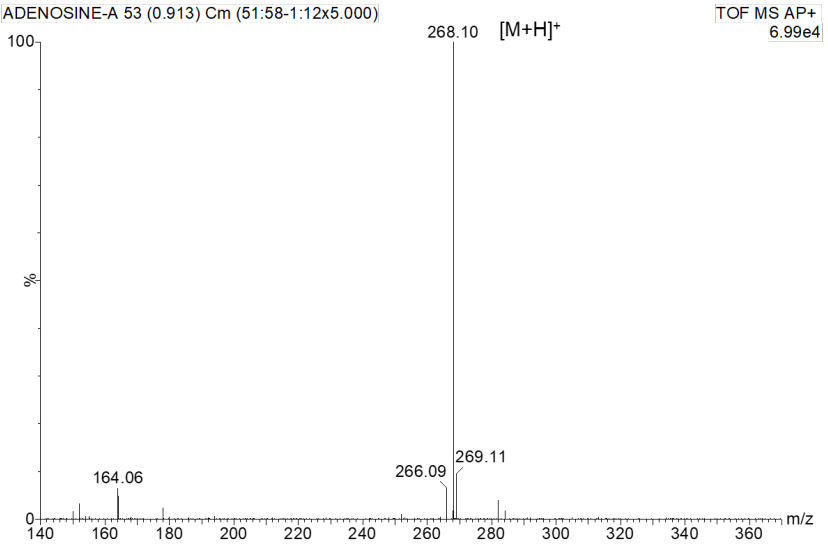

Figure 4.6: Mass spectra of adenosine acquired in positive ion mode using prototype II FAPA ionization source on the Waters Xevo G2-S mass spectrometer. Ion observed at *m/z* 268.10 is the protonated molecule $[M+H]^+$ which is the base peak for adenosine ($C_{10}H_{13}N_5O_4$, M_r 267). A weak ion at *m/z* 266.09 is the hydride abstracted ion $[M-H]^+$ which has a relative intensity $6.45\ \%$ to the base peak.

4.3 A compact flowing atmospheric pressure afterglow (Prototype III)

The previous prototype II design was bulky making integration with the Waters universal source housing difficult, therefore a compact ionization source prototype III was designed which would maintain the existing performance of the source while making it easier to integrate and the component parts were manufactured in-house in the modelling workshop (Faculty of Medicine, Health and Life Sciences, Swansea University). The design of this third prototype remained based on the pin-to-capillary geometry but scaled down reducing the discharge cell volume by 95 % miniaturising the source to allow easy retrofitting to the ion block and allow positioning within the universal source housing but still allowing the source to retain at least the same if not improved performance in terms of analytical performance. This made the mounting of prototype III on the ion block possible which had the benefit of fixed geometry improving reproducibility of measurements. The FAPA afterglow was positioned in the same relative position as the APCI corona pin, optimising the relative sample-source-inlet orifice position. Further the source was positioned radially to the orifice which was expected to improve stability of the signal which would benefit analytical sensitivity.

A schematic and photograph of prototype III is shown in figure 4.7. The discharge cell is made of quartz tube (o.d. 10 mm, i.d. 8 mm, length 10 mm) to contain the electrodes. A sharpened tungsten pin (o.d. 0.75 mm, length 6 mm) acts as the cathode and a stainless steel tube (o.d. 3.18 mm, i.d. 1.35 mm, length 8.5 mm) acts as the anode. Helium gas is delivered via either a stainless steel

or a polyether ether ketone (PEEK) tube (o.d. 1/16") into the outer stainless steel case and diffuses into the discharge cell via small orifices in the ceramic isolator and was operated at a maximum pressure of 10 *psi* - the limiting factor for this being the mass spectrometer pumping capacity. The high voltage cable was connected to an external high voltage power supply by a terminal pin via a ballast resistor (4.7 Ω, 10 W) housed in a external diecast box. The discharge cell was housed inside a chamber captive assembly which is mounted directly onto the ion block on the Waters Xevo G2-S mass spectrometer providing a fixed geometry for the ion source with respect to the orifice and sample, as shown in figure 4.8.

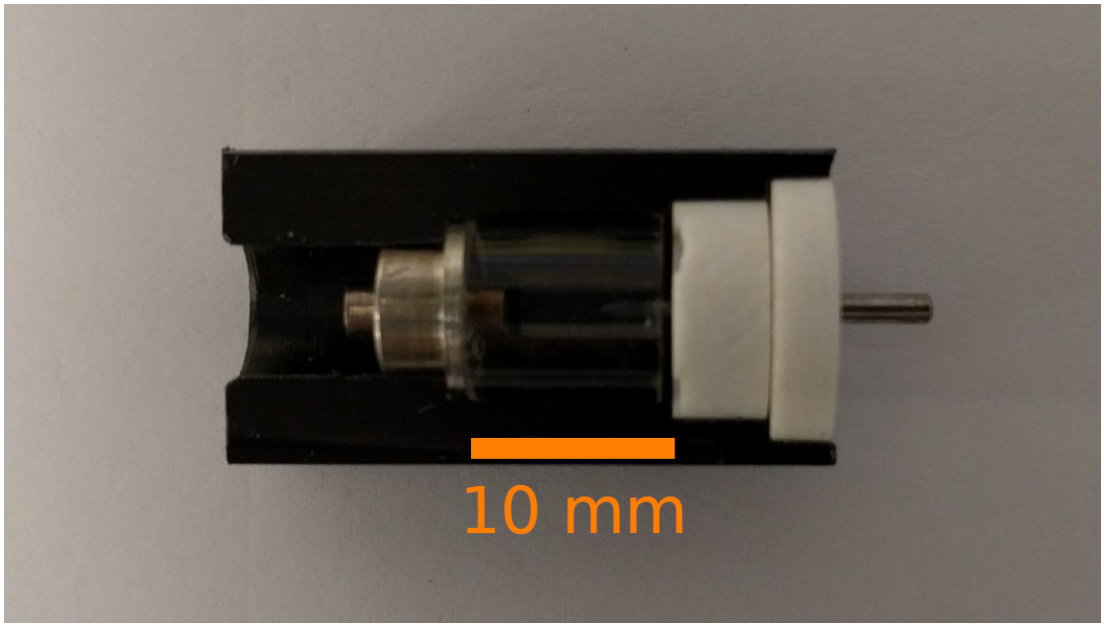

Figure 4.7: Photograph of prototype III FAPA ionization source. The components are shown here held in a black plastic cradle. A sharpened tungsten pin (o.d. 0.75 mm, length 6 mm) acts as the cathode, is on the right. passing through two ceramic isolating spacers and a stainless steel tube (o.d. 3.18 mm, i.d. 1.35 mm, length 8.5 mm) which acts as the anode can be seen on the left passing through a stainless steel cap, in the centre is the discharge cell made of quartz tube (o.d. 10 mm, i.d. 8 mm, length 10 mm). The cathode is attached to a external high voltage power supply via a ballast resistor (4.7 Ω, 10 W) housed in a external diecast box (not shown).

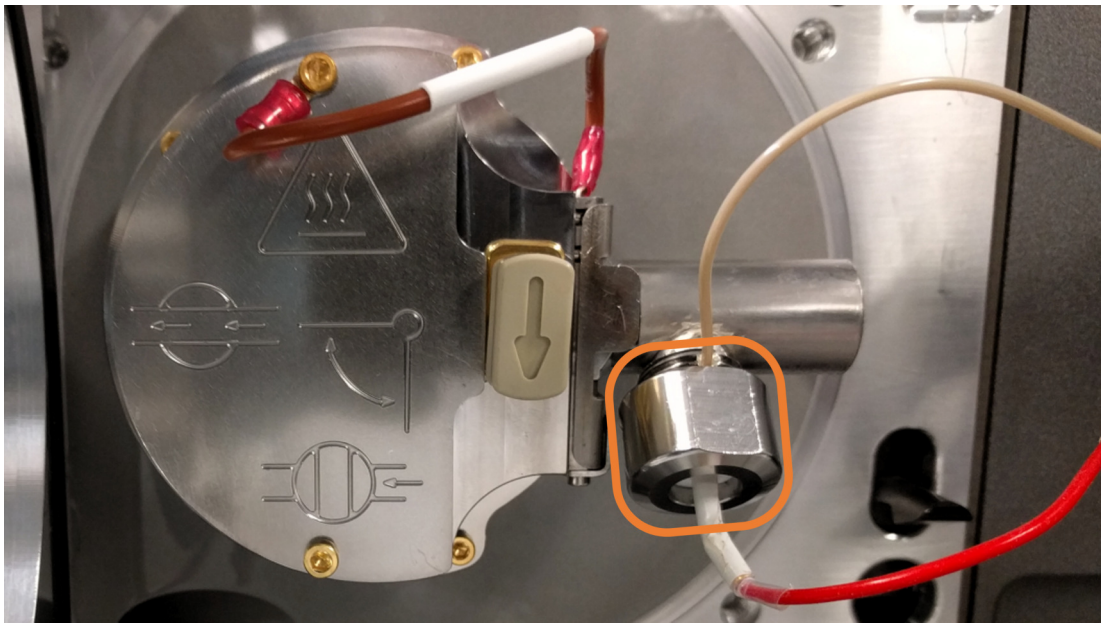

Figure 4.8: Photograph of prototype III FAPA ionization source installed on the Waters Xevo G2-S mass spectrometer. Shown in the centre is the ionization source block of the mass spectrometer with the chamber captive assembly connected on the right hand side. The discharge cell and electrodes are enclosed inside the chamber captive assembly, outlined in orange. The cathode is connected via the red cable (bottom right) to a high voltage power supply via a ballast resistor (4.7 Ω, 10 W) housed in a external diecast box (not shown). The helium gas used in the discharge cell is introduced via the beige PEEK tubing on the right.

4.3.1 Characterisation of prototype III

The FAPA prototype III discharge conditions was characterised on the bench by varying the discharge current (I_{GD}) and helium gas pressure (P_{He}) to determine the ionization source power. The source was placed inside the chamber captive assembly and mounted in on a laboratory bench clamp, while the anode was mechanically connected to ground and the voltage recorded from the power supply console.

Power output of prototype III at varying current

A study of the power output of the source was conducted by varying I_{GD} from 5 to 25 mA, this was repeated at two different P_{He} 34 kPa (5 psi) and 69 kPa (10 psi). The power output, as given by equation 4.1 where V_{GD} is the glow discharge voltage, increased linearly with increasing I_{GD}. This is characteristic of glow discharges operating in the abnormal glow region [88, 90], at a rate of change of 0.5 $V\ mA^{-1}$. Remarkably little deviation is seen in the power between the two P_{He}, varying by a maximum of 180 mW, at 25 mA.

$$Power = V_{GD}.I_{GD} \tag{4.1}$$

Power output of prototype III at varying pressure

A further study of the power output was conducted by varying the P_{He} from 14 to 55 kPa (2 to 8 psi) which was repeated at two different I_{GD} 10 and 20 mA. At both I_{GD} the power showed an increase between 14 and 55 kPa relative to STP, of 0.66 W at 10 mA and 1.1 W at 20 mA. It can also be seen that

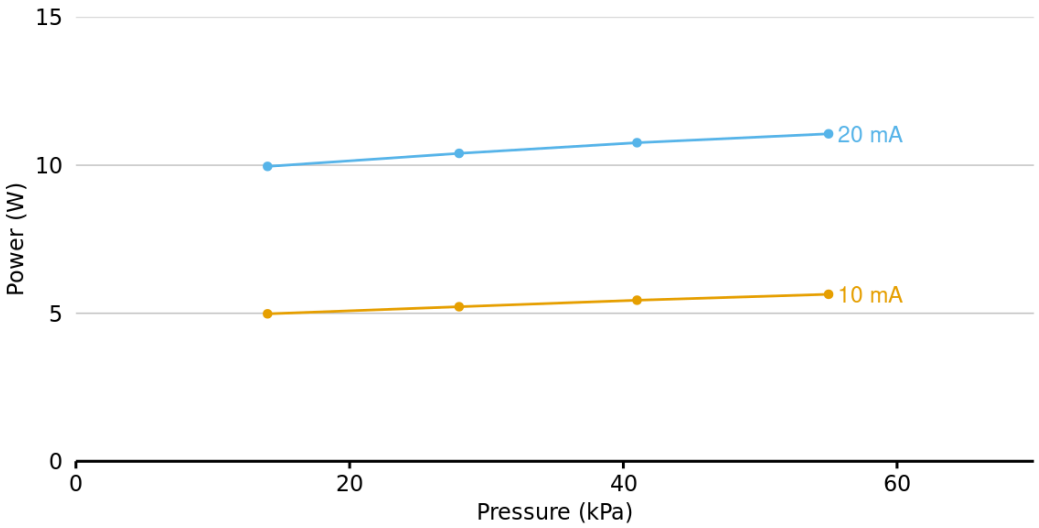

Figure 4.9: Plot of the power as at different I_{GD}. Measurements at two different P_{He} are shown 34 kPa (5 psi) and 69 kPa (10 psi). The power output increased linearly with increasing I_{GD}, this is typical of the abnormal glow discharge regime where the voltage increases with increasing current, at a rate of 0.5 $V\ mA^{-1}$.

prototype III is obeying Paschen's law [102], with increased voltage and power required with increasing pressure. The power regime of the FAPA prototype III is extremely stable across the measured discharge current (I_{GD}) and helium gas pressure (P_{He}).

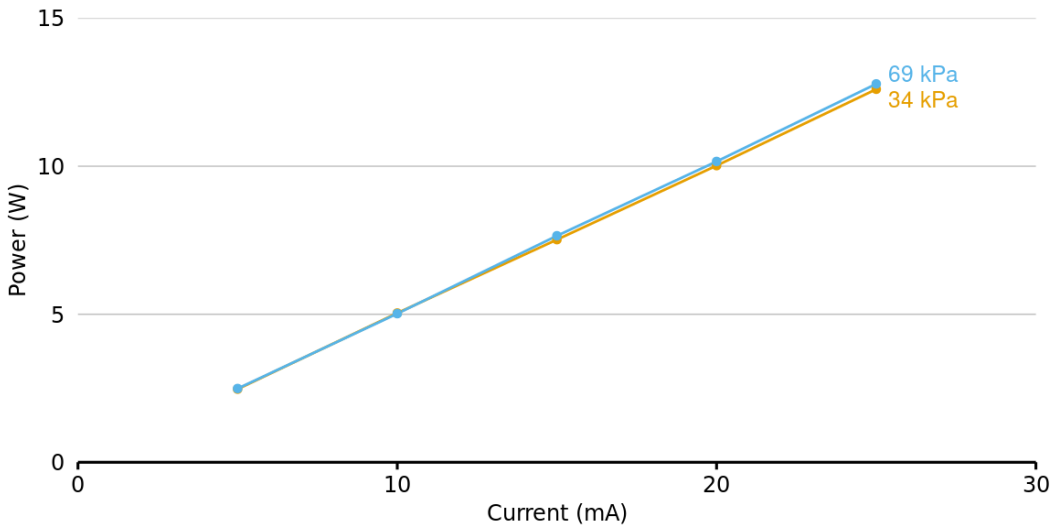

Figure 4.10: Plot of the power as at P_{He} between 14 and 55 kPa. Measurements at two different I_{GD} of 10 and 20 mA is shown. The power output increases with increased pressure, obeying Paschen's law where voltage increases with the increase in product of pressure and electrode distance.

4.3.2 Thermodynamic gas temperature of prototype III

The thermodynamic gas temperature of prototype III was measured using an infra-red thermal camera. The images in figure 4.11 show the ignited glow discharge of prototype III operating at 20 mA and -400 V with the overlaid infrared thermography showing the maximum induced thermodynamic gas temperature in the centre of the discharge being 96.3 $°C$ compared to the background laboratory temperature of 20.5 $°C$ after 20 minutes of operation, which is twice the temperature of prototype II (46.3 $°C$). Increasing the current to 50 mA and -525 V increased the maximum thermodynamic gas temperature in the centre of the discharge to 146.5 $°C$, equivalent to an increase of 1.67 $°C\ mA^{-1}$.

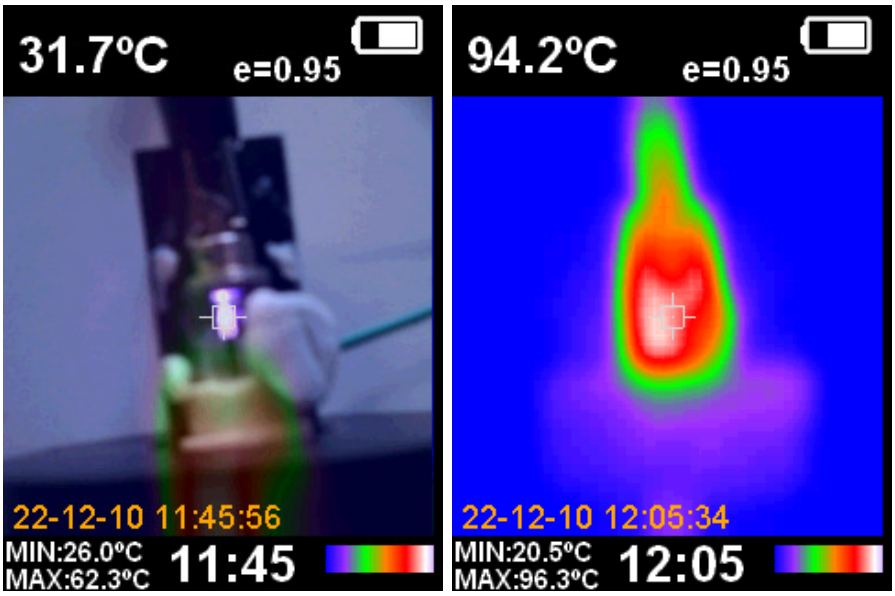

(a) (b)

Figure 4.11: Infrared thermography of prototype III. Image of the ignited glow discharge of prototype III can be seen between the pin-and-capillary (4.11a). Overlaid infrared thermography showing maximum thermodynamic gas temperature of 96.3 $°C$ at the centre of the discharge after 20 minutes operation at 20mA (4.11b).

4.3.3 Background mass spectrum of prototype III

A background mass spectrum was acquired in positive ion mode on the Waters Xevo G2-S mass spectrometer with the source positioned radially to the mass spectrometer inlet. The helium was started at 0 minutes and the glow discharge "ignited" after 0.5 minutes. After conditioning the source for 30 minutes there were several common background ion identified in the mass spectrum as shown in figure 4.12 with prototype III operating at 5 mA, including phthalic anhydride m/z 149, dibutylphthalate m/z 279, diisoctyl phthalate m/z 391, n-butyl benzenesulfonamide m/z 214, oleamide m/z 304, and polysiloxane m/z 335, 429, 445, and 462. At 30 mA a similar set of background ions was observed with diisoctyl phthalate m/z 391 seeming to increase in intensity relative to the polysiloxane ion at m/z 429. This was a much "cleaner" background in contrast with the background mass spectrum seen in figure 4.3 for prototype II where the m/z 214 ion of n-butyl benzenesulfonamide dominated the spectrum.

4.3.4 Compound analysis with prototype III

A study of low-molecular mass compounds was undertaken to asses FAPA prototype III ability analyse a range of chemistries, from polar such as caffeine (Log P = -0.1) to non-polar such as heptane (Log P = 4.4). A record of the ions observed for the compounds studied is shown in table 4.2. The predominant ions observed are the protonated molecule $[M + H]^+$ which is typical of API-*like* ionization observed with APGD ionization sources [71, 33]. For several compounds the base peak was the hydride abstracted ion $[M - H]^+$, which suggesting the presence of the NO^+ reagent ion in the source proceeding

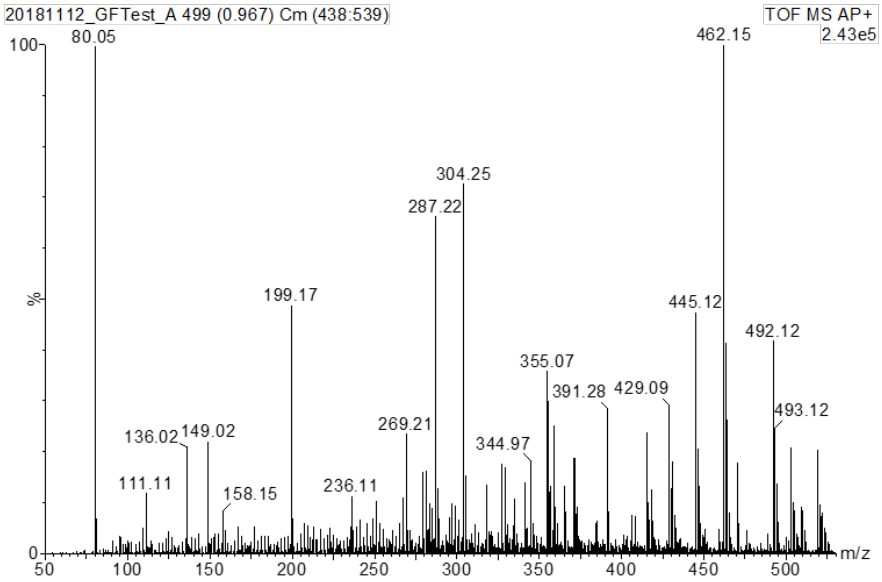

Figure 4.12: Mass spectrum showing background ions acquired in positive ion mode using the FAPA prototype III ionization source using the Waters Xevo G2-S mass spectrometer. Common background ions identified included phthalic anhydride *m/z* 149, dibutylphthalate *m/z* 279, diisoctyl phthalate *m/z* 391, n-butyl benzenesulfonamide *m/z* 214, oleamide *m/z* 304, and polysiloxane *m/z* 335, 429, 445, and 462.

via equation 4.2 or alternatively the $O^{-\bullet}$ ion via equation 4.3. The formation of the dehydrated protonated molecule $[M+H-H_2O]^+$ is also observed (figure 4.13) and is typical of alcohols where the hydroxyl group is protonated and fragments [21] and is also known for some carboxylic acids and aldehydes. For some of the aromatic hydrocarbons the molecular ion $[M]^{+\bullet}$ is also observed and is the base peak of anthracene (figure 4.14). For two of the ester containing compounds, hexadecyl hexadecanoate and tripalmitin, ammonium adduct ions were observed however no ammonium acetate was added so its presence is likely to have come from residue in the atmosphere or source surfaces.

$$NO^+ + MH \longrightarrow M^+ + HNO \tag{4.2}$$

$$O^{-\bullet} + MH \longrightarrow M^{\bullet} + OH^{-} \tag{4.3}$$

Table 4.2: List of compounds studied using the FAPA prototype III ionization source on the Waters Xevo G2-S mass spectrometer. Compounds analysed in positive ion mode. The base peak observed for each compound is recorded along with any other significant ions observed along with the relative intensity. The base peak is prominently the protonated molecule $[M+H]^+$, other ions commonly observed include the hydride abstracted molecular ion $[M-H]^+$ and also the dehydrated protonated molecule $[M+H-H_2O]^+$.

Compound	Base peak	Observed ions (%)
Methylimidizole	83 $[M+H]^+$	
Toluene	91 $[M-H]^+$	92 $[M]^{+\bullet}$ (30)
Heptane	113 $[M-3H+O]^+$	
Dimethyl-γ-pyrone	125 $[M+H]^+$	
D-Lucine	132 $[M+H]^+$	
Cinnamaldehyde	133 $[M+H]^+$	131 $[M-H]^+$ (10)
Acetaminophen	152 $[M+H]^+$	
2-Amino-4-Methyl-5 -Nitropyridine	154 $[M+H]^+$	
Nicotine	163 $[M+H]^+$	161 $[M-H]^+$ (<5)
Anthracene	178 $[M]^{+\bullet}$	179 $[M+H]^+$ (50)
Caffeine	195 $[M+H]^+$	194 $[M]^{+\bullet}$ (15)
Hexadecylamine	242 $[M-H]^+$	
Methyl stearate	299 $[M+H]^+$	
Sulfadimethoxine	311 $[M+H]^+$	
Cholesterol	369 $[M+H-H_2O]^+$	385 $[M-H]^+$ (6)
Terfenadine	470 $[M-H]^+$	472 $[M+H]^+$ (80)
Hexadecyl hexadecanoate	481 $[M+H]^+$	498 $[M+NH4]^+$ (40)
Tripalmitin	551 $[fragment]^+$	824 $[M+NH4]^+$ (30)
Estradiol	255 $[M+H-H_2O]^+$	271 $[M+H]^+$ (80), 269 $[M-H]^+$ (40)
Estriol	287 $[M-H]^+$	

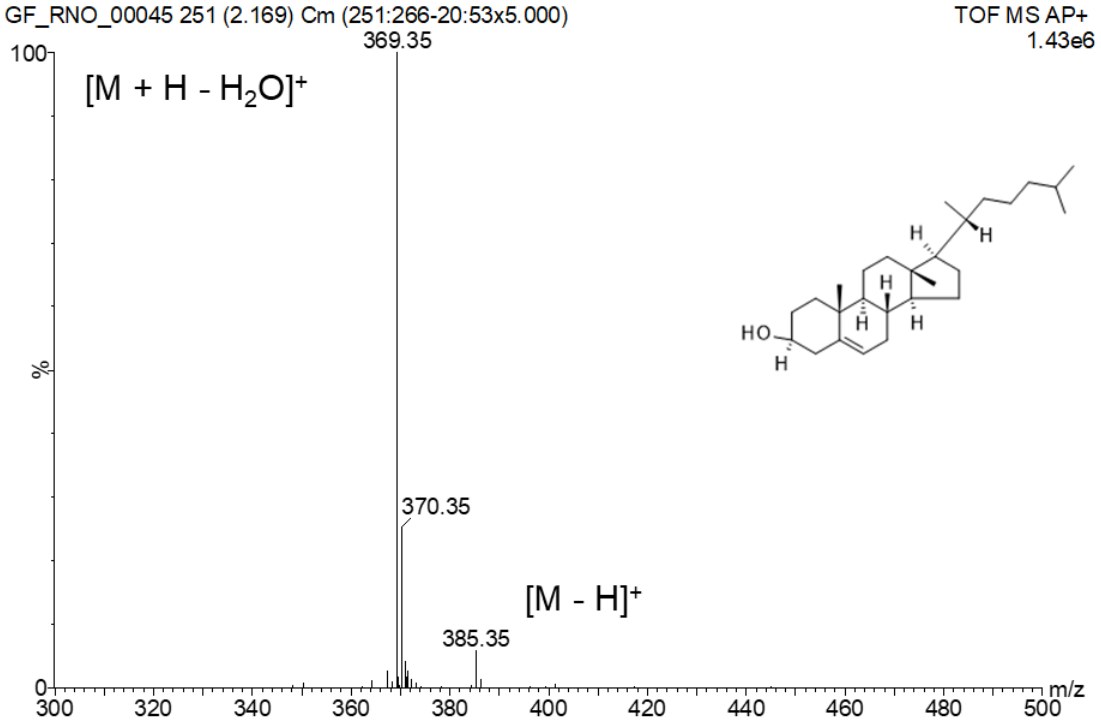

Figure 4.13: Mass spectra of cholesterol acquired in positive ion mode using the FAPA prototype III ionization source on the Waters Xevo G2-S mass spectrometer. Base peak observed was the dehydrated protonated molecule ($[M + H - H_2O]^+$) at *m/z* 369, also observed was the deprotonated molecule ($[M - H]^+$) at *m/z* 385 at ∼6 % relative intensity of the base peak.

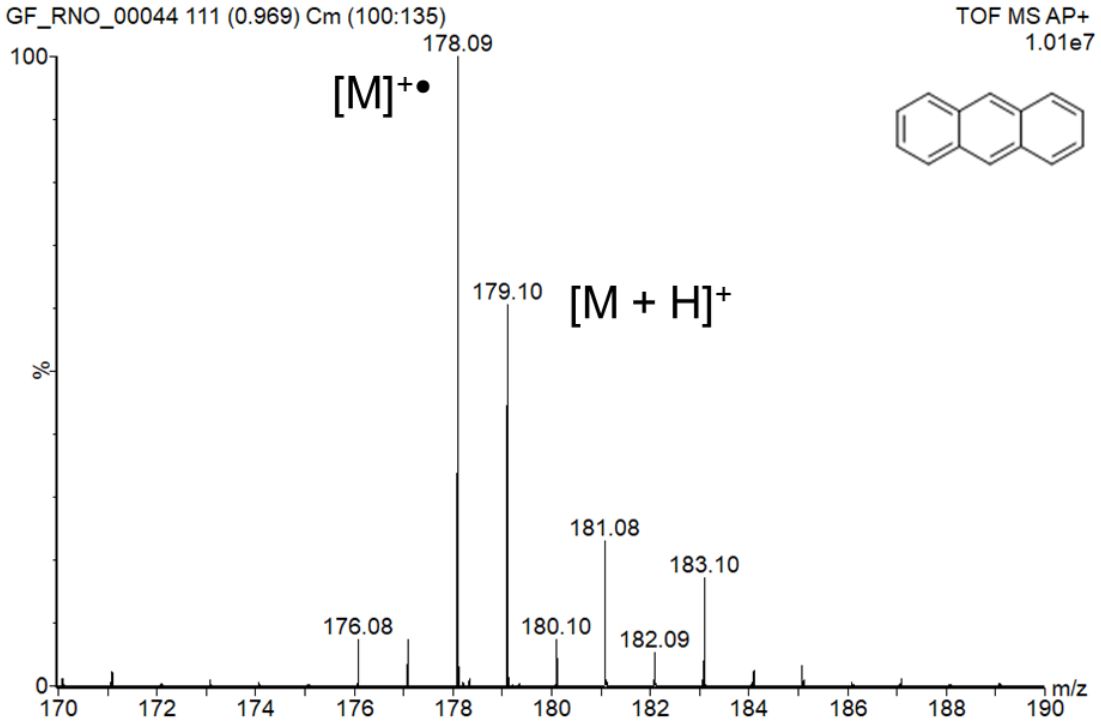

Figure 4.14: Mass spectra of anthracene acquired in positive ion mode using the FAPA prototype III ionization source on the Waters Xevo G2-S mass spectrometer. Base peak observed was the molecular ion ($[M]^{+\bullet}$) at *m/z* 178, also observed was the protonated molecule ($[M+H]^{+}$) at *m/z* 179 at ∼50 % relative intensity of the molecular ion.

Fatty acid methyl esters

The FAPA prototype III ionization source has shown the ability to ionise a range of individual compounds. For real world applications compounds tend to exist in mixtures which can be chromatographically separated or alternatively a shotgun mass spectrometry approach, where all ions are measured simultaneously, can be applied. A solution containing even-numbered saturated fatty acid methyl esters (FAMEs) from C4:0 to C24:0 with equal concentration by mass was studied to determine the ability of the ionization source to analyse mixtures. A mass spectrum of the FAMEs solution was recorded as shown in figure 4.15, the protonated molecules ($[M+H]^+$) are seen for the compounds from C6:0 to C24:0.

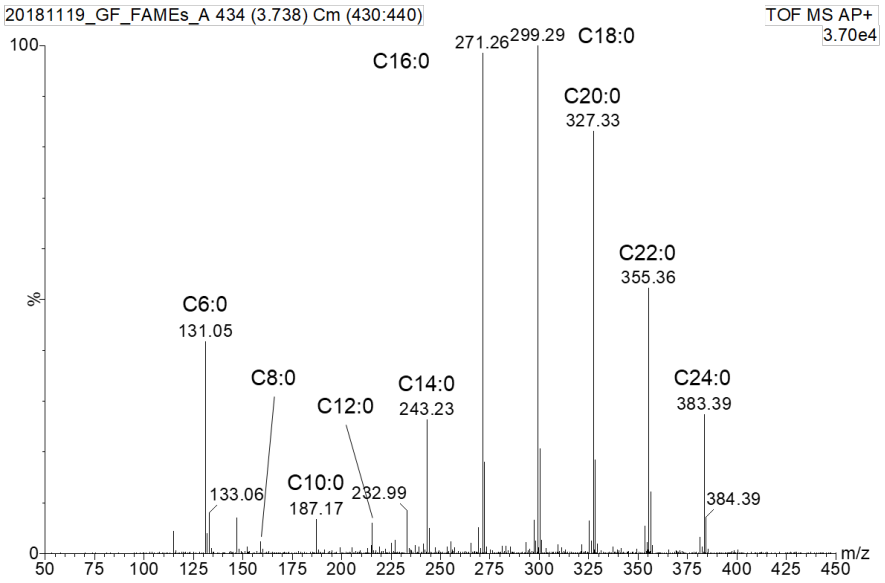

Figure 4.15: Mass spectra of C4:0 to C24:0 even-numbered saturated FAMEs standard using the FAPA prototype III ionization source. Base peak *m/z* 299 for protonated molecule ($[M+H]^+$) of methyl stearate. The lowest mass component methyl butyrate (C4:0) is not observed, as the standard was old it is suspected that with its high vapour pressure the compound had evaporated either in storage or during the transfer process to the ionization source.

4.4 A capillary-to-capillary geometry (Prototype IV)

The prototypes (II and III) described so far have used a pin-to-plate geometry. Difficulties arose with the prototype II design from interchanging the source on the mass spectrometer with the power wiring and gas line weakening and getting damaged with repeated use. An alternative design was needed and hollow cathodes offered a potential solution. Hollow cathodes are common ionization sources in vacuum glow discharge in inorganic mass spectrometry [27, 89], and also as line sources in atomic absorption spectroscopy [103]. The halo-FAPA design uses an annular geometry with the anode and cathode tubes inside one-another but the discharge is maintained between the tubes and not within a hollow-cathode [104]. Hollow-cathode offered the possibility of combining the gas and power into a single part which would reduce the number of components and therefore points of failure as well as possibly higher charge densities which could improve analytical sensitivity.

A photograph and schematic of the FAPA prototype IV is shown in figure 4.16. The discharge cell is made of quartz tube of the same dimensions used in prototype III and contains the electrodes. A stainless steel tube (o.d. 3.18 mm, id. 1.35 mm, length 8.5 mm) acts as the anode and another stainless steel tube (o.d. 1/16") acts as a cathode replacing the sharpened tungsten pin. Helium gas is delivered via a polytetrafluoroethylene (PTFE) tube (o.d. 1/8") and fits over the end of the cathode tube and was operated using a variable flow meter. The high voltage cable was connected using a wire tap connector to the bare cathode tube via a ballast resistor (4.7 Ω, 10 W) housed in an external diecast box. As

with the prototype III the discharge cell was housed inside a chamber captive assembly (figure 4.8) that was mounted directly on the Waters Xevo G2-S mass spectrometer ion block, orientated radially to the inlet.

(a) (b)

Figure 4.16: Schematic (a) of the FAPA prototype IV showing the stainless steel tube (o.d. 1/16") acts as a cathode, and stainless steel tube (o.d. 3.18 mm, id. 1.35 mm, length 8.5 mm) acts as the anode sitting within a discharge cell made of quartz tube. Hatched areas inert quarts and machined ceramic. Photograph (b) of the assembled ionization source in the chamber captive assembly, the PTFE tube (o.d. 1/8") for the delivery of the helium discharge gas and the yellow wire tap connector for connecting to the high voltage power supply is shown.

Changing the shape of the cathode from a sharp pin to a hollow tube there is a consequential change in the surface area of the electrode. An estimate of the volume of the cathode glow was made to compare prototype III and IV, using equation 4.4.

$$V = \pi a^2 . \pi d \tag{4.4}$$

Where V is the cathode glow volume, d is the diameter of the electrode, a is the estimated length of the cathode covered by the cathode glow. The volume of the cathode glow for prototype III was 5.8 mm^3 and for prototype IV was 14.1 mm^3, a 242 % increase in the volume of the cathode glow.

4.4.1 Characterisation of prototype IV

The FAPA prototype IV ionization source discharge conditions were characterised on the bench by varying the helium gas flow rate (Q_{He}), the inter-electrode distance (d_e), and the discharge current (I_{GD}) to determine its power output. As with prototype III the ionization source was placed in the chamber captive assembly and mounted on a laboratory bench clamp.

A study of the power output of the source was conducted by varying I_{GD} from 10 to 40 mA, this was repeated at four different Q_{He} from 0.2 to 1.0 $L\ min^{-1}$. The power increased in general linearly with increasing current at a rate of 0.62 $W\ mA^{-1}$, with a slight up-tick at higher currents, as shown in figure 4.17. Prototype IV is operating in the abnormal glow discharge regime (figure 1.3) [88], as suggested by the linear increase in voltage with increasing current. Little deviation is seen at different flow rates particularly at 10 mA where the standard deviation is only 0.21 but increasing at the higher currents of 40 mA to a standard deviation of 1.03 which suggest that the source is stable in its operation.

A further study of the power output at different inter-electrode distances from 1 to 5 mm was conducted, this was repeated at four different I_{GD} from 10 to 40 mA. At each I_{GD} the power increased linearly as the inter-electrode distance increased as shown in figure 4.18. At 10 mA the power output increases at a rate of 0.62 $W\ mm^{-1}$, while at 40 mA the power output increases at a greater rate of 1.69 $W\ mm^{-1}$.

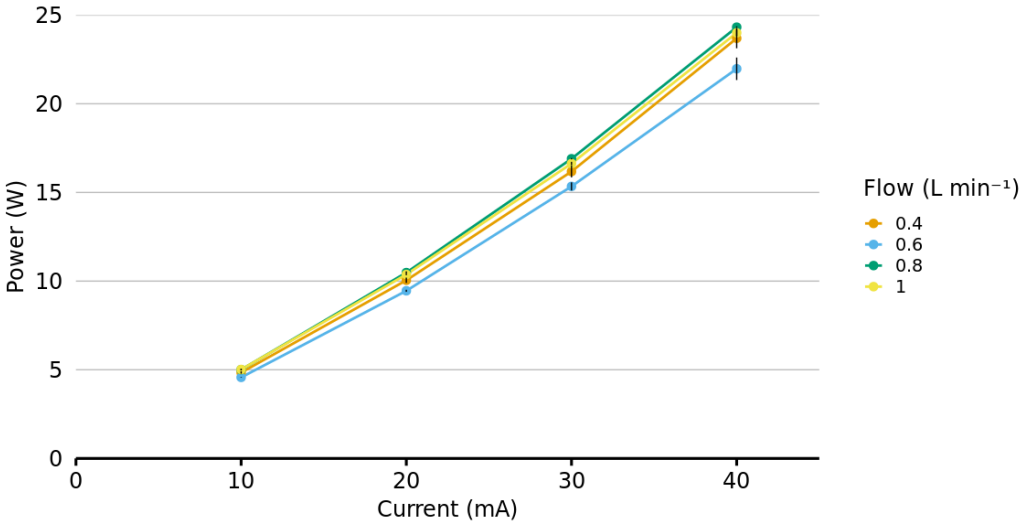

Figure 4.17: Plot of the power output of the prototype IV ionization source at different discharge currents (I_{GD}) from 10 to 40 mA. Four different gas flow rates (Q_{He}) from 0.2 to 1.0 $L\ min^{-1}$ are shown for comparison. The power increased in general linearly with increasing I_{GD}, at a rate of 0.62 $W\ mA^{-1}$. This suggests that the prototype IV is operating in the abnormal glow discharge regime [88].

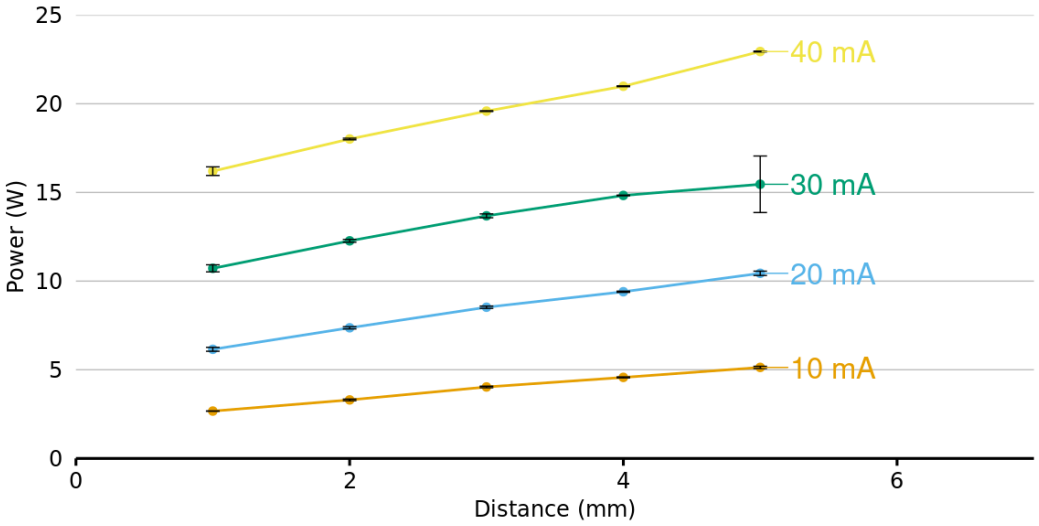

Figure 4.18: Plot of the power output of the prototype IV ionization source at different inter-electrode distances from 1 to 5 mm. Repeated at four different I_{GD} from 10 to 40 mA. The increasing power with inter-electrode distances indicates that prototype IV is obeying Paschen's law with the voltage being a function of the product of pressure and electrode distance.

4.4.2 Thermodynamic gas temperature of prototype IV

The thermodynamic gas temperature of prototype IV was measured using an infra-red thermal camera. The images in figure 4.19 show the ignited glow discharge of prototype III operating at 20 mA and -349 V with the overlaid infrared thermography showing the maximum thermodynamic gas temperature in the centre of the discharge being 78.3 $°C$ compared to the background laboratory temperature of 23.3 $°C$ after 20 minutes of operation.

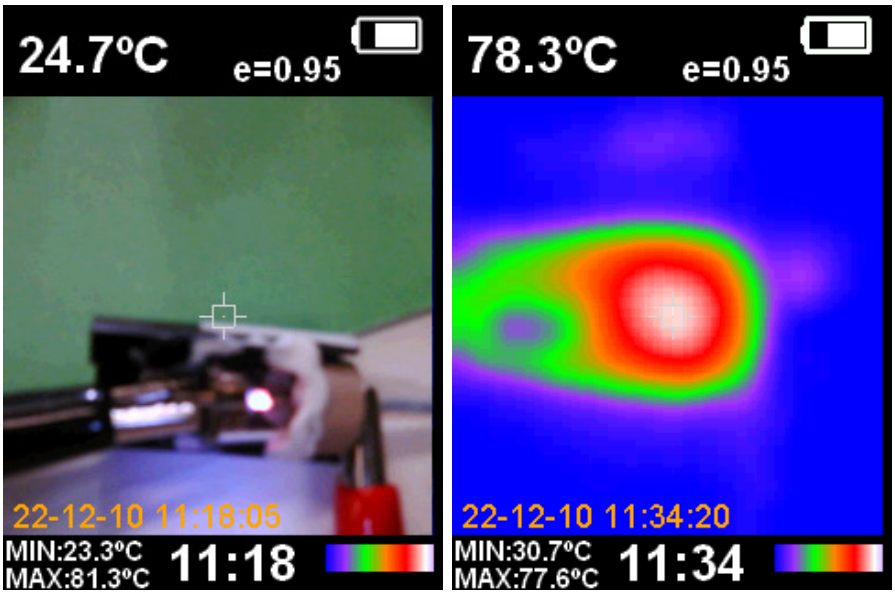

(a) (b)

Figure 4.19: Infrared thermography of prototype IV. Image of the ignited glow discharge of prototype IV can be seen between the pin-and-capillary (4.19a). Overlaid infrared thermography showing maximum thermodynamic gas temperature of 78.3 $°C$ at the centre of the discharge after 20 minutes operation at 20 mA (4.19b).

4.4.3 Background mass spectrum of prototype IV

A mass spectrum of background ions for the FAPA prototype IV ionization source in positive ion mode on the Waters Xevo G2-S mass spectrometer with the source positioned radially to the inlet was acquired, shown in figure 4.20. Several common ions can be readily identified in the mass spectrum, including phthalic anhydride m/z 149 as the base peak and diisooctyl phthalate m/z 391. High levels of plasticiser are seen after 30 minutes of conditioning in the background spectra compared to the previously investigated prototypes (II and III) which could be as a result of outgassing from the use of PTFE tubing or the plastic wire tap connector supplying the gas and power respectively. The use of plastics allowed much greater flexibility in terms of positioning of components however it is evident that the inert quartz and stainless-steel produces less interference in the high temperature environment of the source in the background spectrum.

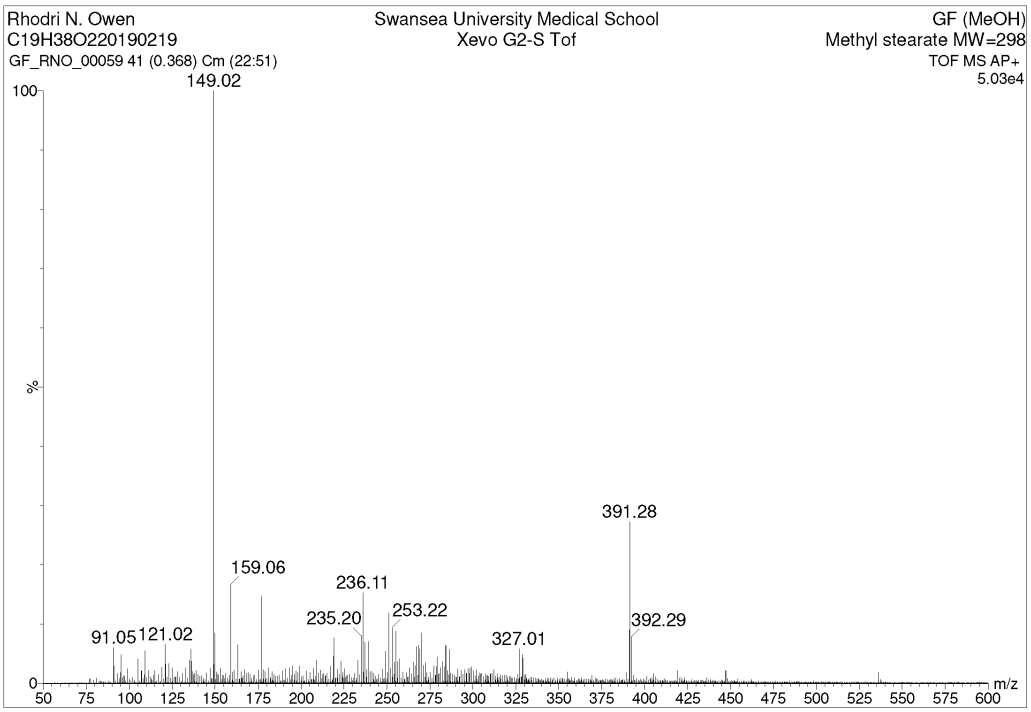

Figure 4.20: Mass spectra showing background ions using the FAPA prototype IV ionization source in positive ion mode on the Waters Xevo G2-S mass spectrometer. Several common ions can be readily identified in the mass spectrum, including phthalic anhydride *m/z* 149 as the base peak and diisooctyl phthalate *m/z* 391. High levels of plasticiser are seen in the background spectra compared to the previously investigated prototypes (II and III) which could be as a result of the use of PTFE tubing or plastic wire tap connector supplying the gas and power respectively.

4.4.4 Analysis of small molecules using prototype IV

A study of low molecular mass compounds was undertaken to assess prototype IV capabilities against a range of chemistries. In positive ion mass spectrometry the protonated molecule ($[M + H]^+$) is the predominant species, with also some dehydrated protonated molecule ($[M + H - H_2O]^+$) and hydride abstracted molecule ($[M - H]^+$) observed as was previously seen for prototype III. In a study of 2-Amino-4-methyl-5-nitropyridine ($C_6H_7N_3O_2$, M_r 153.05 $g\ mol^{-1}$) the protonated molecule ($[M+H]^+$) at m/z 154 can be readily identified in figure 4.21, along with a possible fragment ion at m/z 108 from the loss of the nitro functional group, the accurate mass measurement for the ion was 108.0666 (theoretical m/z 108.0687 δ -2.1 mDa, -19.44 ppm) which is outside the normal tolerance for the instrument (± 3 ppm) and so can not be confirmed. The compound sodium lauryl sulfate ($C_{12}H_{25}SO_4Na$, M_r 288.37 $g.mol^{-1}$) was selected for study using prototype IV by negative ion mass spectrometry. The resulting mass spectrum is shown in figure 4.22. Intense ions for the anion ($[M]^-$) at m/z 265 can be readily identified.

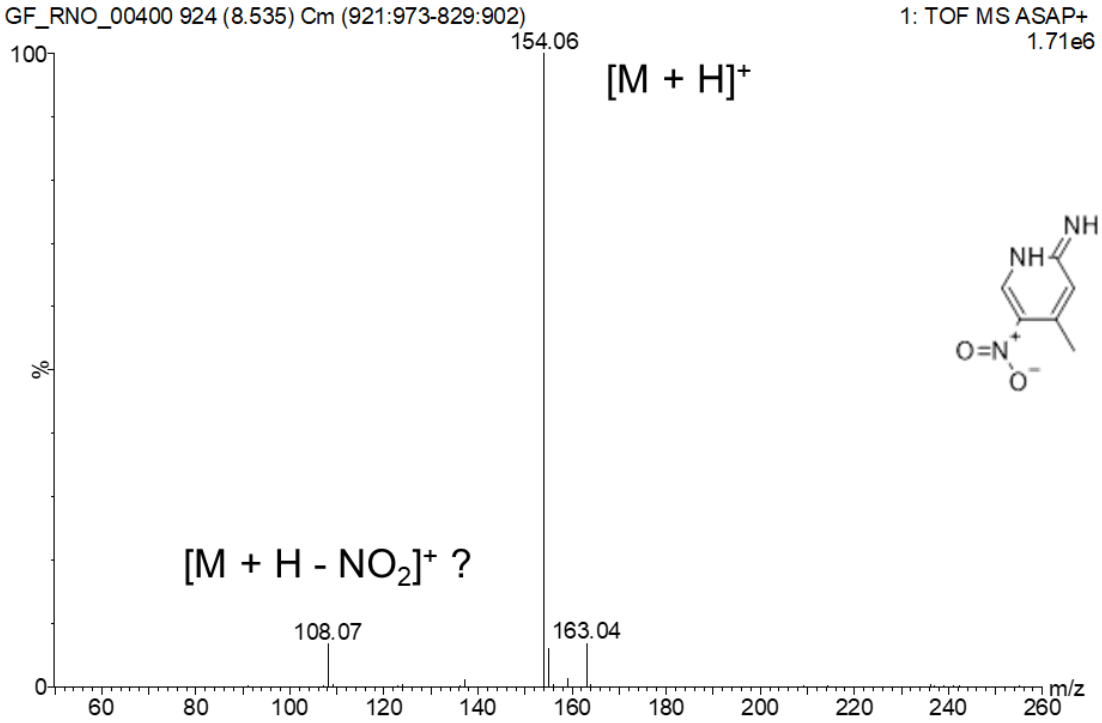

Figure 4.21: Mass spectrum of 2-amino-4-methyl-5-nitropyridine acquired using the FAPA prototype IV ionization source. An intense protonated molecule ($[M+H]^+$) at *m/z* 154 can be readily identified, along with a possible fragment ion at *m/z* 108 from the loss of the nitro functional group , the accurate mass measurement for the ion was 108.0666 (theoretical *m/z* 108.0687 δ -2.1 mDa).

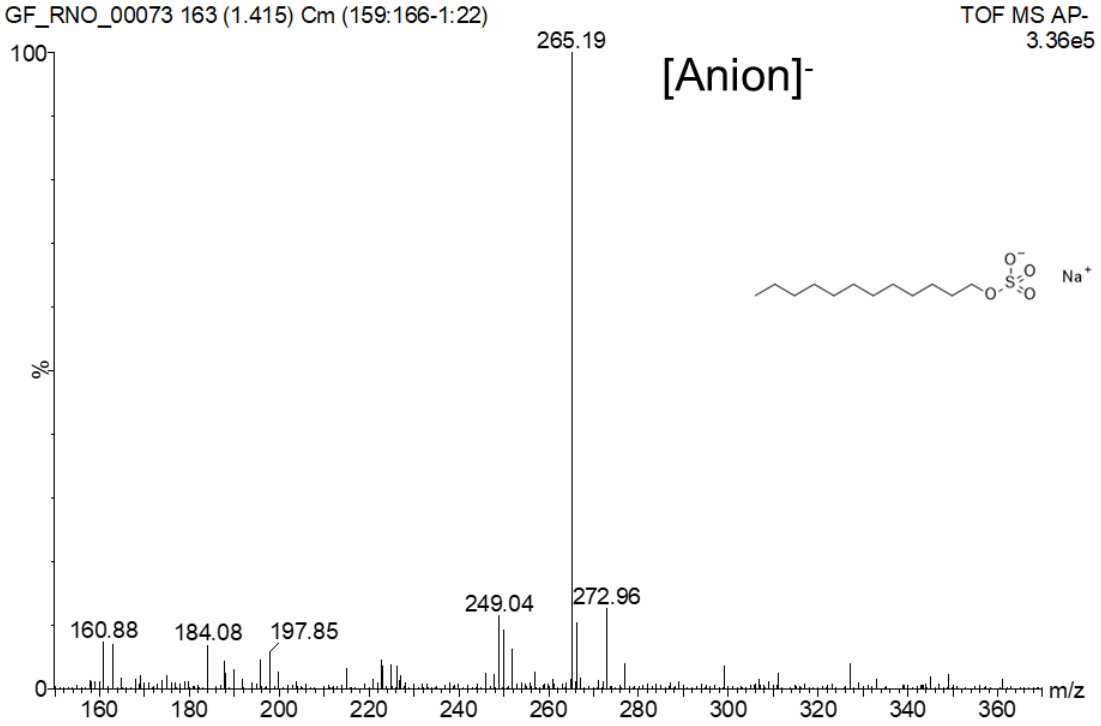

Figure 4.22: Negative mass spectrum of sodium lauryl sulfate acquired using the FAPA prototype IV ionization source. Intense ions for the anion ($[M]^-$) at *m/z* 265 can be readily identified.

4.4.5 Analytical figures of merit for prototype IV

A study to determine the analytical figures of merit for prototype IV was undertaken, three fatty acid derivative compounds were selected, namely hexadecylamine ($C_{16}H_{35}N$, M_r 241), methyl stearate ($C_{19}H_{38}O_2$, M_r 298),and phytosphingosine ($C_{18}H_{39}NO_3$, M_r 317). As outlined in chapter 2 the figures of merit are range of reliable response, limit of detection, and coefficient of variability. The compounds were prepared at seven concentrations of 1, 5, 10, 50, 100, 500, and 1000 $\mu mol\ L^{-1}$ by serial dilution. Samples were syringed onto the end of a glass capillary and introduced into the source using a atmospheric-pressure solids analysis probe with three replicates at each concentration. Calibration curves have been prepared for each of the compounds under study in figure 4.23. Table 4.3 was prepared showing the DL, SEM, and R^2 for each of the compounds. The DL were consistently in the low $pmol\ \mu L^{-1}$ with linearity over three orders of magnitude ($R^2 > 0.97$). The errors in the replicates are however large which is in part down to the use of the solids analysis probe which is generally only used for qualitative analysis. Improvement in sample introduction methods is clearly needed to increase reproducibility such as using chromatography. However there are tentative signs that the source may prove to be analytically sensitive for non-polar biomolecules studied with further refinement.

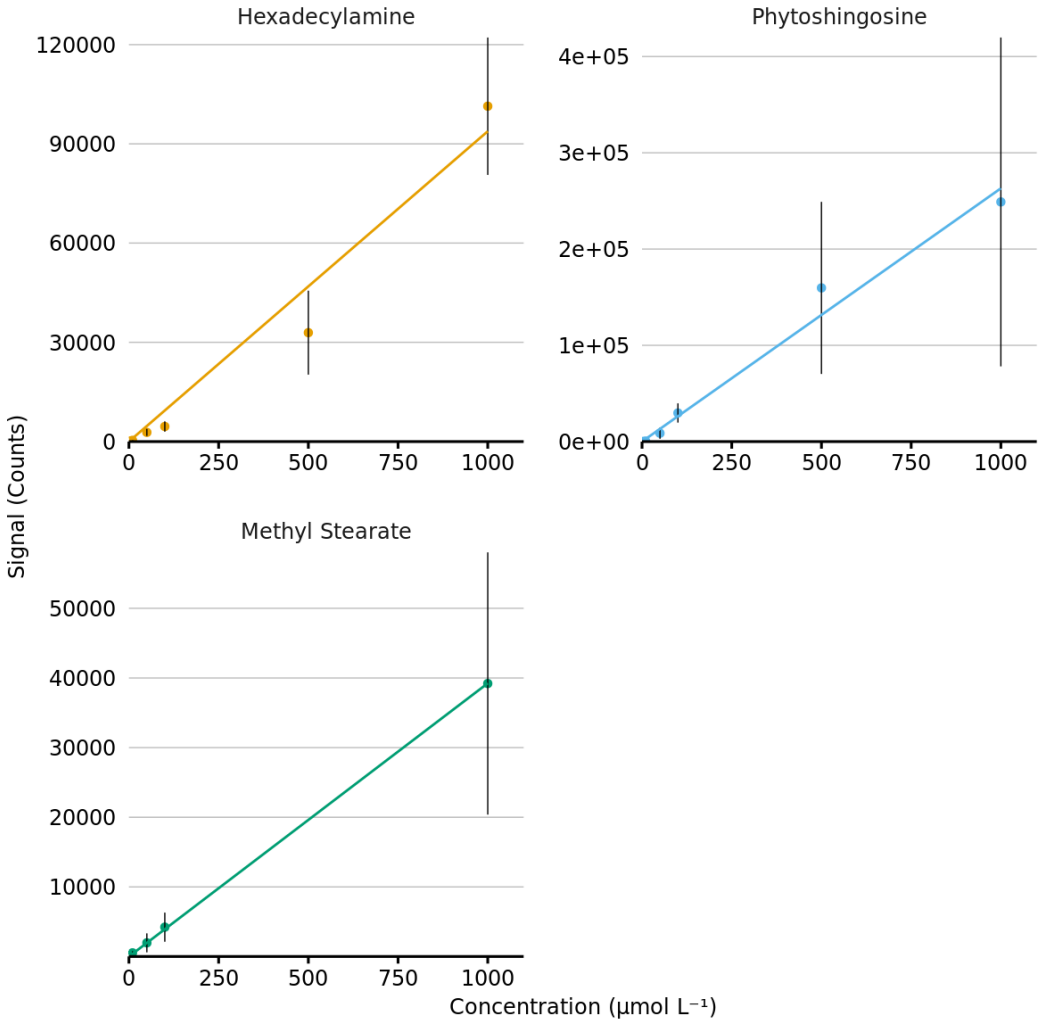

Figure 4.23: Calibration curves acquired using the FAPA prototype IV ionization source ($N = 7, n = 3$), for hexadecylamine ($C_{16}H_{35}N$, M_r 241), phytosphingosine ($C_{18}H_{39}NO_3$, M_r 317), and methyl stearate ($C_{19}H_{38}O_2$, M_r 298).

Table 4.3: Summary of the figures of merit for selected analytes acquired using the FAPA prototype IV ionization source. Listed is the observed ion, DL, standard error of the mean, and coefficient of determination for each compound.

Compound	Observed m/z	DL ($pmol\ \mu L^{-1}$)	SEM	R^2
Hexadecylamine	242	3.08	11	0.9965
Methyl stearate	299	1.95	4	0.9999
Phytosphingosine	318	1.47	9	0.9796

4.5 Discussion and Summary

Three prototype FAPA ionization sources (II, III, and IV) are described in this chapter. The discharge conditions of each prototype source were characterised on the bench and all three operated in the abnormal glow region, that is the region where the voltage increases proportionally with increasing current (figure 1.3), which is characteristic of FAPA sources. Prototype II demonstrated the proof of concept that FAPA sources could be successfully interfaced with the Waters Xevo G2-S mass spectrometer, however, its size and positioning made it unsuitable for routine analysis especially where high reproducibility would be required. More compact prototypes (III and IV) were developed which provided a robust mounting point directly onto the ion block using the capacitive chamber assembly. This had three outcomes; firstly the prototype was positioned optimally, taking the place of the APCI corona needle, with respects to the sample probe and inlet. Secondly the consistent position improved reproducibility between measurements, and finally the afterglow was orientated radially to the inlet to provide greater stability and precision. Analysis using prototype II also highlighted the need for external heating. The measured thermodynamic gas temperature was 46.3 $°C$, which is similar to what had previously been reported for the prototype [71] but contrasts with that reported in the literature of 125 $°C$ for other FAPA sources [105]. This means that compounds with low vapour pressures would not normally be amiable to ionization using this prototype without external volatilisation such as heating or ablation.

The predominant ions observed with all three prototypes in positive mass spectrometry are protonated molecules ($[M + H]^+$), other common ions were

hydride abstracted ions ($[M-H]^+$), molecular ions ($[M]^{+\bullet}$), and dehydrated ions ($[M+H-H_2O]^+$). Less commonly observed were oxygen substituted ions ($[M+O-nH]^+$) with hydrocarbons and ammonium adduct ions ($[M+NH_4]^+$) for some esters. In negative ion mass spectrometry de-protonated molecules ($[M-H]^-$) and anions were observed. Prototype IV exhibited DL in the low $pmol\ \mu L^{-1}$ with good linearity, $R^2 > 0.91$, over three orders of magnitude. This compares favourably with previously reported values for prototype II of 7 $pmol\ \mu L^{-1}$ [71] but these sources have yet to reached DLs as low as 4 *amol* reported for the herbicide ametryn [33].

In summary, FAPA mass spectrometry has demonstrated an ability to ionise a range of sample chemistries using a simple capillary. Use of an ASAP probe, with heated gas nebulizer, extended the range of compounds capable of analysis particularly those with low vapour pressures. It can be easily retrofitted to existing instrumentation with only limited modifications. In the next chapter a more compact design is described and characterised which will address limitations with the existing designs (prototype III and IV) in terms of ease of retrofitting, use with existing sample introduction methods, and transfer and interoperability between different instruments.

Chapter 5

Characterisation and optimisation of a micro-glow discharge ionization source

5.1 Introduction

In this chapter the development of a much more compact micro-glow discharge ionization source, referred to as "prototype V", which was designed and fabricated in-house is investigated, as the development of the helium plasma ionization source [106, 36, 37, 107] and the μFAPA ionization source [34] has shown the possibility of $sub-mm$ plasma ionization sources for use in mass spectrometry. However, the μFAPA appeared to report a loss of sensitivity with respect to larger ionization source designs [34]. The aim of this study is to investigate the optimal operating conditions of prototype V, primarily the discharge current, voltage, the helium discharge gas flow, the desolvation gas flow and temperature, the sample

phase ("dry" verses "wet"), and volume. Due to the change in physical scale and operating conditions it is not known whether the prototype V source will have similar characteristics to FAPA. Optimization of the operating conditions of both the micro-discharge and the mass spectrometer source settings was undertaken to ensure reproducible and analytically useful sample data could be generated.

Multiple methods for introducing samples in all phases of matter (solid, liquid and gas) into the ionization source would be advantageous for semi-volatile and non-volatile compounds. The current range of ADI sources rely on surface desorption of the analytes which means samples must be volatile at room temperature such as with the LTP. Other ionization sources employed techniques to volatilise the analytes most commonly (i) heating by an external source such as with DART and ASAP, or (ii) ablation such as with desorption electrospray ionization (DESI) and laser ablation electrospray ionization (LAESI). A study of the prototype V source used in combination with two direct sample introduction methods namely a solids analysis probe and a flow infusion system using the APCI IonSABRE probe at 50 $\mu L\ min^{-1}$ in combination with a loop-injector (loop volume = 1 μL). Further results of the micro-glow discharge ionization source used in combination with LC extending the capabilities of the prototype V source for the analysis of more complex mixtures are presented.

For all experiments the Xevo G2-S time-of-flight mass spectrometer (Waters, Wilmslow, UK) was used, operating conditions were as specified in chapter 2, if not noted. The prototype V ionization source is fitted to the Universal Source Housing axially, or on-axis, to the mass spectrometer entrance with the sample introduction probe positioned perpendicularly.

5.2 Design of prototype V

A schematic of prototype V is shown in figure 5.1. The body of the ionization source consists of a PEEK union. The anode, a stainless-steel probe tip assembly (o.d. 640 μm) is attached to one end of the union and a PEEK thumb nut was used to connect a helium gas line (PEEK tubing) to the other side of the union. A crimp ring terminal was used to make an electrical connection from the anode electrode to the mass spectrometer internal power supply and was operated in constant current mode (1-35 μA) and the source housing of the instrument acts as the counter electrode, nominally at 0 V. The gas flow rate (0.05-0.5 $L\ min^{-1}$) was regulated by a variable area flow meter. An image of the prototype V source is shown in figure 5.2. The characteristic purple glow from the positive column of the helium discharge can be seen at the tip of the ionization source extending towards the mass spectrometer orifice. Seen above the discharge is the tip of a soda glass capillary which is used in some of the experiments to introduce samples perpendicular to the glow discharge.

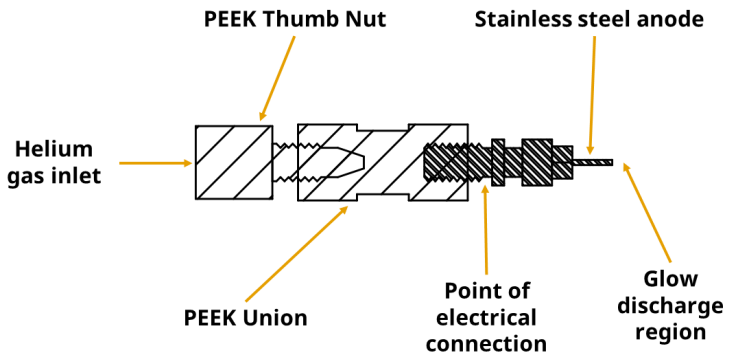

Figure 5.1: Schematic of the prototype V source. Consisting of a PEEK union body. A stainless-steel probe tip assembly (o.d. 640 μm) is attached to one end, which acts as the anode, it is connected by a crimp ring terminal to the internal power supply of the instrument (not shown) operating in a constant current mode. A PEEK thumb nut is used to connect a helium gas line to the other end of the body, the gas flow rate (0.05-0.5 $L\ min^{-1}$) is regulated by a variable area flow meter (not shown).

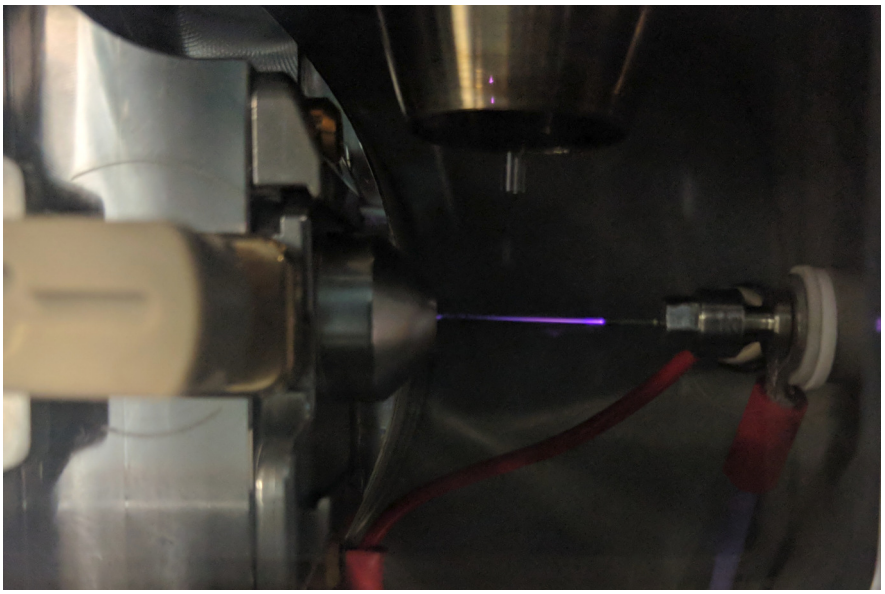

Figure 5.2: An image of the prototype V source positioned (right) *in situ* axially to mass spectrometer inlet (left). The characteristic purple glow of the helium glow discharge is visible. Orthogonal to the glow discharge is the tip of the soda glass capillary tube used to present the sample.

5.3 Characterisation of the micro-glow discharge

Initial characterisation of prototype V micro-glow discharge was conducted on the bench with the source mounted in a laboratory bench clamp. A flat steel plate was used as a counter electrode mechanically fixed to earth as shown in figure 5.3. To determine the power output of prototype V the inter-electrode gap (d_e), discharge current (I_{GD}), and helium gas flow (Q_{He}) were varied and the voltmeter response recorded.

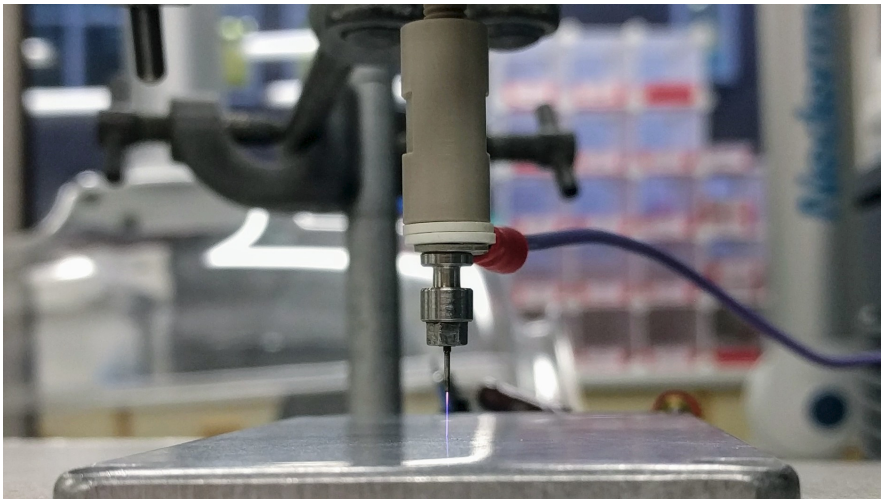

Figure 5.3: Prototype V set up on laboratory bench clamp. The ionization source (top) is positioned opposite a flat steel plate that was used as a counter electrode, and mechanically fixed to earth.

5.3.1 Effect of altering the current I_{GD} on the micro-glow discharge power

A study of the power was conducted by increasing the current from 5 to 35 μA in increments of 5 μA and was repeated at three d_e. To calculate the power output the voltage was measured across a resistor R_2 (200 $k\Omega$) attached to the grounded counter electrode as shown in figure 5.4, the use of resistors as a voltage divider was necessary as the maximum output voltage was in excess of the voltmeter capacity. If the two resistors R_1 and R_2 are equal the voltage is halved. Alternatively if the resistors are of non-equal values then the voltage is proportional to $\frac{R_2}{R_1+R_2}$. The power P can be calculated by combining equations 5.1 and 5.2 and then substituting into equation 5.4 to give equation 5.5.

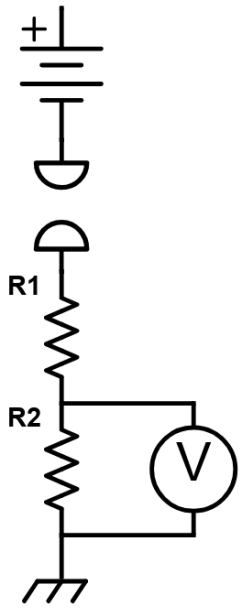

Figure 5.4: Electrical schematic showing voltmeter. Two resistors (R_1 (2 $k\Omega$), R_2 (200 $k\Omega$)) are placed in series on the ground counter-electrode and the voltage V_m is measured across the R_2.

$$V_{in} = I.(R_1 + R_2) \tag{5.1}$$

$$V_m = I.R_2 \tag{5.2}$$

$$V_{in} = \frac{V_m}{R_2}.(R_1 + R_2) \tag{5.3}$$

$$P = I_{GD}.V_{in} \tag{5.4}$$

$$P = I_{GD}.\frac{V_m.(R_1 + R_2)}{R_2} \tag{5.5}$$

Where P is the power, I_{GD} is the discharge current, V_{in} is the input voltage, V_m is the measured voltage, and R_1 (2 $k\Omega$) and R_2 (200 $k\Omega$) are resistors. The calculated power of the ionization source is shown in figure 5.5 at I_{GD} of 5 to 35 μA. At short d_e of 5 and 10 mm the power output increases exponentially with increased I_{GD} from 1.4 mW to 66.6 mW. At larger d_e of 20 mm the relationship is linear increasing from 1.4 mW to 13.5 mW at a rate of 0.4 $mW\ \mu A^{-1}$. Larger d_e for micro-glow discharges have reported to increase discharge temperatures resulting in growth in conductivity [89], which could explain the change in behaviour observed when compared to smaller d_e values.

5.3.2 Effect of altering the helium flow rate Q_{He} on the the micro-glow discharge power

The current and voltage required to start and sustain a glow discharge is governed by the pressure and inter-electrode distance as defined in Paschen's law [102]. A study of the power output was conducted by varying the Q_{He} from 0.1 to 0.5 $L\ min^{-1}$ in 0.1 $L\ min^{-1}$ increments at an I_{GD} of 15 μA. The power output

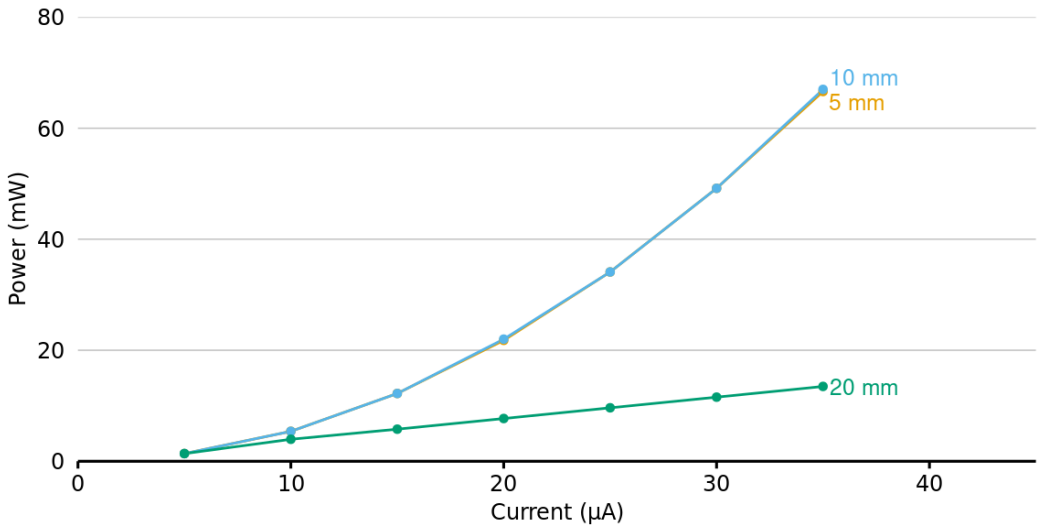

Figure 5.5: Plot of the power at different I_{GD} from 5 to 35 μA. Conducted at a set Q_{He} of 5 $L\ min^{-1}$. Effect of inter-electrode distance (d_e) from 5 to 20 mm shown for comparison. The power output increases exponentially with increased I_{GD} from 1.4 mW to 66.6 mW, while at larger d_e of 20 mm the relationship is linear increasing from 1.4 mW to 13.5 mW.

measured at d_e of 5 and 10 mm remains fairly constant across all gas flow rates varying by $\pm$ 0.085 mW as shown in figure 5.6. The power output at a d_e of 20 mm shows an inverse relationship with the Q_{He} going from 12.2 mW at 0.1 $L\ min^{-1}$ down to 5.8 mW at 0.5 $L\ min^{-1}$ a rate change of -16 $mW\ L\ min^{-1}$. Flow is not a direct proxy of pressure, however in this arrangement the pressure is likely to increase at the exit of the electrode at higher flow rates. At 0.5 $L\ min^{-1}$ the difference in $p.d$ is only a factor of 2 greater at 20 mm than at 10 mm suggesting that at greater electrode distances the breakdown voltage is moving towards the minima on the plot of Pashen's law (figure 3.1).

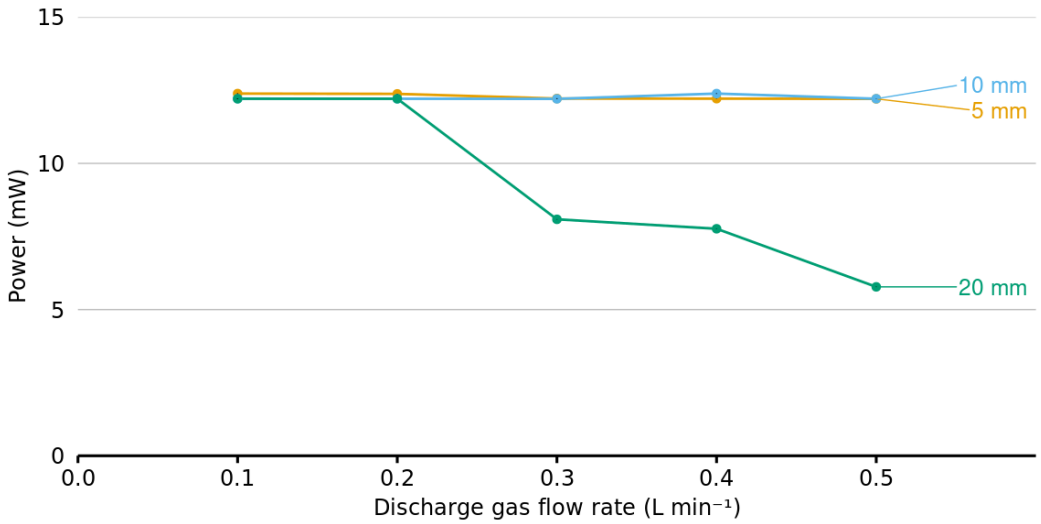

Figure 5.6: Plot of the power output at a range of gas flow rates from 0.1 to 0.5 $L\ min^{-1}$ at a I_{GD} of 15 μA. The measurements repeated at three values of d_e 5, 10, and 20 mm. The power output measured at d_e 5 and 10 mm remains fairly constant, varying by $\pm$ 0.085 mW. At 20 mm an inverse relationship with the gas flow rate is observed, at a rate change of -16 $mW\ L\ min^{-1}$.

5.3.3 Temperature measurements of the micro-glow discharge

The afterglow temperature in a typical FAPA ionization source is in the hundreds of degrees Celsius [32]. Prototype V however has a considerably lower power consumption than the previous prototypes employed in chapter 4, and therefore the thermodynamic gas temperature of the micro-glow discharge was measured using an infra-red thermal camera. The images in figure 5.7 show no measurable difference between the background temperature of the laboratory at 22.4 $°C$, and the thermodynamic gas temperature in the micro-glow discharge and electrodes. Prototype V can therefore be considered to have a "cold plasma" which suggests it is more alike to the LTP, though it must be noted the LTP is a radio frequency

dielectric barrier discharge ionization source, than comparable FAPA ionization sources. This reduces the utility of the source for direct desorption of low vapour pressure compounds unless the micro-glow discharge can ablate samples from a surface, but also this means that those samples which are thermally labile will be subject to less thermal decomposition using prototype V.

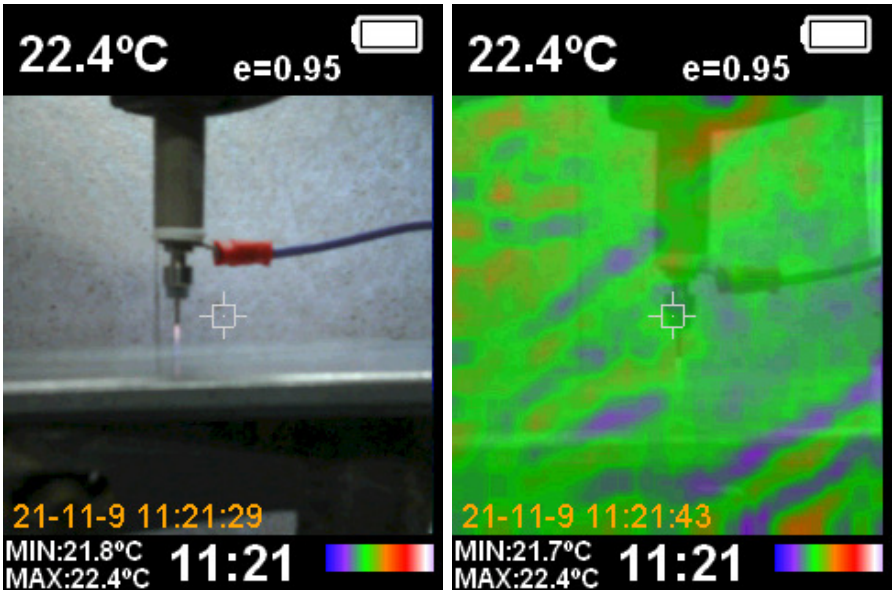

(a) (b)

Figure 5.7: Photograph of prototype V, (a) showing the micro-glow discharge, and (b) with heat map overlay. No significant variation is seen in the region of the micro-glow discharge with respect to the background temperature of the laboratory of $22.4\ ^{\circ}C$.

5.4 Set-up and integration of prototype V with the Waters Xevo G2-S mass spectrometer

The set-up of prototype V with the Waters Xevo G2-S mass spectrometer required only minimal modification. A Waters universal ESI source enclosure was donated (by Dr William Johnson, Waters Corp., Wilmslow, UK) which allowed a 10 mm o.d. hole to be machined into the housing axially to the mass spectrometer inlet at the in-house model workshop (Faculty of Medicine, Health, and Life Science). This allowed prototype V to be orientated axially to the mass spectrometer inlet at a d_e between 5 and 15 mm. The ionization source was connected to the instrument internal constant current power supply using the APCI needle terminal. The instrument settings were as follows; cone voltage -30 V, cone offset -80 V, ion source block temperature 120 $°C$, cone gas 0 $L\ h^{-1}$, desolvation gas flow $0-600$ $L\ h^{-1}$, desolvation temperature 50-650 $°C$. Prototype V primary settings were, discharge current $5-35$ μA, discharge gas flow $0.1-0.5$ $L\ min^{-1}$, inter-electrode gap $5-15$ mm. All data were acquired in full scan continuum mode at m/z 50 to 2,000. Nominal masses (at a resolution of *circa* 20,000) are reported other than where compound identification was required where accurate mass measurements were made using known background ions as reference lock-masses.

The Waters universal source enclosure has a interchangeable probe assembly which can be used with a solids probe such as the ASAP [53] ADI technique and is a simple and rapid sample introduction method. This provides sampling versatility as the solids probe can be dipped in powders and liquids, rubbed on surfaces, or a set volume of a solution can be pipetted or syringed into the end of the capillary.

5.4.1 Background mass spectrum

A mass spectrum of the background ions was acquired in positive ion mode on the Waters Xevo G2-S mass spectrometer using the source in the axial position with respects to the inlet. The mass spectrum presented in figure 5.8 shows several protonated molecules ($[M+H]^+$) that can be seen and readily identified, including m/z 149 phthalic anhydride, m/z 391 diisooctyl phthalate, which are all common background ions. The high intensity of plasticizer in the background is believed to be from the outgassing of the PEEK body and other plastic components such as the power cable. Other ions, such as m/z 257, are present but are of unknown origins are likely from any plastic components or trace impurities in the helium gas.

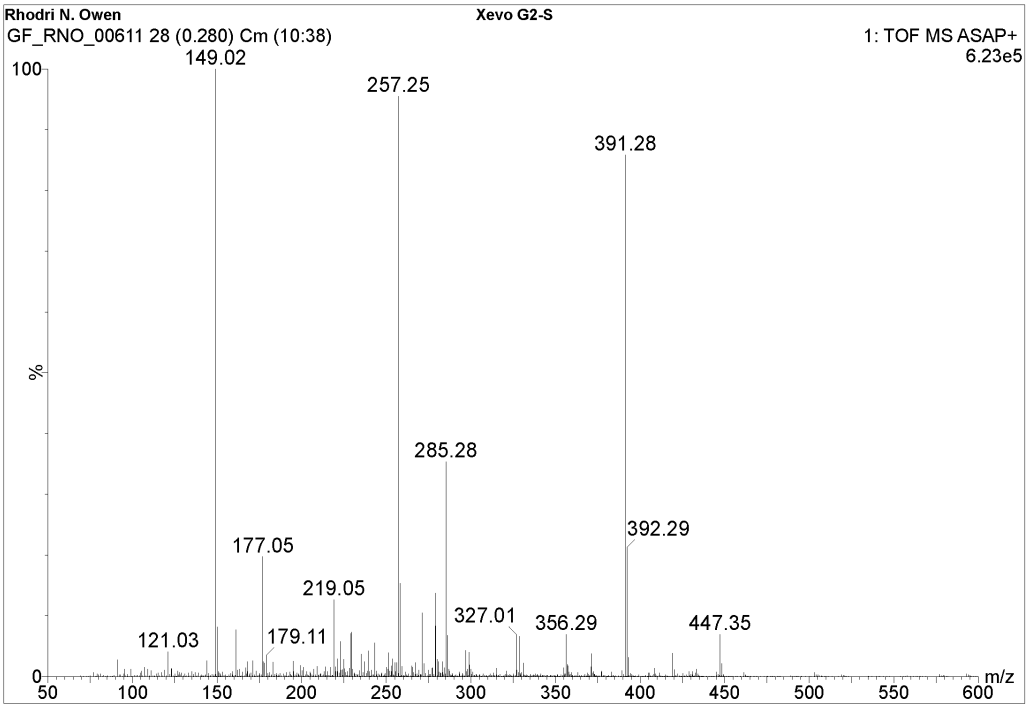

Figure 5.8: Representative background spectrum of the prototype V source. Observed protonated molecules ($[M+H]^+$) included *m/z* 149 phthalic anhydride and *m/z* 391 diisooctyl phthalate. A persistent ion at *m/z* 257 was observed of unknown origin. The high intensity of plasticizer in the background is believed to be from the PEEK body and other plastic components such as the power cable.

5.5 Optimisation of prototype V

To understand the nature of the glow discharge and operating conditions of prototype V, various parameters were assessed to optimise the sample introduction and ionization process. These included desolvation gas flow rate and desolvation gas temperature, sample volume, discharge gas flow rate, discharge current, and sample phase.

Three compounds were selected for optimising the parameters, 2,6-dimethyl-γ-pyrone, methyl dodecanoate and hexadecylamine because of the range of physical properties they possessed, some of which are listed in table 5.1. These compounds were prepared at a concentration of 100 $ng\ \mu L^{-1}$.

Table 5.1: List of compounds used in the optimisation of prototype V. A selection of physical properties are listed namely melting point (Mpt), boiling point (Bpt), and vapour pressure at standard temperature (P).

Compound	Formula	M_r	Mpt ($^\circ C$)	Bpt ($^\circ C$)	P (Pa)
2,6-Dimethyl-γ-pyrone	$C_7H_8O_2$	124	132	251	n/k
Methyl dodecanoate	$C_{13}H_{26}O_2$	214	5	267	547.96
Hexadecylamine	$C_{16}H_{35}N$	241	97	323	0.02

5.5.1 Effects of desolvation gas temperature

A number of ADI techniques rely on the ion source to provide a mechanism for sample sublimation or evaporation to the gas phase. Conventional FAPA sources have a relatively high afterglow temperature 350 $^\circ C$ when compared to the DART [6] or LTP [11] ionization sources *circa. 30-50* $^\circ C$. Higher operating temperatures would allow for easier desorption of compounds with low equilibrium vapour pressures though thermally labile compounds known to

decompose at high temperatures. An assessment of the effect of the desolvation gas temperature on the abundance of the protonated molecule ($[M + H]^+$) was studied using the three analytes 2,6-dimethyl-γ-pyrone, methyl dodecanoate and hexadecylamine. The samples were placed into the end of the soda glass capillary tube and introduced into the source at set temperatures from 50 $°C$ to 650 $°C$ at 50 $°C$ increments.

The peak area from the extracted ion chromatogram (XIC) for each compound ($n = 3$) was recorded and the mean peak area plotted for each temperature value, in figure 5.9. Methyl dodecanoate, a liquid at room temperature, has a low melting point and an equilibrium vapour pressure of 547.96 Pa at 25 $°C$ which is evident as the abundance of the protonated molecule is at a maximum at 50 $°C$. Hexadecylamine has a equilibrium vapour pressure of 0.02 Pa at 25 $°C$ which is five orders of magnitude less than methyl dodecanoate and exhibits a maximum abundance of the protonated molecule plateauing at around 350 to 450 $°C$ and gave no signal at 50 $°C$. All samples including 2,6-dimethyl-γ-pyrone showed a marked reduction in abundance of the protonated molecule above 450 $°C$ suggesting sample decomposition is occurring at an increasing rate, as might be expected with respect to vaporization and ionization. This demonstrates that optimal desolvation gas temperature must be assessed for each compound, however as a general rule 350 $°C$ would appear to provide optimal balance between ionization and decomposition on abundance of the protonated molecule for many compounds with lower vapour pressures.

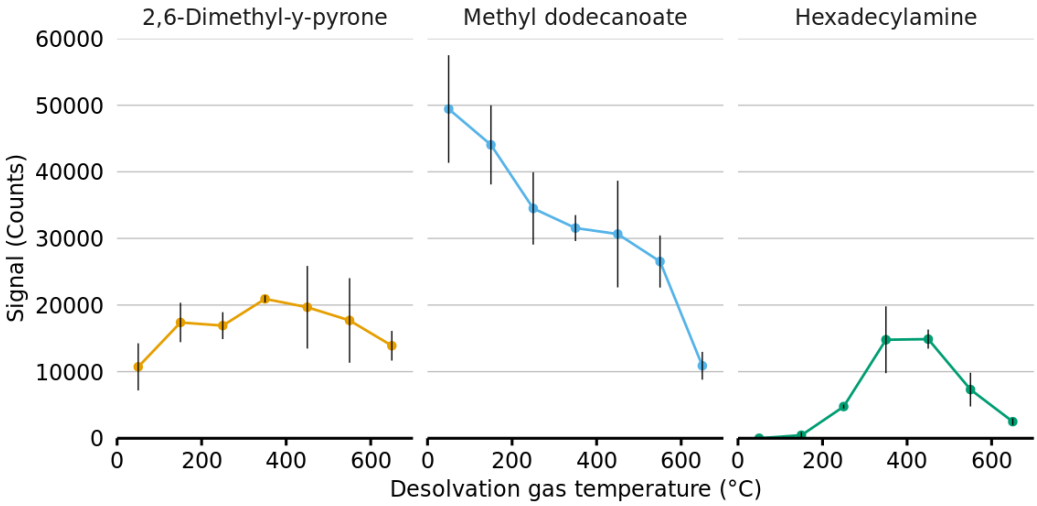

Figure 5.9: Plot of abundance of the protonated molecule at various temperatures. The peak area from the XIC ($n = 3$) for the three selected compounds is plotted at each desolvation gas temperature from 50 to 650 $^{\circ}C$ in 50 $^{\circ}C$ increments, showing the temperature effect on the abundance of the protonated molecule. This demonstrates that optimal desolvation gas temperature must be assessed for each compound, however as a general rule 350 $^{\circ}C$ would appear to provide optimal balance between ionization and decomposition on abundance of the protonated molecule.

5.5.2 Effects of desolvation gas flow rate

Desolvation gas is used in the transfer of heat to the sample to assist desolvation and carry the sample towards the ion source and mass spectrometer orifice. A study of the gas flow rate was made using the three compounds. The desolvation gas temperature was set at 350 $°C$ and the gas flow rate was increased from 100 to 600 $L\ h^{-1}$ in increments of 100 $L\ h^{-1}$ to assess the effects of the flow rate on the abundance of protonated molecules ($[M + H]^+$) recorded.

The peak area from the XIC for each compound ($n = 3$) was recorded and the mean peak area plotted for each gas flow rate value, in figure 5.10. For the analytes 2,6-dimethyl-γ-pyrone and methyl dodecanoate increasing the desolvation gas flow rate had the effect of reducing the abundance of the protonated molecule which might be hypothesised as a result of more volatile compounds having less resident time in the path of the micro-glow discharge. This has a two-fold effect of reducing the number of molecules available to be ionised and also removing some of the ions formed before they reach the sampling orifice. Hexadecylamine showed a different profile with the abundance of the protonated molecule increasing with increased desolvation gas flow rates up to 400 $L\ h^{-1}$ with only marginal increase in intensity by increasing the flow rates further. For less volatile compounds, such as hexadecylamine, the increase flow rate would appear to aid desorption and in turn ion formation but only until such a point at which that the number of molecules available for ionization are being reduced by the increasing flow rate. As a general guide the optimal flow rate would appear to exist at around 400 $L\ h^{-1}$ though optimisation for each compound, or compound class, would provide higher sensitivity.

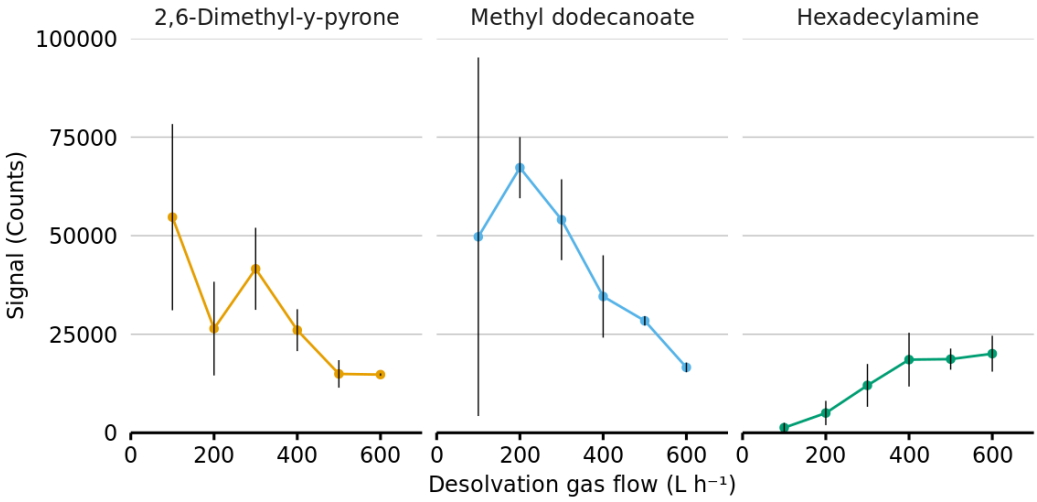

Figure 5.10: Plot of abundance of the protonated molecule from the XIC ($n = 3$) against the desolvation gas flow rates. Comparison at six different flow rates from 100 to 600 $L\ h^{-1}$ in increments of 100 $L\ h^{-1}$, for the three selected compounds are shown.

5.5.3 Effect of altering discharge current (I_{GD})

The I_{GD} will influence the system power ($P = I_{GD}.V$) and consequently the energy ($E = P.t$) available to generate reagent ions and excited species in the micro-glow discharge. These ions and excited species can then go on to directly ionise the analyte or form intermediary reagent ions which can subsequently ionise the analyte molecules. A study was made using the three compounds on the effect of I_{GD} on abundance of the protonated molecule. The I_{GD} was varied from 5 to 20 μA in increments of 5 μA to assess the effect.

The peak area from the XIC for each ion ($n = 3$) was recorded and the mean peak area was plotted at each I_{GD} in figure 5.11. No observable relationship was found between the change in I_{GD} and the abundance of the protonated molecule which is not surprising given the power output as shown in figure 5.6 doesn't fluctuate considerably in this range.

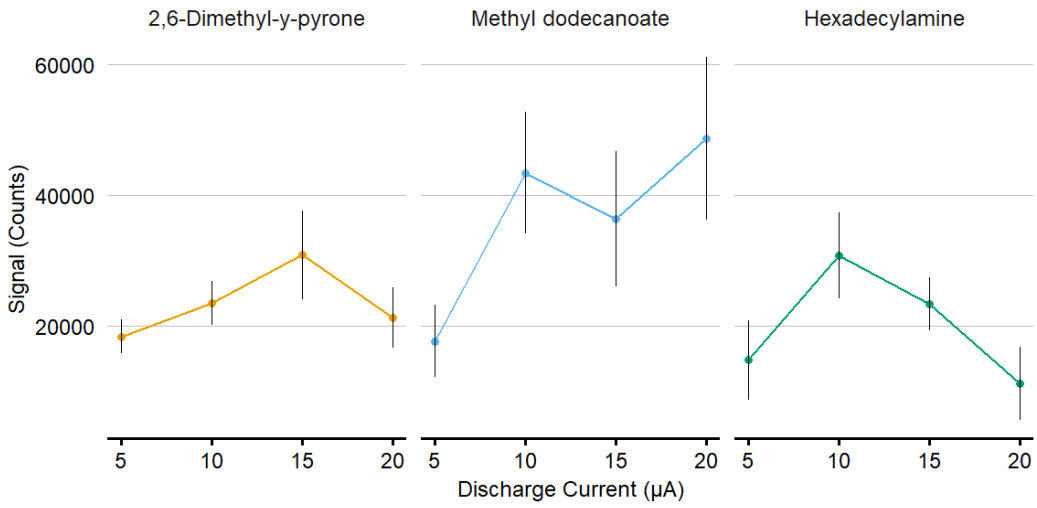

Figure 5.11: Plot of abundance of the protonated molecule with changing discharge current (I_{GD}). Three selected compounds showing profile of the effects on the peak area from the XIC (n = 3) at four different I_{GD} from 5 to 20 μA in increments of 5 μA. No observable relationship was found between the change in I_{GD} and the abundance of the protonated molecule.

5.5.4 Effect of altering helium gas flow rate (Q_{He})

Prototype V is positioned axially, as this is expected to provide higher sensitivity, to the mass spectrometer orifice and perpendicular to the sample probe. Altering Q_{He} will increase the number of helium gas atoms available for excitation and ionization, increasing the possibility of more sample ions being formed as the analyte crosses the path between the ionization source and orifice. Additionally, with the flow of the desolvation gas being perpendicular to the mass spectrometer orifice and the flow of helium discharge gas, the cross-flow of the discharge gas may increase the transport of ions towards the orifice. It should be noted that the latter effect may be limited as others have shown laminar flow to only be present in the afterglow at flow rates of greater than 1.5 $L\ min^{-1}$ [108] and in this current design Q_{He} are much lower (0.1 to 0.5 $L\ min^{-1}$). At these flow rates, which are only between 1.5 and 7.5 % of the desolvation gas flow rate (400 $L\ h^{-1}$), the discharge gas is unlikely to be the dominant process.

The integrated peak area from the XIC for each compound ($n = 3$) was recorded and the mean area plotted for each helium discharge Q_{He} value in figure 5.12 from 0.1 to 0.5 $L\ min^{-1}$ in increments of 0.1 $L\ min^{-1}$. All compounds showed an increasing trend in abundance of the protonated molecule with increased gas flow rates. Above 0.4 $L\ min^{-1}$ the effect was reversed for 2,6-dimethyl-γ-pyrone and methyl dodecanoate being most pronounced with the latter; the effect was not as notable with hexadecylamine. This suggests flow rates in the region of 0.4 $L\ min^{-1}$ is optimal for abundance of the protonated molecule.

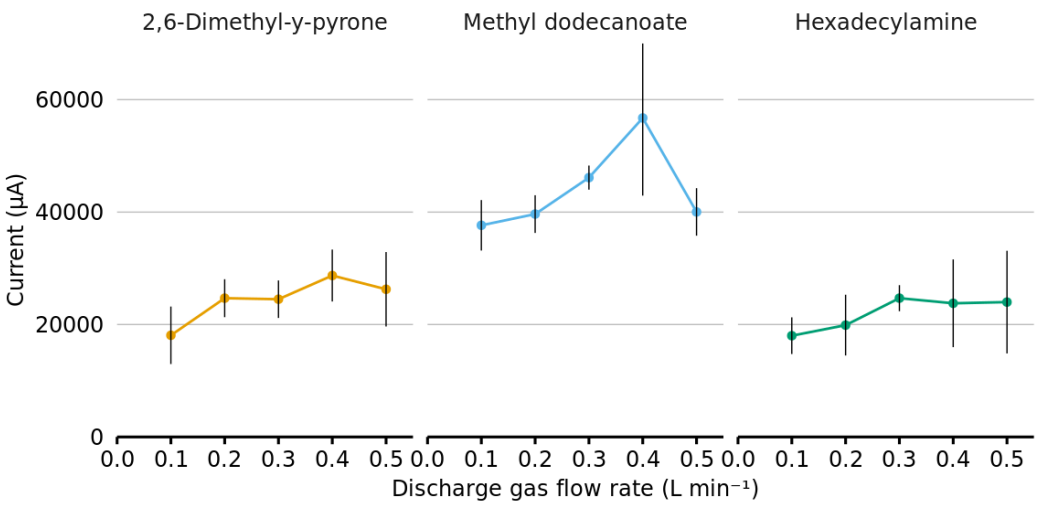

Figure 5.12: Plot of abundance of the protonated molecule at each helium discharge gas flow rate (Q_{He}). Three selected compounds showing profile of the effects on the peak area from the XIC ($n = 3$) at five different Q_{He} from 0.1 to 0.5 $L\ min^{-1}$ in increments of 0.1 $L\ min^{-1}$. All compounds showed an increasing trend in abundance of the protonated molecule with increased Q_{He}.

5.5.5 Effects of wet and dry sample introduction

Samples can be introduced into the source "wet" with the analyte remaining in the solution phase or alternatively "dry" where the solvent is allowed to evaporate leaving the analyte *in situ* in the solid phase prior to introduction into the source. In the "wet" method matrix affects from the solvent can effect the desorption-ionization process. For example a solvent with a high boiling point could keep the analyte solvated for longer in the desolvation gas flow increasing the overall time of the abundance of the protonated molecule is recorded. For this reason, a study of the effects of the "wet" and "dry" method was undertaken. An aliquot of the analyte solution is placed on a soda glass capillary, and half the samples ("dry") were allowed to dry in the laboratory atmosphere while the other half were analysed immediately ("wet").

The peak area from the XIC for each compound ($n = 3$) was recorded and the mean peak area was plotted in figure 5.13 for both "wet" and "dry" samples. The pattern observed in general shows a decreasing abundance of the protonated molecule with "dry" samples with respect to "wet" samples. This was particularly pronounced for methyl dodecanoate, which has a high vapour pressure, with a 41 % decrease in signal. Reproducibility of the measurements was also greater for "dry" samples with a RSD of 11.6 % (range 6.6 - 16.5) compared to "wet" samples which had an RSD of 25.7 % (range 23.0 - 30.5). Even though its boiling point is high, as listed in table 5.1, it is suspected that the effect observed is as a result of the analyte evaporating with the solvent when drying in the laboratory atmosphere. The samples with lower vapour pressure show less variation with hexadecylamine having a minor 6.36 % change in abundance between the dry

and wet sampling in favour of the dry method.

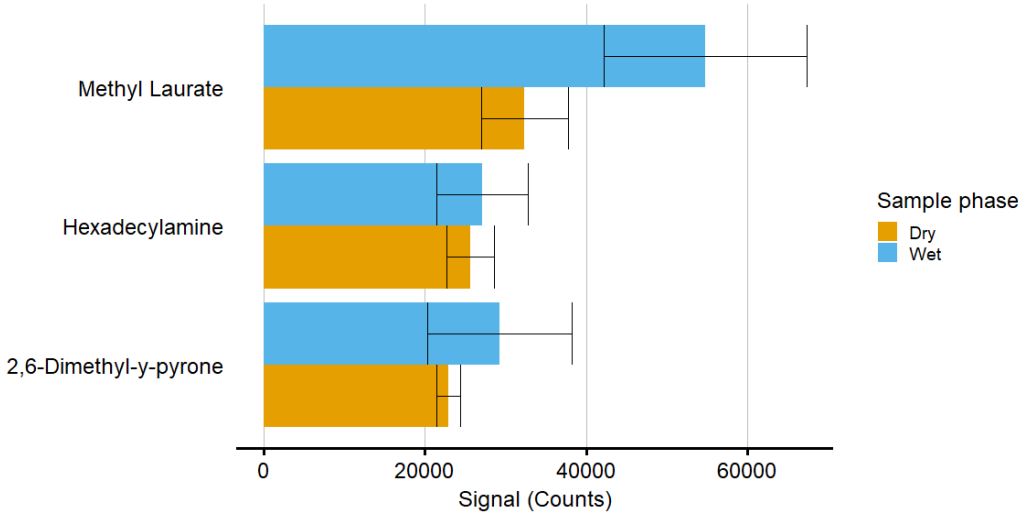

Figure 5.13: Bar plot of comparing abundance of the protonated molecule of "wet" and "dry" sample method. The pattern observed in general shows a decreasing abundance of the protonated molecule with the "dry" sample with respect to the "wet" sample. The phase of the sample as seen in representative mass spectra shown in figure A.4 (Appendix A) does not seem to affect the ion species formed. Higher vapour pressure appears to showed increased effect, it is particularly pronounced for methyl dodecanoate (40.85 % decrease in signal).

5.5.6 Effect of sample volume

The effect on sample volume on abundance of the protonated molecule was investigated to determine whether the volume and analyte concentration affects the ionization capacity of the source. Sample volumes from 0.5 to 4.0 μL were investigated for the three compounds (2,6-dimethyl-γ-pyrone, methyl dodecanoate and hexadecylamine).

The integrated peak area from the XIC for each compound ($n = 3$) was recorded and the mean area was plotted in figure 5.14 at each sample volume. For all compounds the abundance of the protonated molecule was linear across the sample volume range. Within this range the effect of the sample volume of the compounds appear to be negligible and no saturation of the signal was observed.

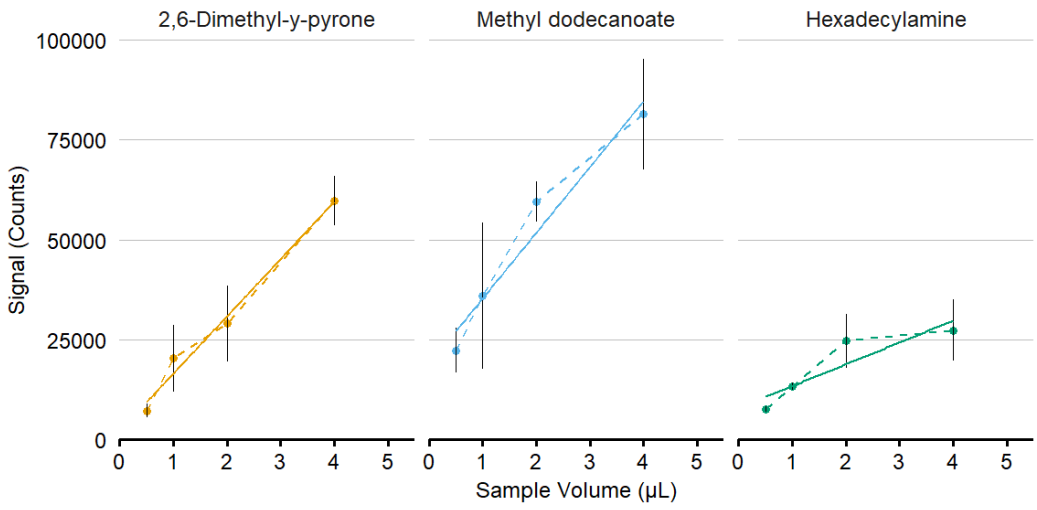

Figure 5.14: Plot of abundance of the protonated molecule with increasing sample volume. For all three compounds examined the abundance of the protonated molecule was in general linear across the sample volume range.

5.5.7 Protonation versus charge transfer when altering discharge conditions

Altering the discharge conditions has previously been shown to suppress protonation in favour of charge transfer [109], and it is suggested that the "hotter" gas temperature reduces the available protonated-water clusters for protonation. This effect is achieved by increasing the current and reducing the discharge gas flow rate, consequently increasing the power and slowing mass transfer of ions and excited species in the afterglow. By selecting a low gas flow rate of 0.1 $L\ min^{-1}$ and high current 20 μA the three samples were studied and the peak areas from the XIC for the molecular ion $M^{+\bullet}$ and protonated molecule $[M+H]^+$ ions were monitored.

The abundance of the $M^{+\bullet}$ ion from charge transfer is negligible under these conditions, as recorded in figure 5.15, suggesting that the formation of hydrated water clusters ($n(H_2O)H^+$) remains unaffected even at the most extreme conditions available to prototype V. This is perhaps not surprising given that this ionization source produces a "cold" plasma as shown in figure 5.7. Therefore, the opportunity to tune this ionization source to favour charge transfer or protonation will not be possible with the current power supply. Alternatives such as using charge transfer reagents or APPI reagents such as carbon disulfide or toluene may need to be employed to selectively modify the dominant ionization processes.

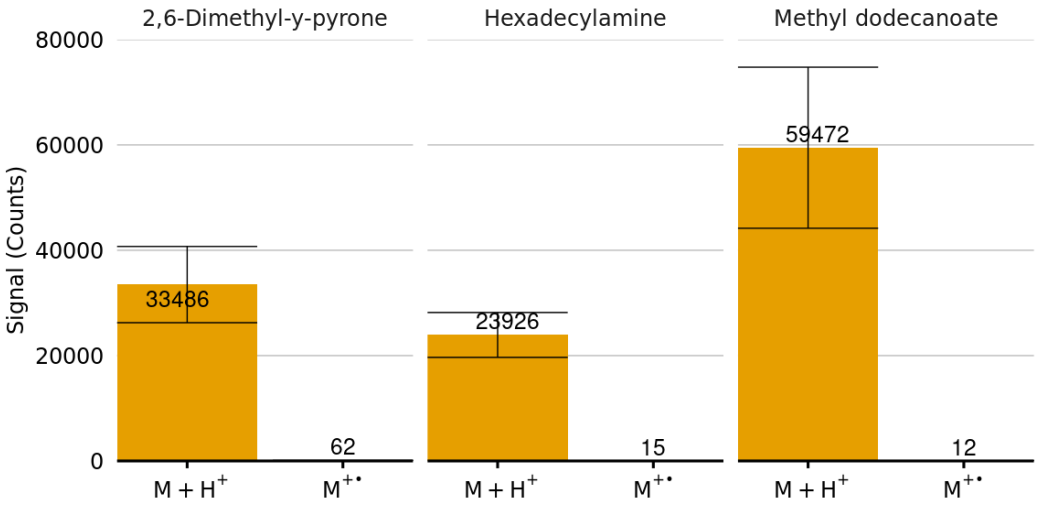

Figure 5.15: Bar graph of the abundance of the $M^{+\bullet}$ and $[M+H]^+$ ions. Shown are the three compounds under study, with a discharge gas flow rate of 0.1 $L\ min^{-1}$ and current 20 μA. The intensity of the $M^{+\bullet}$ ion from charge transfer is negligible under these conditions suggesting that the formation of hydrated water clusters ($n(H_2O)H^+$) remains unaffected. A mass spectrum of 2,6-dimethyl-γ-pyrone is shown in figure A.5 (Appendix A) showing the relative intensities.

5.5.8 Comparison of prototype V with atmospheric-pressure chemical ionization

A study of 19 compounds was undertaken using prototype V to determine the range of compound chemistries amenable to ionization using this technique, further the integrated ion abundance of the conventional corona discharge APCI source was also recorded and a comparison made of the two sources selectivity for the compounds. The results were tabulated and normalized to 1 for the APCI source and are presented in figure 5.16. For eight (42 %) of the compounds prototype V out performed the APCI source by between 1 and 2 times. Based on the structures of the compounds it would appear that prototype V has a propensity to readily ionise hydroxyl and ester containing compounds.

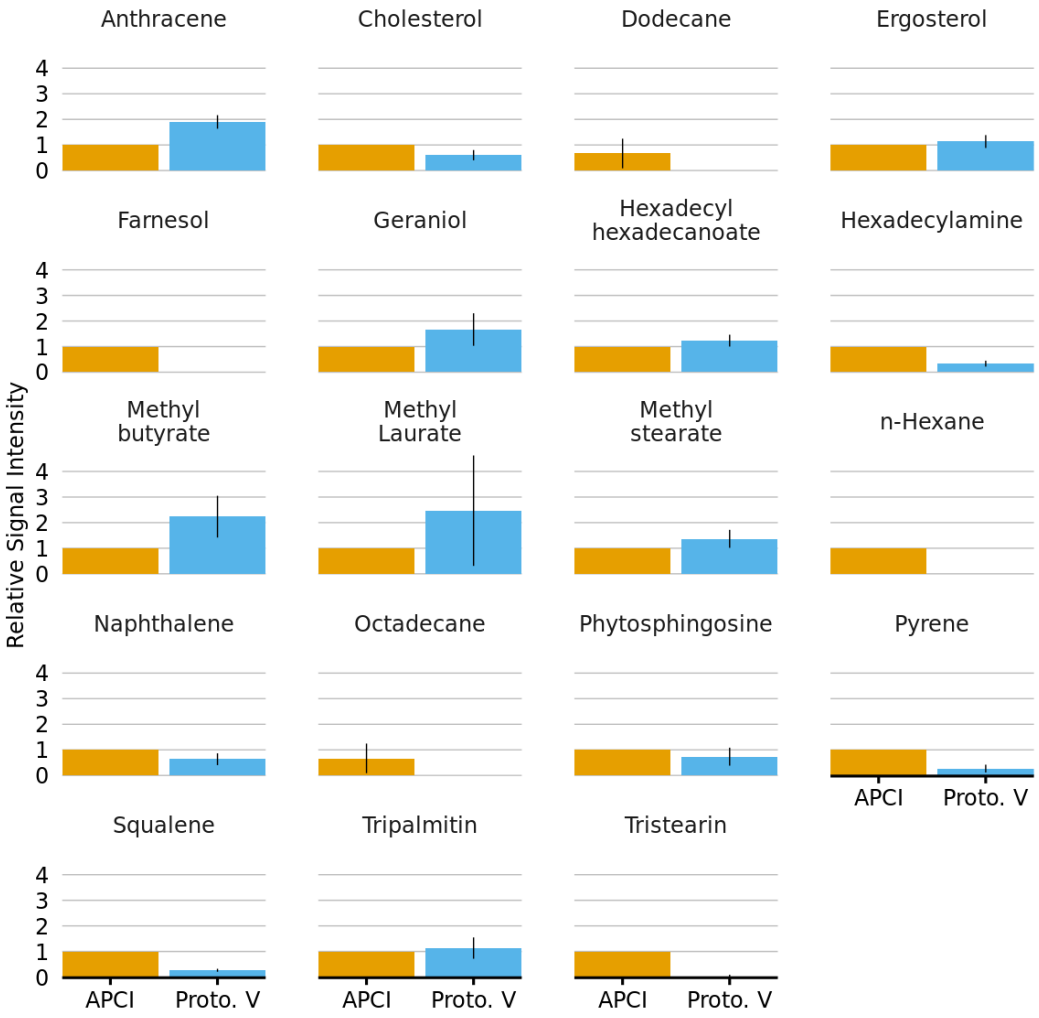

Figure 5.16: Comparison of prototype V with APCI for 19 compounds. The mean intensity of the peak area for each compound ($n = 3$) was normalized to 1 with respect to the response of the APCI source. For eight (42 %) of the compounds prototype V out performed the APCI source by between 1 and 2 times.

5.6 Analytical figures of merit for prototype V comparing different sample introductory methods

A heated inlet system would be important for extending the mass range and types of analytes that would be capable of being analysed, as prototype V described has a relatively "cold" plasma. A study to determine the analytical figures of merit for prototype V was conducted these are DL, range of reliable response, and reproducibility.

5.6.1 Solids analysis probe

Briefly, the ASAP probe consist of a metal assembly into which a soda glass capillary tube (1.9 mm o.d.) can be slotted. Samples can be introduced into the end of the glass capillary as solids, room-temperature liquids, or in solution. Analytes are desorbed from the glass capillary by means of a heated (0-650 $^{\circ}C$) nitrogen desolvation gas (flow rate 0-1,200 $L\ h^{-1}$) and directed towards the ionization source near the mass spectrometer orifice. The probe can be easily used with the adapted universal source housing using the prototype V.

The ASAP probe is conventionally used to provide qualitative data. To determine the performance of prototype V a series of compounds were analysed and analytical figures of merit produced. Five non-polar biomolecules were selected and are listed in table 5.2, including three sex hormones, an animal sterol, and a bacteria sterol. Each compound was weighed and dissolved into dicholromethane/methanol solution (1:1 v/v) to provide a stock solution, before

being further diluted in the same solution of dicholromethane/methanol to a working concentration range of 0.001, 0.005, 0.01, 0.05, 0.1, 0.5, and 1.0 mM.

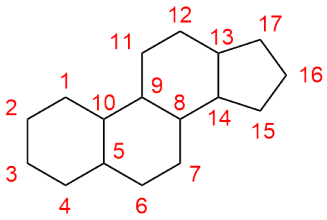

Figure 5.17: Drawing of the steroid ring structure. Carbon atoms numbered according to International Union of Pure and Applied Chemistry (IUPAC), starting at 1 on th "A" ring.

Table 5.2: List of steroids used in the study. A selection of physical properties are listed for reference namely the molecular formula, molecular mass (M_r), melting point (Mpt), boiling point (Bpt), and vapour pressure (P) at STP. (Structures for the compounds listed shown in in figure A.6)

Compound	Molecular Formula	M_r	Mpt ($°C$)	Bpt ($°C$)	P (Pa)
Estrone	$C_{18}H_{22}O_2$	270.37	255	445	3.3E-8
Estradiol	$C_{18}H_{24}O_2$	272.38	173	446	8.5E-7
Testosterone	$C_{19}H_{28}O_2$	288.42	155	433	2.3E-6
Cholesterol	$C_{27}H_{46}O$	386.65	149	360	1.1E-7
Ergosterol	$C_{28}H_{44}O$	396.66	160	250	1.4E-7

Analysis was conducted under optimal conditions determined earlier in this chapter namely with the desolvation gas at 350 $°C$ and 400 $L\ h^{-1}$ and prototype V operating at 15 mA and 0.4 $L\ min^{-1}$. The sample solution was syringed into the end of the glass capillary and allowed to dry in the laboratory atmosphere before being introduced into the desolvation gas flow. The peak area was recorded ($n = 3$) and calibration curves prepared using the mean peak area for each compound are presented in figure 5.18.

A summary of the analytical figures of merit is provided showing the DL, SEM, and coefficient of determination (R^2) for each of the compounds in table

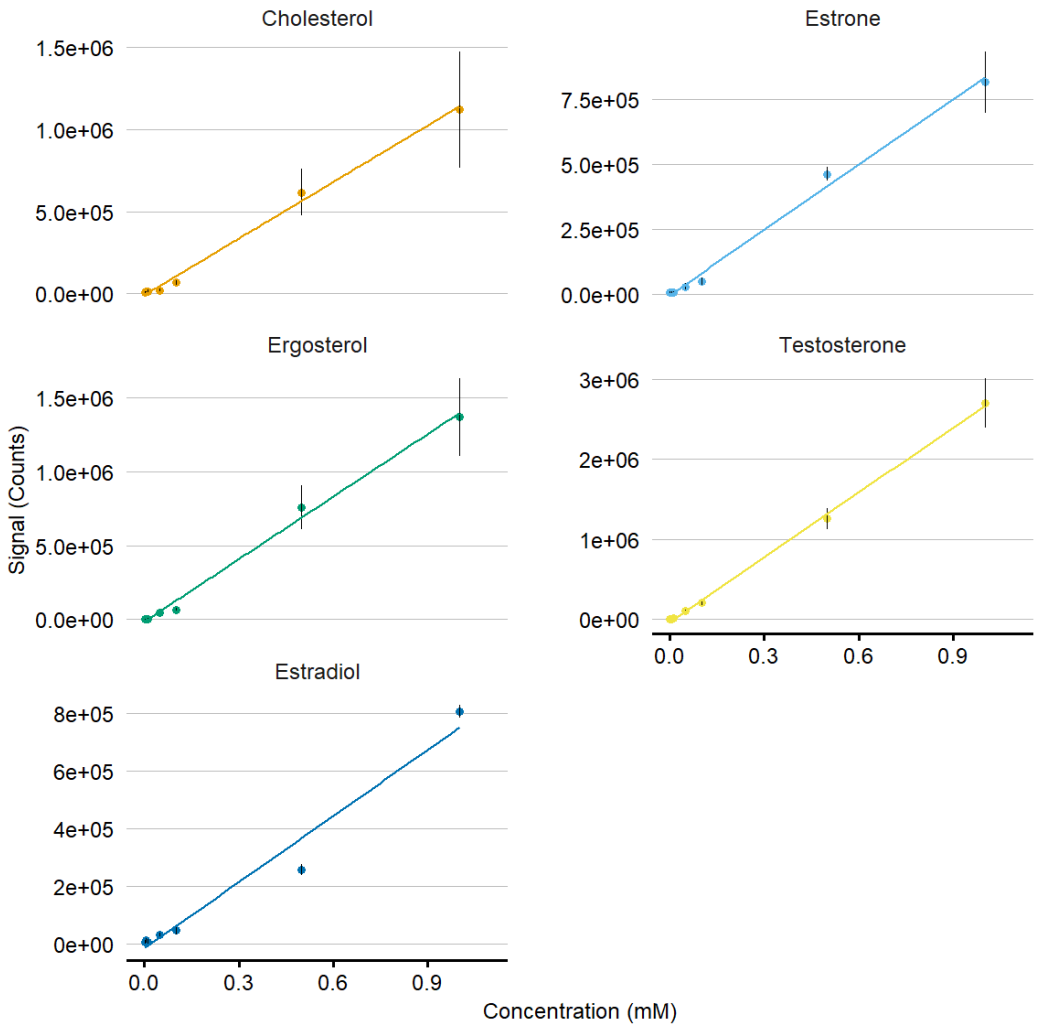

Figure 5.18: Plot of the abundance of the ions against concentration for five compounds using a solids analysis probe (mass spectra shown in figure A.8). Linear regression analysis of the base peak ($N = 7; n = 3$) for each compound cholesterol (*m/z 369*), estrone (*m/z 271*), ergosterol (*m/z 379*), testosterone (*m/z 289*), and estradiol (*m/z 255*).

5.3. The base peak for estrone and testosterone was the protonated molecule $[M + H]^+$ at m/z 271 and 289, respectively, the dehydrated molecular ion $[M + H - H_2O]^+$ was also observed for both compounds at relative intensities

of 40 % and 20 % respectively to the base peak. While for the compounds estradiol, cholesterol, and ergosterol the base peak was the dehydrated molecular ion $[M + H - H_2O]^+$ at m/z 255, 369, and 379, respectively. Weak protonated molecules were observed for cholesterol and ergosterol with a relative intensity of 10 %, while for estradiol it was at 65 % of the base peak. The difference in the ion forming the base peak can be explained in part by the different functional groups present in the compounds. For those compounds with hydroxyl group at carbon-3 position, protonation leads to the formation of a OH_2^+ group which is unstable and likely fragments leading to dehydration of the ion with a stable charge remaining on the steroid fused ring system (figure A.7). While for compounds containing a carbonyl group (testosterone) at carbon-3 position the formation of the protonated COH^+ group is in contrast relatively stable and so remains intact. It is less clear why the protonated molecule is the base peak for estrone at there is a hydroxyl group on the carbon-3 position, while the carbonyl group is at the carbon-17 position, the 'A ring' is highly conjugated and may make the hydroxyl group more acidic making the carbonyl group at position 17 the preferred protonation site. The conjugated 'A ring' in estradiol along with a second hydroxyl group on the 17 position may also explain the increased relative intensity of the protonated molecule when compared to the sterols (cholesterol and ergosterol) under investigation in the study.

Analytical figures of merit for three fatty acid derivative

Analytical figures of merit were also prepared for three fatty acid derivative compounds hexadecylamine ($C_{16}H_{35}N$, M_r 241), methyl stearate ($C_{19}H_{38}O_2$, M_r 298),and phytosphingosine ($C_{18}H_{39}NO_3$, M_r 317) that were previously studied

Table 5.3: Analytical figures of merit for the steroids used in the study using a solids analysis probe. Listed is the observed ion, the sensitivity, DL, SEM, and coefficient of determination for each steroid. (†Reported for the lowest measured concentration)

Compound	Observed m/z	DL ($pmol\ \mu L^{-1}$)	SEM (%)†	R^2
Estrone	271	12.2	37	0.9938
Estradiol	255	27.0	91	0.9678
Testosterone	289	0.1	3	0.9988
Cholesterol	369	13.1	63	0.9949
Ergosterol	379	6.0	61	0.9945

using prototype IV, the results for which were listed in table 4.3. The samples were prepared in the same manner at concentrations of 1, 5, 10, 50, 100, 500 and 1000 $\mu mol\ L^{-1}$, and analysed using the optimised conditions for prototype V.

The sample solutions were syringed (1 μL) into the end of a glass capillary and allowed to dry in the laboratory atmosphere before being introduced into the desolvation gas flow for analysis. The peak area from the XIC for each sample was recorded ($n = 3$) and calibration curves of the mean peak area piloted in figure 5.19. A summary of the analytical figures of merit is provided in table 5.4.

For two of the fatty acid derivative there was an improved DL when using prototype V when compared to the prototype IV ionization source, for hexadecylamine 3.08 to 1.44 $pmol\ \mu L^{-1}$ and for phytoshingosine 1.47 to 0.002 $pmol\ \mu L^{-1}$. For methyl stearate the DL showed a marginal decline from 1.95 to 3.62 $pmol\ \mu L^{-1}$. The sensitivity also showed an improvement of two-orders of magnitude when using prototype V ionization source.

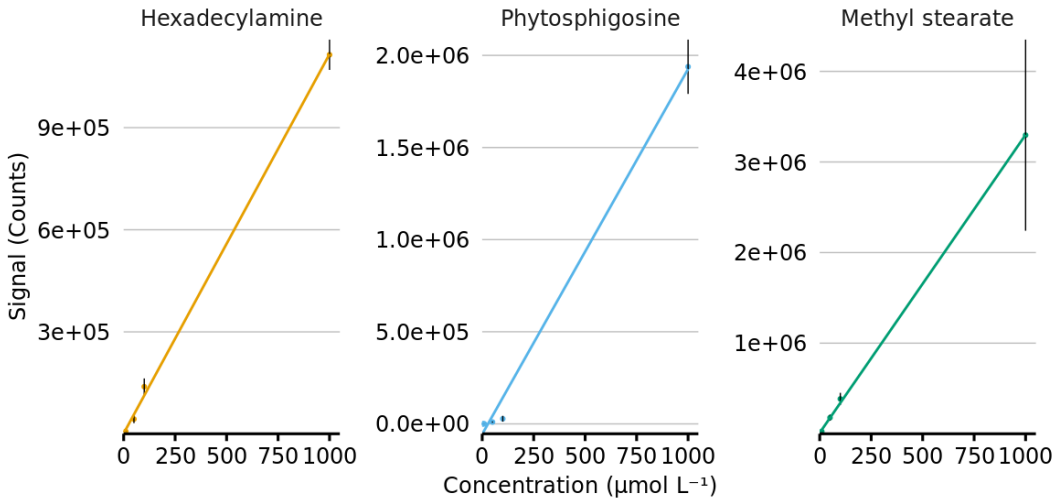

Figure 5.19: Plot of the abundance of the protonated molecule against concentration for hexadecylamine ($C_{16}H_{35}N$, M_r 241), methyl stearate ($C_{19}H_{38}O_2$, M_r 298),and phytosphingosine ($C_{18}H_{39}NO_3$, M_r 317). (Mass spectra of the ions observed are shown in figure A.9).

Table 5.4: Analytical figures of merit for the three compounds used in the study using a solids analysis probe. Listed is the observed ion, DL, SEM, and coefficient of determination for each steroid. (†Reported for the lowest measured concentration.)

Compound	Observed m/z	DL ($pmol\ \mu L^{-1}$)	SEM (%)†	R^2
Hexadecylamine	242	1.44	52	0.9991
Methyl Stearate	299	3.62	66	0.9997
Phytoshingosine	318	0.002	16	0.9933

Reproducibility of sample introduction methods

Reproducibility using prototype V ionization source was poor with the SEM ranging between 16 and 66 at the lowest concentration. In all experiments 1 μL of the analyte was placed on the glass capillary using a syringe. Previously a pipette was used and this showed much greater variation in reproducibility of replicates. A study of a pipette and syringe was made to understand the introduction of

human error in the sample deposition process. Methyl stearate at 0.1 *nmol*, and 0.5 *nmol* was deposited on the end of a glass capillary using either a pipette or syringe and allowed to dry in the laboratory atmosphere. The peak area from the XIC for each method was recorded ($n = 5$) and the results plotted as a boxplot that allows easy visualisation of the distribution of the measurements relative to the median value, including minimum, maximum, first quartile (25 %), and third quartile (75 %), in figure 5.20.

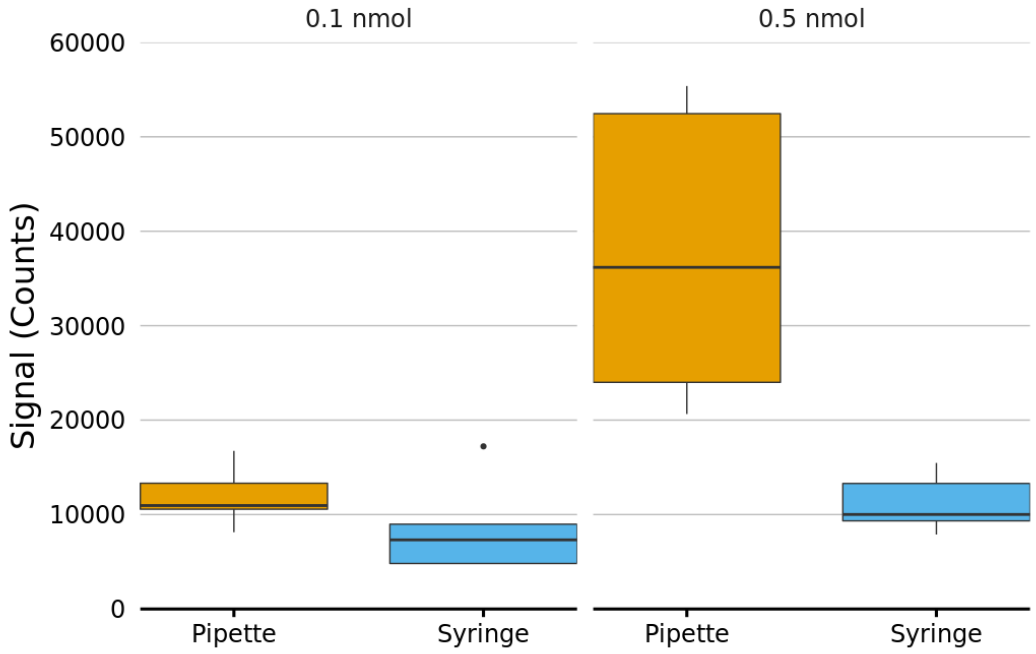

Figure 5.20: Boxplot of the abundance of the protonated molecule using a pipette and a syringe. The abundance of the protonated molecule of methyl stearate ($n = 5$) using the syringe is lower compared to the pipette at both 0.1 and 0.5 *nmol*, but has higher precision. (XIC 0.1 *nmol* shown in figure A.10).

The pipette provided higher abundance of the protonated molecules (median = 10,953) compared to the syringe (median = 7,319) at 0.1 *nmol*. However this was at the expense of the precision, for the pipette the abundance of the

protonated molecules at the 25^{th} and 75^{th} quartiles were 10,567 and 13,317 respectively, and for the syringe the 25^{th} and 75^{th} quartiles were 4,820 and 8,980. At 0.5 *nmol* the variance is more pronounced, for the pipette the median is 36,178 compared to 10,009 for the syringe. The precision of the pipette can also be seen to be much poorer at this concentration where the the 25^{th} and 75^{th} quartiles were 24,000 and 52,499. This clearly demonstrates the need to use a syringe for the delivery of sample solution to improve precision and reproducibility between replicates and to improve linearity of the data.

5.6.2 Infusion by loop injection

On the Waters Xevo G2-S mass spectrometer the ASAP probe can be quickly and easily be exchanged for a APCI IonSABRE probe (heated nebulizer). The benefit of the APCI probe is the ability to continuously introduce a stream of nebulised analyte-solvent vapour to the ionization source. The APCI probe was connected to the fluidics system of the mass spectrometer operating at flow rate of 50 $\mu L\ min^{-1}$, with a rheodyne placed inline fitted with a 1 μL loop, for use with prototype V.

The set of five steroids listed in table 5.2 were analysed in triplicate. A syringe was used to introduce each sample using the 1 μL loop which was overfilled by 4 μL to ensure proper filling of the loop and elimination of any air bubbles. The mean peak area from the XIC for each sample was recorded and calibration curves of the mean peak area piloted in figure 5.21. A summary of the analytical figures of merit are provided in table 5.5.

The DL for the loop injector is in the 0.5 to 25.0 $pmol\ \mu L^{-1}$ range, with

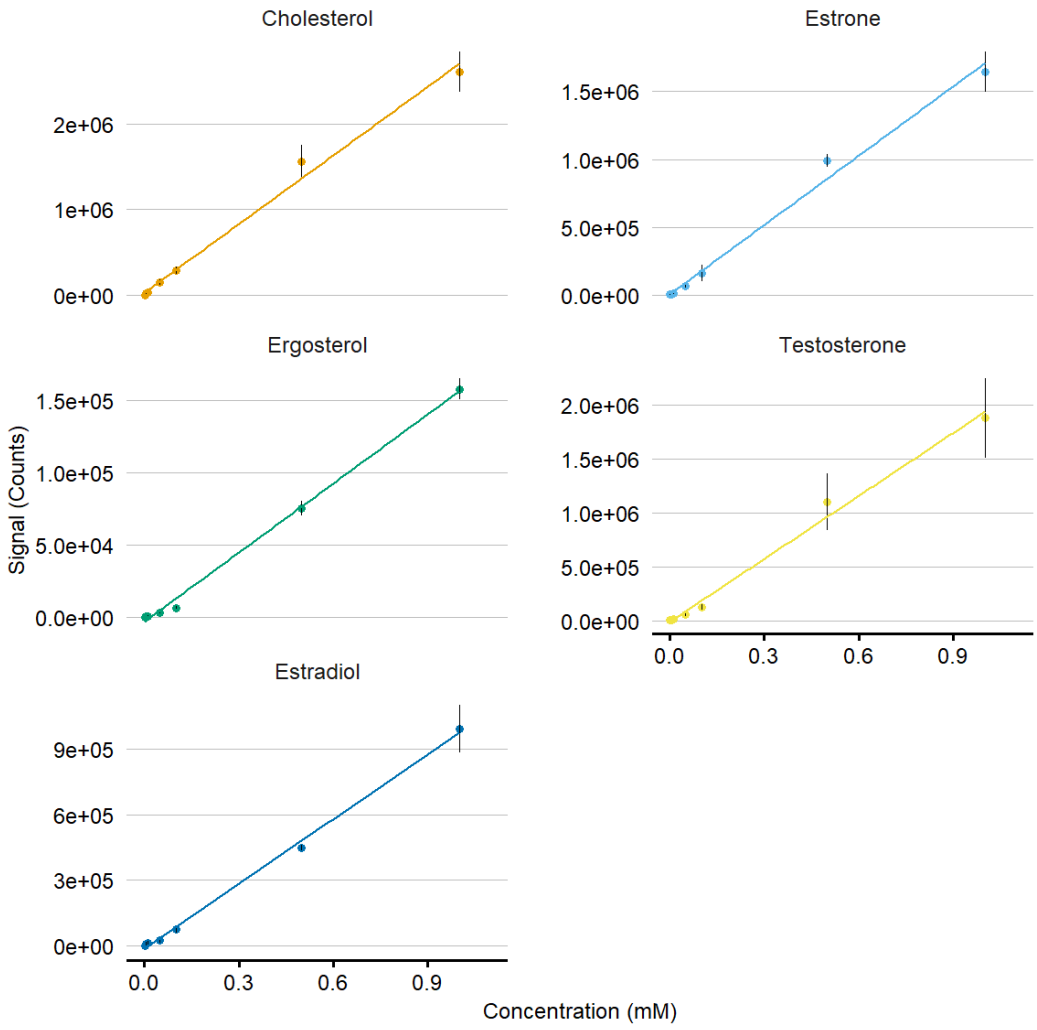

Figure 5.21: Plot of the abundance of ions against concentration for five compounds using loop injection. Linear regression analysis of the base peak for each compound cholesterol (*m/z 369*), estrone (*m/z 271*), ergosterol (*m/z 379*), testosterone (*m/z 289*), and estradiol (*m/z 255*). (Mass spectra of the ions observed are shown in figure A.11.)

an improvement of 2 times, based on the mean DL when compared to the same compounds analysed using the solids analysis probe (0.1 to 27.0 $pmol\ \mu L^{-1}$). Linearity remains high across the concentration range with R^2 of between 0.9908

Table 5.5: Analytical figures of merit for the steroids used in the study using loop injection. Listed is the DL, SEM, and coefficient of determination for each steroid. (†Reported for the lowest measured concentration.)

Compound	DL ($pmol\ \mu L^{-1}$)	SEM†	R^2
Estrone	2.6	17	0.9908
Estradiol	25.0	89	0.9973
Testosterone	0.6	9	0.9918
Cholesterol	0.5	9	0.9920
Ergosterol	1.0	4	0.9968

and 0.9973. The reproducibility at the lowest concentration has in general improved and the SEM is in the range of 4 to 17 $pmol\ \mu L^{-1}$, however, there is an outlier at 89 $pmol\ \mu L^{-1}$ for estradiol which also preformed poorly when analysed using the probe (91 $pmol\ \mu L^{-1}$) and so this may be an issue related to the ionization of the compound. It was discussed in the previous section that the base peak of estradiol was the dehydrated protonated molecule, but that the protonated molecule was at about 65 % relative intensity and any changes in the relative intensities could alter the precision of the measurements resulting in higher than normal SEM values.

5.6.3 Liquid chromatography mass spectrometry using prototype V

In the previous section it was demonstrated how flow-infusion for sample introduction could be interfaced with prototype V ionization source. The APCI probe can also be easily interfaced to a HPLC system allowing its combination as an inlet with prototype V. Modern chromatography systems have the ability to use an autosampler to automate the analysis of large batches of samples without

the need of the operator to be present during the data acquisition. A major advantage of these systems is its ability to separate and concentrate individual compounds present in a complex mixture or matrix. But generally the analysis time can be lengthy taking up to an hour to separate components, unless UHPLC system is used which has fast throughput times which can therefore be a limiting factor.

A study of five steroids cholesterol, estrone, ergosterol, testosterone, and estradiol was undertaken. Each sample was analysed three times and the peak area recorded for the base peak. Calibration curves were prepared from the mean peak areas from the XIC and are plotted in figure 5.22. A summary of the analytical figures of merit is provided in table 5.6.

Table 5.6: Analytical figures of merit for the steroids used in the study using HPLC. Listed is the DL, SEM, and coefficient of determination for each steroid. (†Reported for the lowest measured concentration.)

Compound	DL ($pmol\ \mu L^{-1}$)	SEM (%)†	R^2
Estrone	0.02	0.2	0.9991
Estradiol	7.5	2	0.9997
Testosterone	0.3	12	0.9923
Cholesterol	0.4	9	0.9975
Ergosterol	0.5	6	0.9968

The DL for HPLC with prototype V is in the range of 0.02 to 7.5 $pmol\ \mu L^{-1}$ for the five compounds studied, which is an improvement compared to the mean value 1.8 $pmol\ \mu L^{-1}$ of 7 and 3 times when compared to the solids analysis probe and loop injection, respectively. The linearity over the concentration range remains high with an R^2 of between 0.9923 and 0.9997. There is a significantly improved reproducibility between replicates at the lowest concentration with an

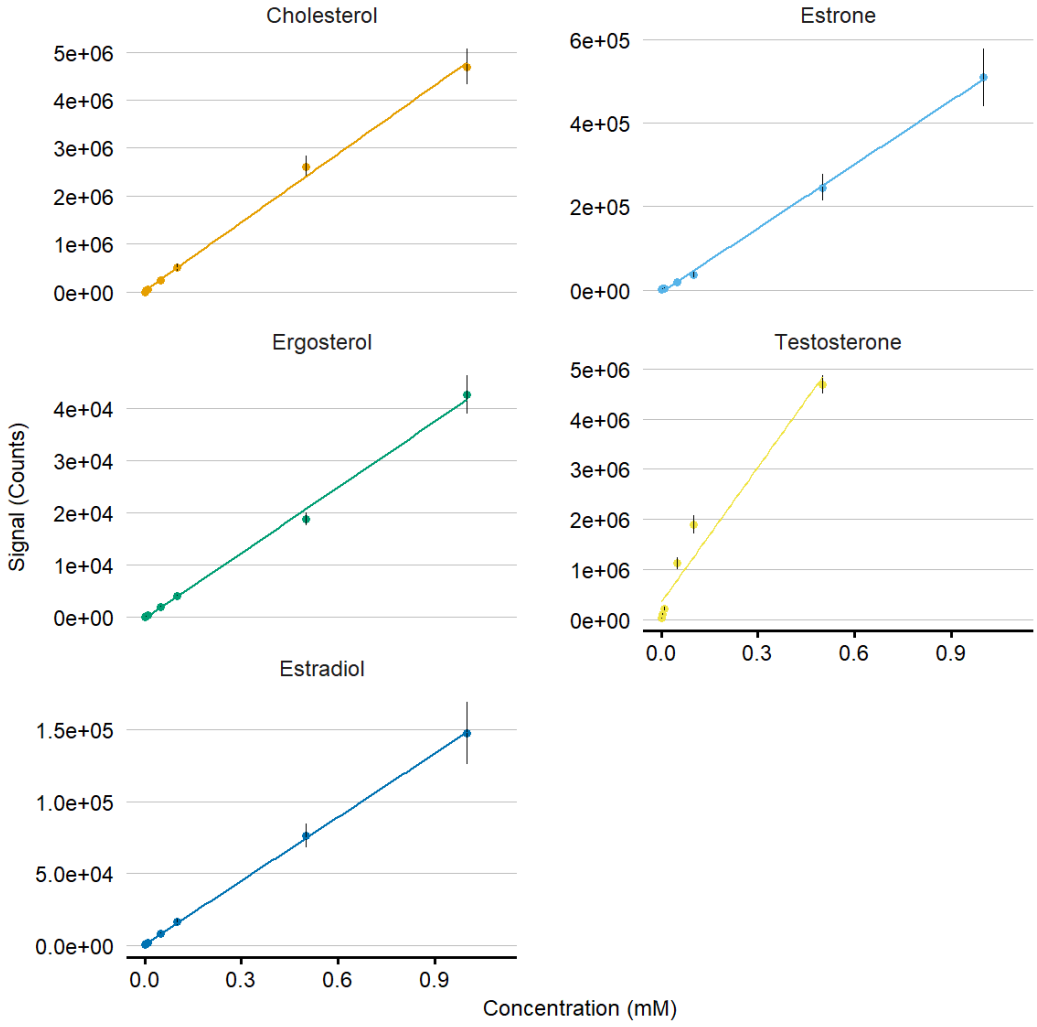

Figure 5.22: Plot of the abundance of ions against concentration for five compounds using HPLC. Linear regression analysis of the base peak for each compound cholesterol (*m/z 369*), estrone (*m/z 271*), ergosterol (*m/z 379*), testosterone (*m/z 289*), and estradiol (*m/z 255*). (Mass spectra of the ions observed are shown in figure A.11.)

SEM of 5.8 on average (range 0.2 to 12), compared to 25.6 for the loop injection and 51.0 for the solids analysis probe.

A study comparing prototype V, with ESI source, on the Waters Xevo G2-S mass spectrometer was conducted. Testosterone was selected as the model

compound due to the prototype V sensitivity. Samples at six concentrations were prepared at 0.001, 0.005, 0.01, 0.05, 0.1, and 0.5 mM and analysed using HPLC in combination with both ESI and prototype V in turn. The peak area from the XIC for the sample was recorded ($n = 3$) and the mean peak areas were plotted. A linear regression plot is presented in figure 5.23.

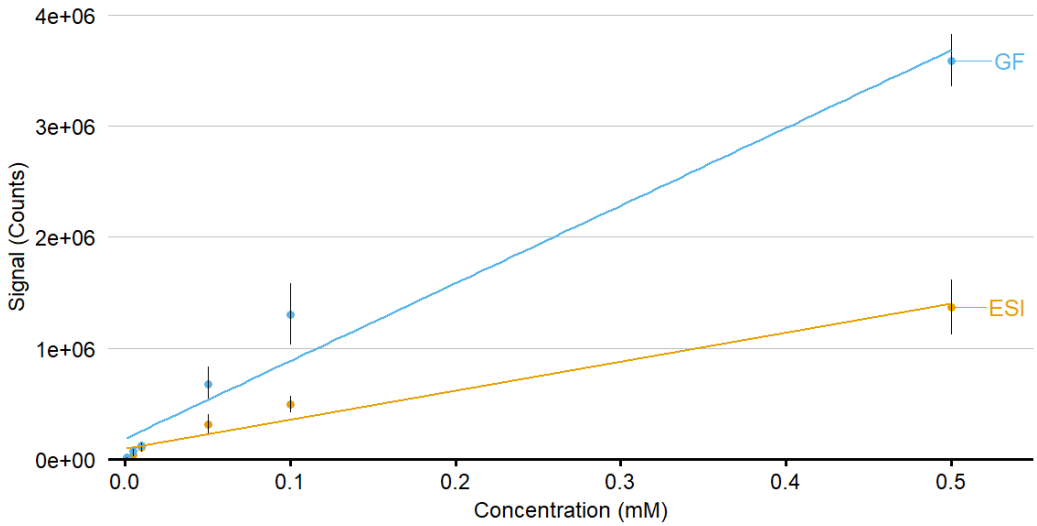

Figure 5.23: Plot of the abundance of the protonated molecule against concentration for testosterone (*m/z 289*) using HPLC. Comparing ESI and prototype V (GF) ionization sources ($N = 6$, $n = 3$).

As previously described and is seen in figure 6.5 the sensitivity of prototype V is high at $7.00 \times 10^{+6}$, less than half as (0.4 times) sensitive when compared with ESI at $2.61 \times 10^{+6}$. The DL of prototype V is lower at 0.6 $pmol\ \mu L^{-1}$ compared to 2.3 $pmol\ \mu L^{-1}$ for ESI, a 0.25 times improvement. Overall prototype V for this compound was more sensitive and had a lower DL, however, this may not be replicated for all compounds as testosterone is non-polar ($LogP = 3.3$) and ESI is reported to have lower DL in general, particularly for ionic and polar compounds [110].

5.7 Discussion and Summary

In this chapter a helium micro-glow discharge ionization source, "prototype V", has been described, and the characteristics of prototype V examined first on the bench in terms of, discharge current (I_{GD}), discharge gas flow rate (Q_{He}), thermodynamic gas temperature, inter-electrode distance (d_e) and power output (P). Based on the current-voltage relationship of the source which increases proportionally at d_e of between 5 and 10 mm supports the proposal that prototype V operates in the glow-to-arc region (figure 1.3) similar to the FAPA prototypes described in chapter 4. The "cold plasma" of prototype V determined from its thermodynamic gas temperature is unusual for glow discharges but as the power density is lower as it operates in the μA regime rather then mA this can be easily understood along with the fact the discharged is not confined in a cell may allow further cooling. At the larger d_e of 20 mm there would appear to be a marked change in the discharge's behaviour with the voltage current relationship more consistent with the "normal glow" where the voltage is constant with varying

current. This could be as a result of a change in the breakdown voltage based on Paschen's law as a result of $P.d_e$ changing.

The integration of prototype V ionization source with the Waters Xevo G2-S mass spectrometer was also reported. It allowed prototype V to be used in combination with existing sample introduction methods and could facilitate multi-modal platform using multiple ionization sources either simultaneously or sequentially. Furthermore the optimisation of the source operating conditions *in situ* in the mass spectrometer were examined namely, the desolvation gas flow rate and temperature, the discharge current, the discharge gas flow rate, the effect of sample volume and sample phase ("wet vs "dry"), and the tuning of ionization process were all examined. The optimal operating conditions were determined using the interchangeable probe assembly with the solids analysis probe. Optimal conditions were found to be; the desolvation gas is 400 $L\ h^{-1}$ at 350 $°C$, the optimal helium discharge gas rate is 0.4 $L\ min^{-1}$, while prototype V is capable of operating over 5-10 mm inter-electrode distances without any measurable change in power output. The "dry" sample introduction method provided better reproducibility (RSD 11.6 % compared to 25.7 %), however this was, in general, at the expense of ion abundance when compared to the "wet" introduction method. Reproducing previous reports [109] of tuning the ionization process to favour charge transfer over protonation could not be reproduced with this design as it is suspected the power output of the source is insufficient given the "cool" thermodynamic gas temperature of 22.4 $°C$.

The development of analytical figures of merit for prototype V ionization source was reported using a ASAP probe, flow infusion using the APCI IonSABRE II probe with a 1 μL loop and a HPLC system. These were limit

of detection, range of reliable response, and reproducibility. For the probe in combination with prototype V, the DL was in the range of 0.1 - 27.0 $pmol\ \mu L^{-1}$ and good linearity over four orders of magnitude (R^2 0.9678 - 0.9988) was reported which is comparable to DL reported with prototype II on the Thermo Scientific LTQ Orbitrap XL mass spectrometer of 7 $pmol\ \mu L^{-1}$ with cinnamaldehyde [71]. DLs in sub-femtomole concentration range have been previously reported using some FAPA ionization sources, 0.004 $fmol$ for ametryn and 0.24 $fmol$ for isoproturon [33], however the DL is generally specific to a compound or class of compounds. On this basis the *probe-source* combination would be a powerful tool for qualitative determination of compounds at low concentrations and for measurements where the highest level of precision was not the main factor. Overall the use of the loop injector using the same operating conditions proved to be more reproducible and sensitive. The loop injector delivers the sample in a discreet and focused packet compared to the probe where the sampling probe is introduced manually into the desolvation gas stream and the analyte is desorbed over a short but less predictable period. Both techniques are rapid and show the suitability in combination with prototype V for the analysis of known target compounds particularly in combination with high resolution instruments capable of separation of isotopologues. The coupling of HPLC with prototype V reported DL in the range of 0.02 - 7.53 $pmol\ \mu L^{-1}$ and good linearity over four orders of magnitude ($R^2 > 0.99$). In comparison the lower limit of detection for estrone, estradiol, and testosterone by LC-ESI-MS/MS was reported as 0.1, 0.3, and 0.1 pg, respectively [111], and by LC-APCI-MS/MS was reported as 0.2, 0.08, and 0.04 $ng\ mL^{-1}$, respectively [112], both of which are in a similar range to prototype V. Initial studies with testosterone tentatively reported enhances sensitivity of

prototype V when compared with ESI. However, it must be noted that this effect could be compound dependent.

In summary, a compact helium micro-glow discharge ionization source was developed, and its micro-glow discharge has been characterised. The micro-discharge differed to that observed for the conventional FAPA discharges in that it was cooler but not withstanding this the source operates in the abnormal glow region of the voltage current plot. Prototype V exhibits low detection limits in the picomole range for testosterone, estrone, estradiol, cholesterol, and ergosterol using both the solids probe and heated nebulized liquid (from flow-infusion and LC), suggesting that it could have utility as a high sensitivity source for a range of compounds.

Chapter 6

Assessment of prototype V for the analysis of polar and non-polar compounds

6.1 Introduction

A study of prototype V is made with a broad range of sample chemistries and compound types were selected to reflect the breadth of samples that are analysed by mass spectrometry in university, public sector, and commercial laboratories. It was shown in chapters 1 and 3 that a range of ionization pathways are available to APGD sources, and this study aims to identify the ions predominantly formed by prototype V ionization source. Previous studies of FAPA have primarily focused on the analysis of explosives, pharmaceuticals, and agrochemicals [113, 34, 12, 33, 64]. The types of compounds selected for this study include not only "small molecule" fine chemicals and pharmaceuticals, but

also synthetic polymers, carboxylic acids, PAH, synthetic oils, biodiesel covering a range of predominantly non-polar compounds which are less amenable to analysis by ESI. In addition non-polar lipids (fatty acids, hydroxy fatty acids, sterols, and sophorolipids) and polar oligopeptides have been selected to determine the capabilities of prototype V ionization source. Previous studies of FAPA have primarily focused for bio-analysis. These compounds and biomolecules have a range of physical and chemical properties some of which are tabulated in chapter 2 such as melting point and water n-octanol partition coefficient (Log P) along with vapour pressure, EI and PA amongst others, all effect their propensity to volatilise and ionise. It is suspected that the primary ionization processes of prototype V will mirror that of API and will rely on the Brønsted acid-base reactions where the PA(molecule) > PA(H_3O^+) of 697 $kJ\ mol^{-1}$ resulting in the formation of protonated molecule.

A range of sample introduction techniques was used in the study namely solids analysis probe, flow infusion ("shotgun") with loop injection, and HPLC to establish the versatility of prototype V depending on the type of sample. Data in this study were acquired using a Waters Xevo G2-S time-of-flight mass spectrometer operating in full scan mode m/z 50-1,200 in either positive or negative mode, further details of sample preparation, operating and instrument conditions is provided in chapter 2. Data was processed using Waters MassLynx 4.1 and the ions observed are discussed in the following sections. Peak areas for ions of interest were integrated from the XIC, and accurate mass measurement [114] of ions was conducted from known background ion (e.g. m/z 391.2848 diisooctyl phthalate) that were used as lock-mass.

6.2 Prototype V source for the analysis of small molecules

Molecules can be classified by their physical properties including, lipophilicity, structure, or functional groups, and in chemistry and life sciences molecular mass is sometimes used to classify molecules. "Small molecules" can be defined as those with molecular mass less than 500 $g\ mol^{-1}$ following Lipinski's rule of five [115] which are considered bioactive. Lipinski specified his rules for bioactive or orally active pharmaceuticals, specifically (i) they have no more than 10 hydrogen bond acceptors, (ii) they have no more than five hydrogen bond donors, (iii) they have a Log P value less or equal to five, and (iv) their molecular mass less than 500 $g\ mol^{-1}$. More generally compounds are considered to be "small molecules" when they have a molecular mass below about 900 $g\ mol^{-1}$ [116].

6.2.1 LC-MS of six compounds

Isolation and identification of small molecules is important for fine chemicals and pharmaceutical industry as well as for the identification of bioactive components in natural products. Six compounds which meet Lipinski's rule of five were selected namely caffeine, chloramphenicol, cumarin, 1-isoquinolinol, 4-hydroxybenzyl alcohol and 4-methoxybenzyl alcohol. These compounds were selected as they had water n-octanol partition coefficient of less than 5, ranging from -0.1 (caffeine) to 1.4 (cumarin) and covered a mass range from 124 to 322 $g\ mol^{-1}$. Pairs of compounds were also selected, such as 4-hydroxybenzyl alcohol and 4-methoxybenzyl alcohol that share the same base structure except for the

substitution of a hydrogen for a methyl group. This significantly changes their lipophilicity (0.2 verses 1.1 respectively) and their phase at room temperature solid (M.pt. 124.5 $°C$) compared to liquid (M.pt. 25 $°C$). A second pair, cumarin which has antifungal properties [117] and 1-isoquinolinol have similar ring structures, masses (146.0 and 145.1 $g\ mol^{-1}$, respectively) and Log P values of 1.4 and 1.3, respectively. The compounds were prepared at a concentration of 1 μM and analysed by LC-MS. Solvent A was water with 2 % acetonitrile and 0.2 % acetic acid, Solvent B was acetonitrile with 0.2 % acetic acid, column Fortis C_{18} 3 μm, 2.1 $\times$ 150 mm. The gradient was optimised, the starting conditions were 30 % Solvent B for 5 minutes, rising to 70 % B at 20 minutes and held at 70 % for a further 5 minutes, before re-equilibrating to 30 % B over 5 minutes.

A base peak ion chromatogram is shown in figure 6.1 with the seven compounds clearly separated between 5 and 30 minutes. The compounds generally eluted in order of increasing lipophilicity, though exceptions are noted such as caffeine (Log P = -0.1) eluted after 4-hydroxybenzyl alcohol (Log P = 0.2). Another exception was 1-isoquinolinol (Log P = 1.3) eluted before 4-methoxybenzyl alcohol and chloramphenicol both with Log P of 1.1. In this case it could be as a result of isoquinolinol having a tautomeric isoquinolin-1-one form with different hydrophilicity (figure 6.2). Data clearly identifying the physical and chemical properties of each tautomer is not readably available, however differences in hydrogen bonding were reported for amide and hydroxy groups in proteins and peptides [118] suggesting solvation and functional group interaction could change the partition coefficient. The analysis was repeated five times and the average intensity of the peak area was calculated for each compound (table 6.1). The integrated peak areas vary by almost two orders of magnitude between the

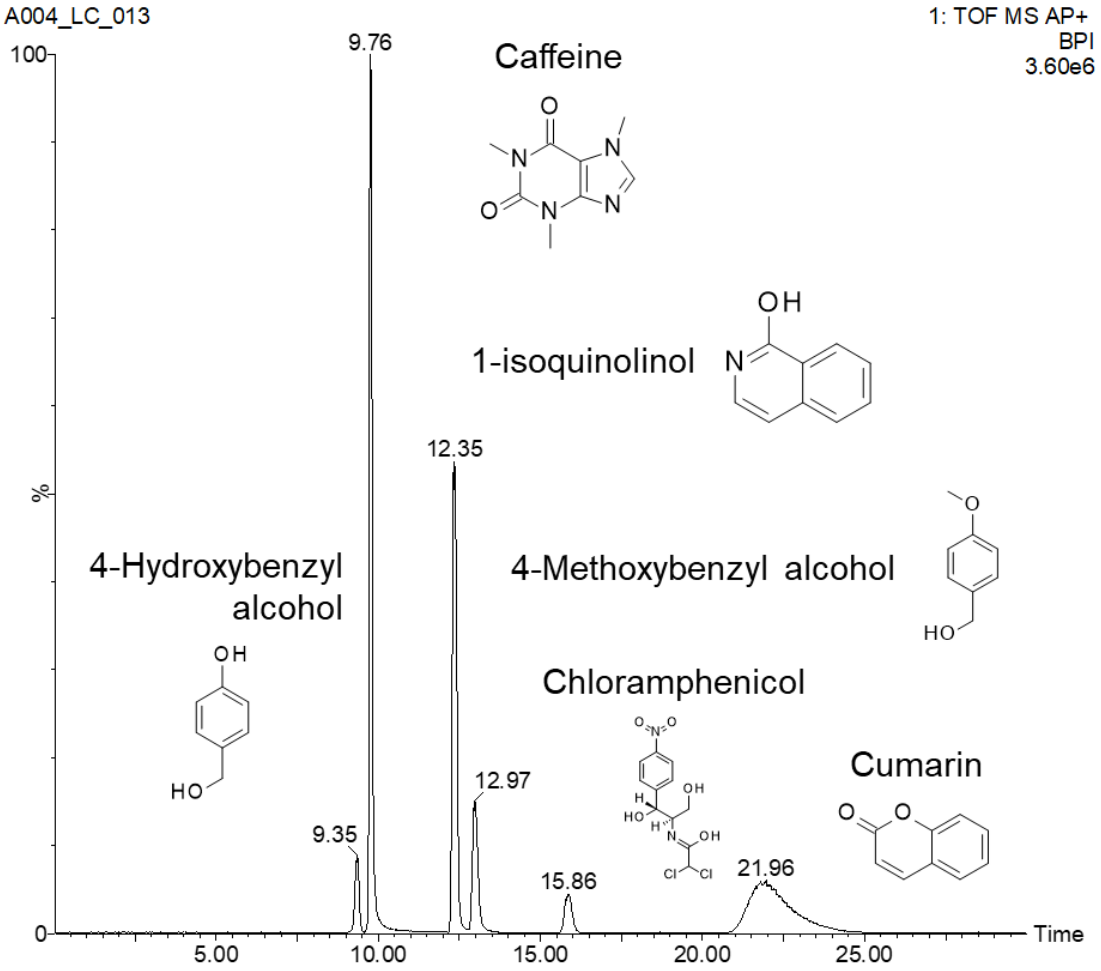

Figure 6.1: Base peak ion chromatogram of six compounds separated by prototype V source mass spectrometry. In order the compounds eluted 4-hydroxybenzyl alcohol at t_R 9.35 min, caffeine at t_R 9.76 min, 1-isoquinolinol at t_R 12.35 min, 4-methoxybenzyl alcohol at t_R 12.97 min, chloramphenicol at t_R 15.86 min, and cumarin at t_R 21.96 min. (Mass spectra of the observed ions is shown in figure A.13.)

compounds even-though the samples were prepared in equimolar concentrations suggesting differences in ionizability and PA of the compounds.

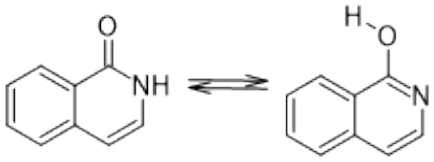

Figure 6.2: Tautomer forms of isoquinolin-1-one and isoquinolin-1-ol.

Table 6.1: List of the six compounds separated by of LC-MS. The ion associated with each compound is listed, along with the retention time (t_R), and the intensity of the peak area ($N = 5$).

Compound	m/z [Ion]	t_R (min)	Peak Area
4-Hydroxybenzyl alcohol	107.05 $[M + H - H_2O]^+$	9.1-9.8	1.47E+5
Caffeine	195.09 $[M + H]^+$	9.4-10.1	1.10E+6
1-Isoquinolinol	146.06 $[M + H]^+$	11.7-12.8	8.28E+5
4-Methoxybenzyl alcohol	121.06 $[M + H - H_2O]^+$	12.4-13.7	3.15E+5
Chloramphenicol	323.02 $[M + H]^+$	14.3-18.7	3.13E+4
Cumarin	147.04 $[M + H]^+$	18.3-21.9	9.02E+5

6.2.2 Low-average molecular mass polymers

Polymers are large molecules made of repeating units, or monomers, where they occur widely in nature and are also made synthetically. Polysaccharides, peptides, and polynucleotides are examples of important polymers in biochemistry. The first synthetic polymer was Bakelite developed in the early 1900 and since then a wide range of polymers have been developed which are used ubiquitously. Small polymers are used as internal reference standards in mass spectrometry [119] for accurate mass measurement. Environmental plastic pollution has been highlighted as a major problem and detection of microplastics is an emerging area of interest [120, 121, 122].

A study of three low average-molecular mass polymers, namely polyethylene glycol, polypropylene glycol and polyethylenimine, was undertaken using prototype V ionization source. The samples were prepared at concentrations of 1 $\mu g.\mu L^{-1}$, and 1 μL was syringed on the end of a glass capillary before being introduced into the source. The resulting mass spectra presented in figure 6.3 show the protonated molecule for all three polymers with the repeating units seen for each polymer of, m/z 44.03 for polyethylene glycol, m/z 58.04 for polypropylene glycol, and m/z 43.04 for polyethylenimine. Using high resolution mass spectrometry the accurate mass measurement was recorded of one of the polyethylene glycol ions at m/z 459.280, and a report was produced listing all the possible composition within an uncertainty, δ[123], of 1.0 mDa in table 6.2. Of the five possible compounds that were listed the calculated m/z of 459.2805 (-0.5 mDa) was the only one that corresponded to the molecular formulae of the protonated molecule of polyethylene glycol $[(C_2H_{4+2}O_1)_{10} + H]^+$.

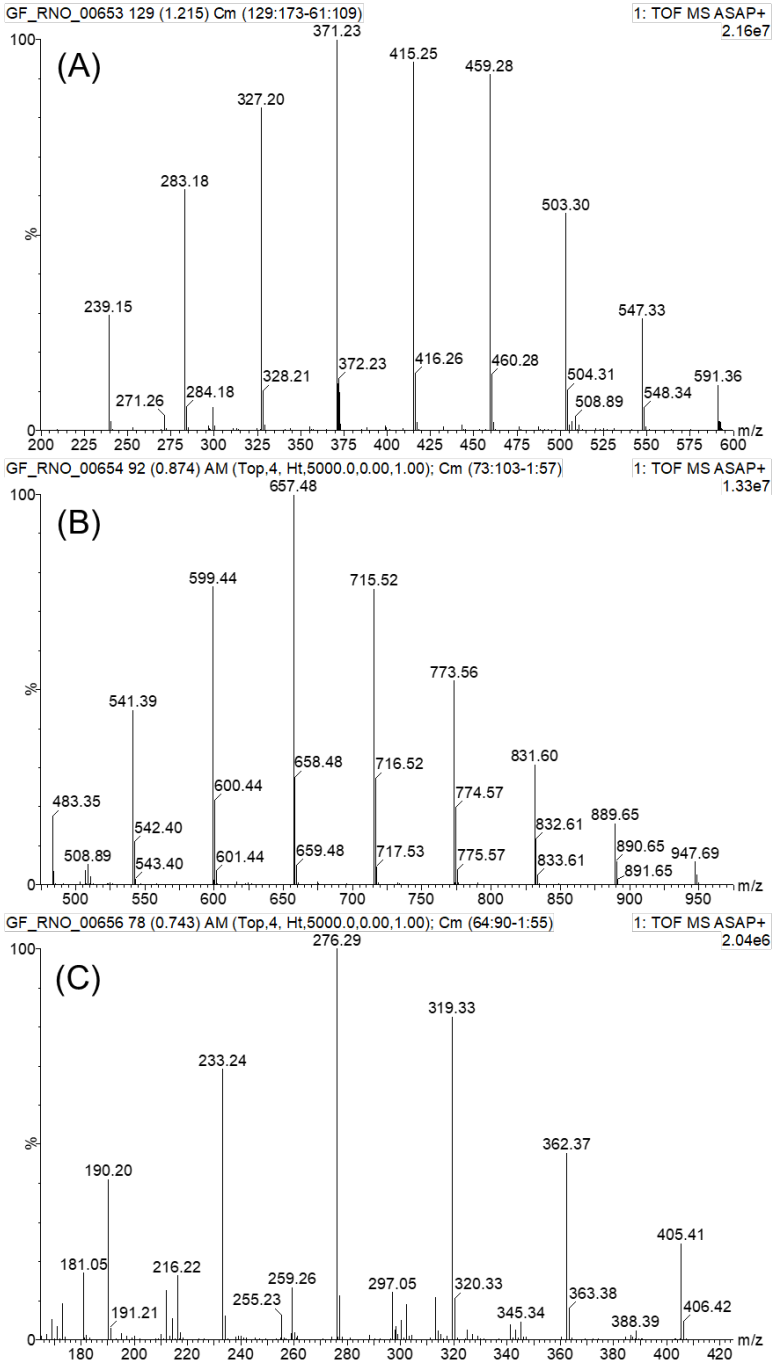

Figure 6.3: Mass spectra of low molecular weight polymers using prototype V ionization source. Polyethylene glycol *m/z* 239.15 to 591.36 with repeating unit m/z 44.03 (A). Polypropylene glycol *m/z* 483.35 to 947.69 with repeating unit m/z 58.04 (B). Polyethylenimine *m/z* 190.20 to 405.41 with repeating unit m/z 43.04 (C).

Table 6.2: Elemental composition report using accurate mass measurement of the polyethylene glycol ion at *m/z* 459.2800, showing all possible options for an ion with elements C, H, N, and O composition within 1.0 mDa. For each calculate *m/z* the corresponding uncertainty, δ, in mDa with respect to the measured *m/z*, the degree of unsaturation (DBE), the % confidence of the isotope profile, and empirical formula of the ion is listed.

Calc. m/z	δ (mDa)	DBE	Conf (%)	Formula
459.2800	0.0	17.5	1.83	$C_{33}H_{35}N_2$
459.2805	-0.5	-0.5	66.13	$C_{20}H_{43}O_{11}$
459.2805	-0.5	5.0	11.18	$C_{19}H_{37}N_7O_6$
459.2792	0.8	0.0	16.70	$C_{18}H_{41}N_3O_{10}$
459.2792	0.8	5.5	4.17	$C_{17}H_{35}N_{10}O_5$

6.2.3 Analysis of compounds containing benzoic acids

Negative ion mass spectrometry is not as commonly used as positive ion mass spectrometry because fewer compound classes undergo de-protonation [57]. Nonetheless, it is more sensitive for certain compound classes e.g. electro-negative species and as there are generally fewer background ions generated can lead to clearer mass spectra.

In this study a selection of five benzoic acids were selected for analysis, namely 3-nitrobenzoic acid, 2,5-dihydroxybenzoic acid, 4-fluorobenzoic acid, pentafluorobenzoic acid, and pentafluorocinnamic acid. They are generally non-polar in character with Log P values of between 1.6 and 2.4. The samples were prepared to a stock concentration of 1 mM in methanol, and further diluted to working concentrations of between 5 and 500 $pmol\ \mu L^{-1}$.

Analysis of 4-fluorobenzoic acid by loop-injection

The compound 4-fluorobenzoic acid was selected and analysed at a concentration of 100 $pmol\ \mu L^{-1}$ by direct infusion using a 1 μL injection loop. A mass spectrum is presented in figure 6.4 showing the base peak as the de-protonated molecule $[M-H]^-$ at m/z 139.0. Also observed was an ion at m/z 95.0 at relative intensity 13.4 %, of the base peak, which would appear to be the result of fragmentation of the bond between the carbonyl group and the aromatic ring, resulting in the formation of a stable 4-fluorobenzyl fragment ion.

Separation of five benzoic acid compounds by LC-MS

To establish analytical figures of merit using prototype V in negative-ion with chromatography, a study involving the five benzoic acid compounds was conducted using HPLC to separate the components in the sample. An Agilent 1100 series HPLC was used with a Fortis C_{18} column 3 μm, 2.1 $\times$ 150 mm. Solvent A was water with 2 % acetonitrile and 0.2 % acetic acid, and solvent B was acetonitrile with 0.2 % acetic acid. The initial conditions in this study were, the gradient at 0 minutes was 0 % solvent B increasing to 95 % solvent B at 20 minutes at a rate of 0.2 $mL\ min^{-1}$. A chromatogram is presented in figure 6.5 showing the separation of the compounds between 10 to 20 minutes. Four of the compounds are clearly separated and identifiable namely, 2,5-dihydroxybenzoic acid (t_R = 11.82, $LogP$ = 1.6), pentafluorobenzoic acid (t_R = 13.20, $LogP$ = 2.0), 3-nitrobenzoic acid (t_R = 13.54, $LogP$ = 1.8), and 2,3,4,5,6-pentafluorocinnamic acid (t_R = 14.99, $LogP$ = 2.4). No distinct peak can be seen for the compound 4-fluorobenzoic acid, and when a XIC for the ion

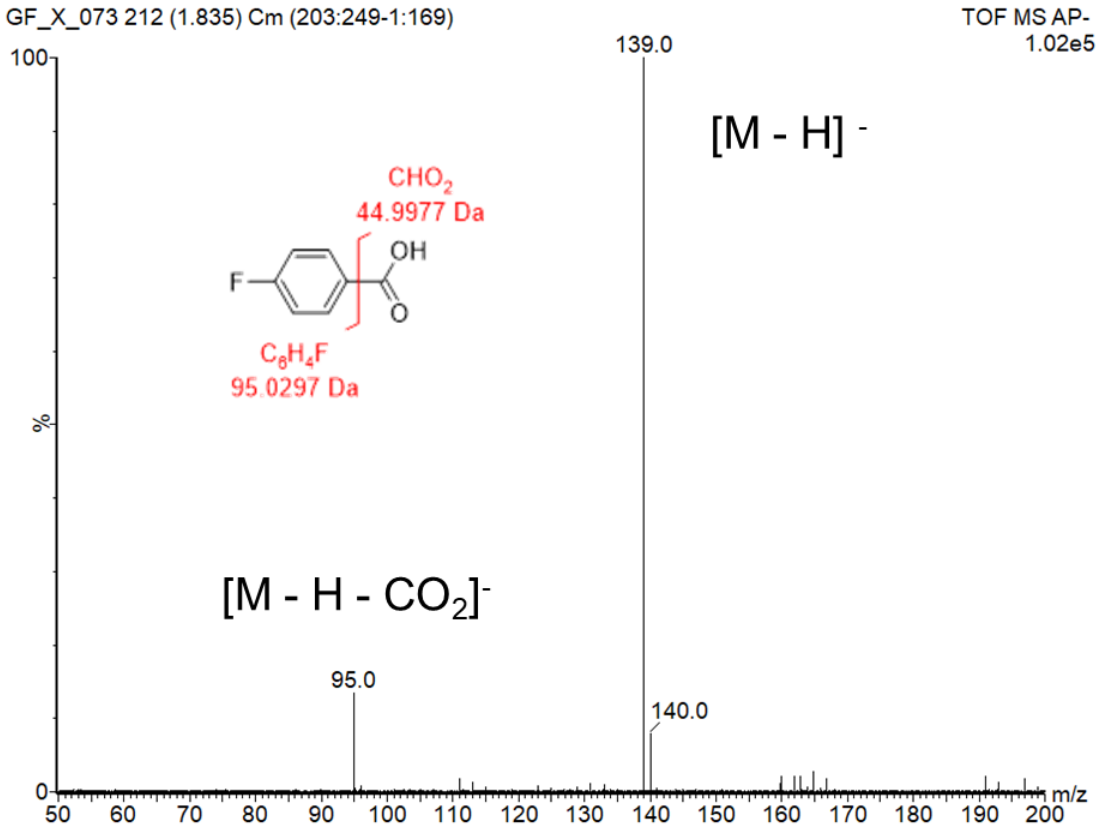

Figure 6.4: Mass spectrum of 4-fluorobenzoic acid by negative-ion mass spectrometry using prototype V. The base peak ions at *m/z* 139.0 is the de-protonated molecule $[M-H]^-$, also observed was an ion at *m/z* 95.0 $[M-H-CO_2]$ (13.4 % intensity of the base peak) possibly resulting from fragmentation occurring at the bond of the benzyl ring and CO_2 group of the de-protonated molecule.

at m/z 139 was made it was shown as co-eluting at $t_R = 13.54\ min$ and had a relative intensity of only 1.9 %.

The initial HPLC method provided good separation of the compounds, however, as the first compound did not elute until $t_R = 11.82\ min$ it was not optimal in terms of maximising efficiency. The method was therefore optimised by altering the gradient conditions as follows, at 0 minutes 45 % solvent B at a rate of 0.2 $mL\ min^{-1}$, increasing to 18 min at 85 % solvent B.

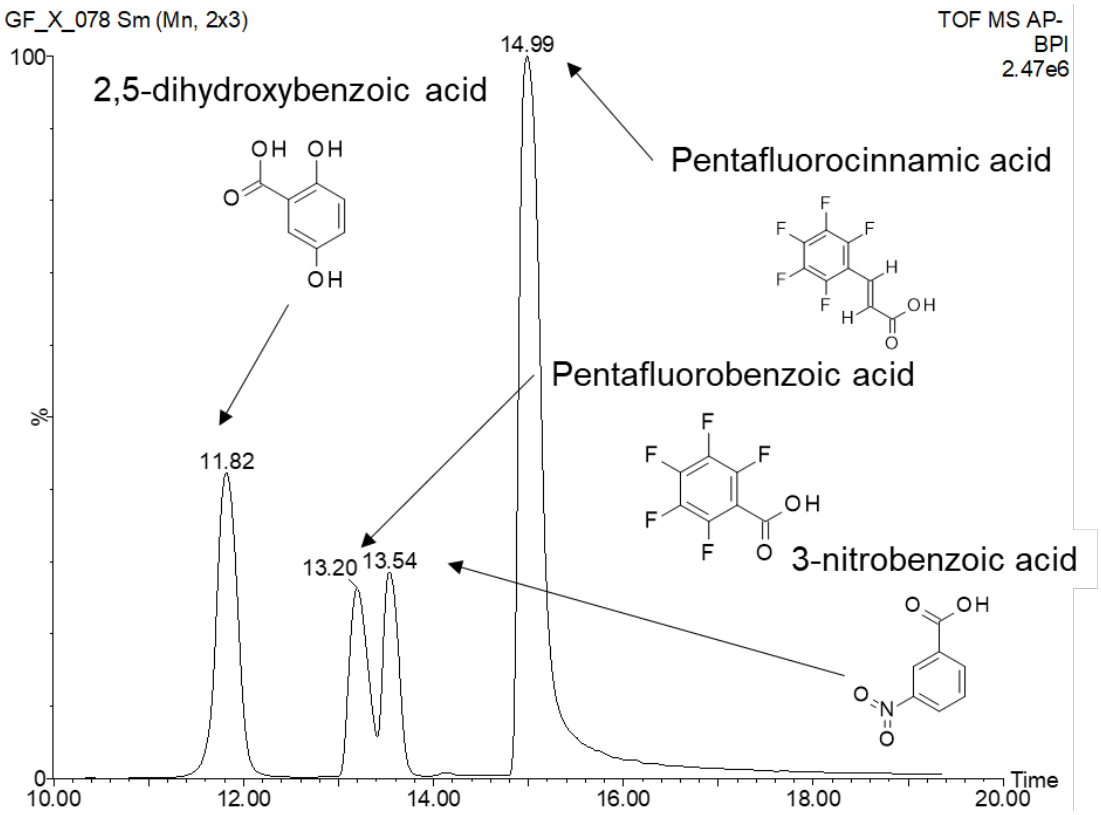

Figure 6.5: Chromatogram at t_R 10 to 20 min of five benzoic acid compounds at 100 μM. Four of the compounds could be readily separated and identified 2,5-dihydroxybenzoic acid (t_R = 11.82, $LogP$ = 1.6), pentafluorobenzoic acid (t_R = 13.20, $LogP$ = 2.0), 3-nitrobenzoic acid (t_R = 13.54, $LogP$ = 1.8), and 2,3,4,5,6-pentafluorocinnamic acid (t_R = 14.99, $LogP$ = 2.4). The compound 4-fluorobenzoic acid ($LogP$ = 2.1) appeared to co-elute at t_R = 13.54 with the 3-nitrobenzoic acid and had weak ions (relative intensity of 1.9 % of the base peak).

Analytical figures of merit for benzoic acid compounds by LC-MS

In the previous chapter the analytical figures of merit were all conducted in positive-ion using prototype V. Therefore to gain an understanding of the analytical capabilities in negative-ion of prototype V an experiment using three of the benzoic acid compounds was undertaken by LC-MS. A series of five dilutions were prepared at concentrations of 500, 100, 50, 10 and 5 μM and the analysis

was conducted in triplicate. The linear regression plots are presented in figure 6.6 and a summary of the results has been tabulated in table 6.3. Over three-orders of magnitude the DL is between 122 and 153 $pmol\ \mu L^{-1}$, which is an order of magnitude greater than for the compounds examined in positive-ion by prototype V.

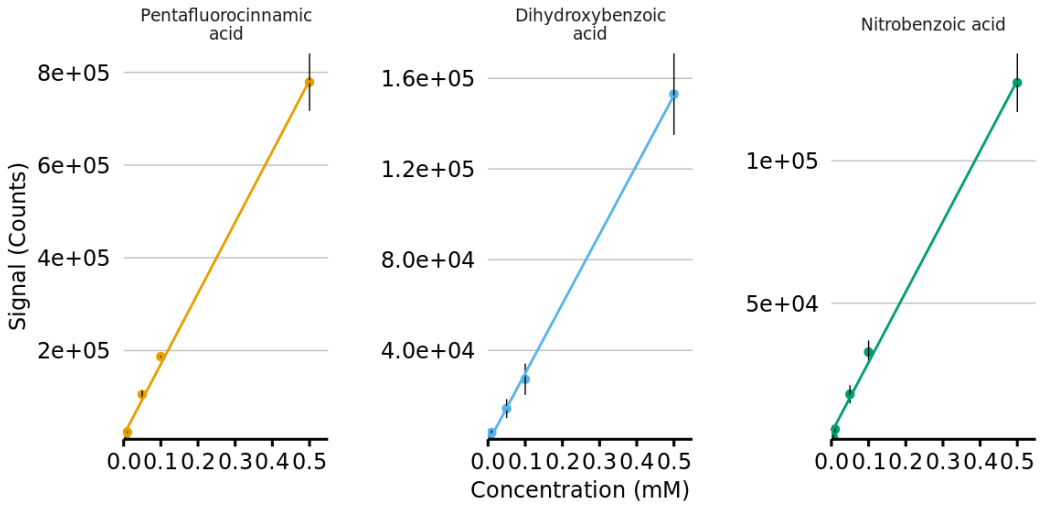

Figure 6.6: Linear regression plots of three benzoic acid compounds. The DL was 122, 177, and 125 $pmol\ \mu L^{-1}$ for pentafluorocinnamic acid ($R^2 = 0.9983$), dihydroxybenzoic acid ($R^2 = 0.9995$), and nitrobenzoic acid ($R^2 = 0.9978$), respectively.

Table 6.3: Analytical figures of merit for three benzoic acid compounds. Listed is the observed ion, DL, SEM and coefficient of determination for each compound.

Compound	Observed m/z	DL ($pmol\ \mu L^{-1}$)	SEM	R^2
Pentafluorocinnamic acid	237	122	22	0.9983
Dihydroxybenzoic acid	153	177	9	0.9995
Nitrobenzoic acid	166	125	14	0.9978

Therefore in negative-ion, prototype V is capable of the analysis of compounds

which typically undergo de-protonation, specifically benzoic acids. Optimised LC-MS method in negative-ion mode has been developed to quickly analyse in less than eight minutes and separate the majority of compounds (80 %) in the sample. In negative-ion mode prototype V has a DL in the pico-mole range for the compounds investigated with good linearity over three orders of magnitude (R^2 >0.998).

6.3 Prototype V for petroleomics characterisation

"Petroleomics" is the analysis and classification of petrochemicals. Mass spectrometry has been used widely for the characterisation of fossil fuels. This usually involve the use of ultra-high resolution mass spectrometry such as FT-ICR of crude oils [124, 125]. However, more recently distillates, additives and biofuels are routinely analysed by GC-MS and LC-ESI-MS as well as ADI methods [126, 127, 128]. Analysis of these fuels and oils provides critical information on the composition and therefore a greater understanding of how the components may interact or degrade over time [129].

6.3.1 Analysis of poly-aromatic hydrocarbons by LC-MS

PAH are non-polar molecules consisting of two or more aromatic rings made up of only hydrogen and carbon. They are commonly found in oil and coal deposits formed by geological processes and can also be generated in industrial processes such as by wood burning or in tobacco smoke [130]. Exposure to PAH has been

linked to increased risk of cancer, the mechanism is due to the formation of deoxyribonucleic acid (DNA) adducts with epoxides and other PAH metabolites leading to mutation and replication error [131]. PAH have been shown to bind with the aryl hydrocarbon receptor increasing the production of cytochrome P450 enzymes which in turn metabolise the PAH into "toxic" epoxides [132].

A study was undertaken by LC-MS using prototype V to qualitatively separate and identify the 16 components in a PAH calibration mix. The sample was prepared at a concentration of 10 $\mu g\ mL^{-1}$ in acetonitrile for analysis. A Fortis 3 μm diphenyl column was used in the analysis, solvent A was water and solvent B was acetonitrile. A gradient starting at 0 minutes was 35 % solvent B held for five minutes before increasing to 95 % solvent B at 20 minutes at a rate of 0.2 $mL\ min^{-1}$ and held for 5 minutes, then returning to the start conditions. The compounds were identified from their respective XIC and were recorded in table 6.4. Ten distinct ions were observed which using accurate mass measurement was possible to confirm the elemental composition to with an uncertainty δ of less than 1.5 mDa. In five instances the compounds were structural isomers, and it was not possible to identify the individual compounds with this approach, as is seen in the representative mass spectra in figure A.14. If tandem mass spectrometry or ion mobility spectrometry was available further isolation of the compounds may have been achievable.

6.3.2 Analysis of Mobil Jet Oil II

According to the manufacturer Mobil Jet Oil II has been developed for air craft type gas turbines, and has been tested for stability at operating temperatures of

Table 6.4: List of the 16 compounds identified using prototype V in the PAH calibration mix. Listed is the retention time (t_R), integrated peak area, observed *m/z* and calculated *m/z* of the ion, and uncertainty (δ).

Compound	t_R (min)	Area	Obs m/z	Calc. m/z	δ (mDa)
Naphthalene	11.34	911	128.0619	128.0626	-0.7
Acenaphthylene	12.15	4,833	153.0700	153.0704	-0.4
Acenaphthene	13.04	1,763	155.0864	155.0861	0.3
Fluorene	13.19	940	167.0860	167.0861	-0.1
Anthracene Phenanthrene	14.03	3,604	178.0773	178.0783	-1.0
Fluoranthene Pyrene	15.05	3,571	203.0849	203.0861	-1.2
Benz[a]anthracene Chrysene	16.57	3,623	229.1026	229.1017	0.9
Benzo[a]pyrene Benzo[b]fluoranthene Benzo[k]fluoranthene	17.62	11,737	253.1014	253.1017	-0.3
Benzo[ghi]perylene Indeno[1,2,3-cd]pyrene	18.53	4,017	276.0949	276.0939	1.0
Dibenz[a,h]anthracene	18.81	1,785	278.1111	278.1096	1.5

204 $°C$. It is approved against U.S. Military Specification MIL-PRF-23699. It has been reported that compounds listed in the material safety data sheets [133] could be toxic if a person is inadvertently exposed to them, in particular tricresyl phosphate could react and act as a neurotoxin while n-phenyl-1-naphthylamine is a known skin sensitizer [134].

Flow infusion with prototype V

A study of Mobil Jet Oil II using flow infusion with prototype V was conducted, a 1 μL of oil diluted in 1,000 μL of acetonitrile before 1 μL was injected by loop for analysis. A mass spectrum of the sample is shown in figure 6.7 showing a complex mixture of ions and what appear to be overlapping polymeric series

making interpretation difficult.

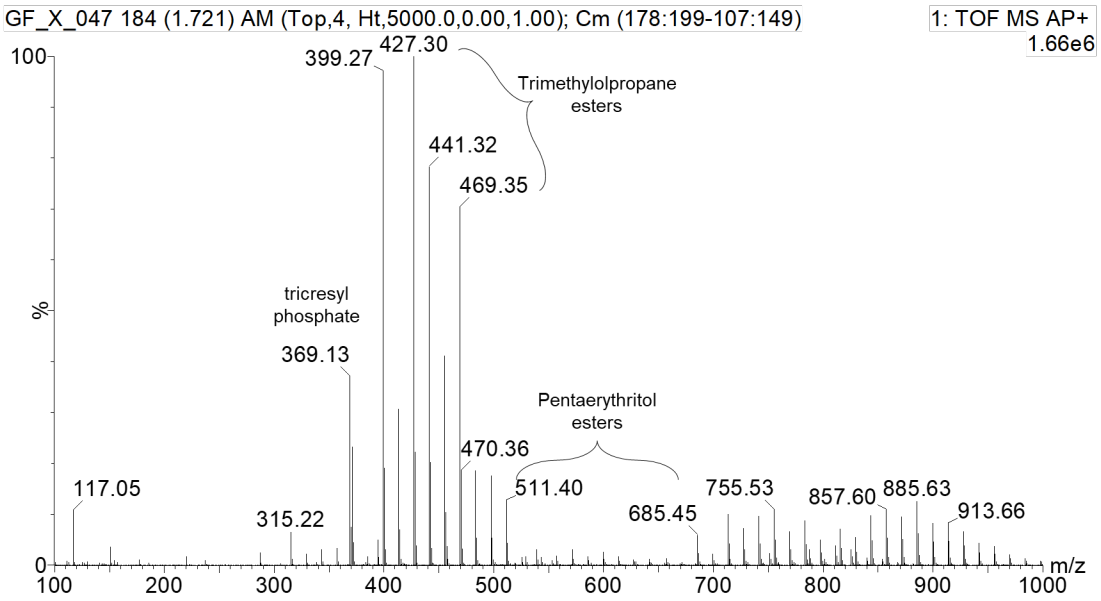

Figure 6.7: Mass spectrum of Mobil Jet Oil II by micro-glow discharge mass spectrometry. Sample introduced using flow infusion and 1 μL injection loop. The spectrum is complex and consists of overlapping polymeric series making interpretation more complex.

In addition to the components listed in the material safety data sheets in other oils, poly(alkyl) methacrylates and alkyl diphenylamies have also been noted [126]. A Kendrick mass analysis was conducted on the mass spectrum in figure 6.7, that involves the calculation of the Kendrick mass and the KMD using the method described in chapter 2, and the resultant data are plotted in figure 6.8. Using a combination of known compounds, accurate mass measurement and data from the Kendrick mass analysis it is possible to assign putative formulae to the ions observed. The KMD are tabulated along with the m/z values and empirical formula of the base unit in table 6.5. Separately ions corresponding to the n-phenyl-1-naphthylamine and tricresyl phosphate are observed at m/z 220.1119 (theoretical 220.1126 $\delta - 0.7\ mDa$) and m/z 369.1259 (theoretical

369.1256 $\delta 0.3$ mDa), respectively.

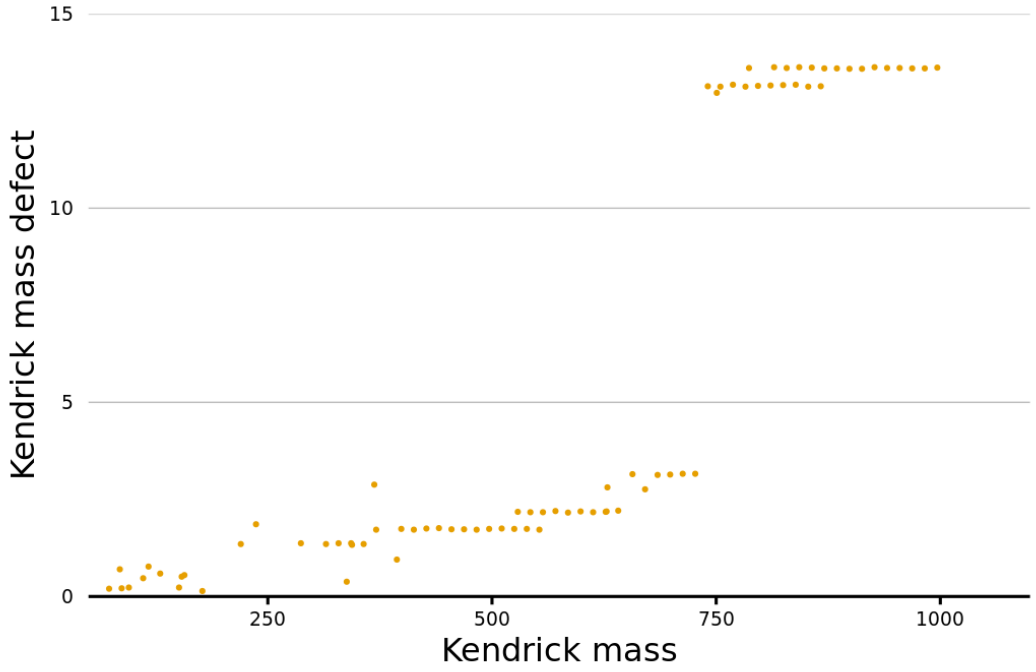

Figure 6.8: Plot of the Kendrick mass against the KMD using the method described in chapter 2 [87]. Six-series of compounds with repeating CH_2 units can be identified from their common KMD at 1.4, 1.7/1.8, 2.2, 3.1/3.2, 13.1/13.2, and 13.6.

Table 6.5: List of compounds identified by prototype V in Mobil Jet Oil II. Shown are the KMD values taken from figure 6.8, the corresponding observed *m/z* of the ions, the calculated empirical formula of the base unit and repeating unit, and where identified the compound name.

KMD	Observed m/z	Base Unit	Putative compound name
1.4	287.1844-357.2650	$C_5H_6O_5$+$n(CH_2)$	
1.7/1.8	371.2437-553.4485	$C_7H_8O_6$+$n(CH_2)$	Trimethylolpropane esters
2.2	529.3752-641.4977	$C_7H_8O_8$+$n(CH_2)$	Pentaerythritol esters
3.1/3.2	657.4214-727.4985	$C_7H_4O_{11}$+$n(CH_2)$	
13.1/13.2	741.5162-867.6583	$C_6H_2O_{11}$+$n(CH_2)$	
13.6	787.5211-997.7560	$C_{11}H_{12}O_{13}$+$n(CH_2)$	

LC-MS of Mobil Jet Oil II

Another approach to investigating the components in this oil is by LC-MS using prototype V. An isocratic mobile phase was used to separate the compounds and an experiment was conducted using increasing proportions of acetonitrile at 60, 80 and 90 % which are seen in figure 6.9. At the lowest concentration of acetonitrile examined (60 %) the components did not seem to be well retained on the column and co-eluted near the beginning of the analysis, while at the highest concentration of acetonitrile (90 %) there was good separation and higher resolution. A summary of the compounds identified at 90 % concentration of acetonitrile is included in table 6.6, which had distinct retention times. Many of the polymeric compounds appeared to co-elute, as seen in figure A.15, sometimes at multiple retention times making identification of the retention times for the compounds difficult.

Table 6.6: List of compounds identified by prototype V using LC-MS in Mobil Jet Oil II.

Compound	t_R (min)	Observed m/z	Theoretical m/z	δ (mDa)
n-phenyl-1-naphthylamine	2.50	220.1134	220.1126	0.8
tricresyl phosphate	2.67	369.1261	369.1256	0.5

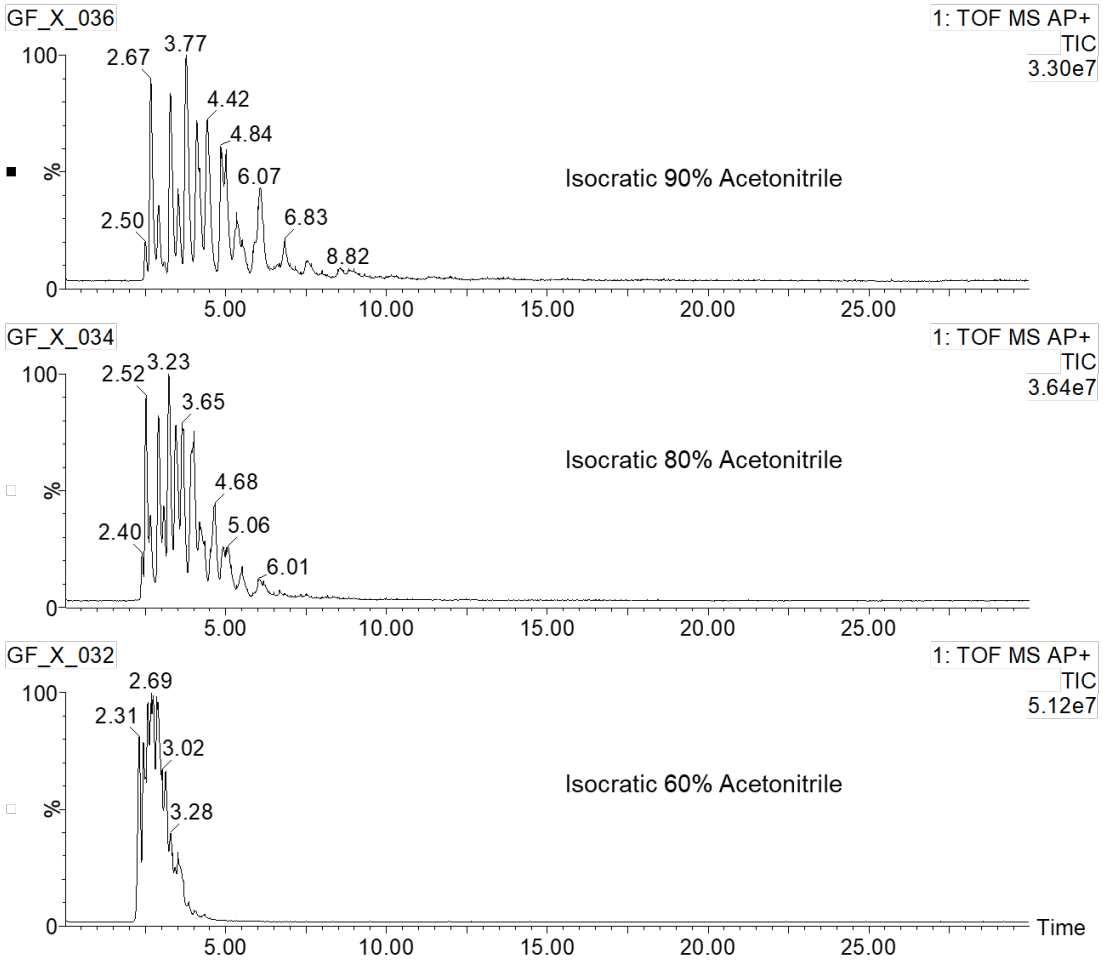

Figure 6.9: Total ion chromatogram (TIC) chromatogram of Mobil Jet Oil II by LC-MS using prototype V. Increasing the percentage of solvent B (acetonitrile) in the LC mobile phase improves separation of the compounds found in the jet oil, as seen in figure A.15.

6.3.3 Analysis of biodiesel

An alternative to fossil based fuels are those of biological origin, such as plants and micro-organisms. UK Government had set a target of 10 % green renewable energy use for road and rail transport by 2020 as part of a strategy to reduce greenhouse gas emissions. Problems associated with FAMEs in biodiesel have been ascribed to cloudiness and stability at low temperatures [129]. The cold filter plugging point is set by national standards to ensure the biodiesel will provide trouble free flow in engines at a minimum operating temperature. A biodiesel standard (ERM - EF001) was analysed using prototype V in combination with a solids-analysis probe, and the resulting mass spectra is presented in figure 6.10. Observed in the mass spectra are the methyl esters of unsaturated palmitic acid (m/z 271.3), stearic acid (m/z 299.3), arachidic acid (m/z 327.3), behenic acid (m/z 355.4), the monounsaturated oleic acid (m/z 297.3), and the polyunsaturated linolenic acid (m/z 293.3). The prototype V ionisation source could be an useful method for the rapid detection and qualitative analysis of components in biodiesel.

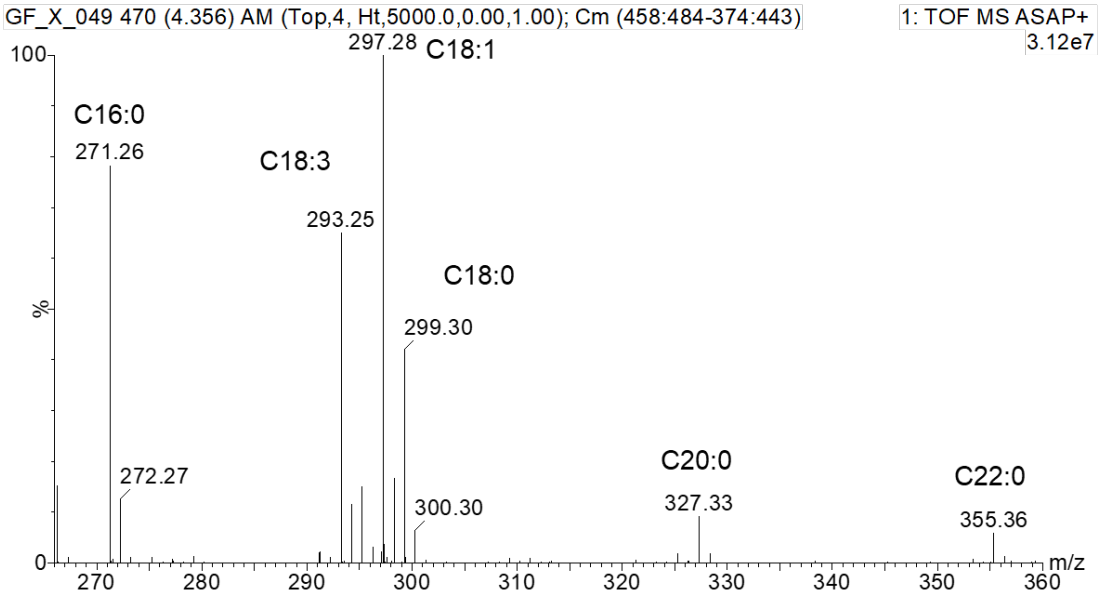

Figure 6.10: Mass spectrum of biodiesel by solids analysis probe using prototype V. Observed are intense ions for unsaturated palmitic acid methyl ester (C16:0, *m/z* 271.3), stearic acid methyl ester (C18:0, *m/z* 299.3), arachidic acid methyl ester (C20:0 *m/z* 327.3), and behenic acid methyl ester (C22:0, *m/z* 355.4). Also observed are the monounsaturated oleic acid methyl ester (C18:1, *m/z* 297.3) and polyunsaturated linolenic acid methyl ester (C18:3, *m/z* 293.3).

6.4 Prototype V ionisation source for bio-analysis

6.4.1 Bio-analysis of lipids from yeast and other biological sources

Yeast are single-cell eukaryotic microorganisms which are members of the Fungi kingdom. There are over 1,500 species of yeast currently identified. The term yeast is sometimes used synonymously with *Saccharomyces cerevisiae* however yeast is diverse and found in both the Basidiomycota and Ascomycota division phylum. So called "true yeast" including the *Saccharomyces sp.* and *Candida sp.* belong in the Saccharomycetales order.

6.4.2 Comparison of *Saccharomyces cerevisiae* yeast

A species of yeast *Saccharomyces cerevisiae* has been key for over ten thousand years in winemaking, baking, and brewing. In the 1850s the work of Louis Pasteur led to new knowledge concerning the history of alcoholic fermentation by yeast and new methods for culturing pure strains. Once isolated *S. cerevisiae* soon became them most widely adopted single-cell system as a model organism for biological research, due in part to researchers' ability to control and manipulate its life cycle. The strain S288c was adopted as single reference isolate of *S. cerevisiae* for scientific research and it became the first eukaryotic organism to have its genome fully sequenced in 1996 [135].

Four strains of brewers yeast were selected Vermont, WY938a, WLP925, and Lalvin EC-1118. WLP925 is described as a high-pressure lager yeast produced by

White Labs, Lalvin EC-1118 produced by Lallemand is described as a champagne yeast and is classed as *S. cerevisiae var. bayanus*, Vermont is described as an ale yeast, and WY938a is yeast used in the laboratory. Analysis of each yeast was conducted in both positive and negative ion modes mass spectrometry using prototype V.

Lalvin EC-1118

The lipids were extracted from the samples using the MTBE protocol described in chapter 2 [79] and subsequently analysed by flow infusion with prototype V. In negative-ion the mass spectrum shows predominately the de-protonated molecules of fatty acids at m/z 253, 255, 281 and 283 corresponding to the palmitoleic acid (C16:1), palmitic acid (C16:0), oleic acid (C18:1), and steric acid (C18:0) were observed in figure 6.11. Higher mass ions above m/z 400 were also observed which seem to be contaminates of unknown origin as they also appear intensely in the background. The data acquired in positive mode using prototype V is more complex a series of ions m/z 257, 271, 285, and 299 correspond to $C_{16}H_{33}O_2$, $C_{17}H_{35}O_2$, $C_{18}H_{37}O_2$, and $C_{19}H_{39}O_2$ with a potentially related ion at m/z 237 $C_{16}H_{29}O$, these could tentative be assigned as various naturally occurring fatty esters including potentially branched fatty acids as odd-numbered straight chains FAMEs are uncommon in nature, or alternatively they could relate to synthetic polymeric esters and ethers separated by m/z 14 of the CH_2 unit of unknown origins.

Another set of ions observed in positive mode was at m/z 385, 403, 413 and 431 these correspond to $C_{22}H_{41}O_5$, $C_{22}H_{43}O_6$, $C_{24}H_{45}O_5$, and $C_{24}H_{47}O_6$. An associated ion is also observed in negative mode at m/z 163 corresponding

to $C_{16}H_{29}O_2$. One of the ingredients listed on the packaging is "emulsifier", commonly used in dried yeast are sorbitan esters with maximum permitted level of *quantum satis* [136]. The mass-to-charge ratios measured correspond closely to sorbitan monostearate and sorbitan monopalmitate, along with their corresponding dehydrated protonated molecule $[M + H - H_2O]^+$ and also the sorbitan de-protonated molecule $[M - H]^-$.

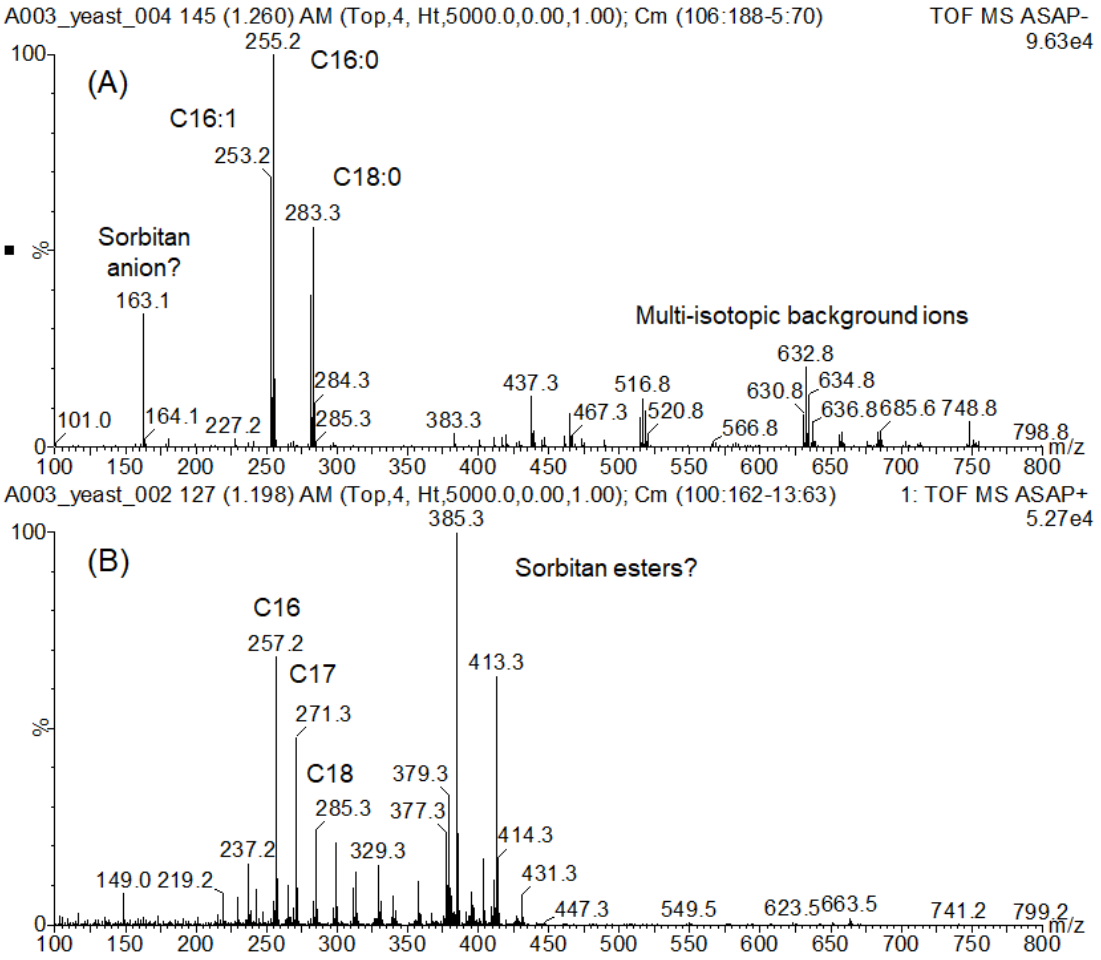

Figure 6.11: Mass spectra of the commercially available *S. cerevisiae* Lalvin EC-1118. Ions observed in negative-ion using prototype V include a series of fatty acids at *m/z* 253, 255, 281 and 283, multi-isotopic ions of unknown origin are seen above *m/z* 500 which also appear in the background (A). In positive mode glow flow, ions are observed at *m/z* 257, 271, 285, and 299 which appear to be FAMEs, also possible a dehydrated fragment an ion at *m/z* 237 is related to the ion at *m/z* 257 (B). Sorbitan esters are used in dried yeast as food additives, ions in panel B at *m/z* 385, 403 and 413 are tentatively assigned as sorbitan monostearate (E 491) and sorbitan monopalmitate (E 495), there is corresponding ion observed at *m/z* 163 which could be the de-protonated ion of free sorbitan in panel A.

Profiling of free fatty acids in yeast by negative-ion mass spectrometry using prototype V

The major free fatty acids identified in yeast are long chain saturated myristic acid (C14:0), palmitic acid (C16:0), stearic acid (C18:0), cerotic acid (C26:0), and the monounsaturated palmitoleic acid (C16:1) and oleic acid (C18:1) [137][138]. The monounsaturated making up *circa* 80 % of all the fatty acids. A study of the four yeast was conducted using prototype V fitted with a 1 μL loop-injector and a comparison of five free fatty acids C14:0, C16:1, C16:0, C18:1, and C18:0 was undertaken, the C26:0 was not sufficiently intense in any of the samples to make a meaningful comparison. The data is presented in figure 6.12, the Lalvin, Vermont and WY938a yeast had relative concentration of monounsaturated fatty acids of 40.5, 42.4 and 49.9 %, respectively, while the WLP925 had only 19.8 %. The palmitic acid was at relative concentrations of 37.7, 28.5, 32.1 and 61.2 % for Lalvin, Vermont, WY938a and WLP925, respectively, and was the most abundant saturated fatty acids in all the samples. The free fatty acids profile of each yeast studied is sufficiently distinct that this method could be develop as a fingerprint identification of unknown yeast against a database, assuming identical growth and analysis protocols are observed.

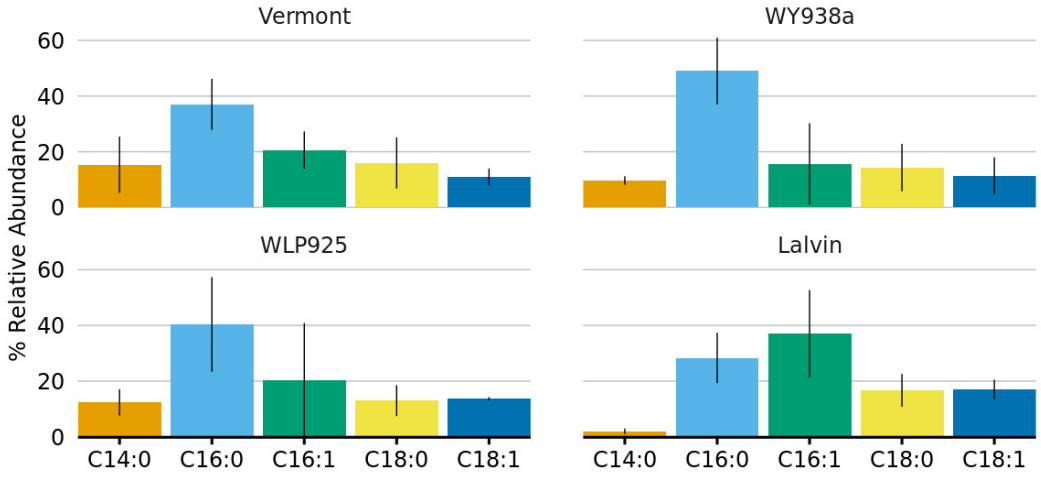

Figure 6.12: Histogram profiling of free fatty acids in yeast by negative-ion mass spectrometry using prototype V ($n = 3$). The palmitoleic acid (C16:1) and palmitic acid (C16:0) are the most abundant free fatty acids.

6.4.3 Negative-ion LC-MS using prototype V of free fatty acids

The conventional approach to analysis of free fatty acids is by GC-MS which requires derivatization into methyl esters or trimethlysilyl-derivatives. Derivatization with electro sprayable reagents for use with LC-MS is also now being used by several groups [139, 140, 141]. Less common is the direct analysis in negative mode. A study of two fatty acids palmitic acid (C16:0) and palmitoleic acid (C16:1) was undertaken to establish if prototype V could ionise such samples delivered by HPLC in negative-ion mode. A stock solution of fatty acids was prepared by dissolving 3.0 mg C16:0 and 0.5 mg C16:1 into 1 mL of dichloromethane:methanol ($1 : 1$ v/v), and then further diluted in dichloromethane:methanol to a working concentration. A Fortis C_{18} 3 μm, 2.1 $\times$ 150 mm was used in the analysis, solvent A was water with 2 % acetonitrile and 0.2 % acetic acid, solvent B was Acetonitrile with 0.2 % acetic acid. A gradient starting at 40 % solvent B held for 5 minutes, increasing to 95 % B at 30 minutes at a rate of 0.2 $mL\ min^{-1}$.

A chromatogram showing the separation of the two compounds at t_R 23.67 and 26.42 minutes for C16:1 (m/z 253) and C16:0 (m/z 255), respectively, is presented in figure 6.13. The peak area of the C16:0 was calculated to be 6.18 times the intensity of the C16:1 peak which is in very close agreement to the ratio of the prepared stock concentration of 11.71 μM compared with 1.97 μM for C16:0 and C16:1, respectively. This suggests that LC-MS using prototype V would be a suitable method for quantitative measurement for the analysis of free fatty acids in food and nutritional supplements. This method with prototype V could provide

characterisation of fatty acid in a high throughput setting, such as factories, or remote locations were limited sample preparation and rapid confirmation of components is required.

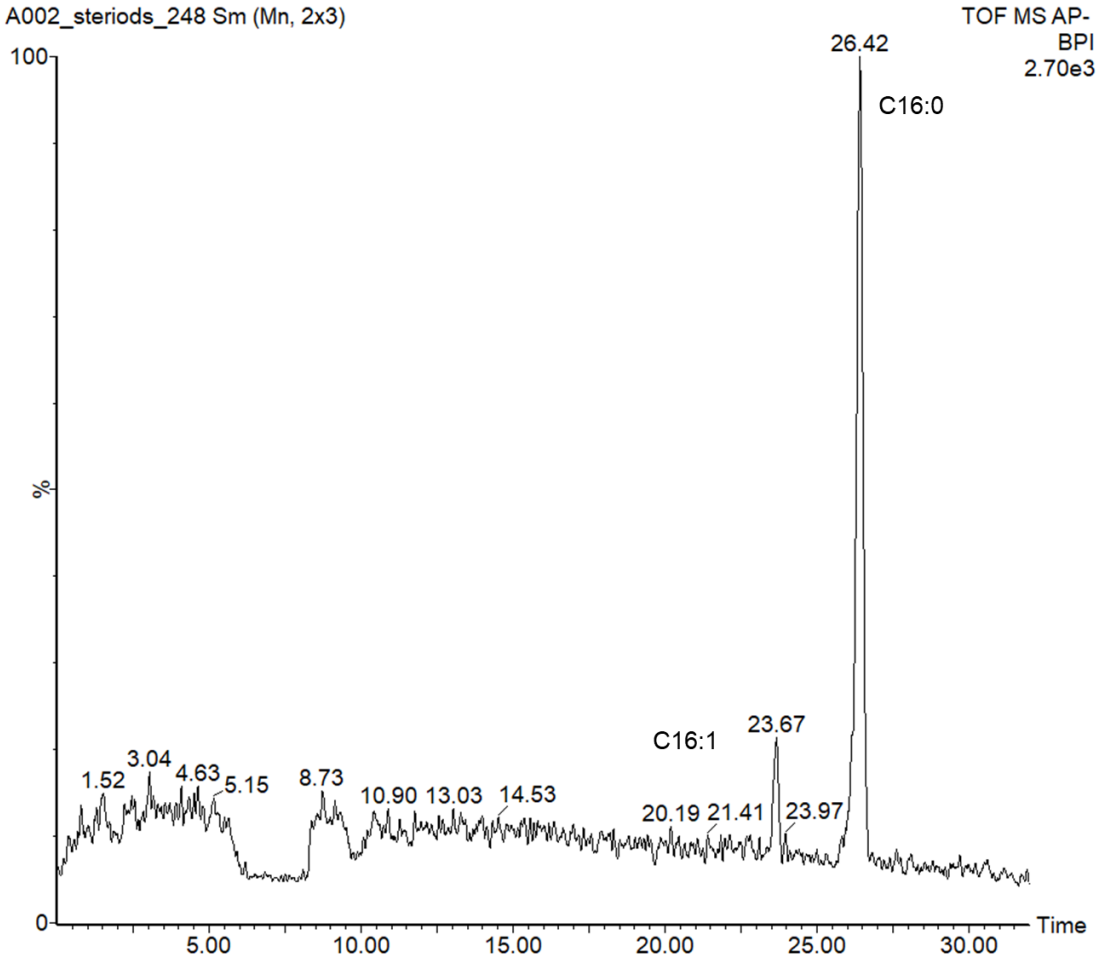

Figure 6.13: Base peak ion (BPI) chromatogram over 35 minutes of free fatty acids palmitic acid (C16:0) and palmitoleic acid (16:1) by negative-ion mass spectrometry using prototype V. The peak area of the C16:0 was calculated to be 6.18 times the intensity of the C16:1 peak which is in very close agreement to the ratio of the prepared stock concentration of 11.71 μM compared with 1.97 μM for C16:0 and C16:1, respectively.

6.4.4 Characterisation of hydroxy-fatty acids from plant cutin

A plant cuticle is a protective coating of young shoots, leaves and other plant organs. They are made up of two major components cutan which is believed to be a hydrocarbon polymer [142], and cutin a polyester consisting of C16 and C18 hydroxy-fatty acids monomers [143].

A study by negative-ion mass spectrometry using prototype V of the three cutin monomer extracts from apple, tomato, and chrysanthemum was undertaken using flow infusion to determine the qualitative relative abundance of the hydroxy fatty acids present from each plant source. The mass spectra of each sample is presented in figure 6.14 showing distinct differences in ion intensities. The ion at m/z 287.2 is the base peak in all samples corresponding to a mixture of the 9,16- and 10,16-dihydroxyhexadecanoic acid structural isomers, a much weaker ion corresponding to 16-hydroxyhexadecanoic acid at m/z 271.2 can also be observed in all samples. A targeted analysis of the five most common hydroxy-fatty acids found in cutin was undertaken and is presented as a stacked bar plot in figure 6.15. The tomato can be seen to almost predominately consist of 9,16-/10,16-dihydroxyhexadecanoic acid (9,10-diOH-C16:0; 92.19 %) this is also the main component for the apple and chrysanthumum, while 9,10,18-trihydroxystearic acid (9,10,18-triOH-C18:0) is in relatively high abundance at 32.41 and 23.93 % respectively in the latter plants. The relative abundance 16-hydroxyhexadecanoic acid (16-OH-C16:0) is low in all three plant extracts, with very low abundance of 18-hydroxyoleic acid (18-OH-C18:1; 0.02 %) and 9,10,18-triOH-C18:0 (0.11 %) in the tomato extract.

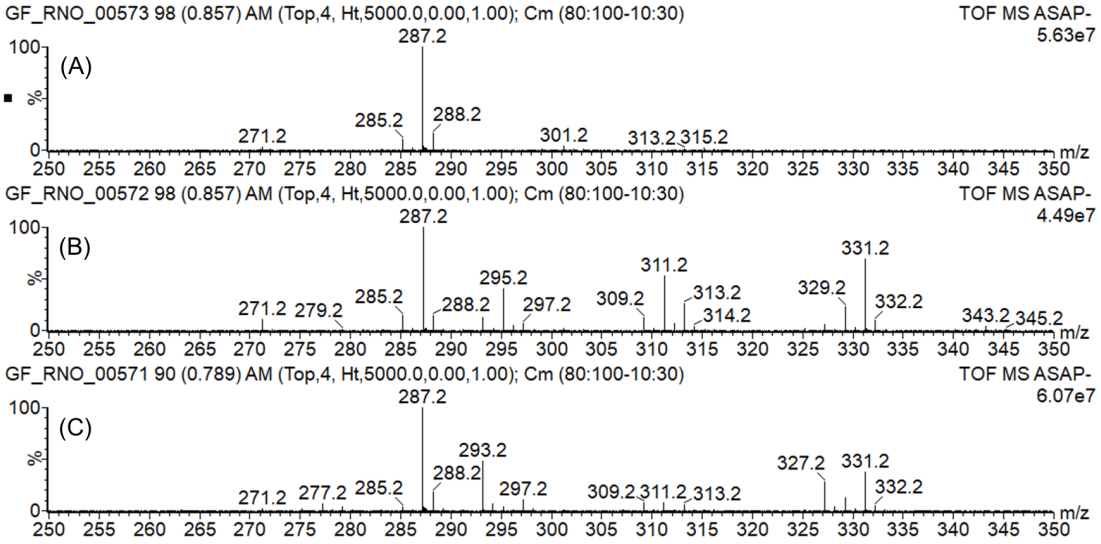

Figure 6.14: Mass spectra of three plant extracts by negative-ion mass spectrometry using prototype V. Observed are ions for the cutin monomer hydroxy fatty acids of tomato (A), apple (B) and chrysanthemum (C). The ion at *m/z* 287.2 is the base peak in all samples corresponding to 9,16-/10,16-dihydroxyhexadecanoic acid, a much weaker ion corresponding to 16-hydroxyhexadecanoic acid at *m/z* 271.2 can also be observed in all samples.

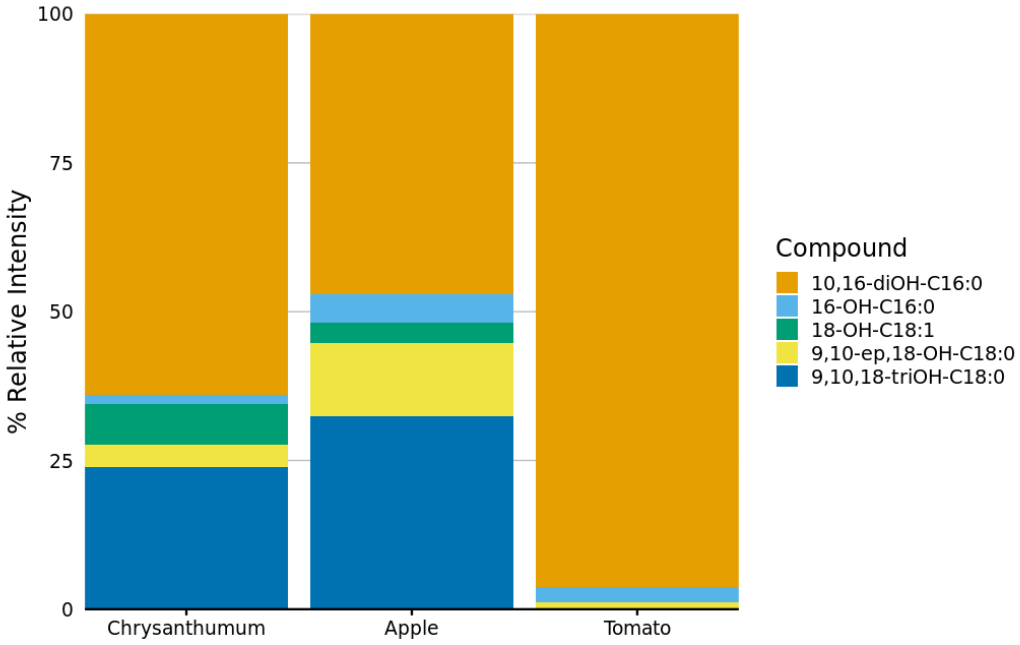

Figure 6.15: Histogram of cutin monomer hydroxy fatty acids of tomato, apple and chrysanthemum. The tomato can be seen to almost predominately consist of dihydroxyhexadecanoic acid (9,10-diOH-C16:0; 92.19 %), this is also the main component for the apple and chrysanthumum while 9,10,18-trihydroxystearic acid (9,10,18-triOH-C18:0) is in relatively high abundance of 32.41 and 23.93 % respectively.

6.4.5 Characterisation of lactonic sophorolipid from yeast

Glycolipids are of interest as potential bio-surfactants due to the perception of their low-toxicity and biodegradability [144]. Lactonic sophorolipid is a glycolipid produced by *Candida* sp. and *Starmerella* sp. yeast [145]. Structurally they consist of a β-1,2 bonded disaccharide (sophorose) head and a lipophilic tail made up of C16 or C18 fatty acid. A study to characterise a lactonic sophorolipid standard, 1',4"-sophorolactone 6',6"-diacetate, was undertaken. The mass spectrum is presented in figure 6.16, the base peak is the protonated molecule at m/z 689.4, also observed are the dehydrated ions ($[M + H - H_2O]^+$) at m/z 671.4 and 653.4. Ions at m/z 467.3 and 485.3 could be related and would appear to correspond to the fragment ions $C_{26}H_{43}O_7$ and $C_{26}H_{45}O_8$, respectively.

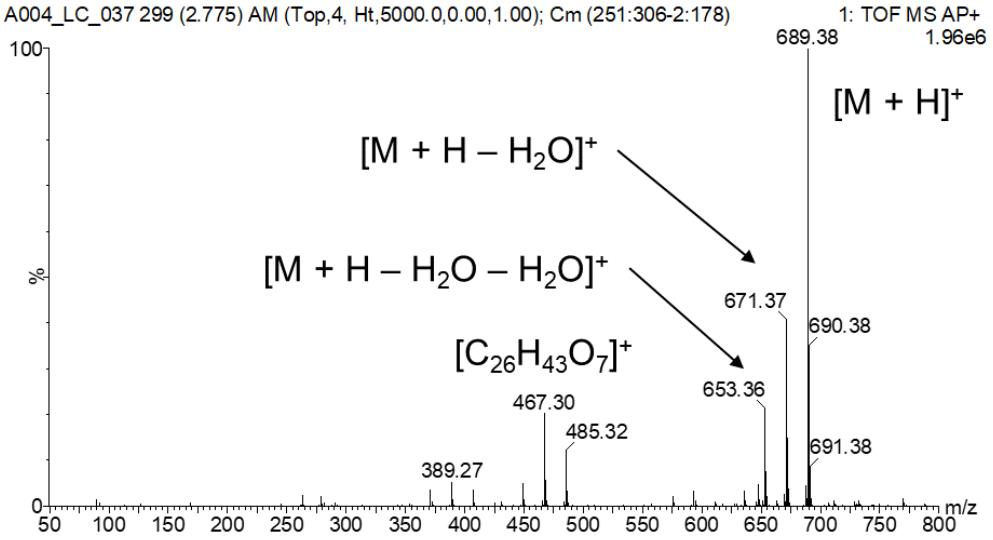

Figure 6.16: Mass spectrum of lactonic sophorolipid. Base peak at m/z 689.4 is the protonated ion, also observed is the dehydrated ions at m/z 671.4 and 653.4. Other ion are observed in the spectrum are at m/z 467.3 and 485.3 which would appear to correspond to the fragment ions $C_{26}H_{43}O_7$ and $C_{26}H_{45}O_8$ respectively.

6.4.6 Characterisation of *Candida albicans*

Candida albicans is commonly used as a model organism for fungal pathogenesis studies. *Candida* sp cause 750 million fungal infections worldwide per year, and there is an unmet need for improved treatments as *Candida albicans* can cause a life-threatening systemic infections of *candidemia* and *candidiasis*. It is estimated that several million people infected with oral and oesophageal candidiasis and further 75 million women contracting vulvovaginal candidosis annually.

Azoles are the treatment and prophylaxis of choice for invasive fungal infections caused by *Candida* sp. These antifungals act by reducing the production of ergosterol ($C_{28}H_{44}O$, Mr 396.65), which is responsible for plasticity in the cell membrane in yeast, by inhibiting sterol CYP51 (14α-demethylase) production (figure 6.17). Resistance is developing to the current class of azoles, such as fluconazole, and new classes of azole antifungal compounds is being actively investigated [146].

Monitoring of sterols produced by *C. albicans* treated with antifungal agents in the laboratory has traditionally been undertaken using GC-MS and involves the extraction and derivatization of the sterols produced by yeast prior to analysis. A study was undertaken to assess prototype V's ability to characterise *C. albicans* specimens comparing two methods. The first method was the shotgun approach using flow infusion without the need for chromatographic purification. The second method used reverse-phase HPLC. Two specimens of *C. albicans* were selected a wild-type SC5314 and a knock-out K41 strain with the deletion of the *ERG3* gene which encodes for the sterol-C5-desaturase enzyme.

Using the shotgun method 1 μL of the sample was injected using a

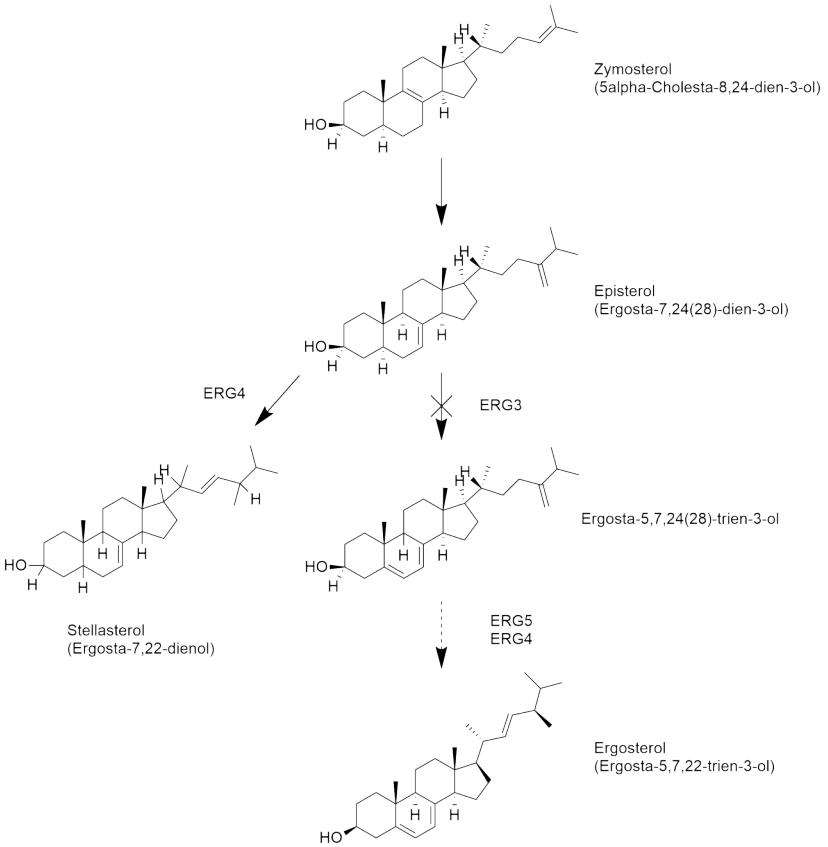

Figure 6.17: Biosynthetic pathway of ergosterol. The gene *ERG3* encods the enzyme which catalyses the conversion of episterol (ergosta-7,24(28)-dien-3-ol) to ergosta-5,7,24(28)-trien-3-ol and ultimately ergosterol.

loop-injection. A mass spectrum of the two yeast samples acquired sequentially is shown in figure 6.18 where a distinct difference in the ion distribution of the samples were observed. In the K41 sample the dehydrated protonated molecule ($[M+H-H_2O]^+$) for stellasterol also known as ergosta-7,22-dien-3-ol ($C_{28}H_{46}O$, Mr 398.35) and episterol ($C_{28}H_{46}O$, Mr 398.35) was observed at m/z 381.36, while the $[M+H-H_2O]^+$ ion of ergosterol was observed in the SC5314 sample at m/z 379.34.

As stellasterol and episterol are isomers, distinguishing the two compounds

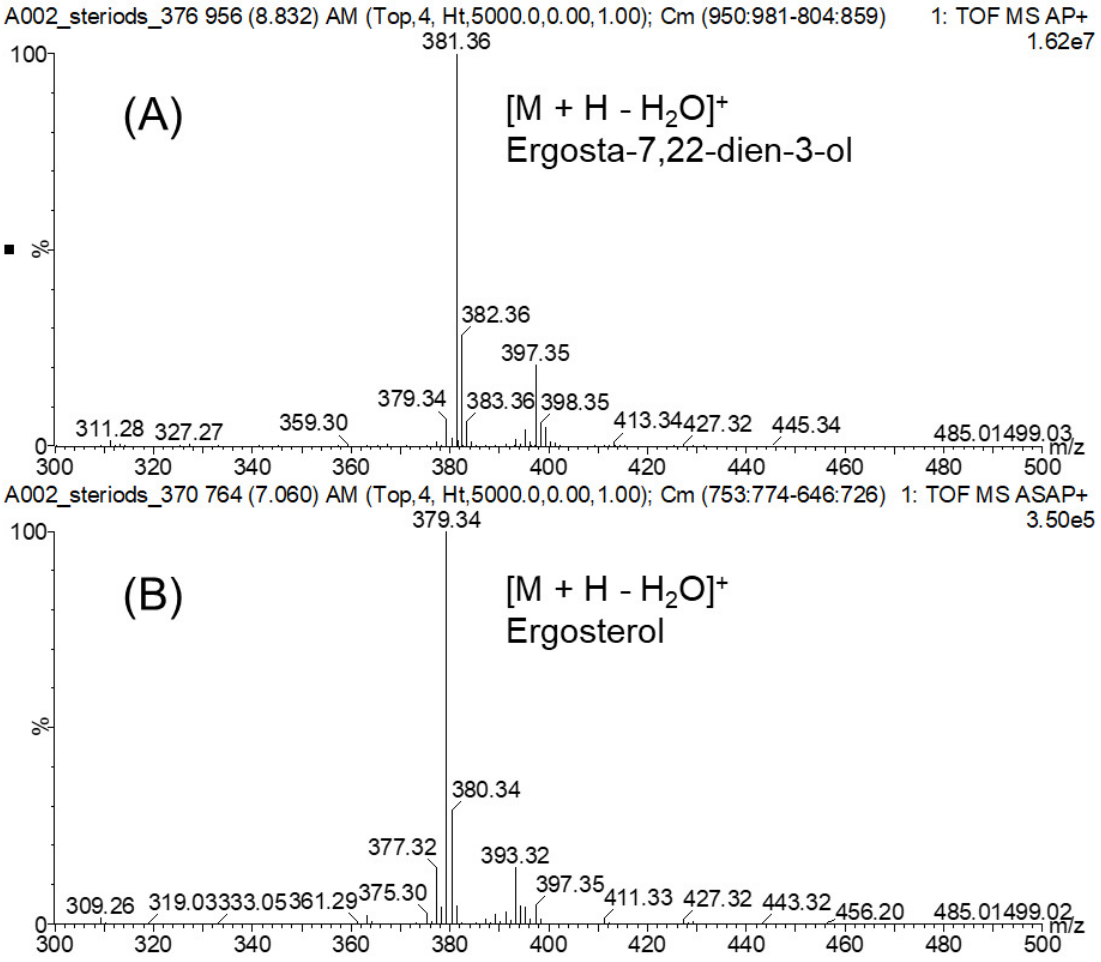

Figure 6.18: Mass spectra of pathogenic yeast *C. albicans*. Observed for the knock-out K41 (ERG3) mutant is a ion at *m/z* 381.36 which corresponds to the dehydration of the protonated molecule of ergosta-7,22-dien-3-ol (A). For the wild-type SC5314 an ion at *m/z* 379.34 which corresponds to the dehydration of the protonated molecule of ergosterol (B).

in the K41 sample is not possible using the shotgun method. The use of reversed-phase LC-MS offers the possibility of separating isomeric ions based on their polarity. The LC conditions were as follows, solvent A was water with 0.2 % acetic acid and solvent B was acetonitrile with 0.2 % acetic acid. The gradient was set at 40 % solvent B at 0 to 5 minutes increasing to 95 % at 15 minutes at

0.200 $mL\ min^{-1}$ and held for 5 minutes, using a Fortis C_{18} column 3 μm, 2.1 $\times$ 150 mm. A XIC of the ions at m/z 381.36 and 379.34 is shown in figure 6.19. For the SC5314 sample, ergosterol was detected at $t_R = 20.91\ min$. For K41 mutant ions are observed at $t_R = 21.52\ min$, with weaker responses at 19.06 and 20.55 min. This might suggest that there are three isomers that share the same m/z ratio, however as the Xevo G2-S does not have MS/MS capability it is not possible to further assign each peak to a specific compound.

Prototype V has shown its capability to analyse sterols isolated from *C. albicans* by two methods. No derivatization was used requiring less sample preparation time with respect to GC-MS and direct measurement of the sterols was possible with intense dehydrated molecules $[M + H - H_2O]^+$ observed. The use of chromatography was shown to provide additional confirmation of compounds by the use of retention times, which would be enhanced when used in combination with standards and MS/MS capability to provide further structural data on the compounds under examination from their fragmentation patterns.

6.4.7 In situ derivatization of sterols

As has been demonstrated rapid analysis of sterols in *C. albicans* and free fatty acids can be achieved without lengthy derivatization step using micro-glow discharge mass spectrometry. For sterols and steroids the characteristic $[M - 17]$ ion is generally observed. When there are many similar compounds with hydroxyl groups in a specimen this can lead to greater complexity in the analysis and assignment of ions. Direct *in situ* derivatization would be highly advantageous in such circumstances and various methods have been suggested [147]. In this study

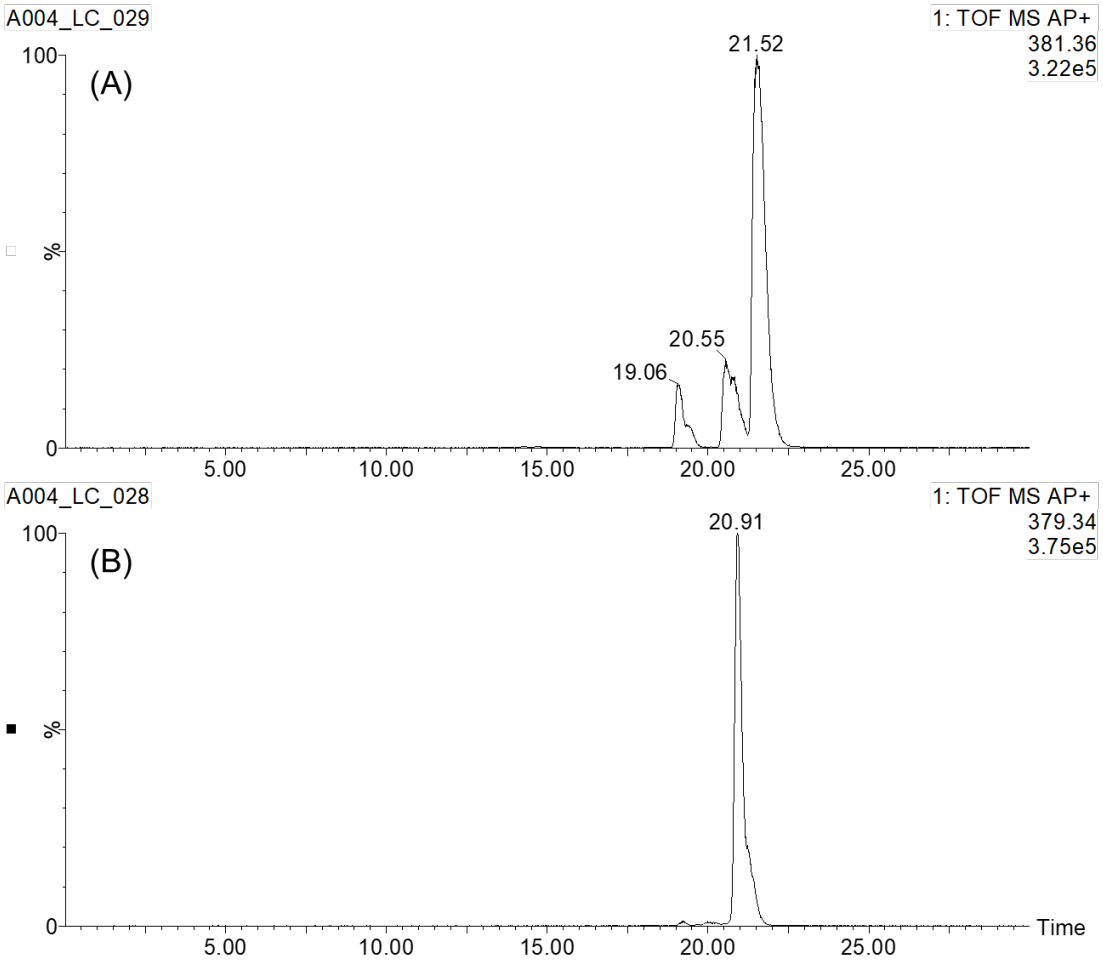

Figure 6.19: XIC of pathogenic yeast *C. albicans*. For the knock-out K41 (ERG3) the ion at *m/z* 381.36 is observed at $t_R = 21.52 min$ (A) weaker peaks are also observed at $t_R = 19.06\ min$ and $t_R = 20.55\ min$ which may relate to other isomers such as episterol. For the wild-type SC5314 an ion at *m/z* 379.34 is observed at t_R 20.91 min (B).

the assessment of five basic amine compounds as *in situ* derivatization agents was undertaken. Cholesterol, used as the target compound, was prepared at a concentration of 1 $mg\ mL^{-1}$ and mixed in turn 1:1 (v/v) with each basic amine, and 1 μL of the resulting solutions was syringed on the end of a glass capillary for analysis using prototype V, and repeated for each mixture. The resulting peak

intensities from the XIC was recorded ($n = 3$) in table 6.7.

Table 6.7: *In situ* derivatization of cholesterol. The *m/z* of adduct ion (molecule-base [M+B])formed in the derivatization process is listed , along with the % relative intensity of the ion with respect to the total intensity of the [M+B], [M+1], [M-1] and [M+17] calculated from the XIC.

Derivatization reagent	m/z of product $[M + B]^+$	% relative intensity
Ethylamine	414.41	27.0
Diethylamine	442.44	66.1
Triethylamine	470.47	67.9
Piperidine	454.44	81.3
Pyridine	448.39	55.6

The derivitization reaction involves the elimination of water as a result of the condensation of the hydroxyl group of the cholesterol and amine of the base (figure A.17) The results show that none of the basic amine *in situ* derivatization reagents were able to achieve full conversion. However, of the five reagents tested piperidine performed best resulting in a 81.3 % conversion, with triethylamine and diethylamine providing 67.9 and 66.1 % conversion respectively. In contrast ethylamine performed poorly only converting 27.0 %. This method could be useful for more complex mixtures when using piperidine however as 100 % conversion isn't achieved it may not be an useful approach for quantitative work as variability can occur as there is no direct control of the reaction process.

6.5 Analysis of oligopeptides using prototype V ionisation source

Peptides are polar biochemicals made up of amino acids linked by peptide bonds. Sometimes peptides with twenty or fewer amino acids are referred to as

oligopeptide. In general analysis of peptides are carried out by ESI particularly for higher mass (i.e. >2,000 Da) due in part to its ability to form multiply protonated molecules which could not otherwise be measured in the mass range of the mass analyser. In this chapter, so far, prototype V has been used to analyse predominantly non-polar and neutral compounds which are less amiable to ionization by ESI. A study of three oligopeptides, namely MFRA, Leucin Enkephalin, and Angiotensin I, which are commonly found in the laboratory, were analysed using prototype V to establish its capabilities for the analysis of more polar compounds. The compounds were diluted in water to a working concentration and analysed by flow injection using a 1 μL loop.

MRFA

A mass spectrum of the oligopeptide MRFA is shown in figure 6.20, collected sequentially in positive and negative ion modes. Neither protonated molecule nor the corresponding de-protonated molecule form the base peak in the mass spectrum. The nebulization process and prototype V would appear to impart significant energy causing the formation of fragment ions associated with dehydration at m/z 506.2/504.2, and possibly 464.2/462.2. Also observed is fragment ion associated with the loss of what appears to be a CH_2N2 group from the arginine amino acid. The fragment ions at m/z 375.2/373.2 would appear to correspond with the loss of methionine ($C_5H_{11}NO_2S$, M_r149.2).

Leucine Enkephalin

A spectrum of Leucine Enkephalin is shown in figure 6.21. Observed in the mass spectrum is C-terminal fragmentation ions of the y-series, at m/z 393.2 (y_4), 336.2

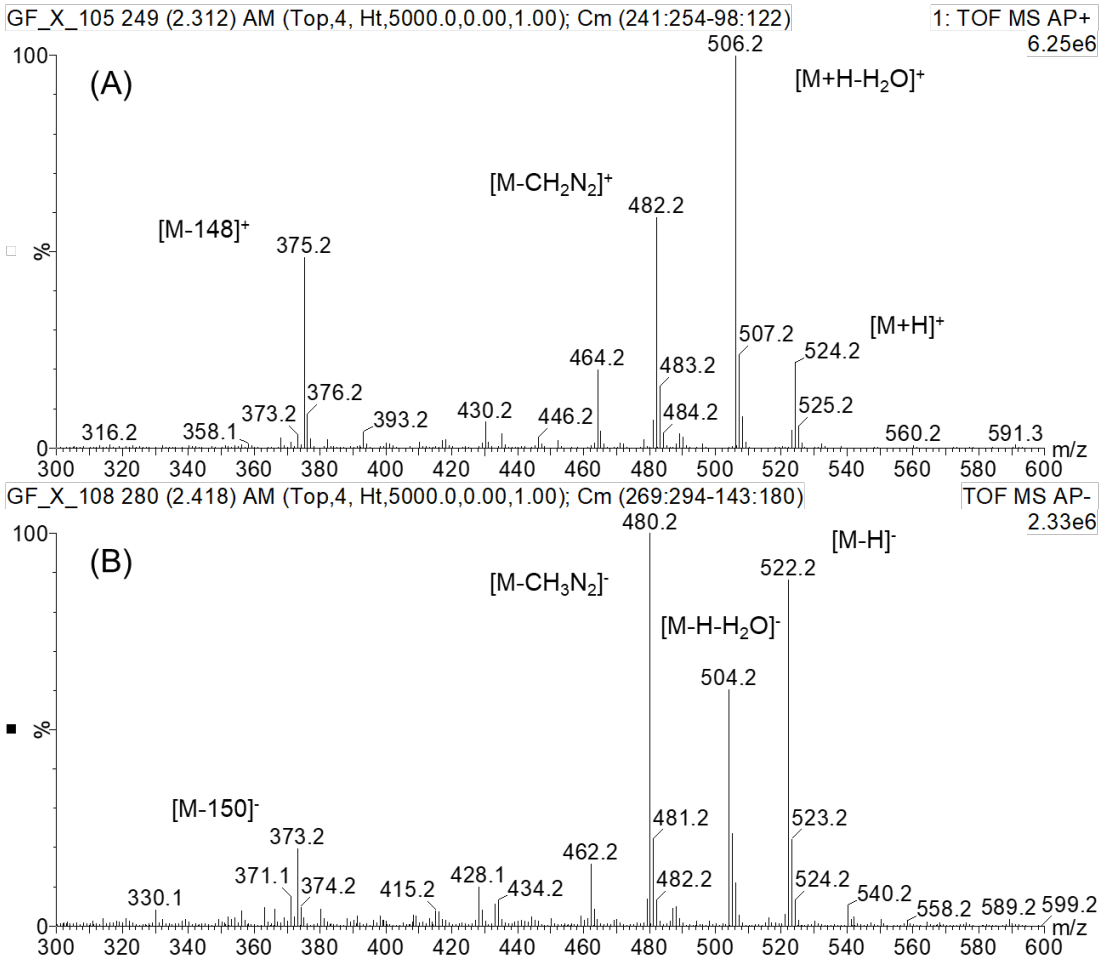

Figure 6.20: Mass spectrum of the oligopeptide MRFA. The protonated molecule can be seen along with the dehydrated ion $[M + H - H_2O]$ at *m/z* 506.2, loss of CH_2N_2 at *m/z* 482.2 and a fragment ion at *m/z* 375.2 (A). In negative ion mode the corresponding de-protonated molecule is observed along with fragment ions at *m/z* 504.2 [M-19], 480.2 [M-43] and 373.2 [M-150] (B).

(y_3), and 279.2 (y_2). There are also N-terminal fragmentation ions of the b-series at *m/z* 425.2 (b_4) and 221.1 (b_2). Ions for the b_3 fragment and the a-series were not observed. An as yet unassigned intense ion at *m/z* 301.2 is also observed. Fragmentation such as this is in *de novo* peptide sequencing often associated with low-energy collision-induced dissociation (CID) or post source decay (PSD).

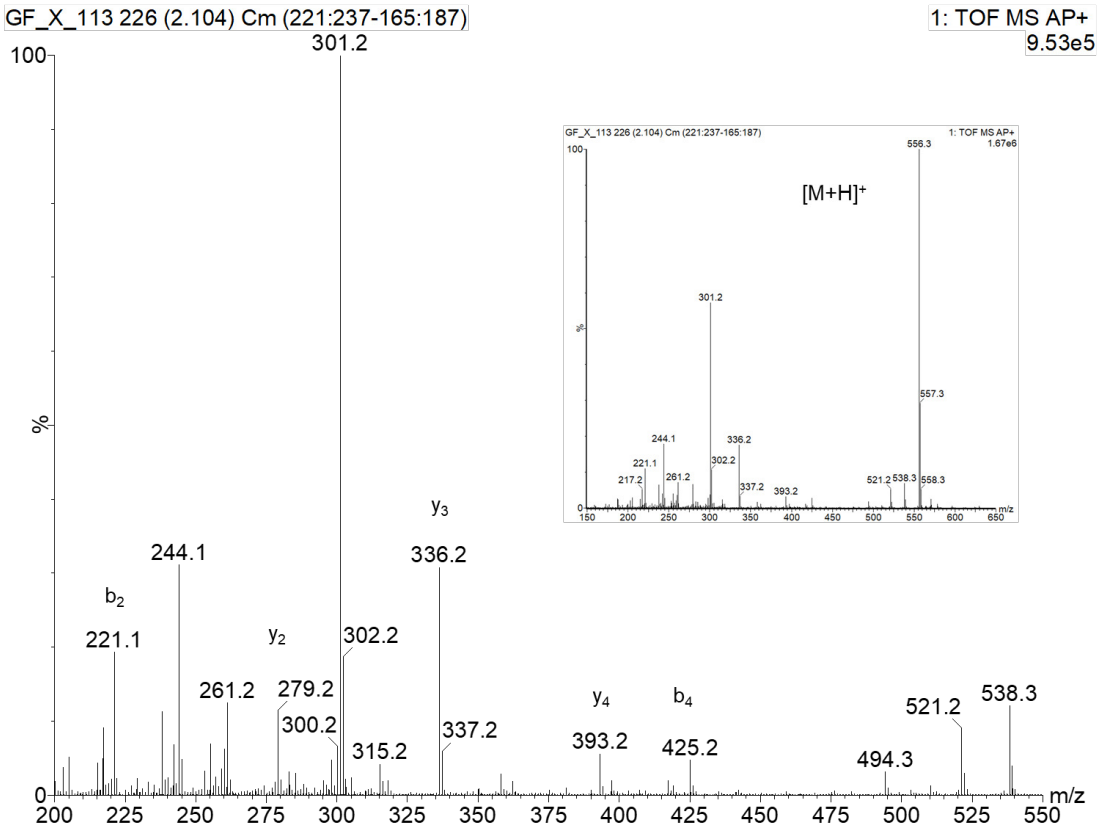

Figure 6.21: Mass spectrum of the oligopeptide Leucine Enkephalin. Intense fragment ions from the y- and b- series, namely y_2 *m/z* 279.2, y_3 *m/z* 336.2, y_4 *m/z* 393.2 and the b_2 *m/z* 221.1, b_4 *m/z* 425.2. The protonated molecule can be seen at *m/z* 556.3 (inset).

Angiotensin I

A spectrum of Angiotensin I is shown in figure 6.22. The weak protonated molecule at m/z 1296.7 can be observed, and unusually for prototype V, a sodium adduct ion $[M + Na]$ at m/z 1318.7 and $[M - H + 2Na]^+$ at m/z 1340.7 can be tentatively assigned. As with the other oligopeptides studied so far, fragment ions are observed in the mass spectrum specifically those of the y-series at m/z 513.3, 650.3, 763.4, 926.5, and 1025.6.

The spectrum for these oligopeptides suggests that prototype V is potentially

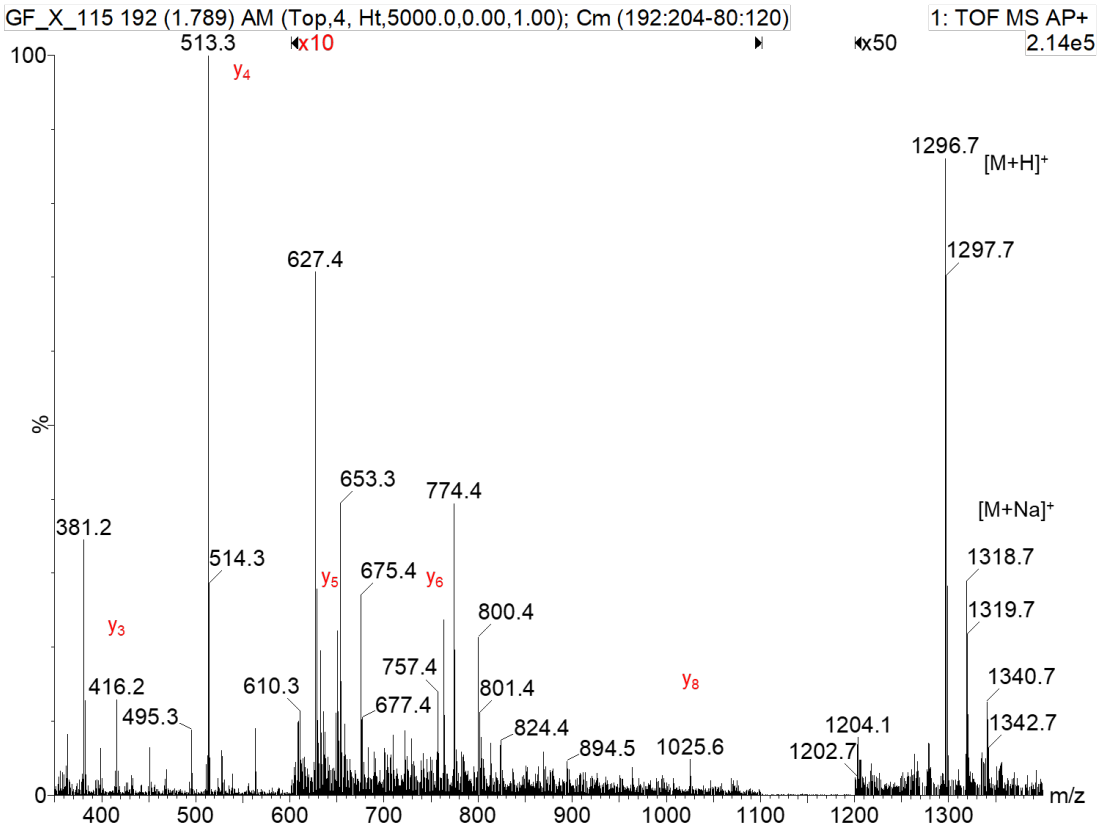

Figure 6.22: Mass Spectrum of the oligopeptide Angiotensin I. The y_4, y_5, y_6, y_7, and y_8 fragment ions shown at *m/z* 513.3, 650.3, 763.4, 926.5 (not marked), and 1025.6. The protonated molecule at *m/z* 1296.7 is magnified x50 and unusually there appears to be a $[M + Na]^+$ adducted ion at *m/z* 1318.7.

more energetic than had previously been observed. This results in greater fragmentation which is could make identifying molecular species harder if there are multiple components but it has the potential benefit of providing structural data of compounds.

6.6 Discussion and summary

A broad range of compounds has been studied by prototype V. The study of "small molecules" provided confirmation that prototype V is suitable as a source for fine chemicals and pharmaceuticals both in positive and negative modes.

More complex mixtures studied using prototype V was undertaken, using several sample introduction techniques including LC. The flow infusion, or shotgun, method in combination with statistical analysis such as Kendrick mass plots can be used to differentiate a range of components by micro-glow discharge mass spectrometry with accurate mass measurement for targeted and untargeted analysis providing additional component for compound identification. The study of samples by LC-MS in combination with prototype V allowed separation of individual components reducing competitive ionization, allowed identification of compounds with overlapping isotopic profiles, and also the semi-quantitative analysis which could not be easily achieved by high resolution alone.

The use of prototype V has expanded the range of biomolecules analysed by APGD to sterols and fatty acids which could be used as a routine method for yeast, plants, as well as for food an dietary supplements. Further it has shown how prototype V can be used without derivatization for rapid characterisation using flow infusion or LC-MS. To the authors knowledge this is only the second time FAPA, or similar APGD, have been used to measure oligopeptides. Typically the protonated molecule ($[M + H]^+$) was observed using prototype V though extensive fragmentation of the oligopeptides was also seen for example in figure 6.21 suggesting that significant internal energy is imparted by this prototype to these molecules.

The predominant ions observed using prototype V in positive mode are protonated molecules ($[M + H]^+$), while compounds with hydroxyl/alcohol functional groups the dehydrated ions ($[M + H - H_2O]^+$) is observed as was shown in table 6.1. In negative mode the de-protonated molecule ($[M - H]^-$) is primarily observed, the DL is in the $pmol\ \mu L^{-1}$ range with high linearity ($R^2 > 0.998$) achievable with the source.

In summary, prototype V shows capability to ionise a wide range of sample chemistries, from polar to non-polar, providing rapid analysis using a probe and flow infusion. This prototype V ionization source is capable of handling the higher flow rates, e.g. $0.2\ mL\ min^{-1}$, of solvent:analyte delivered by LC adding an extra capability as part of a multimodal sample introduction and ionization platform.

Chapter 7

Assessment of prototype V using ultra high pressure liquid chromatography mass spectrometry

7.1 Introduction

A study of prototype V using a Waters ACQUITY Class I UPLC coupled to a Waters Xevo TQ-S mass spectrometer is made. In previous chapters (5 and 6) prototype V was shown to be compatible with the high flow rates of HPLC using a APCI IonSABRE II (heated nebuliser) probe to deliver the sample into the source and ionization region. The aim of this study is an assessment of the operation of prototype V ionization source using UHPLC which has the capability of separating compounds more rapidly than traditional HPLC. By some

estimates ESI is one to two orders of magnitude more sensitive than EI [110]. In chapter 5 prototype V tentatively showed improved sensitivity to testosterone when compared directly to ESI, however, it is not known whether this will be the case with all compound classes and sample chemistries. Therefore a comparison of prototype V is also made against ESI, and APCI.

Three sets of analytical standards were selected for the comparative study covering polar to non-polar chemistries namely, the "six-mix" standard which contains five "small molecules", an APGC standard containing non-polar PAH, and an extractables & leachables (E&L) screening standard which contains compounds commonly used in industrial polymer additives and preservatives. Based on the findings in previous chapters it is expected that the predominant ions observed with the prototype V source will be $[M + H]^+$ and some $[M]^{+\bullet}$ ions.

For all experiments the Waters Xevo TQ-S triple quadrupole mass filter was used at Waters Corp. Research Laboratories in Wilmslow, UK, operating conditions are specified in chapter 2, if not noted. Low resolution data in full scan or multiple reaction monitoring (MRM) mode were acquired. Data was processed using Waters MassLynx 4.1 and the ions observed are discussed in the following sections, peak areas for ions of interest are integrated from the XIC.

7.2 Analytical figures-of-merit

A study using prototype V was conducted to analyse the"six-mix" solution. The "six-mix" solution contained five compounds namely, caffeine ($C_8H_{10}N_4O_2$, M_r 194.08, $LogP$ = -0.1), acetaminophen ($C_8H_9NO_2$, M_r 151.06, $LogP$ = 0.5),

sulfadimethoxine ($C_12H_14N_4O_4S$, M_r 310.07, $LogP = 1.6$), hydroxyprogesterone ($C_{21}H_{30}O_3$, M_r 330.22, $LogP = 3.2$), and verapamil ($C_{27}H_{38}N_2O_4$, M_r 454.28, $LogP = 3.8$), which would all appear to conform to Lipinski's rule of five [115], as described in chapter 6. Data was acquired in MRM mode on the Xevo TQ-S for the following transitions acetaminophen 152 > 109.9, caffeine 195.1 > 138.0, sulfadimethoxine 311.2 > 155.9, hydroxyprogesterone 331.2 > 109.0, and verapamil 455.3 > 165.0. In MRM mode the product ions are measured from one or more precursor ion, selected in $Q1$, with the aim of maximising selectivity and sensitivity.

Until now the prototype V ionization source has been operated with the APCI IonSABRE II (heated nebuliser) probe in constant current mode at 10 μA (*cf.* chapter 5 and 6). Data was acquired with the APCI probe ($n = 3$) and linear regression analysis for each of the five compounds is presented in figure 7.1. A summary of the data is made in table 7.1

Table 7.1: List of results from the linear regression analysis of prototype V in combination with the APCI probe. Listed is the linear dynamic range (1 d.p.), coefficient of variability (R^2), the lowest detectable concentration on column in picograms, the SEM at the lowest concentration, and the calculated instrument detection limit (DL).

Compound	Linear dynamic range	Lowest Conc. (pg)	DL (pg)	SEM	R^2
Acetaminophen	2.7	10.00	1.9	120.9	0.9986
Caffeine	3.7	1.00	1.2	63.6	0.9870
Sulfadimethoxine	3.7	0.50	0.2	31.8	0.9935
Hydroxyprogesterone	4.0	2.50	3.8	36.8	0.9969
Verapamil	4.7	0.03	0.1	37.1	0.9997

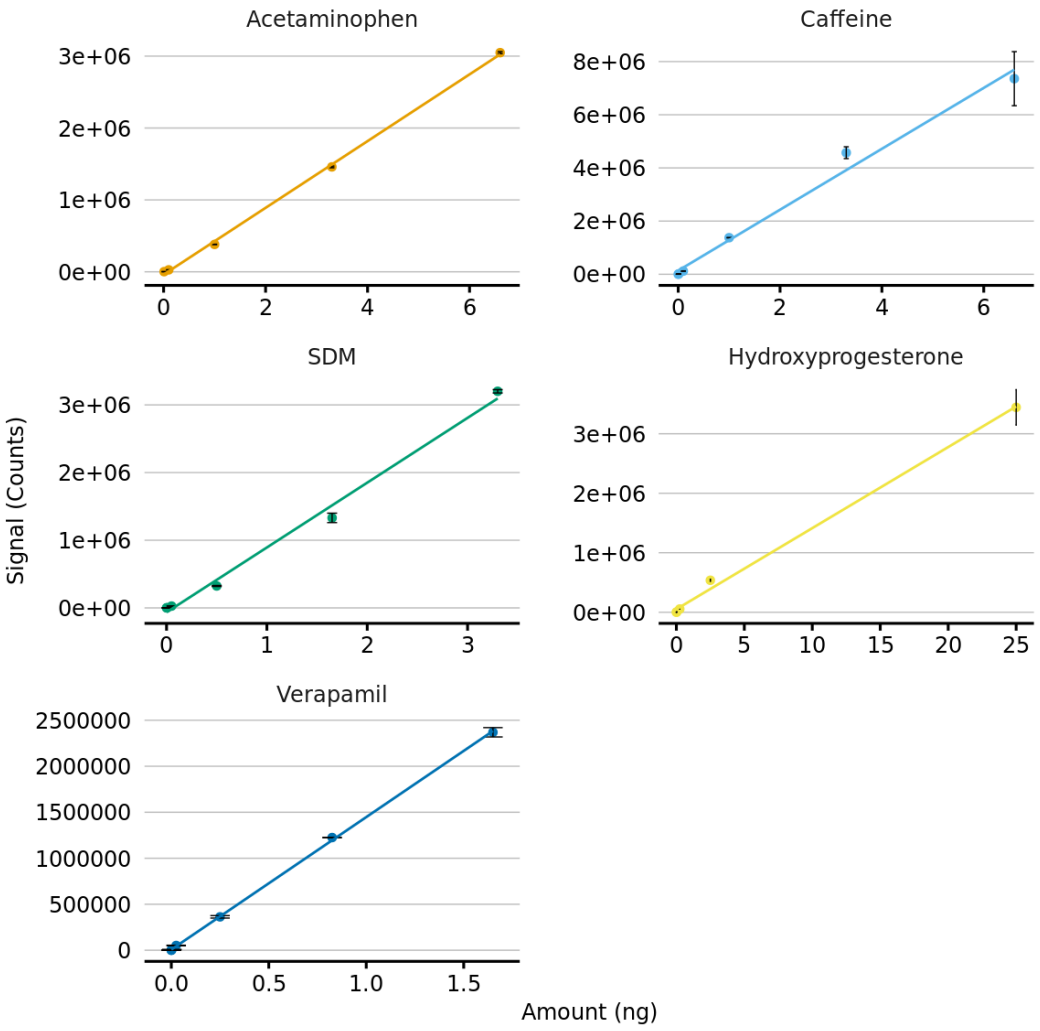

Figure 7.1: Linear regression plot for the five compounds for prototype V using the APCI probe ($n = 3$) to deliver the sample.

A second study was conducted using the ESI probe (capillary voltage 0 kV) in place of the APCI probe, with prototype V in voltage control mode at +3 kV. Whereas, the APCI probe emits a plume of vapourised analytes the ESI probe emits a spray of solvated analyte molecules. Data was acquired with the ESI probe ($n = 2$) and linear regression analysis for each of the five compounds is presented in figure 7.2. A summary of the data is made in table 7.2

Table 7.2: List of results from the linear regression analysis of prototype V in combination with the ESI probe. Listed is the linear dynamic range (1 d.p.), coefficient of variability (R^2), the lowest detectable concentration on column in picograms, the SEM at the lowest concentration, and the calculated instrument detection limit of (DL).

Compound	Linear dynamic range	Lowest Conc. (pg)	DL (pg)	SEM	R^2
Acetaminophen	2.3	10.00	12.8	214.8	0.9997
Caffeine	2.3	10.00	0.7	714.9	0.9999
Sulfadimethoxine	4.3	0.05	0.02	66.0	0.9880
Hydroxyprogesterone	4.3	25.00	2.1	335.1	0.9951
Verapamil	3.6	0.03	0.04	44.4	0.9998

The data indicates that in general the prototype V source is capable of routine detection of compounds at on column concentrations in the low picograms with high linearity $R^2 > 0.98$ over 2 to 4 orders of magnitude. The results demonstrate that the performance of the ionization source is compound specific. For acetaminophen and caffeine which are both polar ($LogP < 1$) and for the non-polar hydroxyprogesterone there was no detectable signal below 10, 1, and 2.5 pg, respectively. Whereas for sulfadimethoxine and verapamil the ionization source was capable of detection at on column concentrations of 50 fg or less. The DL for sulfadimethoxine was lower by an order of magnitude (200 to 20 fg) when using the ESI probe as the sample introductory method and there were

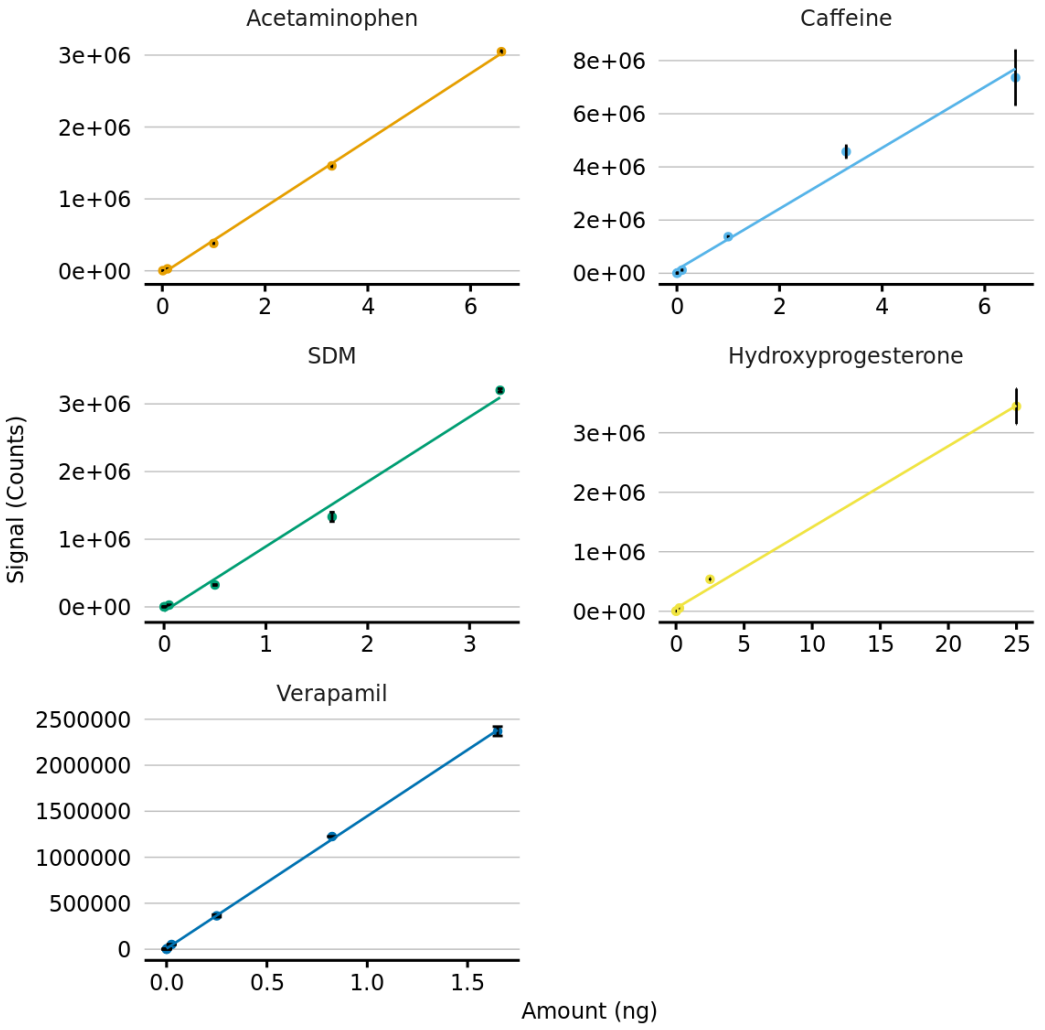

Figure 7.2: Linear regression plot for the five compounds for prototype V using the ESI probe ($n = 2$) to deliver the sample.

also marginal improvements in the DLs for caffeine, hydroxyprogesterone and verapamil. This suggests that the samples may degrade more with the APCI probe compared to when they are in a solvated spray. However an increase in the DL was observed for acetaminophen (1.9 to 12.8 pg). One reason for the ionization source's poorer sensitivity to acetaminophen, with respects to the other

compounds in this study, could be explained by the presence of the hydroxyl group on the phenyl ring. Previous experiments have shown the propensity for alcohol or hydroxyl containing compounds to lose the OH group by the well-established mechanism forming a stable $[M + H - H_2O]^+$ ion (equation 7.1).

$$MOH + H^+ \rightarrow MOH_2^+ \rightarrow M^+ + H_2O \tag{7.1}$$

Considering the polarity by plotting the DL against the water n-octanol coefficient ($LogP$) in figure 7.3 we can see that in general, with the exception of hydroxyprogesterone, the more polar compounds with a Log P value of less than 1 have higher DL when compared to those compounds with a $LogP$ value grater then 1, this suggest that prototype V is more suited for the analysis of less polar compounds.

Analysis of the six-mix solution by ESI was also undertaken and compared at the equivalent of 1 pg on column of sulfadimethoxine in positive ion using MRM mode. Prototype V ionization source was at least an order of magnitude less sensitive compared to the standard ESI method for these specific compounds.

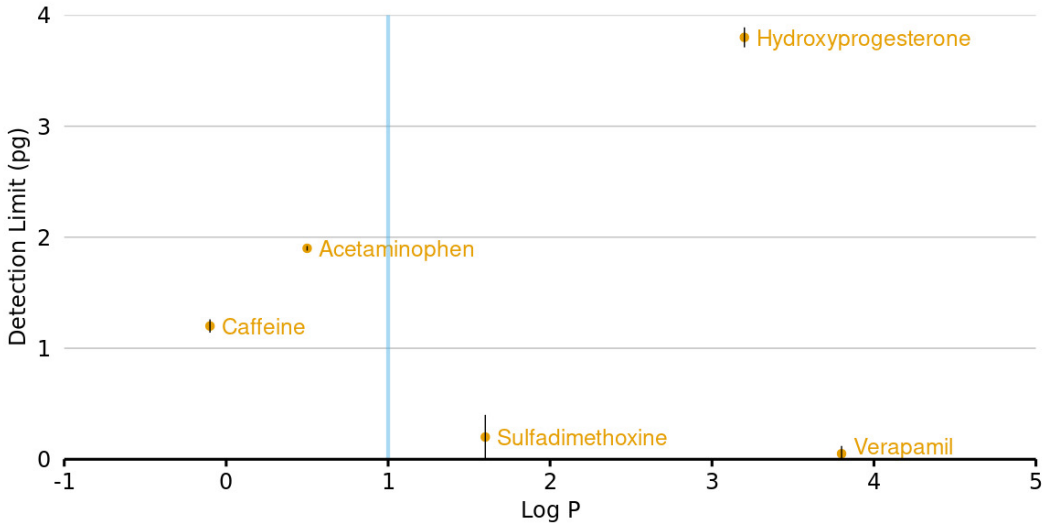

Figure 7.3: Plot of Log P against the DL for the five compounds using prototype V fitted with the APCI IonSABRE II (heated nebuliser) probe to deliver the sample. In general, with the exception of hydroxyprogesterone, the more polar compounds with a Log P value of less than 1 have higher DL when compared to those compounds with a $LogP$ value greater than 1, this suggest that the the prototype V source is more suited for the analysis of less polar compounds.

7.3 Analysis of APGC standard by direct infusion

The APGC standard contains eight compounds namely 2,3,7,8-tetrachloro-dibenzo-p-dioxin ($C_{12}H_4Cl_4O_2$, M_r 319.90, $LogP$ 6.4), phenanthrene ($C_{14}H_{10}$, M_r 178.08, $LogP$ 4.5), hexachlorobenzene (C_6Cl_6, M_r 281.81, $LogP$ 5.7), octafluoronaphthalene ($C_{10}F_8$, M_r 271.99, $LogP$ 4.0), 1,2-dichlorobenzene ($C_6H_4Cl_2$, M_r 145.97, $LogP$ 3.4), anthracene ($C_{14}H_{10}$, M_r 178.08, $LogP$ 4.4), endosulfan ($C_9H_6Cl_6O_3S$, M_r 403.82, $LogP$ 3.8), and benzo[*ghi*]perylene ($C_{22}H_{12}$, M_r 276.09, $LogP$ 6.6) were selected as they are non-polar compounds which may be better suited to prototype V. A study was conducted using the flow infusion method at a flow rate of 20 $\mu L\ min^{-1}$ and the compounds were initially detected in full scan mode. The ions observed are recorded in table 7.3. Five of the potential compounds were identified by their m/z using prototype V, however the ion at m/z 179 could represent either phenanthrene, anthracene, or more likely both. ESI performed poorly in comparison with this set of compounds where only a weak ion at m/z 179 was observed, the ion of benzo[*ghi*]perylene may also have tentatively been observed.

Further analysis was undertaken using MS/MS. A collision energy of 35 eV was used to fragment ions of the precursor ion at m/z 178 for the phenanthrene/anthracene compound. Observed are transitions 176.9, 175.9, 150.9, and 149.7 corresponding to the sequential loss of hydrogen. Also observed are the fragments 164.9, 151.9, and 138.9 a transition of 13 equivalent to the loss of CH. The fragmentation pattern for both prototype V and ESI are similar, and no noticeable difference is observed (figure 7.4).

Table 7.3: List of compounds from the APGC standard detected by prototype V and ESI. The *m/z* is recorded along with the corresponding ion species where observed.

Compound	Prototype V m/z	Electrospray m/z
1,2-Dichlorobenzene	-	-
Phenanthrene	178 $[M]^{+\bullet}$/179.1 $[M+H]^+$	179.1 $[M+H]^+$
Anthracene	178 $[M]^{+\bullet}$/179.1 $[M+H]^+$	179.1 $[M+H]^+$
Octafluoronaphthalene	-	-
Benzo[*ghi*]perylene	277.1 $[M+H]^+$	*weak*
Hexachlorobenzene	-	-
2,3,7,8-Tetrachloro-dibenzo-p-dioxin	319.7 $[M]^{+\bullet}$	-
Endosulfan	404.7 $[M+H]^+$	-

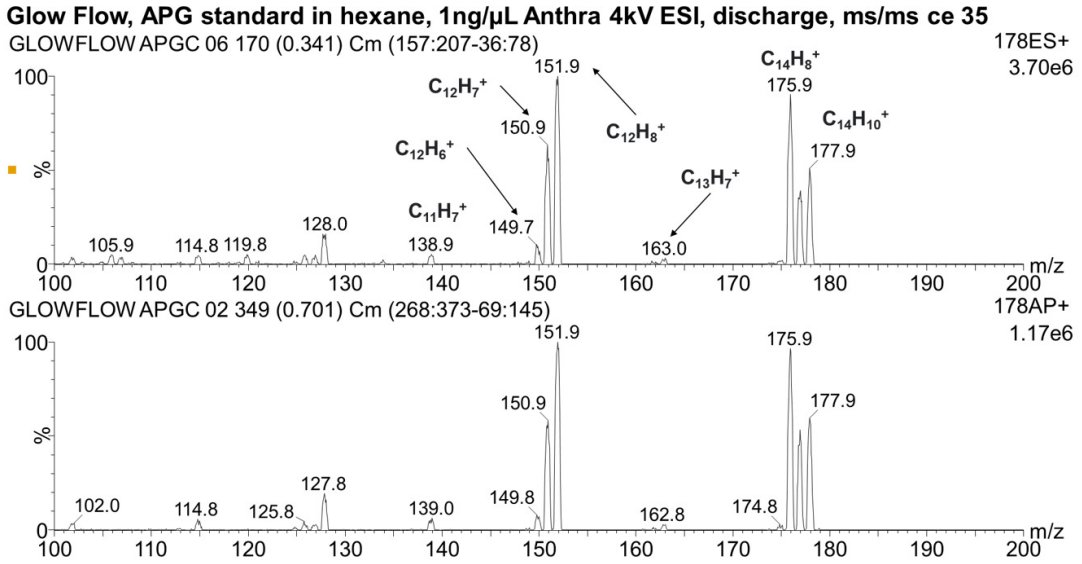

Figure 7.4: MS/MS mass spectrum of the fragment ions for the precursor ion at *m/z* 178 for the phenanthrene/anthracene. Top panel is ESI and the bottom panel is prototype V. The collision energy was set to 35 eV. The fragmentation pattern for both prototype V and ESI are similar and no noticeable difference is observed.

A MS/MS study was also conducted for the Benzo[*ghi*]perylene compound (collision energy of 70 eV) and the fragments of the precursor ion at m/z 277 were recorded in figure 7.5. The signal for prototype V is an order of magnitude greater than ESI for the fragment ions. A series of fragment ions 276.0, 273.9,

and 271.9, equivalent to the loss of hydrogen atoms from the precursor ion are observed. Also observed is a fragment ion 247.9 a transition of 26 from m/z 273.9 equivalent to the loss of C_2H_2. A clearer fragmentation pattern was observed with prototype V due to the signal intensity being an order of magnitude higher. For both compounds examined this would appear to be the result of fragmentation of the ring structure.

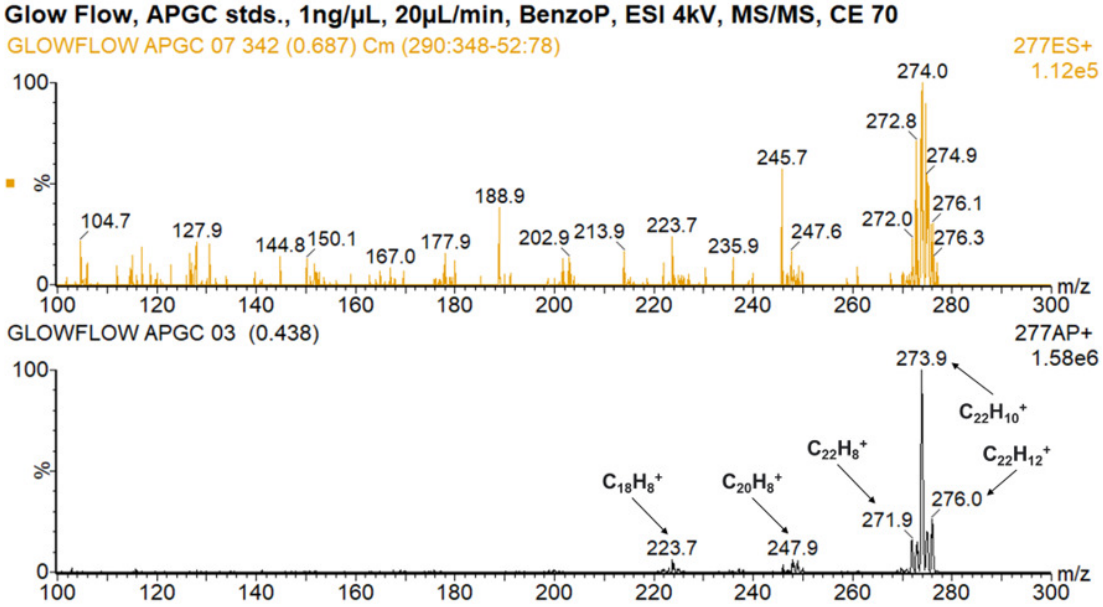

Figure 7.5: MS/MS mass spectrum of the fragment ions for the precursor ion at m/z 277 of Benzo[*ghi*]perylene. Top panel is ESI and the bottom panel is prototype V. A much clearer fragmentation pattern was observed with prototype V due to the signal intensity being an order of magnitude higher. The collision energy was set to 70 eV.

7.4 Comparison of prototype V for detection of extractables and leachables with electrospray ionization and atmospheric-pressure chemical ionization

Analysis of 18 compounds which are commonly detected extractables and leachables (E&L) in plastics manufacture was undertaken with the compounds listed in table A.1 and figure A.18. Prototype V was operated in constant current mode at 10 μA, and was compared to ESI and APCI with a corona discharge of 2 μA. The mass spectrometer was operated in full scan mode with polarity switching to gather data of positive and negative ions generated simultaneously, three measurements were undertaken with volumes of 1, 5, and 10 μL injected via the UHPLC using a water (with 0.1 % formic acid and 1 mM ammonium acetate) and methanol gradient over 15 minutes at 0.3 $mL\ min^{-1}$. A Waters CORTECS UPLC C_{18}, 1.6 μm, 2.1 x 100 mm column was used [148].

Positive ion

The peak area for the protonated molecule $[M + H]^+$ was tabulated for the 5 μL injection and the signal intensity was normalised to the ESI data to compare. Prototype V and APCI sources showed reduced sensitivity with respects to ESI. The results for positive ion mode are shown in figure 7.6 with only nine of the 18 compounds detected as some are only ionizable in negative ion mode.

However, the data for the protonated molecule is not necessarily representative for the compounds studied. As can be seen in figure 7.7 the protonated molecule

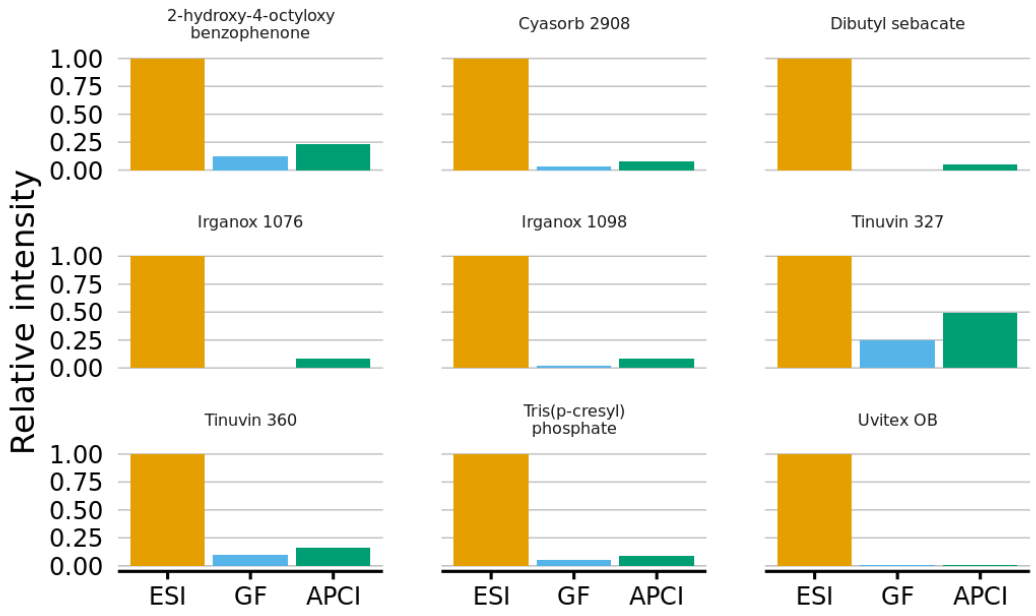

Figure 7.6: Histogram showing the relative abundance of the protonated molecule normalised to 1.00 for ESI. The comparison is of the 5 μL ($n = 1$) injection via Waters UHPLC, using a Waters CORTECS UPLC C_{18}, 1.6 μm, 2.1 x 100 mm column. Only nine of the 18 compounds gave ions in positive ion mode. The ESI source outperforms both prototype V (GF) and APCI sources in positive ion mode.

is not discernible in the mass spectrum of Ethanox 330 ($C_{54}H_{78}O_3$, M_r 774.60, $LogP$ 16.33) by ESI as the abundance of protonated molecule is low and can not be distinguished from the background noise, while intense ions are observed for the ammonium, sodium and potassium adducted molecular ions at m/z 792.4, 797.3, and 813.3.

Tinuvin compounds do not appear to form sodium adduct ions and there was no measurable signal. The hydroxyl group on the aromatic ring of Tinuvin maybe sterically hindered due to the presence of an ortho substituent making sodium adduction difficult. This would suggest that formation of sodium adducts may

be preferred when a suitable heteroatom for bonding exists and is not sterically hindered. The formation of $[M + Na]^+$ ions however does not appear to readily occur using either prototype V or APCI, both of which used the APCI IonSABRE II probe to nebulize the sample. This difference could therefore be due to the different mechanism that forms the ions in the gas-phase when compared to the solvated-phase for ESI [149].

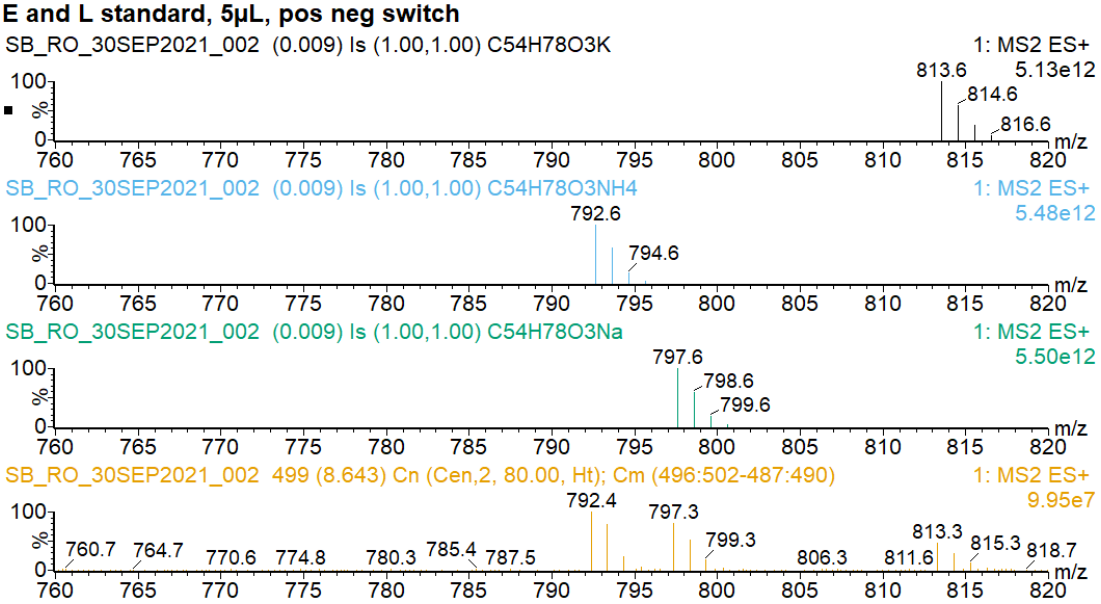

Figure 7.7: Mass spectrum of Ethanox 330 from the E&L standard by ESI in positive ion mode for the 5 μL injection via Waters UHPLC, using a Waters CORTECS UPLC C_{18}, 1.6 μm, 2.1 x 100 mm column.. A series of intense ions are observed at *m/z* 792.4, 797.3, and 813.3 corresponding to $[M + NH4]^+$, $[M + Na]^+$, and $[M + K]^+$ adducted ion species, respectively. The protonated molecule is not observed.

Negative ion

In negative ion mode a similar number of the compounds proved to be ionizable, only nine of the 18 E&L analytes gave a response. The peak area for the de-protonated molecule $[M-H]^-$ was tabulated for the 5 μL injection and the signal intensity was normalised to the ESI data. The results for negative ion mode are shown in figure 7.8, only nine of the 18 compounds were detected as some are only ionizable in positive ion mode. Five out of the nine showed improved signal intensity with the APCI and prototype V sources relative to ESI. The prototype V ionization source provided the strongest improvement in signal response for three of the compounds Cyasorb 2908, Tinvin 327 and Irganox 1076, which typically possess a hydroxyphenyl group, being 2, 8 and 8 times more intense than ESI, respectively. Switching polarity of the ionization source and extraction cone results in the alteration of the location of processed in the glow discharge where previous modelling work [95] suggest the density of generated positive reagent ions are at the maximum in the cathode dark space (CDS) which is near the cathode. This could result in more negative reagent ions being present at the point the sample is vaporised increasing the frequency of ionization and therefore increase relative signal intensity in negative ion mode.

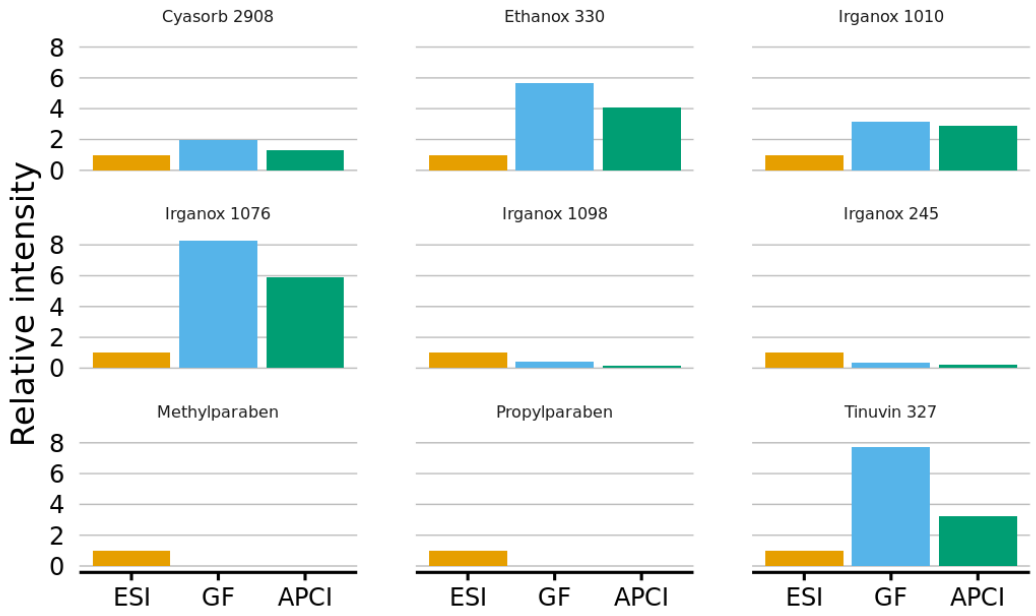

Figure 7.8: Histogram showing the relative intensities of the de-protonated molecule normalised to 1.00 for ESI. The comparison is of the 5 μL ($n = 1$) injection via Waters UHPLC, using a Waters CORTECS UPLC C_{18}, 1.6 μm, 2.1 x 100 mm column. For five of the nine compounds identified in negative ion mode there is an improved sensitivity for prototype V (GF) and APCI sources.

7.5 Discussion and Summary

An assessment of the prototype V ionization source was conducted using three analytical standards covering a broad range of chemistries, from polar to non-polar. The study allowed the source to be assessed using a UHPLC coupled to a triple quadrupole mass analyser providing fast chromatography, with respects to HPLC, and high analytical sensitivity. Prototype V provided DLs in the picogram range with good linearity ($R^2 > 0.98$) over 2-to-4 orders of magnitude, the use of the ESI probe in place of the APCI IonSABRE probe improved the DL in the low picogram range. However, in comparison to ESI, prototype V was an order of magnitude less sensitive for the polar compounds in the "six mix" standard.

The APGC standard had a more non-polar range of compounds, and prototype V was capable of ionising five of the eight compounds. In contrast ESI was only capable of generating ions of sufficient intensity for the identification of one of the compounds. The MS/MS mass spectra for both ionization methods proved to be similar in terms of the fragment ions observed for anthracene, making comparison of mass spectra between techniques possible.

A particular strength of prototype V was demonstrated in negative ion mode in the analysis of E&L standard commonly used in industry as polymer additives and preservatives, offering between 2 and 8 times enhancement of the signal from the integrated peak areas when compared to ESI.

In summary, prototype V in this assessment did not show as high a sensitivity to polar compounds when compared directly to ESI. However, there was improved ionization with respects to ESI for non-polar compounds, which had previously

been seen with PAH in chapter 6. Prototype V demonstrated superior capabilities in negative ion mass spectrometry with over twice the signal enhancement in many instances. This assessment and comparison of prototype V suggests it could be an important addition as part of a multimodal ionization source giving complementary data alongside APCI and APPI on compounds less amenable to ESI, in a step towards the development of a universal ionization source.

Chapter 8

Conclusions

I have investigated a series of APGD sources in this thesis for their potential to ionise chemistries not normally amenable to ionization by conventional atmospheric pressure ionization techniques. In total, four prototype sources (II, III, IV, and V) were designed and constructed, and a variety of parameters were measured to characterise the discharges. A novel micro-glow discharge source (prototype V) was interfaced with the Waters Xevo G2-S TOF mass spectrometer and it was used in combination with a range of sample introduction methods. An investigation using prototype V with a range of non-polar compounds, along with a smaller selection of polar compounds, was conducted to determine the breadth of its analytical capabilities.

The first source that was studied, was prototype II which had a conventional pin-to-capillary geometry and it was demonstrated that compounds with high vapour pressures and low molecular masses could be readily ionise and detected with this FAPA source in combination with the Waters Xevo G2-S TOF mass spectrometer. However, prototype II was large and bulky making the

retrofitting and integration with the Waters universal source housing difficult as the orientation of the inlet is different to the Thermo Scientific Imax housing which it was originally designed for and the space within the Waters housing is more limited. Therefore a second source (prototype III) using the same pin-to-capillary geometry was designed and manufactured in-house to address these limitations. The design reduced the volume of the discharge cell by 95 %, which allowed the source to be mounted directly onto the ion source block inside a capacitive assembly. This had the added benefit of reducing variability and improved reproducibility by maintaining a fixed position relative to the sample and mass spectrometer inlet. A third source design (prototype IV) used a novel capillary-to-capillary geometry, which simplified the source by combining the cathode and the helium gas line in a single part making it easier to operate. The final source that was designed and constructed was a micro-glow discharge ionization source (prototype V) which made use of the mass spectrometer internal power supply which reduced the components required and made operating the source easier as it could be controlled by the instrument software. The current-voltage characteristics of the micro-glow discharge increase linearly, which is consistent with the abnormal glow discharge regime (figure 1.3) seen with FAPA sources. As was shown the source benefits from low power consumption (1.4 to 66.6 mW) and has a "cold" thermodynamic gas temperature which likely contribute the source in general exhibiting "soft" ionization.

To accommodate prototype V, the universal source housing was adapted and it was positioned axially to the mass spectrometer inlet. This had the advantage of allowing the use of the existing set of sample introduction methods. The ASAP probe was operated across a range of desorption temperatures and was

used to analyse solids as well as liquid samples. This method is not particularly suited to routine quantitation but it did demonstrate its ability in combination with the prototype V ionization source to rapidly characterise and identify compounds of interest. Whereas the APCI IonSABRE probe was used for the analysis of compounds in solution either using flow-infusion with a loop-injector or alternatively with chromatography (HPLC and UHPLC). In this configuration prototype V did achieve consistent DL in the low nanogram range with linearity over four orders of magnitude. When the source was used with the ESI probe the DL improved which was in the sub-nanogram range, for sulfadimethoxine this was from 190 to 20 *pg*. In direct comparison with ESI the prototype V source was an order of magnitude less sensitive for polar compounds, however the prototype V source was more sensitive to non-polar compounds and it had up to eight-times the signal intensity for compounds in negative ion mode. Due to its compact and simple design the source could be easily integrated as a multimodal system in conjunction with other ionization sources, and can be readily interfaced with many types of chromatography and sample introduction methods.

A range of compounds have been characterised to understand the breadth of chemistries amiable to ionization using APGD ionization source. In particular small molecules which were generally non-polar were selected for analysis using prototype V. In positive ion mode protonated molecules were formed, also observed were dehydrated molecular ions for hydroxyl containing compounds along with molecular ions for compounds which could not be readily protonated. While in negative ion mode de-protonated molecules were formed using prototype V. Compounds in more complex mixtures could be identified using either statistical analysis such as Kendrick analysis or by employing chromatography to

separate the individual components. In addition to organic molecules prototype V was used for bio-analysis of lipids and oligopeptides extending the range of compounds that have been analysed by FAPA and APGD sources. Fatty acids and omega hydroxy fatty acids could be readily ionised and characterised in negative ion mode using prototype V without derivatization and this approach could be used to provide rapid analysis, in industry. Dehydration is commonly observed for sterols in mass spectrometry never the less these compounds could be easily identified from their masses using prototype V. An alternative approach was the use of *in situ* derivatization which showed some promise however low reaction yields and potential variability means its unlikely that this approach could be used for routine quantitation. In addition to the non-polar lipids, oligopeptides were also studied using prototype V, only the second time to be done so by FAPA, protonated molecules were observed along with extensive fragmentation suggesting that this source is less suited to thermally labile polar compounds.

In summary, a compact d.c. helium micro-glow discharge ionization source has been developed which was easily retrofitted to the Waters universal source housing, however the design also lends itself to integration with a range of other mass spectrometers given its compact nature allowing universal retrofitting. The repositioning of prototype V allowed it to be used with the existing sample introduction methods specifically ASAP probe, APCI IonSABRE, ESI probe, and also in conjunction with HPLC and UHPLC which meant that compounds with different vapour pressures and thermal stability in solid or liquid forms could be readily analysed. The source exhibited high analytical sensitivity in the nanogram range in both positive and negative modes, and was capable of ionising a wide range of compound chemistries from polar to non-polar, in particular it

showed particular sensitivity to non-polar compounds in negative ion mode when compared to ESI.

The source has the potential to operate in conjunction with a range of sample inlets and in combination with other ionization techniques as part of a multimodal platform to analyse the widest range of samples and a step towards an universal source. This micro-glow discharge ionization source would be particularly suited to an open-access laboratory where large volumes of samples with varying chemistries are analysed such as a university or fine chemicals industry, and can complement the existing suite of ionization techniques where compounds could less amenable to ionization by existing atmospheric pressure sources.

References

[1] Dempster, A. J. *Phys. Rev.* **1918,** *11,* 316–325.

[2] Munson, M. S. B.; Field, F. H. *J. Am. Chem. Soc.* **1966,** *88,* 2621–2630.

[3] Horning, M. G.; Casparrini, G.; Horning, E. C. *J. Chromatogr. Sci.* **1969,** *7,* 267–275.

[4] Robb, D. B.; Covey, T. R.; Bruins, A. P. *Anal. Chem.* **2000,** *72,* 3653–3659.

[5] Takáts, Z.; Wiseman, J. M.; Gologan, B.; Cooks, R. G. *Science* **2004,** *306,* 471–473.

[6] Cody, R. B.; Laramée, J. A.; Durst, H. D. *Anal. Chem.* **2005,** *77,* 2297–2302.

[7] Crookes, W. *Phil. Trans. R. Soc. Lond.* **1879,** *170,* 135–164.

[8] Siemens, W. *Ann. Phys. Chem.* **1857,** *178,* 66–122.

[9] Grimm, W. *Spectrochim. Acta B* **1968,** *23,* 443–454.

[10] Houk, R. S.; Fassel, V. A.; Flesch, G. D.; Svec, H. J.; Gray, A. L.; Taylor, C. E. *Anal. Chem.* **1980,** *52,* 2283–2289.

[11] Harper, J. D.; Charipar, N. A.; Mulligan, C. C.; Zhang, X.; Cooks, R. G.; Ouyang, Z. *Anal. Chem.* **2008,** *80,* 9097–9104.

[12] Andrade, F. J.; Shelley, J. T.; Wetzel, W. C.; Webb, M. R.; Gamez, G.; Ray, S. J.; Hieftje, G. M. *Anal. Chem.* **2008,** *80,* 2646–2653.

[13] Fenn, J. B.; Mann, M.; Meng, C. K.; Wong, S. F.; Whitehouse, C. M. *Mass Spectrom. Rev.* **1990,** *9,* 37–70.

[14] Shelley, J. T.; Hieftje, G. M. *J. Anal. At. Spectrom.* **2011,** *26,* 2153–2159.

[15] Yergey, A. L.; Yergey, A. K. *J. Am. Soc. Mass Spectrom.* **1997,** *8,* 943–953.

[16] Kingdon, K. H. *Phys. Rev.* **1923,** *21,* 408–418.

[17] Penning, F. M. *Physica* **1936,** *3,* 873–894.

[18] Stephens, W. E. *Phys. Rev.* **1946,** *69,* 674–674.

[19] Brunnée, C. *Int. J. Mass Spectrom. and Ion Processes* **1987,** *76,* 125–237.

[20] Brunée, C. *Int. J. Mass Spectrom. and Ion Processes* **1987,** *79,* R10.

[21] Chapman, J. R. *Practical Organic Mass Spectrometry: a guide for chemical and biochemical analysis;* J. Wiley: Chichester ; New York, 2nd ed.; 1993.

[22] Gross, J. H. *Mass spectrometry: a textbook;* Springer: Cham, 3rd ed.; 2018.

[23] Kenneth Marcus, R.; Hoegg, E. D.; Hall, K. A.; Williams, T. J.; Koppenaal, D. W. *Mass Spectrom. Rev* **2021,** 1–22.

[24] Meisenbichler, C.; Kluibenschedl, F.; Müller, T. *Anal. Chem.* **2020,** *92,* 14314–14318.

[25] Ai, W.; Nie, H.; Song, S.; Liu, X.; Bai, Y.; Liu, H. *J. Am. Soc. Mass Spectrom.* **2018,** *29,* 1408–1415.

[26] Pawlaczyk, M.; Cegłowski, M.; Frański, R.; Kurczewska, J.; Schroeder, G. *Materials* **2021,** *14,* 6388.

[27] Marcus, R. K.; Broekaert, J. A. C., Eds.; *Glow discharge plasmas in analytical spectroscopy;* J. Wiley: Chichester, England, 2003.

[28] Jakubowski, N.; Stuewer, D.; Toelg, G. *Spectrochim. Acta B* **1991,** *46,* 155–163.

[29] Evetts, I.; Milton, D.; Mason, R. *Biol. Mass Spectrom.* **1991,** *20,* 153–159.

[30] Kuwabara, H.; Tsuchiya, M. *J. Mass Spectrom. Soc. Jpn.* **1982,** *30,* 313–318.

[31] Hiraoka, K.; Fujimaki, S.; Kambara, S.; Furuya, H.; Okazaki, S. *Rapid Commun. Mass Spectrom.* **2004,** *18,* 2323–2330.

[32] Andrade, F. J.; Shelley, J. T.; Wetzel, W. C.; Webb, M. R.; Gamez, G.; Ray, S. J.; Hieftje, G. M. *Anal. Chem.* **2008,** *80,* 2654–2663.

[33] Shelley, J. T.; Wiley, J. S.; Hieftje, G. M. *Anal. Chem.* **2011,** *83,* 5741–5748.

[34] Zeiri, O. M.; Storey, A. P.; Ray, S. J.; Hieftje, G. M. *Anal. Chim. Acta* **2017,** *952,* 1–8.

[35] Yang, Z.; Pavlov, J.; Attygalle, A. B. *J. Mass. Spectrom.* **2012,** *47,* 845–852.

[36] Hassan, I.; Pinto, S.; Weisbecker, C.; Attygalle, A. B. *J. Am. Soc. Mass Spectrom.* **2016,** *27,* 394–401.

[37] Pavlov, J.; Douce, D.; Bajic, S.; Attygalle, A. B. *J. Am. Soc. Mass Spectrom.* **2019,** *30,* 2704–2710.

[38] Jecklin, M. C.; Schmid, S.; Urban, P. L.; Amantonico, A.; Zenobi, R. *Electrophoresis* **2010,** *31,* 3597–3605.

[39] Conrads, H.; Schmidt, M. *Plasma Sources Sci. Technol.* **2000,** *9,* 441.

[40] Na, N.; Zhao, M.; Zhang, S.; Yang, C.; Zhang, X. *J. Am. Soc. Mass Spectrom.* **2007,** *18,* 1859–1862.

[41] Shelley, J. T.; Chan, G. C.-Y.; Hieftje, G. M. *J. Am. Soc. Mass Spectrom.* **2012,** *23,* 407–417.

[42] Penning, F. M. *Sci. Nat.* **1927,** *15,* 818–818.

[43] Mason, R. S.; Miller, P. D.; Mortimer, I.; Mitchell, D. J.; Dash, N. A. *Phys. Rev. E* **2003,** *68,* 016408.

[44] Carroll, D. I.; Dzidic, I.; Stillwell, R. N.; Haegele, K. D.; Horning, E. C. *Anal. Chem.* **1975,** *47,* 2369–2373.

[45] Good, A.; Durden, D. A.; Kebarle, P. *J. Chem. Phys.* **1970,** *52,* 212–221.

[46] Lias, S. G.; Liebman, J. F.; Levin, R. D. *J. Phys. Chem. Ref. Data* **1984,** *13,* 695–808.

[47] Hunter, E. P. L.; Lias, S. G. *J. Phys. Chem. Ref. Data* **2009,** *27,* 413.

[48] Field, F. H.; Lampe, F. W. *J. Am. Chem. Soc.* **1958,** *80,* 5587–5592.

[49] Dzidic, I.; Carroll, D. I.; Stillwell, R. N.; Horning, E. C. *Anal. Chem.* **1976,** *48,* 1763–1768.

[50] Hsu, C. S.; Qian, K. *Anal. Chem.* **1993,** *65,* 767–771.

[51] Owen, B. C.; Gao, J.; Borton, D. J.; Amundson, L. M.; Archibold, E. F.; Tan, X.; Azyat, K.; Tykwinski, R.; Gray, M.; Kenttämaa, H. I. *Rapid Commun. Mass Spectrom.* **2011,** *25,* 1924–1928.

[52] Cooks, R. G.; Ouyang, Z.; Takats, Z.; Wiseman, J. M. *Science* **2006,** *311,* 1566–1570.

[53] McEwen, C. N.; McKay, R. G.; Larsen, B. S. *Anal. Chem.* **2005,** *77,* 7826–7831.

[54] Gong, X.; Zhao, Y.; Cai, S.; Fu, S.; Yang, C.; Zhang, S.; Zhang, X. *Anal. Chem.* **2014,** *86,* 3809–3816.

[55] Liu, P.; Forni, A.; Chen, H. *Anal. Chem.* **2014,** *86,* 4024–4032.

[56] Huang, M.-Z.; Zhou, C.-C.; Liu, D.-L.; Jhang, S.-S.; Cheng, S.-C.; Shiea, J. *Anal. Chem.* **2013,** *85,* 8956–8963.

[57] Hoffmann, E. d.; Stroobant, V. *Mass spectrometry: principles and applications;* Wiley: Chichester ; New York, 2nd ed.; 2001.

[58] Abian, J. *J. Mass Spectrom.* **1999,** *34,* 157–168.

[59] James, A. T.; Martin, A. J. P. *Analyst* **1952,** *77,* 915–932.

[60] Gohlke, R. S. *Anal. Chem.* **1959,** *31,* 535–541.

[61] Newman, K.; Mason, R. S. *J. Anal. At. Spectrom.* **2004,** *19,* 1134–1140.

[62] Zhao, J.; Zhu, J.; Lubman, D. M. *Anal. Chem.* **1992,** *64,* 1426–1433.

[63] Oliva, M.; Zhang, D.; Prada-Tiedemann, P.; Gamez, G. *Talanta* **2021,** *231,* 122333.

[64] Guć, M.; Cegłowski, M.; Pawlaczyk, M.; Kurczewska, J.; Reszke, E.; Schroeder, G. *Measurement* **2021,** *168,* 108326.

[65] Guć, M.; Schroeder, G. *Appl. Sci* **2020,** *10,* 4217.

[66] Fandino, J.; Orejas, J.; Chauvet, L.; Blanco, D.; Guillot, P.; Pisonero, J.; Bordel, N. *J. Anal. At. Spectrom.* **2020,** *35,* 2002–2010.

[67] Hiraoka, K.; Furuya, H.; Kambara, S.; Suzuki, S.; Hashimoto, Y.; Takamizawa, A. *Rapid Commun. Mass Spectrom.* **2006,** *20,* 3213–3222.

[68] Blair, S. L.; Ng, N. L.; Zambrzycki, S. C.; Li, A.; Fernández, F. M. *J. Am. Soc. Mass Spectrom.* **2018,** *29,* 635–639.

[69] Kuwabara, H.; Viden, I.; Tsuchiya, M.; Sugatani, J.; Saito, K. *J. Biochem.* **1986,** *100,* 477–484.

[70] Tsuchiya, M.; Kuwabara, H. *Anal. Chem.* **1984,** *56,* 14–19.

[71] Davies, C. *"Development of an Advanced Ionisation Technique for Mass Spectrometry: the Flowing Atmospheric Pressure Afterglow (FAPA) Ionisation Source",* Thesis, Swansea University, 2018.

[72] Mamyrin, B. A.; Karataev, V. I.; Shmikk, D. V.; Zagulin, V. A. *Journal of Experimental and Theoretical Physics* **1973,** *64,* 4.

[73] Dawson, J. H. J.; Guilhaus, M. *Rapid Commun. Mass Spectrom.* **1989,** *3,* 155–159.

[74] Morris, H. R.; Paxton, T.; Dell, A.; Langhorne, J.; Berg, M.; Bordoli, R. S.; Hoyes, J.; Bateman, R. H. *Rapid Commun. Mass Spectrom.* **1996,** *10,* 889–896.

[75] Waters Corporation, "Analysis of Environmental Contaminants using High Performance Quantitative LC/MS/MS", 2015.

[76] Paul, W.; Steinwedel, H. *Z. Naturforsch. A* **1953,** *8,* 448–450.

[77] Waters Corporation, "ACQUITY UPLC I-Class PLUS System brochure", 2018.

[78] Kim, S.; Chen, J.; Cheng, T.; Gindulyte, A.; He, J.; He, S.; Li, Q.; Shoemaker, B. A.; Thiessen, P. A.; Yu, B.; Zaslavsky, L.; Zhang, J.; Bolton, E. E. *Nucleic Acids Res.* **2021,** *49,* D1388–D1395.

[79] Matyash, V.; Liebisch, G.; Kurzchalia, T. V.; Shevchenko, A.; Schwudke, D. *J. Lipid Res.* **2008,** *49,* 1137–1146.

[80] R Core Team, "R: A language and environment for statistical computing.", 2019.

[81] Okabe, M.; Ito, K. "Color Universal Design (CUD) / Colorblind Barrier Free", 2002.

[82] Miller, J. N.; Miller, J. C. *Statistics and chemometrics for Analytical Chemistry;* Prentice Hall: Harlow, 6th ed.; 2010.

[83] IUPAC, *The IUPAC Compendium of Chemical Terminology: The Gold Book;* International Union of Pure and Applied Chemistry (IUPAC): Research Triangle Park, NC, 4th ed.; 2019.

[84] European Medicines Agency, "ICH Q2(R1) Validation of analytical procedures", Text CPMP/ICH/381/95, European Medicines Agency, 1995.

[85] Barwick, V. "Preparation of calibration curves: A guide to best practice", Technical Report LGC/VAM/2003/032, LGC, 2003.

[86] Marquardt, R.; Meija, J.; Mester, Z.; Towns, M.; Weir, R.; Davis, R.; Stohner, J. *Chemistry International* **2018,** *90,* 175-–180.

[87] Kendrick, E. *Anal. Chem.* **1963,** *35,* 2146–2154.

[88] Llewellyn-Jones, F. *The Glow Discharge;* Methuen: London, 1966.

[89] Fridman, A. A. *Plasma chemistry;* Cambridge University Press: Cambridge, 1st ed.; 2012.

[90] Llewellyn-Jones, F. *Ionization and Breakdown in Gases;* Methuen: London, 1957.

[91] Sommerfeld, A. *Z. Physik* **1928,** *47,* 1–32.

[92] Gearhart, C. A. *Stud. Hist. Philos. Sci. B - Stud. Hist. Philos. Mod. Phys.* **2017,** *60,* 95–109.

[93] Hodgman, S. S.; Dall, R. G.; Byron, L. J.; Baldwin, K. G. H.; Buckman, S. J.; Truscott, A. G. *Phys. Rev. Lett.* **2009,** *103,* 053002.

[94] Hornbeck, J. A.; Molnar, J. P. *Phys. Rev.* **1951,** *84,* 621–625.

[95] Martens, T.; Mihailova, D.; van Dijk, J.; Bogaerts, A. *Anal. Chem.* **2009,** *81,* 9096–9108.

[96] Chan, G. C.-Y.; Shelley, J. T.; Wiley, J. S.; Engelhard, C.; Jackson, A. U.; Cooks, R. G.; Hieftje, G. M. *Anal. Chem.* **2011,** *83,* 3675–3686.

[97] Cody, R. B. *Anal. Chem.* **2009,** *81,* 1101–1107.

[98] Shelley, J. T.; Wiley, J. S.; Chan, G. C. Y.; Schilling, G. D.; Ray, S. J.; Hieftje, G. M. *J. Am. Soc. Mass Spectrom.* **2009,** *20,* 837–844.

[99] Aghaei, M.; Bogaerts, A. *Anal. Chem.* **2021,** *93,* 6620–6628.

[100] Hollas, J. M. *Basic Atomic and Molecular Spectroscopy;* Royal Society of Chemistry: Cambridge, UK, 2002.

[101] Sanz-Medel, A.; Pereiro, R.; Costa-Fernández, J. M. *Basic Chemometric Techniques in Atomic Spectroscopy;* Royal Society of Chemistry: Cambridge, UK, 2013.

[102] Paschen, F. *Ann. Phys. (Berl.)* **1889,** *273,* 69–96.

[103] Andrade-Garda, J. M.; of Chemistry (Great Britain), R. S., Eds.; *Basic chemometric techniques in atomic spectroscopy;* RSC analytical spectroscopy monographs RSC Publishing: Cambridge, 2009.

[104] Pfeuffer, K. P.; Schaper, J. N.; Shelley, J. T.; Ray, S. J.; Chan, G. C.-Y.; Bings, N. H.; Hieftje, G. M. *Anal. Chem.* **2013,** *85,* 7512–7518.

[105] Schilling, G. D.; Shelley, J. T.; Barnes, J. H.; Sperline, R. P.; Denton, M. B.; Barinaga, C. J.; Koppenaal, D. W.; Hieftje, G. M. *J. Am. Soc. Mass Spectrom.* **2010,** *21,* 97–103.

[106] Yang, Z.; Attygalle, A. B. *J. Am. Soc. Mass Spectrom.* **2011,** *22,* 1395–1402.

[107] Gangam, R.; Pavlov, J.; Attygalle, A. B. *J. Am. Soc. Mass Spectrom.* **2015,** *26,* 1252–1255.

[108] Pfeuffer, K. P.; Shelley, J. T.; Ray, S. J.; Hieftje, G. M. *J. Anal. At. Spectrom.* **2013,** *28,* 379–387.

[109] Badal, S. P.; Michalak, S. D.; Chan, G. C.-Y.; You, Y.; Shelley, J. T. *Anal. Chem.* **2016,** *88,* 3494–3503.

[110] Wishart, D. S. *Bioanalysis* **2009,** *1,* 1579–1596.

[111] Wooding, K. M.; Hankin, J. A.; Johnson, C. A.; Chosich, J. D.; Baek, S. W.; Bradford, A. P.; Murphy, R. C.; Santoro, N. *Steroids* **2015,** *96,* 89–94.

[112] Chu, L.; Li, N.; Deng, J.; Wu, Y.; Yang, H.; Wang, W.; Zhou, D.; Deng, H. *Journal of Pharmaceutical and Biomedical Analysis* **2020,** *185,* 113223.

[113] Kuhlmann, C.; Heide, M.; Engelhard, C. *Anal. Bioanal. Chem.* **2019,** *411,* 6213–6225.

[114] Beynon, J. H. *Nature* **1954,** *174,* 735–737.

[115] Lipinski, C. A.; Lombardo, F.; Dominy, B. W.; Feeney, P. J. *Adv. Drug Deliv. Rev.* **1997,** *23,* 3–25.

[116] Veber, D. F.; Johnson, S. R.; Cheng, H.-Y.; Smith, B. R.; Ward, K. W.; Kopple, K. D. *J. Med. Chem.* **2002,** *45,* 2615–2623.

[117] Jia, C.; Zhang, J.; Yu, L.; Wang, C.; Yang, Y.; Rong, X.; Xu, K.; Chu, M. *Frontiers in Cellular and Infection Microbiology* **2019,** *8,* 445.

[118] Habermann, S. M.; Murphy, K. P. *Protein Sci.* **1996,** *5,* 1229–1239.

[119] Williams, C.; Hunter, A.; Stein, B. "Electrospray Accurate Mass Measurement Using Polyethylenimine as an Internal Reference Standard", 2006.

[120] Sullivan, G. L.; Delgado-Gallardo, J.; Watson, T. M.; Sarp, S. *Water Res.* **2021,** *196,* 117033.

[121] Lim, X. *Nature* **2021,** *593,* 22–25.

[122] Geyer, R.; Jambeck, J. R.; Law, K. L. *Sci. Adv* **2017,** *3,* e1700782.

[123] Cody, R. B. *J. Am. Soc. Mass Spectrom.* **2020,** *31,* 1004–1005.

[124] Marshall, A. G.; Rodgers, R. P. *Acc. Chem. Res.* **2004,** *37,* 53–59.

[125] Marshall, A. G.; Rodgers, R. P. *PNAS* **2008,** *105,* 18090–18095.

[126] Barrère, C.; Hubert-Roux, M.; Afonso, C.; Racaud, A. *J. Mass Spectrom.* **2014,** *49,* 709–715.

[127] Ratsameepakai, W.; Herniman, J. M.; Jenkins, T. J.; Langley, G. J. *Energy Fuels* **2015,** *29,* 2485–2492.

[128] Langley, G. J.; Herniman, J.; Carter, A.; Wilmot, E.; Ashe, M.; Barker, J. *Energy Fuels* **2018,** *32,* 10580–10585.

[129] Purghart, V.; Jäckle, H. *Chimia* **2010,** *64,* 196–196.

[130] Ravindra, K.; Sokhi, R.; Van Grieken, R. *Atmos. Environ.* **2008,** *42,* 2895–2921.

[131] Boström, C.-E.; Gerde, P.; Hanberg, A.; Jernström, B.; Johansson, C.; Kyrklund, T.; Rannug, A.; Törnqvist, M.; Victorin, K.; Westerholm, R. *Environ Health Perspect* **2002,** *110,* 451–488.

[132] Nebert, D. W.; Dalton, T. P.; Okey, A. B.; Gonzalez, F. J. *J. Biol. Chem.* **2004,** *279,* 23847–23850.

[133] ExxonMonil Aviation, "Safety Data Sheet | Mobil Jet™ Oil II", 2021.

[134] Winder, C.; Balouet, J.-C. *Environ. Res.* **2002,** *89,* 146–164.

[135] Liti, G. *eLife* **2015,** *4,* e05835.

[136] EFSA Panel on Food Additives and Nutrient Sources added to Food (ANS), *et al. EFSA Journal* **2017,** *15,* e04788.

[137] Tuller, G.; Nemec, T.; Hrastnik, C.; Daum, G. *Yeast* **1999,** *15,* 1555–1564.

[138] Klug, L.; Daum, G. *FEMS Yeast Res.* **2014,** *14,* 369–388.

[139] Zhao, X.; Zhu, S.; Liu, H. *J. Sep. Sci.* **2020,** *43,* 1838–1846.

[140] Qin, Q.; Feng, D.; Hu, C.; Wang, B.; Chang, M.; Liu, X.; Yin, P.; Shi, X.; Xu, G. *J. Chromatogr. A* **2020,** *1614,* 460709.

[141] Marquis, B. J.; Louks, H. P.; Bose, C.; Wolfe, R. R.; Singh, S. P. *Chromatographia* **2017,** *80,* 1723–1732.

[142] van Bergen, P. F.; Scott, A. C.; Barrie, P. J.; de Leeuw, J. W.; Collinson, M. E. *Org. Geochem.* **1994,** *21,* 107–112.

[143] Cutler, D. F.; Alvin, K. L.; Price, C. E., Eds.; *The Plant cuticle: papers presented at an international symposium organized by the Linnean Society of London, held at Burlington House, London, 8-11 September 1980;* Linnean Society symposium series 10; Published for the Linnean Society of London by Academic Press: London ; New York, 1982.

[144] Peng, Y.; Munoz-Pinto, D. J.; Chen, M.; Decatur, J.; Hahn, M.; Gross, R. A. *Biomacromolecules* **2014,** *15,* 4214–4227.

[145] Kurtzman, C. P.; Price, N. P.; Ray, K. J.; Kuo, T.-M. *FEMS Microbiol. Lett.* **2010,** *311,* 140–146.

[146] Warrilow, A. G.; Nishimoto, A. T.; Parker, J. E.; Price, C. L.; Flowers, S. A.; Kelly, D. E.; Rogers, P. D.; Kelly, S. L. *Antimicrob. Agents Chemother.* **2019,** *63,* e02586–18.

[147] Borisov, R. S.; Esparza, C.; Goriainov, S. V.; Zaikin, V. G. *Talanta* **2019,** *200,* 31–40.

[148] Waters Corporation, "Extractables & Leachables Screening Standard Care and Use Manual | Waters", 2020.

[149] Thurman, E. M.; Ferrer, I.; Barceló, D. *Anal. Chem.* **2001,** *73,* 5441–5449.

Appendix A

Supplementary data

A.1 Chapter 2

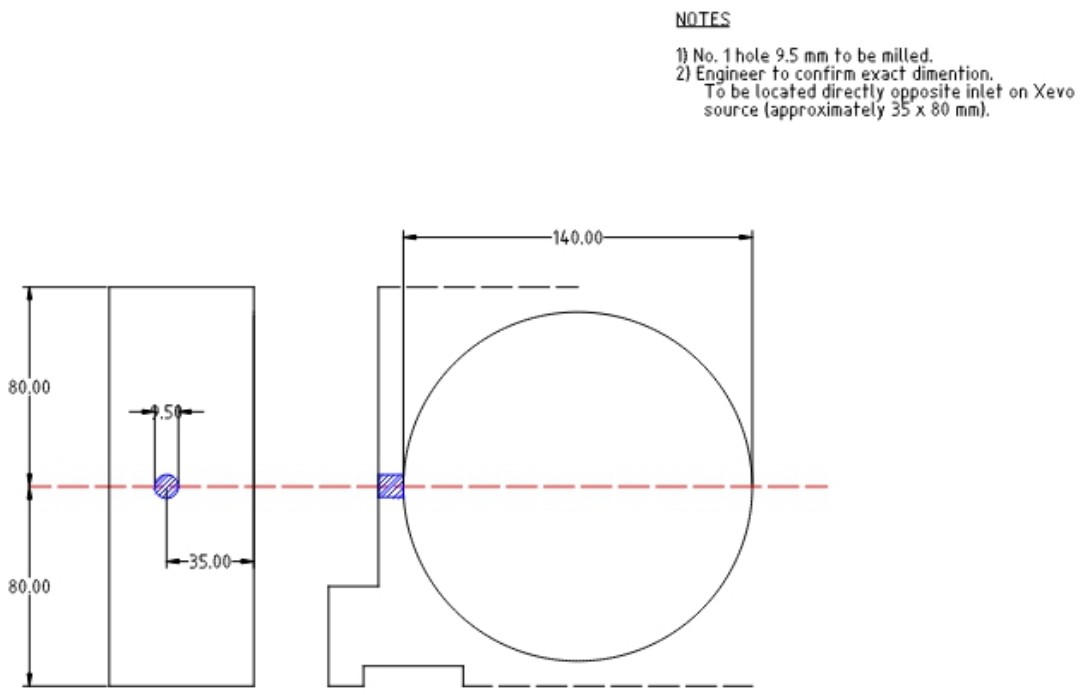

Figure A.1: Drawing of adaption to the universal source enclosure to accommodate prototype V ionization source. A 9.5 mm hole was milled into the body of the enclosure axially (head-on) to the inlet orifice of the mass spectrometer.

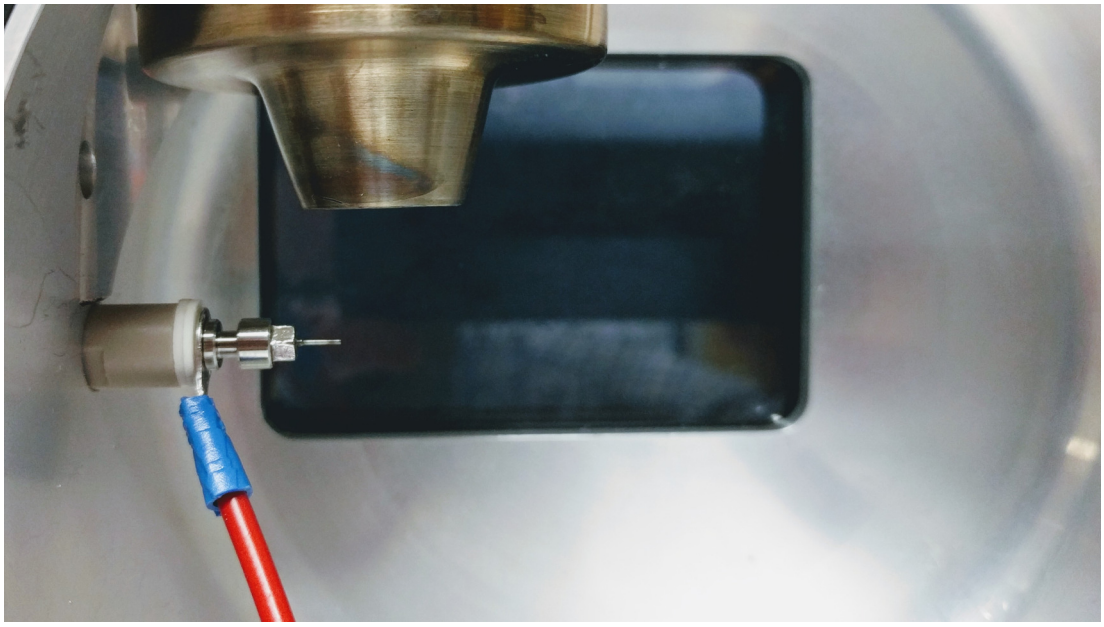

Figure A.2: Image of prototype V ionization source positioned *in situ* within the adapted universal source enclosure. Visible is the prototype V electrode with power connector (left) and end of the heated nebulizer (top).

A.2 Chapter 4

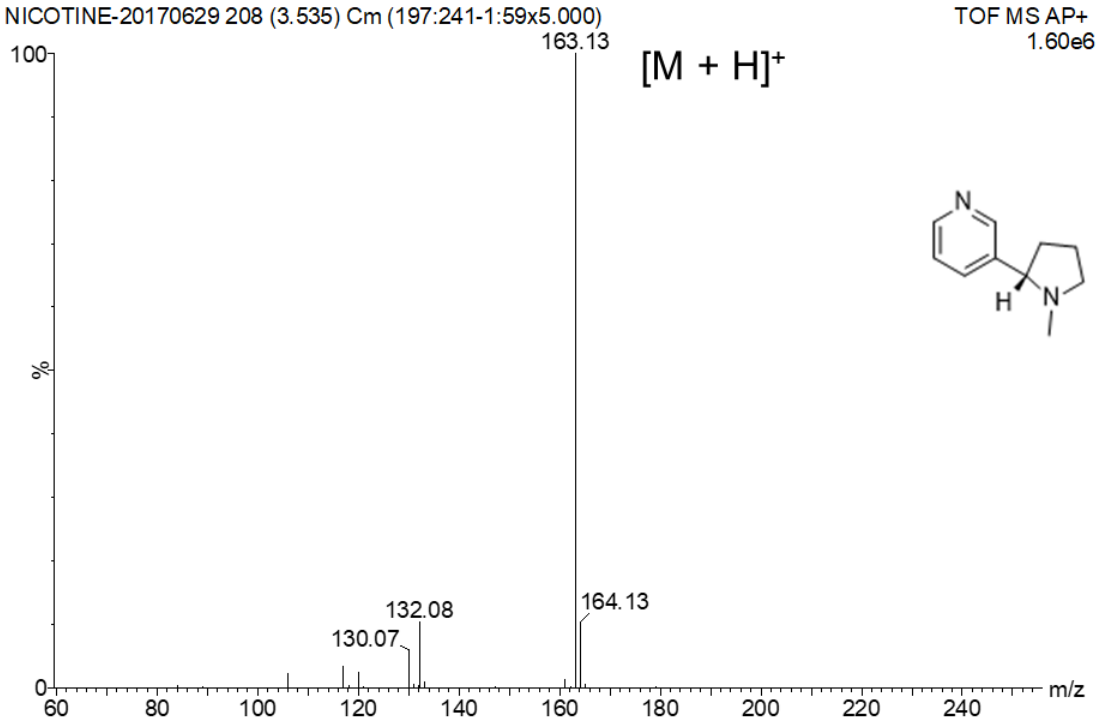

Figure A.3: Mass spectra of nicotine acquired in positive ion mode using the FAPA prototype II ionization source on the Waters Xevo G2-S mass spectrometer. Base peak observed was the protonated molecule ($[M + H]^+$) at *m/z* 163.

A.3 Chapter 5

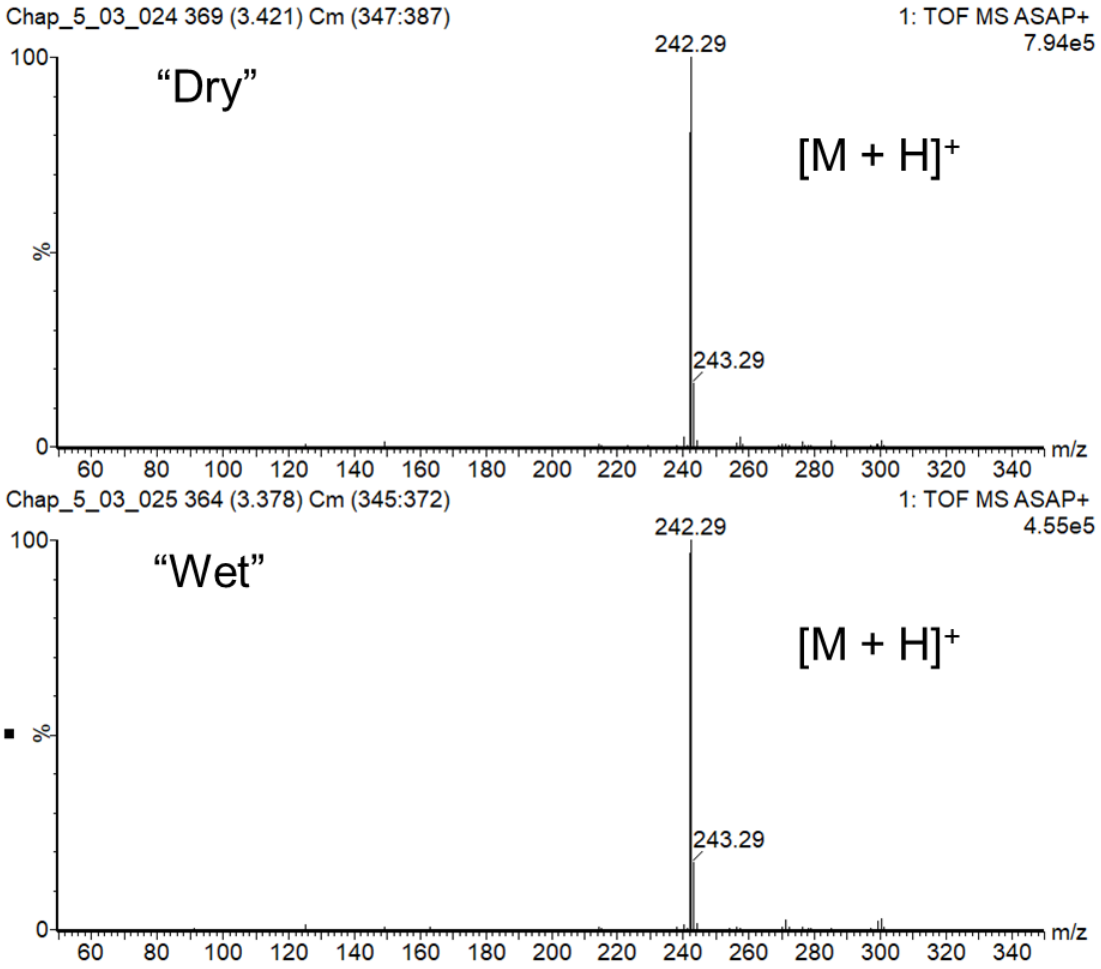

Figure A.4: Mass spectra of hexadcylamine, showing the abundance of the protonated molecule m/z 242.29 comparing both wet and dry conditions in figure 5.13. The phase of the sample does not appear to alter the ion species formed.

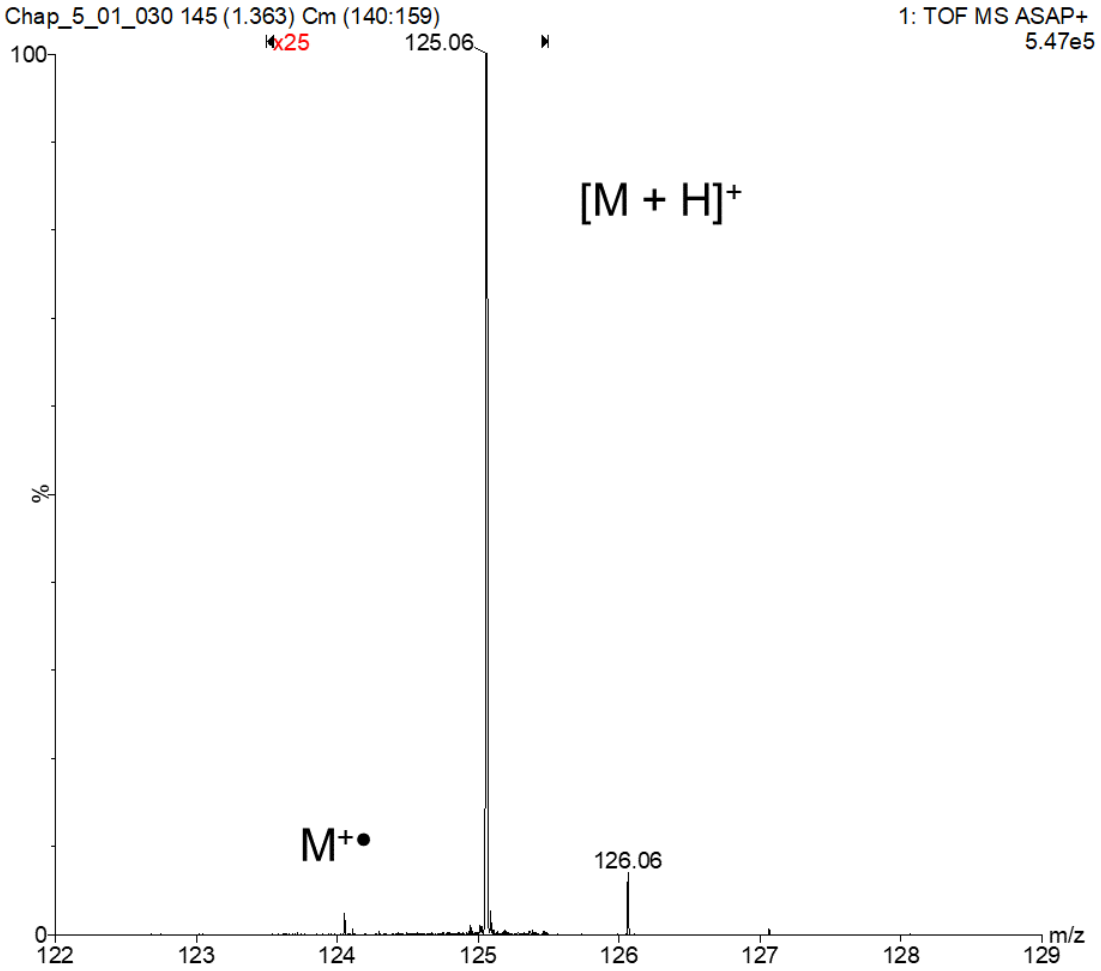

Figure A.5: Mass spectrum of 2,6-dimethyl-γ-pyrone showing the relative intensities of the protonated molecule and molecular ion as recorded in figure 5.15. The spectrum has been magnified to show the molecular ion ($M^{+\bullet}$) which is less than 1 % relative intensity for the base peak for the protonated molecule.

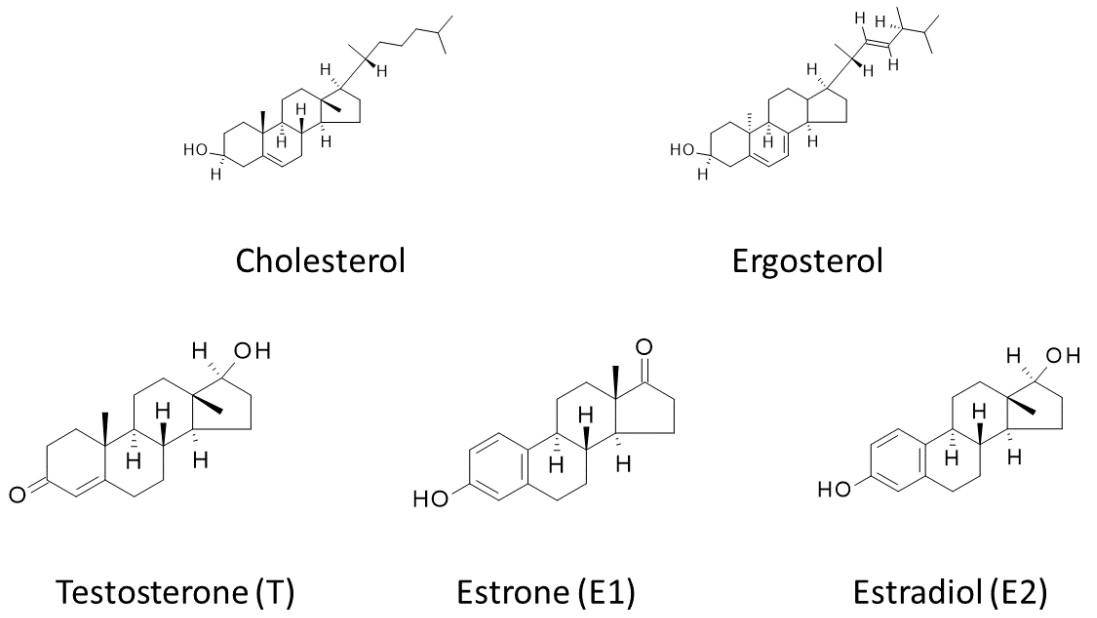

Figure A.6: Structures of the steroid compounds listed in table 5.2. The five steroids were used to develop analytical figures of merit for prototype V in combination with different sample introduction methods.

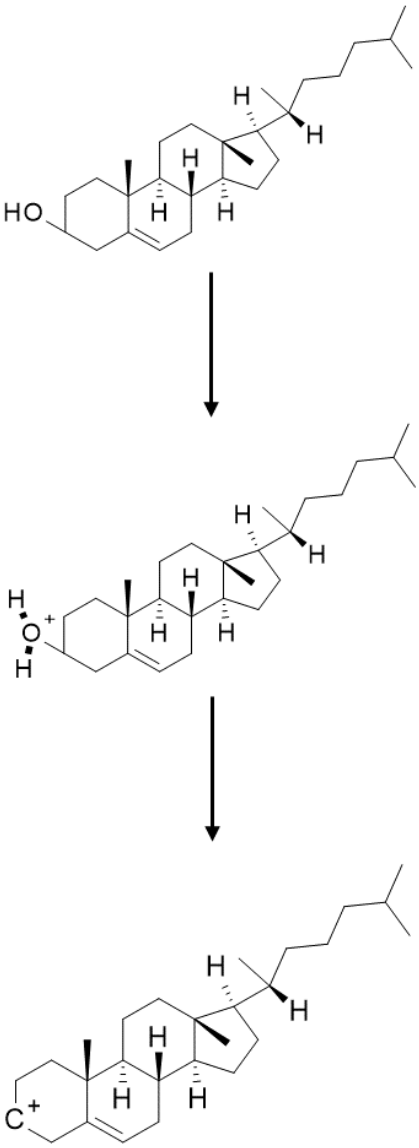

Figure A.7: Fragmentation mechanism of sterol cholesterol in chapter 5. For steroid compounds with hydroxyl group at carbon-3 position, protonation of the hydroxyl group leads to the formation of OH_2^+ which is unstable and likely fragments leading to dehydration of the ion with a stable charge remaining on the steroid fused ring system.

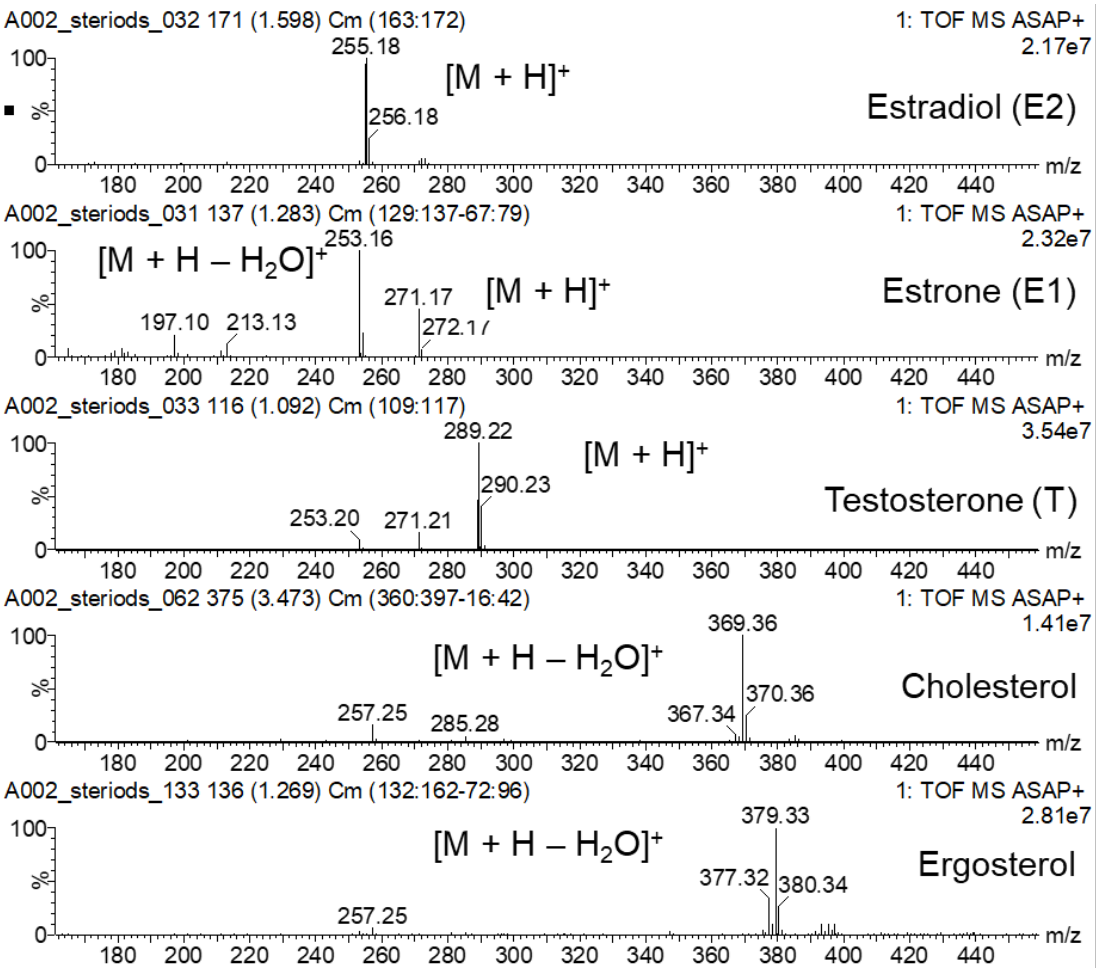

Figure A.8: Mass spectra of typical ions observed for the compounds cholesterol (*m/z 369*), estrone (*m/z 271*), ergosterol (*m/z 379*), testosterone (*m/z 289*), and estradiol (*m/z 255*) analysed using prototype V in conjunction with solids analysis probe, for calibration curves in figure 5.18.

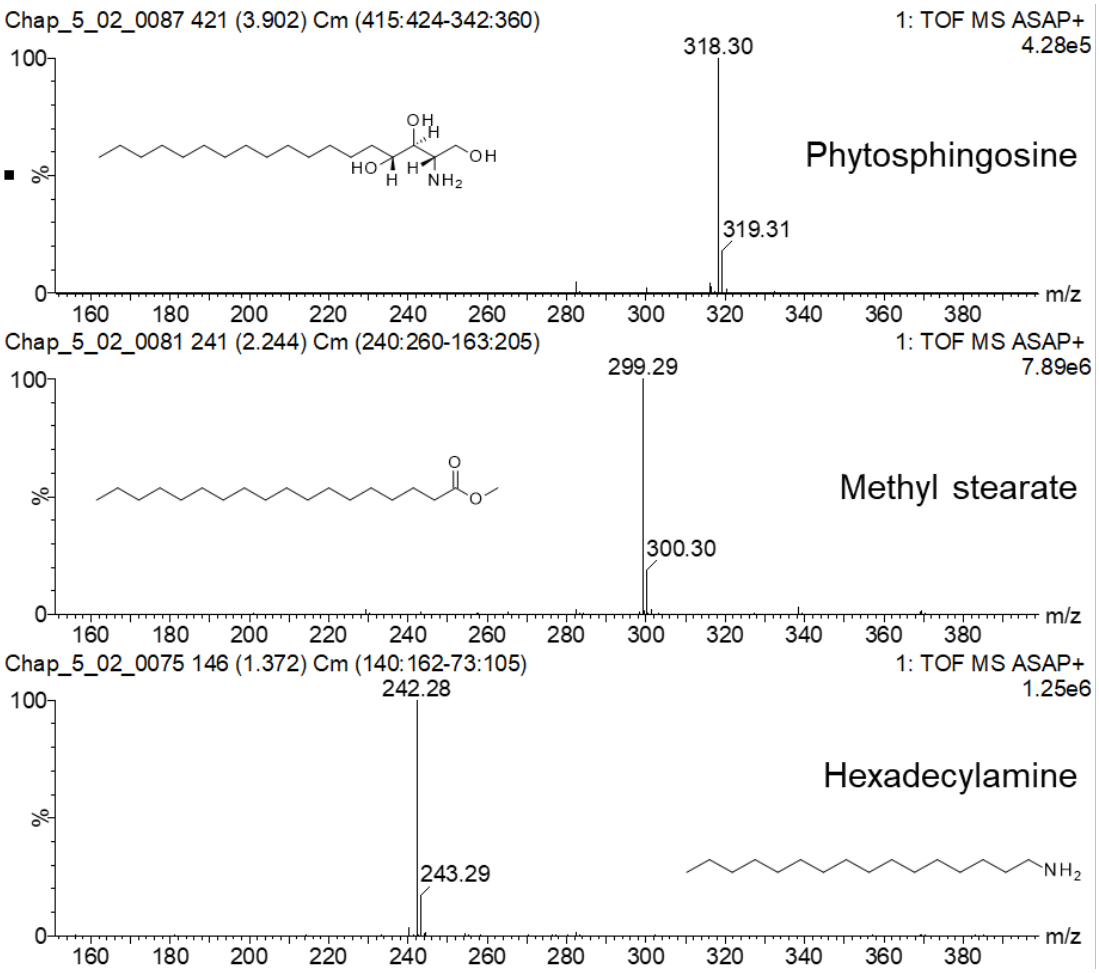

Figure A.9: Mass spectra of typical ions observed for hexadecylamine ($C_{16}H_{35}N$, M_r 241), methyl stearate ($C_{19}H_{38}O_2$, M_r 298), and phytosphingosine ($C_{18}H_{39}NO_3$, M_r 317) analysed using prototype V in conjunction with solids analysis probe, for calibration curves in figure 5.19.

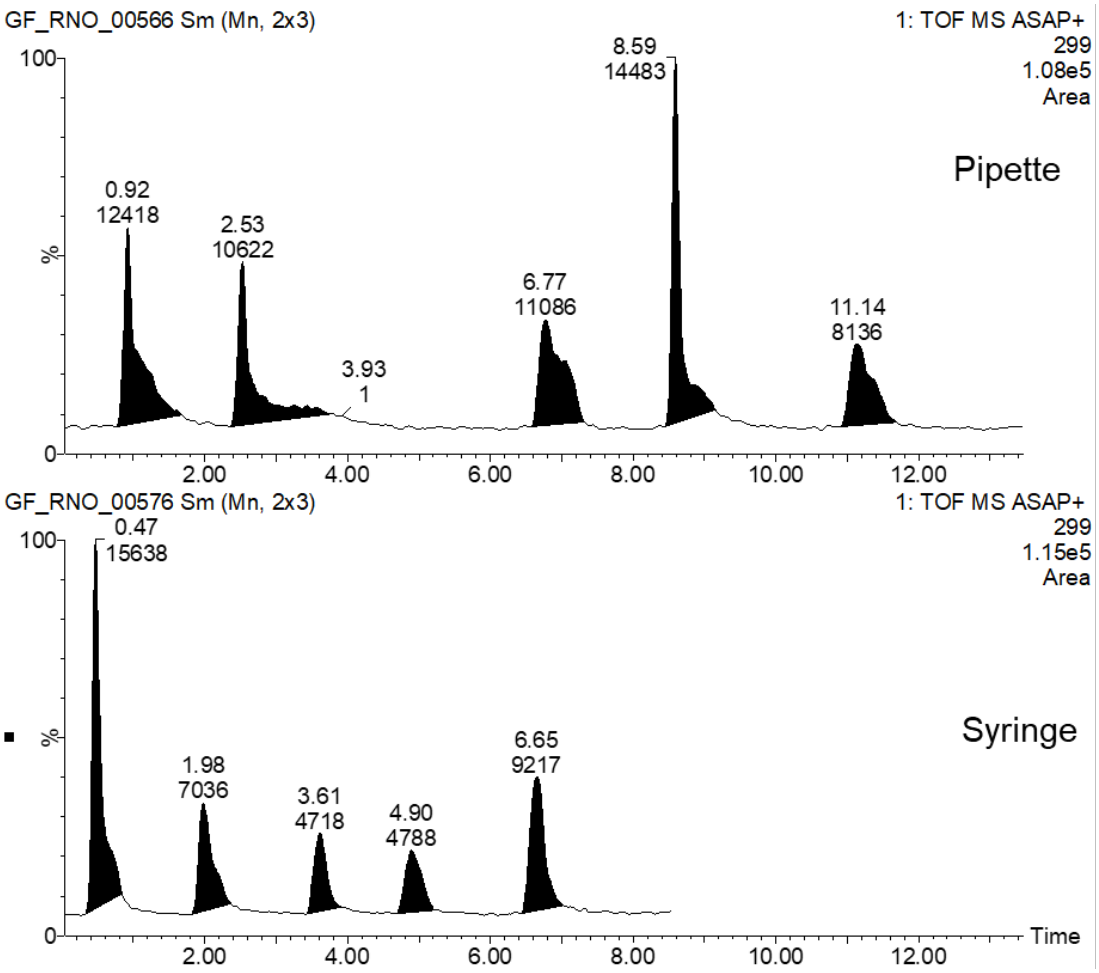

Figure A.10: XIC of methyl stearate ion at 0.1 $nmol$ showing the difference in abundance of the protonated molecule at m/z 299 using a pipette (top) and syringe (bottom) to deposit the sample on the glass capillary.

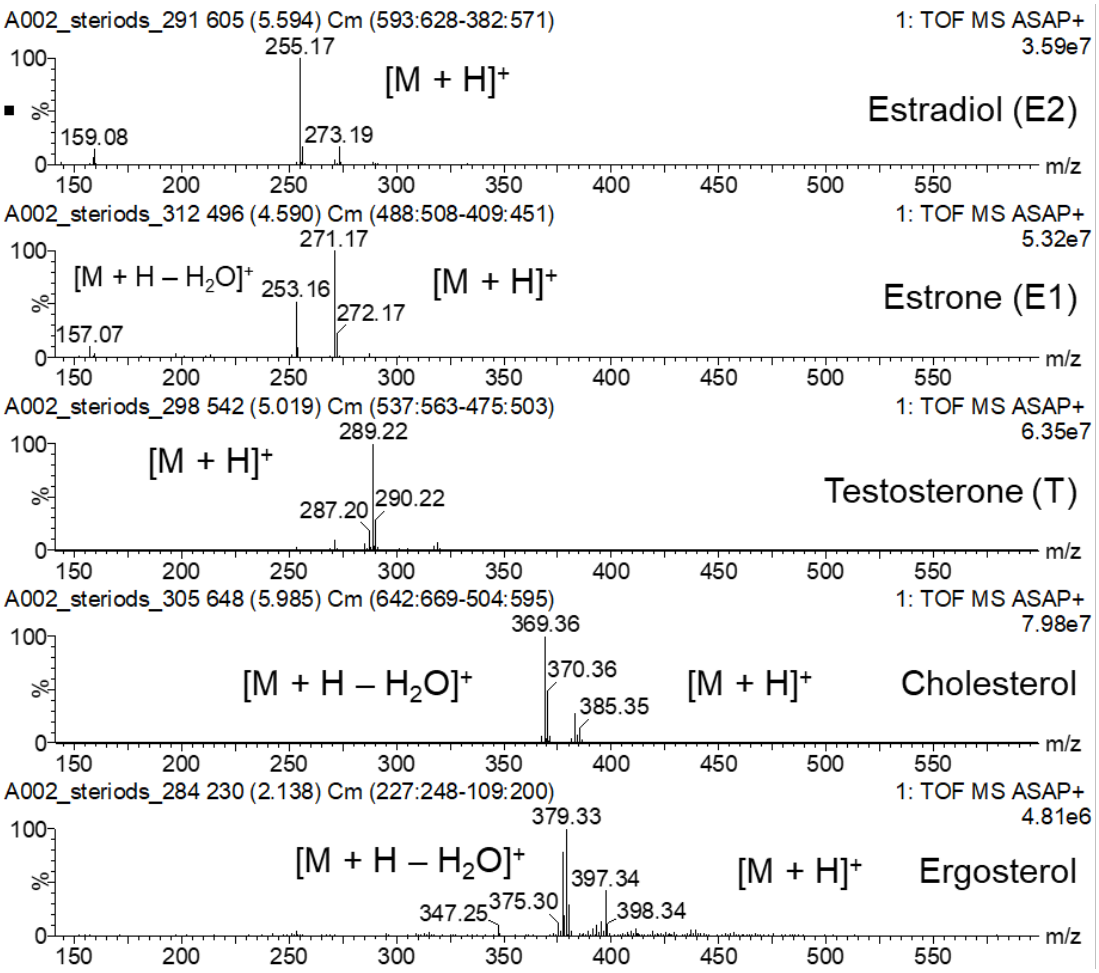

Figure A.11: Mass spectra of typical ions observed for the compounds cholesterol (*m/z 369*), estrone (*m/z 271*), ergosterol (*m/z 379*), testosterone (*m/z 289*), and estradiol (*m/z 255*) analysed using prototype V in conjunction with loop-injection, for calibration curves in figure 5.21.

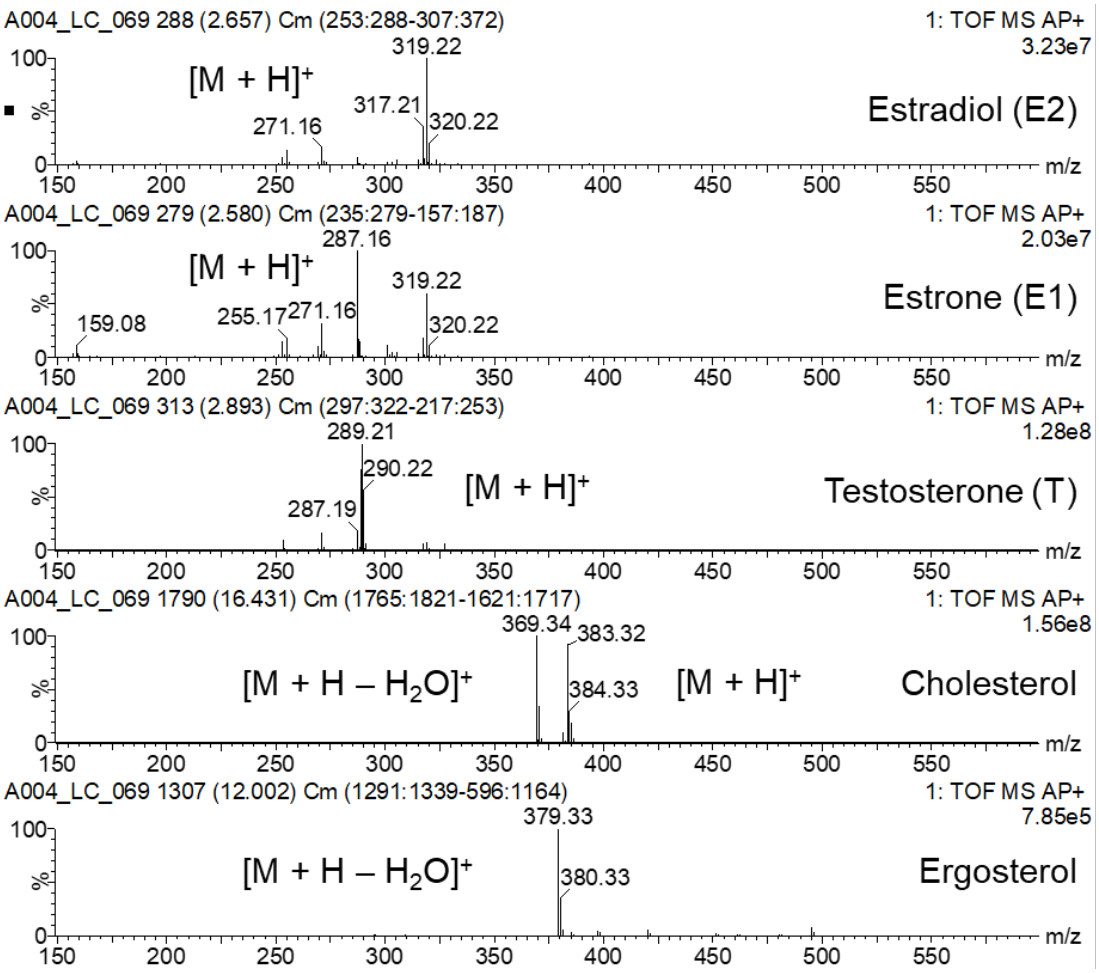

Figure A.12: Mass spectra of typical ions observed for the compounds cholesterol (*m/z 369*), estrone (*m/z 271*), ergosterol (*m/z 379*), testosterone (*m/z 289*), and estradiol (*m/z 255*, weak) analysed using prototype V in conjunction with HPLC, for calibration curves in figure 5.22. Unknown ions at *m/z* 287.1668 (accurate mass measurement *m/z* 287.1647 δ 2.1 mDa $C_{18}H_{23}O_3$) and 319.2291 (accurate mass measurement *m/z* 319.2273 δ 2.3 mDa $C_{20}H_{31}O_3$) in the mass spectra of estrone and estradiol.

A.4 Chapter 6

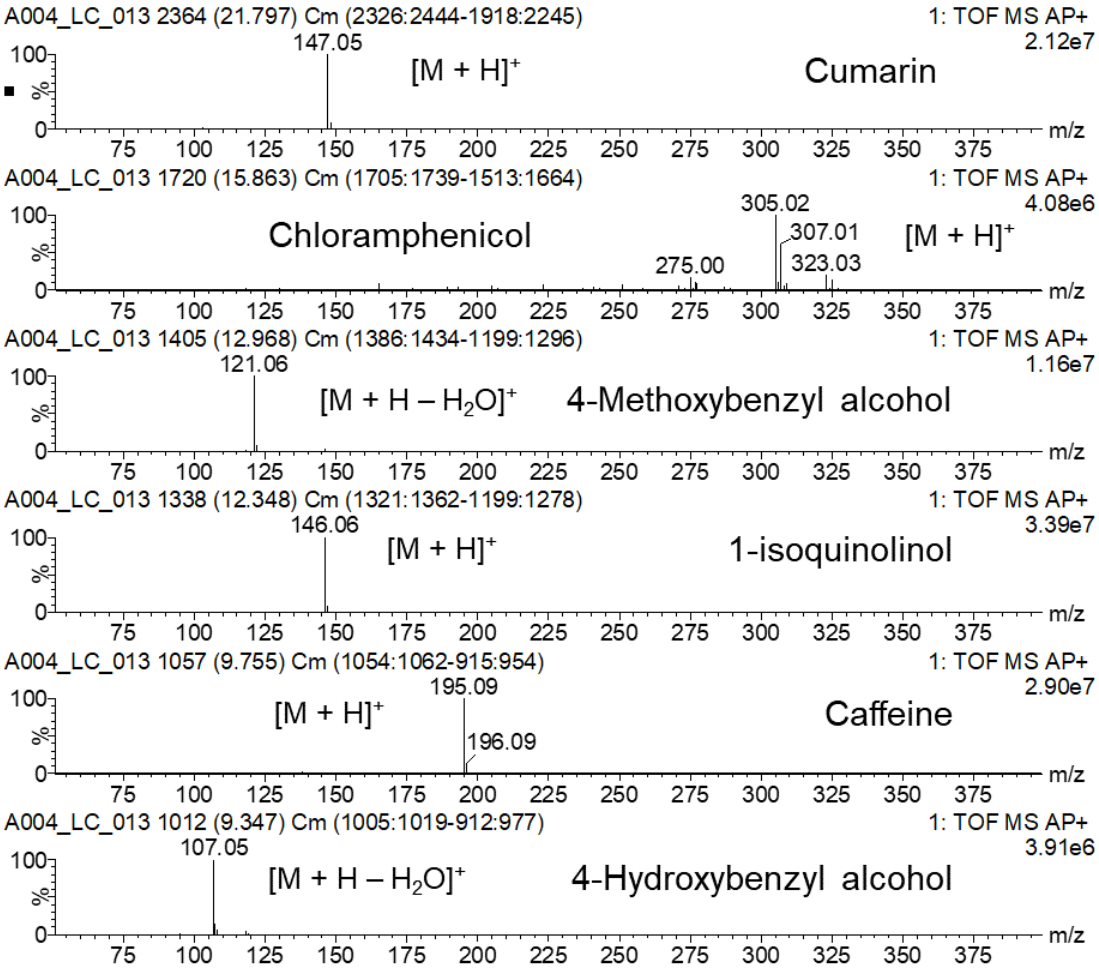

Figure A.13: Mass spectra of the six components identified in the base peak ion chromatogram in figure 6.1, ions observed are annotated in each spectrum.

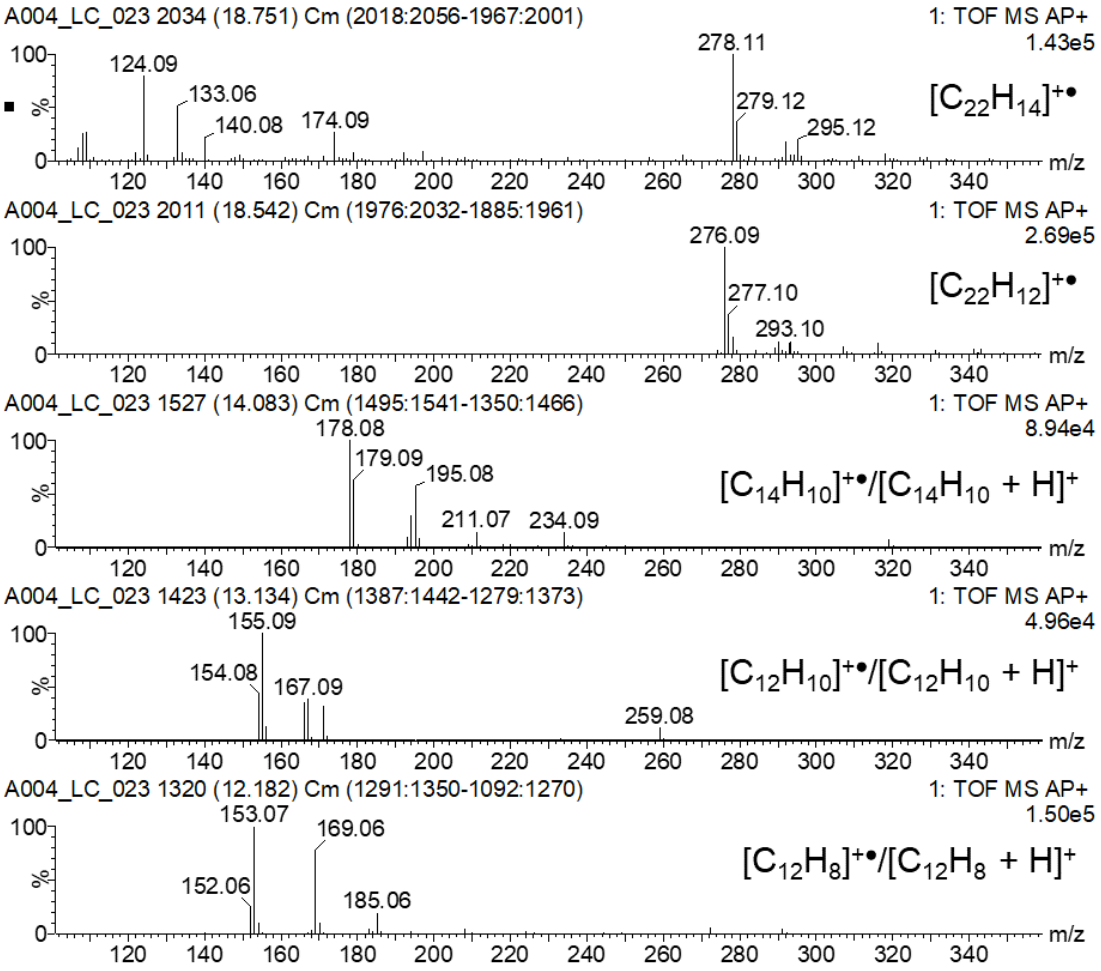

Figure A.14: Representative mass spectra showing five of PAH components listed in table 6.4 analysed by LC-MS using prototype V. Some of the compounds share the same molecular formula and mass, e.g. anthracene and phenanthrene at *m/z* 178 ($M^{+\bullet}$). The ratio of the abundance of the protonated molecule and the molecular ion vary, and do not appear to follow a specific pattern. There is evidence of possible oxygen adduct ions present in the mass spectra.

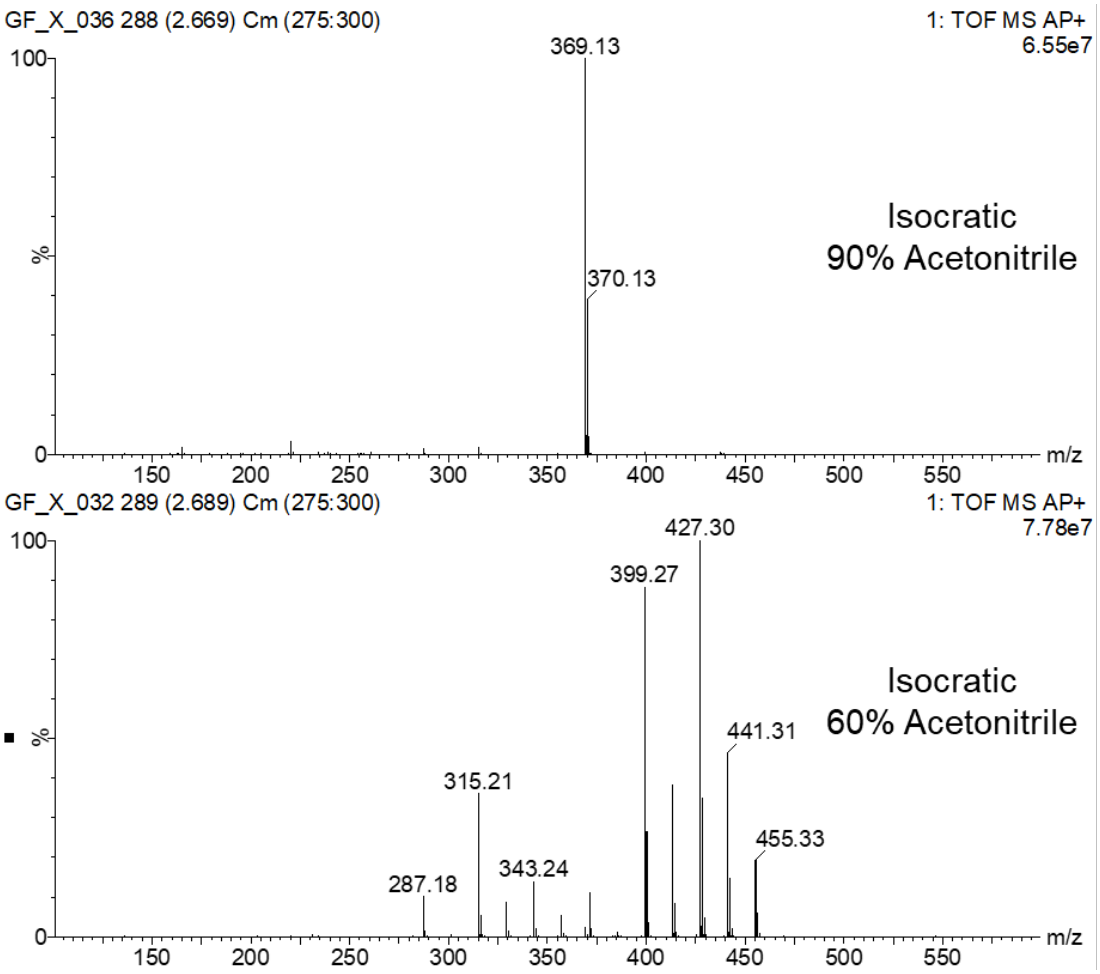

Figure A.15: Mass spectra of Mobil Jet Oil II by LC-MS using prototype V, showing improved separation of the components at 90 % acetonitrile compared to 60 % as shown in the TIC in figure6.1 over the scan range of 275-300. The tricresyl phosphate ion is isolated from other components and can be easily identified (top panel).

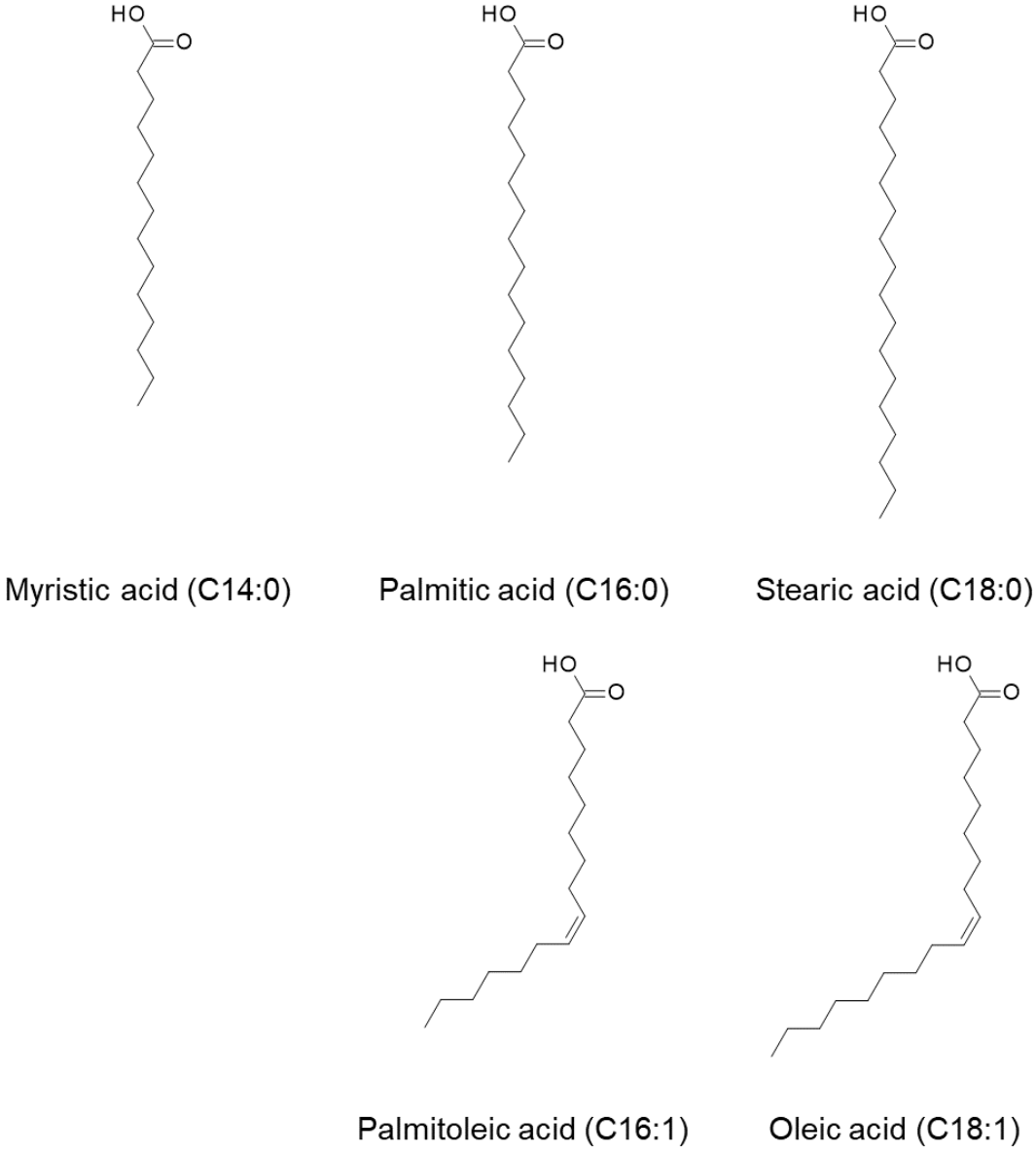

Figure A.16: Structures of free fatty acids identified in figure 6.12.

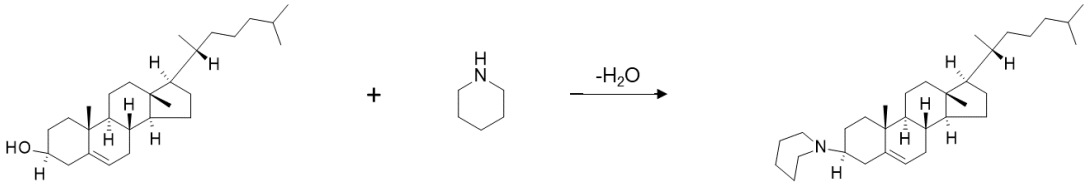

Figure A.17: Mechanism showing the *In situ* derivatization of cholesterol with the base piperidine. Elimination of water takes place between the secondary amine of the piperidine and the hydroxyl of the cholesterol.

A.5 Chapter 7

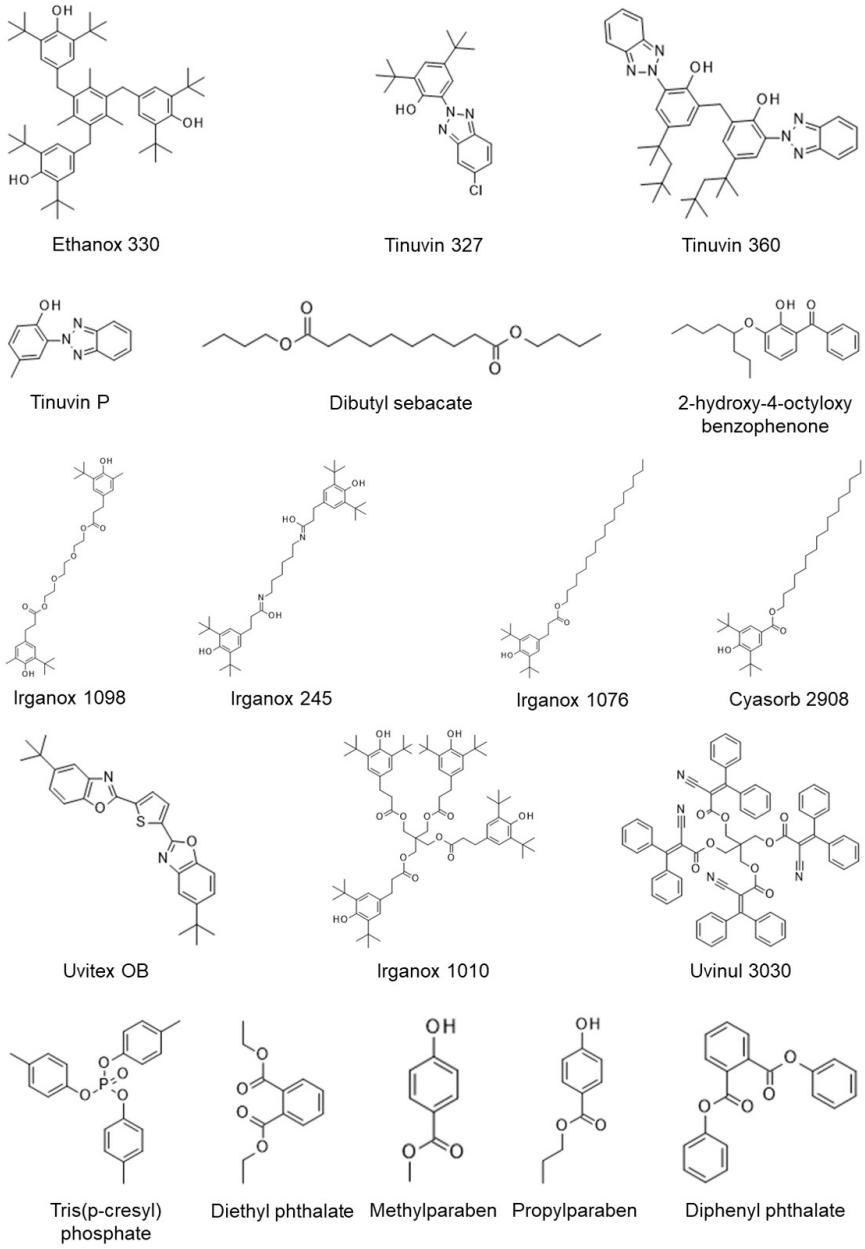

Figure A.18: Structures of the compounds found in the extractables and leachables standard.

Table A.1: List of the compounds found in the extractables and leachables standard. The list includes the compounds name, molecular formula, monoisotopic mass, and Log P.

Compound	Formula	Mass	Log P
Methylparaben	$C_8H_8O_3$	152.0473	1.88
Propylparaben	$C_{10}H_{12}O_3$	180.0786	2.90
Diethyl phthalate	$C_{12}H_{14}O_4$	222.0892	2.71
Tinuvin P	$C_{13}H_{11}N_3O$	225.0902	4.31
Dibutyl sebacate	$C_{18}H_{34}O_4$	314.2457	5.96
Diphenyl phthalate	$C_{20}H_{14}O_4$	318.0892	3.57
2-hydroxy-4-octyloxy benzophenone	$C_{21}H_{26}O_3$	326.1882	7.56
Tinuvin 327	$C_{20}H_{24}ClN_3O$	357.1608	7.54
Tris(p-cresyl) phosphate	$C_{21}H_{21}O_4P$	368.1177	5.11
Uvitex OB	$C_{26}H_{26}N_2O_2S$	430.1715	7.22
Cyasorb 2908	$C_{31}H_{54}O_3$	474.4073	12.48
Irganox 1076	$C_{35}H_{62}O_3$	530.4699	13.53
Irganox 245	$C_{34}H_{50}O_8$	586.3506	7.61
Irganox 1098	$C_{40}H_{64}N_2O_4$	636.4866	9.82
Tinuvin 360	$C_{41}H_{50}N_6O_2$	658.3995	14.48
Ethanox 330	$C_{54}H_{78}O_3$	774.5951	16.33
Uvinul 3030	$C_{69}H_{48}N_4O_8$	1060.3472	12.97
Irganox 1010	$C_{73}H_{108}O_{12}$	1176.7841	18.83

Appendix B

International Journal of Mass Spectrometry

International Journal of Mass Spectrometry 466 (2021) 116603

Contents lists available at ScienceDirect

International Journal of Mass Spectrometry

journal homepage: www.elsevier.com/locate/ijms

Short communication

Towards a universal ion source: Glow Flow mass spectrometry

Rhodri N. Owen *, Steven L. Kelly, A. Gareth Brenton **

Institute of Life Science, Swansea University Medical School, Swansea, Wales, SA2 8PP, United Kingdom

ARTICLE INFO

Article history:
Received 23 October 2020
Received in revised form
3 March 2021
Accepted 12 April 2021
Available online 24 April 2021

Keywords:
Ionization
Ion source
Helium microplasma
Mass spectrometry
Glow discharge
Analytical science

ABSTRACT

A helium-microplasma ion source (Glow Flow) has been developed and characterised. It is engineered to be a simple design, of low-cost and can be readily retrofitted to most modern mass spectrometers. Initial assessment of its performance has shown it to be robust, reproducible and of high sensitivity. Glow Flow provides broad non-specific detection of samples from polar through to non-polar chemistries making it of wide utility. A study of persistent organic pollutants, polyaromatic hydrocarbons, low average-molecular-mass polymers (polyethyleneimine, polyethylene glycol, and polypropylene glycol) and a complex mixture of fatty-acid methyl esters by direct sample introduction using a nebulised heated nitrogen flow was conducted. The ability to make quantitative measurement was investigated using methyl stearate and a linear calibration plot gave a $R^2 = 0.999$ and limit-of-detection of ~100 fmol. This design is extremely stable, in operation. Typical ions commonly observed are intense protonated molecule ions, radical molecular ions, hydride abstracted ions, and oxygen adduct ions. At present this system is valuable to apply to small molecule analysis ($m/z < 1000$), and is easily interfaced to gas and liquid chromatography, and likely to be useful for imaging.

1. In

uce his
plasma
A n ioni-
the ficance
inclu re [3,6]
amo I) and
"no i view of
analy as been
chara nber of
tion, or mass
high ressure
broa own to
and l any of
assig lky and
Furth allow
and i design
gas a uld be
St a high-
assoc c pres-

* Corresponding author.
** Corresponding author.
E-mail addresses: r.n.owen@swansea.ac.uk (R.N. Owen), g.brenton@swansea.ac.uk (A. Gareth Brenton).

https://doi.org/10.1016/j.ijms.2021.116603
1387-3806/

2. Mat

2.1. Hel

ass spec-
ons were
A sc to +30 V,
microp °C, and
trically was ob-
union i ilmslow,
probe t
Manch
nut (55
a heliu
connec
spectro
current
acts as e over a
(0.05− 0.05 to
(Model electrode
Glow F axially to
atmosp acted as
Heiftje er supply
Flow is readback
and at sed from
atmosp o 15 mm
ities to
active i
(RF) di
dischar
area he
[14].

2.2. Ch

High
bispher
dibrom
dustry
Alfa Ae
purcha
ical sta
esters (
glycol,
from Si
(N5.0) 0.5
experi
Sam rates with
methan ion source
concen the source
(**A**), and a
de distance

Fig. 1. (**a**) nd side). (**b**)
Photogra ent internal
power su

the cur
reduced
within t
the sho
the full
electroc

Solv
atmosp
voltage
i.e. 5 k
corresp
dischar
source,
conseq
or the g

$V_b =$

where
sure an

To a
helium-
system
flow ra
increasi
rates fo
current
0.3–0.5
that thi
glow re
voltage
atmosp
normal
current,

3.2. Fig

An e
of the h
Methyl
40 pg μ
and allo
mass sp

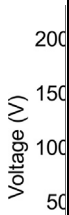

Fig. 3. Pl
different
glow disc
of 20 mm
and the v

50

l scan mode
centrations
ely into the

k area of
obe does
lies on a
r sample
limit-of-
exhibited
the mean

e a broad
nated hy-
prepared
o a glass
the mass
tra were
recorded
lar com-
les while
ular ions
ions and
tensities,
ke many
pathways
d proton-

(2)

(3)

(4)

ocarbons
molecule

Table 1
List of p mass spectra.
Proton a

Comp	d
Bisphe	
Bisphe	3.14 (5%)
Pyrene	9.08 (3%)
Anthra	
Octade	
Diben	5.08 (5%)
Tetrad	
Napht	5.08 (10%)
Dodec	
1,4-Di	
Pentafl	
Hexafl	
2,8-Di	

[M+H] ature was
decrea chain and
sample observed
ionizat s allowed
selecti nately, the
hydroc were not
ment we were
followi ower tem-
others n [24]. We
format ot away in
atom i rapid des-
n gas tem-
$M +$ to observe
rk we will
$[M - H$ hromatog-
t leads to

An
establi
(Suppl
compo
howev
[M + C ion source
signal n our lab-
involving
sitive and

3.4. Lo

Thr on a Xevo
ethyle the Glow
which laboratory
analysi ption [24],
broade per would
prepar good sma-
ASAP p ompounds
desolv ctrometer
volatili [26]). The
observ ecules and
acteris ve plasma
corres or molec-
(Table rce will be
ential for
d be easily

3.5. D d ambient
a range of
FA on a X–Y
1000 n spectrom-
the en cation lies
capilla into the

Table 2
List of ions

Compou	
Polyethy	547.4 (50%), 591.4
Polypro MW ~ Polyethy	9.8 (20%), 947.8 (10%)

Table 3
List of the
mixture fo
sponding
between 5

Commo
Methyl
Methyl
Methyl
Methyl
Methyl l
Methyl
Methyl
Methyl s
Methyl a
Methyl
Methyl l

micropl
heating
control v
coupling
nebulize
which re
the use
the wor
intense
abstract
Howeve
classes s
ing in q
required
to make
adopt m

CRediT

Rhod
draft. **St**
Concept

Declarat

The
relations
interests

Garet
School a
England
marketi
in this a

the editors as part
tional Mass Spec-
nded by the Engi-
(EP/R51312X/1).

found online at

etry: approaching the
. Spectrom. 26 (2011)

s, Phys. Rev. 11 (1918)
electron impact ioniza-
mpact for a long time.
committee in 2013, see

pectrometry. I. General

Desorption Mass Spec-

Horning, Atmospheric
ge ion source for use in
analytical system, Anal.

e optische emissionss-
3 (1968) 443–454.
using an atmospheric

ctrometry of involatile
atrix, J. Mass Spectrom.

metry of some organic
89) 209–225.
urce for the analysis of
nal. Chem. 77 (2005)

spectrometry sampling
ray ionization, Science

mpling/ionization mass
nal. Chem. 83 (2011)

bient desorption/ioni-
ative and quantitative

orption/ionization mass
ning to accurate quan-
4076.
Y. Naito, Definitions of
endations 2013), Pure

Cooks, Z. Ouyang, Low-
ization, Anal. Chem. 80

tatistical Computing, R
ia, 2019. URL, https://

, G. Gamez, S.J. Ray,
source. 1. Ionization of
646–2653.

[19] C.N. McEwen, R. [redacted] 7 (2009) 413.
tissues using sol [redacted] d Physics. A Ready-Reference
cial LC/MS instru [redacted] RC Pr, Boca Raton, 1986.
[20] D.T. Usmanov, L [redacted] ch 2020 *c.F.* https://doi.org/
spectrometric m
ethanol in low p [redacted] odall, C.D. Foley, C.D. Manly,
1187–1195.
[21] K. Merrett, A.B. Y [redacted] ar, L.F. Imperial, E.D. Inutan,
fluoroaromatic c [redacted] nisation Technique for Mass,
[22] E.P.L. Hunter, S. [redacted] ress PhD Thesis.

Appendix C

Spectroscopy Europe

ARTICLE

"GlowFlow", a step towards a unified ionisation source for mass spectrometry?

Rhodri N. Owen, Steven L. Kelly and A. Gareth Brenton
Institute of Life Science, Swansea University Medical School, Swansea, Wales, SA2 8PP, UK

Mass spectrometry is a gold-standard analytical technique and is widely employed over a range of fields, from petrochemical, fine chemical through to medical applications. The types of instrumentation for sample separation, ionisation, mass analysis and detection that have evolved in analytical mass spectrometry are diverse; as the old colloquialism goes "*it is a matter of horses for courses*". Our "GlowFlow" source design based on an Argon flowing glow-discharge may satisfy part of that landscape.

Introduction

One of the earliest, and possibly still the most widely used, ionisation sources is electron ionisation (EI).[1] The ionisation process requires the analyte molecule to be in the gas-phase and introduced directly into a beam of electrons (typically 70 eV) in a high vacuum environment necessary for mass analysis. Gas-phase molecules interact with the fast electron beam, with around 1 in 10^5 molecules excited sufficiently to eject a valance electron forming a molecule ion species.[2] EI persisted until the 1960s as the predominant ionisation method for small molecule work, such as petroleum mixture and non-polar chemical analysis.

DOI: 10.1255/sew.2021.a53

Historically, there has been an imperative to address biological chemistry and, therefore, engage with polar chemical entities. Unfortunately, EI methodologies did not work at all well on biological molecules. They thermally degraded as scientists tried, largely unsuccessfully, to desorb these specimens into the gas phase. The decades to 1990 saw a plethora of methods to achieve viable biological mass spectrometry, with chemical ionisation,[3] field desorption/ionisation,[4] plasma desorption,[5] thermospray,[6] fast-atom bombardment (FAB)[7] and matrix-assisted laser desorption/ionisation[8] invented. Electrospray ionisation (ESI)[9,10] spectacularly achieved this goal, along with other methods such as atmospheric pressure chemical ionisation (APCI).[11]

Atmospheric pressure ionisation (API) was a key enabling technological step in modern mass spectrometry methods.[12] API is now ubiquitous, both simplifying sample introduction by eliminating the "ion source vacuum" components and having led to a diversity of methods available to analysts.

Even with this profusion of new methods no universal ionisation method has emerged, especially one that straddles molecules from non-polar though to polar chemistries.

The success of ESI is that it is a "soft" method which means it produces little, if any, fragmentation and can be used to analyse thermally labile and less volatile molecules. In ESI, ions are generated from Brønsted acid–base chemical reactions,[13] i.e. protonation for positive mode and deprotonation in negative mode, within those droplets generated by an electrosprayed jet of liquid. ESI works best at atmospheric pressure; in fact it was an important part of the enabling technology of ESI that nascent electrosprayed ions needed to be stabilised, otherwise they tended to be clustered with water molecules attached, or even fragment either unimolecularly or by collisional activation.[14] Collisions with a background gas or an intentionally introduced gas stream was a neat solution to these problems, enabling both the declustering of molecule ions (e.g. clustered with numerous water molecules) and internally cooling them so as to reduce fragmentation. Of course, these advances were, in part, serendipitous taking many years of incremental R&D improvements to the original systems.[9,10]

ESI, however, does have some drawbacks, not all molecules can be protonated; for example, hydrocarbons where EI is often the preferred high-sensitivity method. The "Achilles Heel" of EI is that it operates at low pressure which requires complex and costly vacuum systems and sample inlets.

Therefore, an ionisation source that can bridge the techniques of EI and ESI would be highly advantageous, one that operates at atmospheric pressure and can ionise the broadest range of compounds from polar to non-polar. This was the motivation for us to start to investigate GlowFlow, since it showed promise to span a range of chemistries, although with yet to be characterised sensitivity and specificity.

Electrical plasmas, such as a helium atmospheric pressure glow discharge (APGD), could offer such a solution as they potentially have several pathways to form ions.[15] The first step is the formation

of the metastable helium (He^m) in the discharge, a highly energetic atom which has 19.8 eV of energy, enough to directly ionise most organic molecules and has a surprisingly long lifetime of up to 7870 s as it only de-excites through collision.[16] In an intermediate step, the He^m atom ionises atmospheric gases, such as nitrogen or water vapour, or it can directly proceed to ionise sample molecules (M).

The aim of our study was to develop a compact APGD ionisation source that could be retrofitted to existing instrumentation and ionise compounds at atmospheric pressure which are less amenable to ESI. We named our implementation GlowFlow (see Figure 1).

A selection of persistent organic pollutants and analogues was chosen for study as they can bioaccumulate in the environment and can have adverse health implications.

Methods

The design of helium glow-discharge sources is of two general types: either i) a glow discharge cell[15] [see Figure 2(i)] that runs a discharge, typically at tens of watts of power, or ii) a simple nude design [see Figure 2(ii)] which generally operates at lower wattages, typically mW. Our design of the glow flow ionisation source used herein was made from an electrically insulating polyether ether ketone (PEEK), zero-dead volume union [Figure 2(ii)].[17] Attached to one end was a stainless-steel tip which acted as the anode (ID = 0.5 mm) and was connected to the mass spectrometer's internal power supply, operated in constant current mode (1–35 µA), typically set at 15 µA. To the other end of the ionisation source body was a helium gas line connected by a PEEK nut. A flow meter was used to regulate the gas flow rate (0.05–0.5 L min^{-1}). High purity (99.999 %) helium was used for all experiments.

A Waters Xevo G2-S time-of-flight mass spectrometer (Wilmslow, Manchester, UK) was used for the analysis with the GlowFlow source fitted axially to the entrance for improved sensitivity. Standards of anthracene, naphthalene, pyrene, bisphenol A,

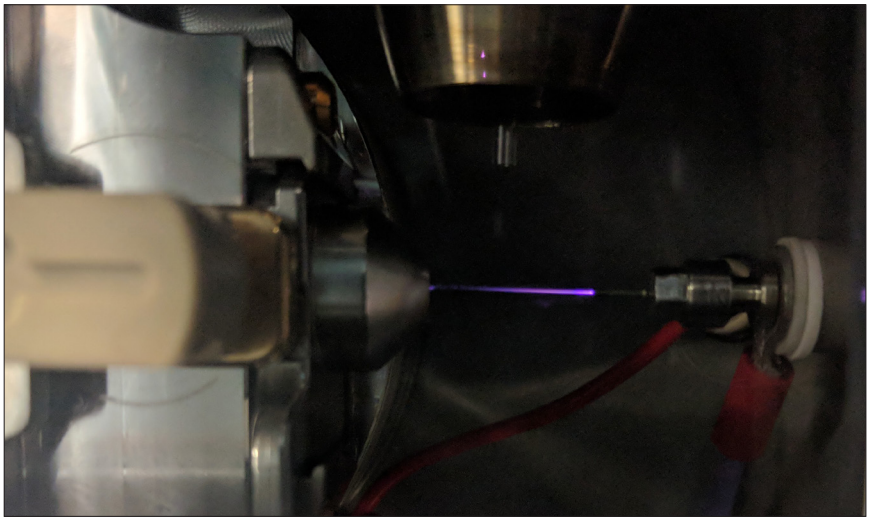

Figure 1. The GlowFlow ionisation source installed on a Waters Xevo G2-S universal source housing. The ionisation source is positioned on the right, with the electrical connection opposite the entrance to the mass spectrometer. A heated nebuliser used to desorb samples is shown at the top.

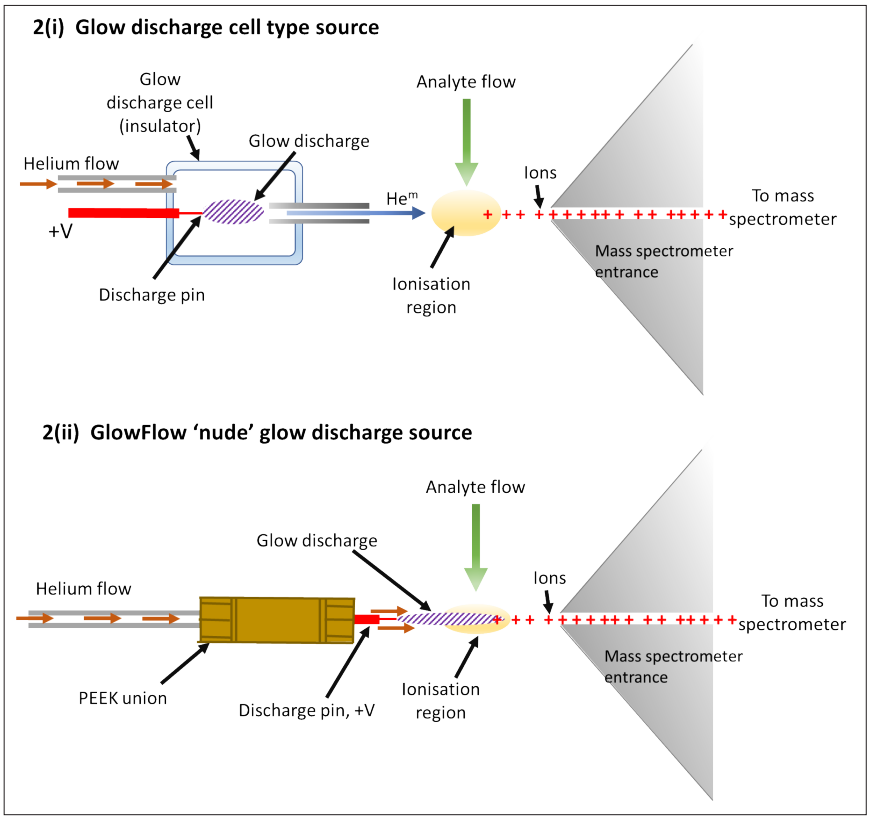

Figure 2. Illustrations of a cell design for a glow discharge and the "GlowFlow" method. i) A formal discharge cell design is commonly used[15] in glow-discharge mass spectrometry with the cell often positioned off-axis at a critical angle to optimise sensitivity. The voltage on the anode is typically several hundred volts, sufficient to sustain the selected constant current required for the glow discharge. To initiate the glow, the voltage will often be raised significantly higher until the discharge ignites after which the voltage settles down again. ii) The GlowFlow design utilises a hollow PEEK union through which helium flows through and then over a sharpened tungsten electrode where the glow discharge forms and flows towards the ionisation region where the analyte flow occurs.

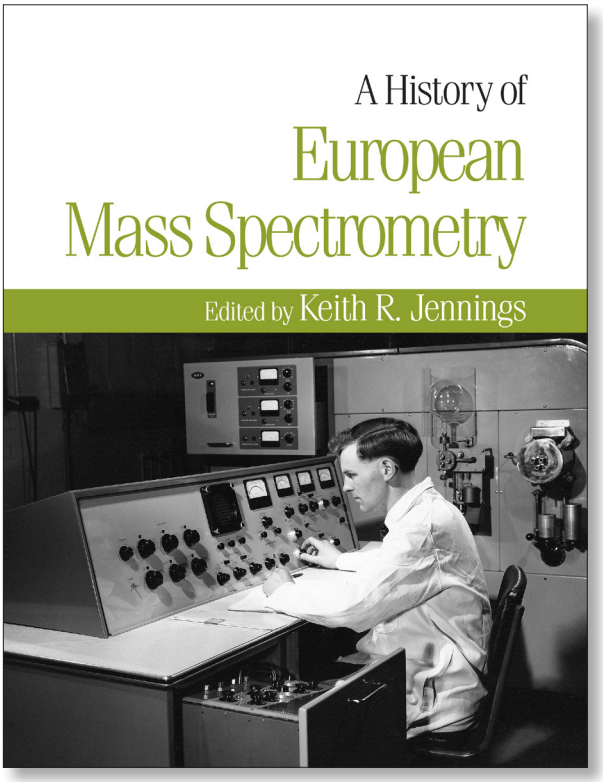

A History of European Mass Spectrometry

Edited by Keith R. Jennings

with contributions from Nico M.M. Nibbering, Andries Bruins, Michael Karas, Bob Bateman, Jochen Franzen, Michael C. ten Noever de Brauw, Peter Roepstorff, Károly Vékey, Jim Scrivens and Alison E. Ashcroft

The construction of Thompson's mass spectrograph in Cambridge followed by Aston's improved instruments and his pioneering work on non-radioactive isotopes is widely known. In the sixty years or so since then, European scientists and engineers have made many major contributions to the development of new instruments and techniques. Accounts of these contributions in the scientific literature necessarily give little idea of the contributors themselves or of the difficulties that had to be overcome before success was achieved.

Most newcomers to mass spectrometry in the last ten years will have little concept of the difficulties faced in obtaining the mass spectra of four solid samples during a working day before the invention of the vacuum lock probe. This was followed by several hours of counting spectra and trying to interpret them. Many will never have seen a magnetic deflection instrument and will be familiar only with mass spectrometers having both the operation of the instrument and the interpretation of the data under computer control.

This book aims to give an insight into how some of the more important developments came about, from the advent of the first commercial instruments to the present day. The various accounts, several of which contain personal reminiscences, both provide a human background to these developments and convey the excitement of being part of the European mass spectrometry community during this period.

Anal. Bioanal. Chem.
"They present a fascinating story of the people who, in the middle of the twentieth century, had a vision of mass spectrometry as one of the most useful analytical methods in chemistry. In my opinion this is the most interesting part of the book, providing an eyewitness account of how many obstacles had to be circumvented to reach the level of quality seen in modern mass spectrometers."

"In conclusion: every scientist, young or old, who works with mass spectrometry will find something of interest in this book."

Mass Matters
"Above all, it is the dedication and enthusiasm of the scientists involved that stands out and makes for engrossing reading."

"The feeling of the humanity of mass spectrometry epitomizes the thread of this book; the recollections veering toward the more social science than the physical science that we may be used to. The logical progression of this book enables the reader to follow the amazing developments that have so heavily influenced physics, chemistry and biology whilst gaining insight to the life and times of the scientists that have accomplished so much over the last sixty or so years. As editor, Keith has certainly achieved a highly interesting and informative book that is easy and enjoyable to read."

impopen.com/mshistory

bisphenol S, 1,4-dioxane, dibenzofuran and 2,8-dibromodibenzofuran (Tokyo Chemical Industry UK Ltd, The Oxford Science Park, Oxford, UK), and dodecane, tetradecane and octadecane (Sigma-Aldrich, Gillingham, Dorset, UK) were prepared at concentrations of 1 µg mL^{-1}. Methyl stearate (Alfa Aesar, Port of Heysham Industrial Park, Heysham, UK) was prepared at a concentration range from 5 pg µL^{-1} to 40 pg µL^{-1}.

Results

The GlowFlow ionisation source operates at gas flow rates of 0.05–0.5 L min^{-1} and can sustain a discharge at currents of 1–35 µA. To characterise the ionisation source's capabilities, a separate experimental rig was made where the glow discharge was positioned perpendicularly to a metal plate which acted as a counter electrode and was connected to earth. A constant current of 10 µA was set on the instrument's internal power supply and the GlowFlow source was moved away from the counter electrode in 5 mm steps from 5 mm to 40 mm and the readback current was recorded. Over relatively short inter-electrode gaps of 5–15 mm the current remained constant, but at the larger inter-electrode gaps >15 mm there was a noticeable reduction in the current (see Figure 3).

The distinct purple glow of the discharge also shortened at inter-electrode gaps >15 mm leaving only a faint glow at the tip of the anode. To prevent the collapse of the glow discharge at larger distances, the actual current supplied must reduce as the voltage is reaching the power supply's maximum operating threshold.

Persistent organic pollutants

Organic compounds that build up in the environment and tend to be classified as persistent organic pollutants. A range of these compounds and their analogues were prepared at concentrations of 1 µg µL^{-1}, they ranged from non-polar hydrocarbons to polar compounds, such as bisphenol. A solids analysis probe was used to introduce samples, consisting of a metal body into which a glass capillary can be inserted. Samples are then syringed into the capillary before it is introduced into the source and a heated nitrogen gas nebuliser (programmable, ambient to 500 °C) desorbs/sublimates the sample for analysis using the GlowFlow ionisation source, with the mass spectrometer in full scan mode. A range of ions were observed in the mass spectrum and the most intense peaks were recorded (Table 1).

Typically, intense protonated molecules were measured for polar tending compounds and radical ions were measured for the more non-polar compounds. In some instances, the $M^{+\bullet}$ and $[M+H]^+$ ions were of equal intensity supporting the hypothesis that GlowFlow, like many other plasma ion sources, can access multiple ionisation pathways (Figure 4A). The base peak for hydrocarbons was M + 15, as seen in Figure 4B for octadecane, suggesting the hydrogen atom displacement by oxygen occurs readily for this class of compounds, following reactions in Scheme 1.[18] Knowing this, sample chemistry could be used to establish the most favourable ionisation pathway and potentially suggests the potential for the ability to tune the source to selectively ionise.

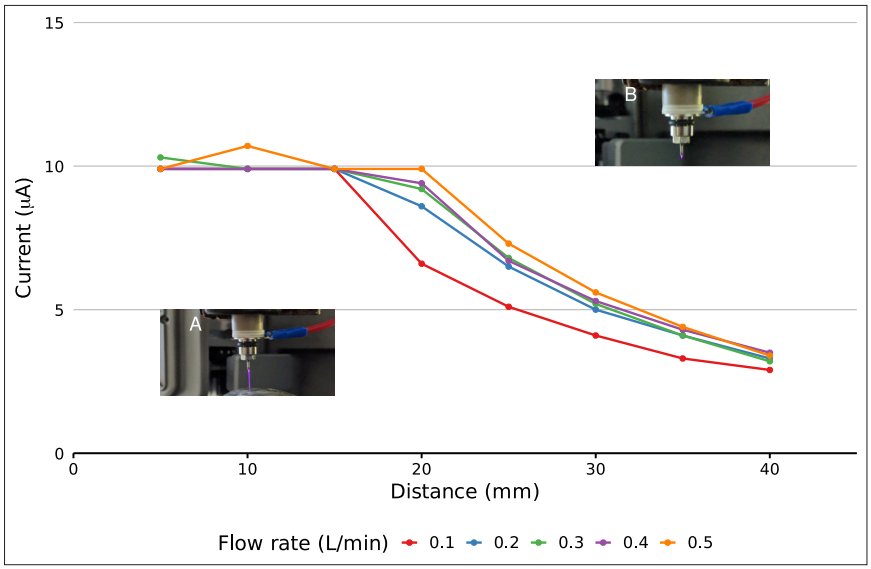

Figure 3. Plot of recorded current as at varying electrode distances. The electrodes were moved in 5 mm steps from 5 mm to 40 mm. A comparison at different gas flow rates was also made. Relatively stable current is seen at 5–15 mm. At larger electrode distances (>15 mm) the current reduces due to a limit in the maximum voltage that can be delivered by the power supply. Panel A shows a long, purple plasma jet at the smaller electrode distances, while in panel B the glow is reduced in length reflecting the lower current.

$$M + O_2^{+\bullet} \rightarrow [M-H]^+ + OH_2^{\bullet}$$

$$[M-H]^+ + O_3 \rightarrow [M-H+O]^+ + O_2$$

Scheme 1. Hydrogen displacement by oxygen as observed in a GlowFlow mass spectrum of hydrocarbon molecules.

Figures-of-merit

The sensitivity and reproducibility of the GlowFlow ionisation source was determined using methyl stearate. Serial dilutions were prepared at concentrations from 40 pg µL^{-1} to 5 pg µL^{-1}. On the end of a glass capillary 1 µL of the solution was syringed and allowed to dry in the laboratory before being introduced by a solids analysis probe into the mass spectrometer. The peak area of the ion at *m/z* 299.29 was recorded and a calibration curve prepared, with five replicates at each concentration (Figure 5). The source lower limit-of-detection (LOD) was determined to be 111 fmol and had a coefficient of variation of 0.9991.

Table 1. List of significant ions observed in the mass spectra using GlowFlow ionisation source to analyse persistent organic chemicals and analogues.

Compound	Formula	Log P	Observed base peak	2nd peak (%)	3rd peak (%)
1,4-Dioxane	$C_4H_8O_2$	–0.3	89 [M+H]		
Hexafluoro-2-propanol	$C_3H_2F_6O$	1.7	167 [M]		
Bisphenol S	$C_{12}H_{10}O_4S$	1.9	251 [M+H]		
Pentafluorobenzene	C_6HF_5	2.5	167 [M]		
Bisphenol A	$C_{15}H_{16}O_2$	3.3	213 [M+H–O]	229.12 (10%)	243.14 (5%)
Naphthalene	$C_{10}H_8$	3.3	129 [M+H]	128 (95%)	145.08 (10%)
Dibenzofuran	$C_{12}H_8O$	4.1	169 [M+H]	168.08 (80%)	185.08 (5%)
Anthracene	$C_{14}H_{10}$	4.4	179 [M+H]	178.10 (70%)	
Pyrene	$C_{16}H_{10}$	4.9	203 [M+H]	202.08 (80%)	219.08 (3%)
Dodecane	$C_{12}H_{26}$	6.1	147 [M–23]	185.19 (90%)	
Tetradecane	$C_{14}H_{30}$	7.2	213 [M–H+O]	211.17 (30%)	
Octadecane	$C_{18}H_{38}$	9.3	269 [M–H+O]	267.20 (40%)	

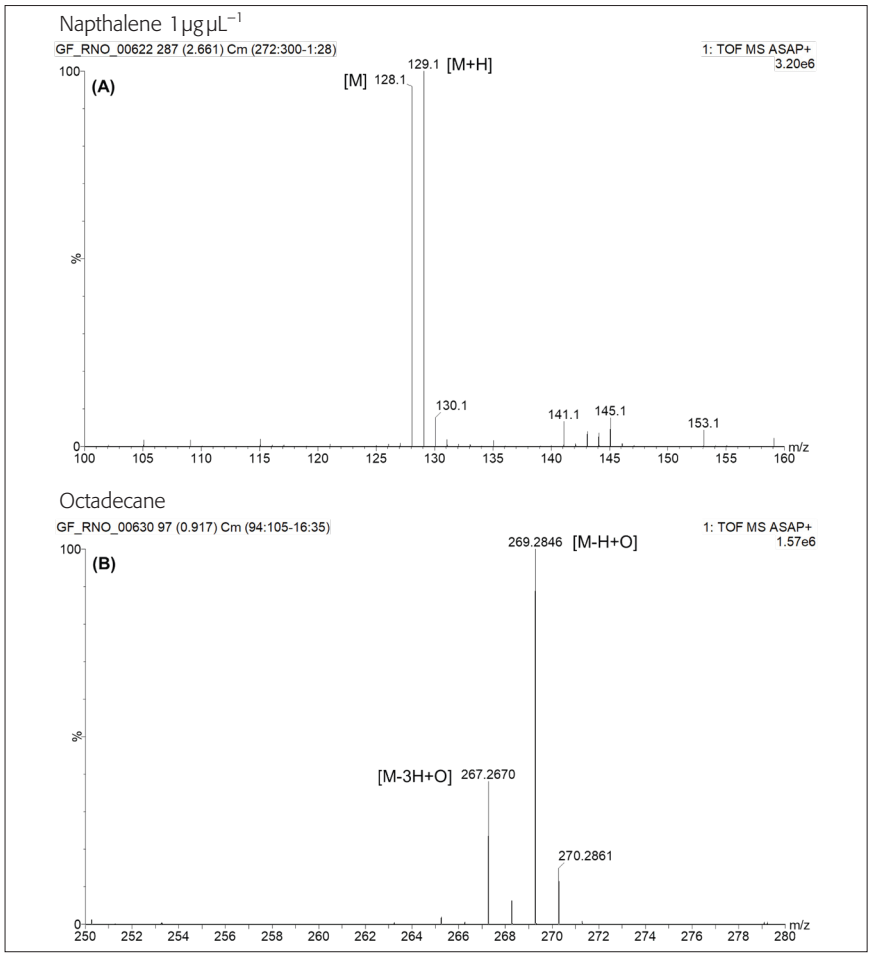

Figure 4. A GlowFlow mass spectrum of naphthalene. Observed at *m/z* 128 is the $M^{+\bullet}$ ion and at *m/z* 129 the $M+H^+$ ion, demonstrating the multiple ionisation pathways available to the GlowFlow ionisation source (A). A GlowFlow mass spectrum of octadecane (B). Intense ions observed at *m/z* 269.2848 which correspond to $C_{18}H_{37}O$ (δ=0.3 mDa; the δ being the difference between the observed *m/z* and calculated exact mass of the monoisotopic peak).

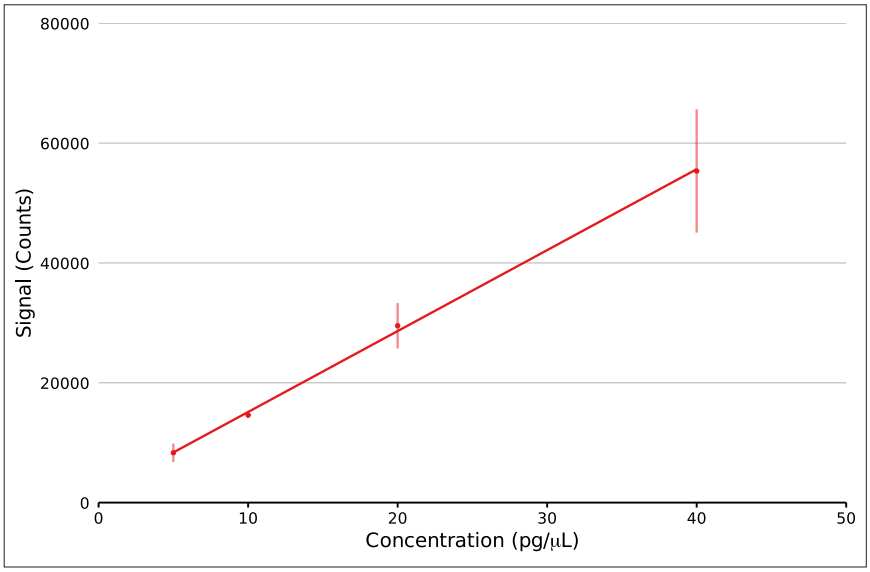

Figure 5. Linear regression plot of methyl stearate ion at *m/z* 299.29 at four concentrations from 5 pg μL^{-1} to 40 pg μL^{-1} (n=5). The lower LOD was calculated.

Conclusion

Our ambition was to develop a high-sensitivity multimodal ionisation source that can analyse both atoms and molecules, polar to non-polar compounds with the broadest range of molecular masses. This study has shown the GlowFlow ionisation source can analyse a range of polar to non-polar compounds and is able to achieve low limits of detection (111 fmol for methyl stearate). Further work to interface this ionisation source with a range of chromatography is being actively undertaken, as well as to assess GlowFlow's breadth of operation over a range of compounds. Our findings to date show that the source works for a wide range of molecules. For non-polar compounds, the ion species we generally observe are not normally the EI radical ion but various ion types, e.g. where a hydrogen atom is displaced by oxygen. For polar species, protonated molecules are commonly observed in GlowFlow, although at reduced sensitivities. Whereas, there appears to be great potential for GlowFlow in negative-ion mode as high sensitivity (recent data show <10 fmol) is often observed, with de-protonated species and occasionally dehydrated species typically observed. The technique readily interfaces to all types of chromatography and due to our compact design can be easily contained within many commercial source designs and be switched rapidly between active/inactive operation. Perhaps the simplicity of GlowFlow lends itself to be integrated with ESI and APCI setups, creating a near universal source assembly?

Competing interests

The GlowFlow™ ionisation source described in this article is marketed and sold by AberMS Ltd. Gareth Brenton is an Emeritus Professor in Swansea Medical School and a director of AberMS Ltd.

Acknowledgements

This work was funded by the Engineering and Physical Sciences Research Council (EP/R51312X/1) and from the ERDF/ Welsh Government funded BEACON project".

References

1. A.J. Dempster, "A new method of positive ray analysis", *Phys. Rev.* **11(4),** 316–325 (1918). https://doi.org/10.1103/PhysRev.11.316
2. Note the terms and definitions we have used follow the revised definitions given by the IUPAC Committee in 2013, see K.K. Murray, R.K. Boyd, M.N. Eberlin, G.J. Langley, L. Liang and Y. Naito, "Definitions of terms relating to mass spectrometry (IUPAC Recommendations 2013)", *Pure Appl. Chem.* **85(7),** 1515–1609 (2013). http://doi.org/10.1351/PAC-REC-06-04-06
3. M.S. Munson, and F.H. Field, "Chemical ionization mass spectrometry. I. General introduction", *J. Am. Chem. Soc.* **88(12),** 2621–2630 (1966). https://doi.org/10.1021/ja00964a001
4. H.D. Beckey, "Field desorption mass spectrometry: A technique for the study of thermally unstable substances of low volatility", *Int. J. Mass Spectrom. Ion Phys.* **2(6),** 500–502 (1969). https://doi.org/10.1016/0020-7381(69)80047-1
5. R. Macfarlane and D. Torgerson, "Californium-252 plasma desorption mass spectroscopy", *Science* **191(4230),** 920–925 (1976). https://doi.org/10.1126/science.1251202
6. C.R. Blakley, J.J. Carmody and M.L. Vestal, "Liquid chromatograph-mass spectrometer for analysis of nonvolatile samples", *Anal. Chem.* **52(11),** 1636–1641 (1980). https://doi.org/10.1021/ac50061a025
7. M. Barber, R.S. Bordoli, R.D. Sedgwick and A.N. Tyler, "Fast atom bombardment of solids as an ion source in mass spectrometry", *Nature* **293(5830),** 270–275 (1981). https://doi.org/10.1038/293270a0
8. F. Hillenkamp, M. Karas, R.C. Beavis and B.T. Chait, "Matrix-assisted laser desorption/ionization mass spectrometry of biopolymers", *Anal. Chem.* **63(24),** 1193A–1203A (1991). https://doi.org/10.1021/ac00024a002
9. J.B. Fenn, M. Mann, C.K. Meng, S.F. Wong and C.M. Whitehouse, "Electrospray ionization–principles and practice", *Mass Spectrom. Rev.* **9(1),** 37–70 (1990). https://doi.org/10.1002/mas.1280090103
10. M. Dole, L.L. Mack, R.L. Hines, R.C. Mobley, L.D. Ferguson and M.B. Alice, "Molecular beams of macroions", *J. Chem. Phys.* **49(5),** 2240–2249 (1968). https://doi.org/10.1063/1.1670391

11. D.I. Carroll, I. Dzidic, R.N. Stillwell, M.G. Horning and E.C. Horning, "Subpicogram detection system for gas phase analysis based upon atmospheric pressure ionization (API) mass spectrometry", *Anal. Chem.* **46(6),** 706–710 (1974). https://doi.org/10.1021/ac60342a009
12. G.A. Harris, A.S. Galhena and F.M. Fernandez,"Ambient sampling/ionization mass spectrometry: applications and current trends", *Anal. Chem.* **83(12),** 4508–4538 (2011). https://doi.org/10.1021/ac200918u
13. The Editors of Encyclopaedia Britannica, *Brønsted-Lowry Theory*. Encyclopedia Britannica (21 April 2021). https://www.britannica.com/science/Bronsted-Lowry-theory [Accessed 2 November 2021]
14. A.G. Brenton, R.P. Morgan and J.H. Beynon, "Unimolecular ion decomposition", *Ann. Rev. Phys. Chem.* **30(1),** 51–78 (1979). https://doi.org/10.1146/annurev.pc.30.100179.000411
15. J.T. Shelley and G.M. Hieftje, "Ambient mass spectrometry: approaching the chemical analysis of things as they are", *J. Anal. At. Spectrom.* **26(11),** 2153–2159 (2011). https://doi.org/10.1039/C1JA10158G
16. S.S. Hodgman, R.G. Dall, L.J. Byron, K.G.H. Baldwin, S.J. Buckman and A.G. Truscott, "Metastable helium: A new determination of the longest atomic excited-state lifetime", *Phys. Rev. Lett.* **103(5),** 053002 (2009). https://doi.org/10.1103/PhysRevLett.103.053002
17. R.N. Owen, S.L. Kelly and A.G. Brenton, "Towards a universal ion source: glow flow mass spectrometry", *Int. J. Mass Spectrom.* **466,** 116603 (2021). https://doi.org/10.1016/j.ijms.2021.116603
18. S.P. Badal, T.D. Ratcliff, Y. You, C.M. Breneman and J.T. Shelley, "Formation of pyrylium from aromatic systems with a Helium:Oxygen Flowing Atmospheric Pressure Afterglow (FAPA) plasma source", *J. Am. Soc. Mass Spectrom.* **28(6),** 1013–1020 (2017). https://doi.org/10.1007/s13361-017-1625-z

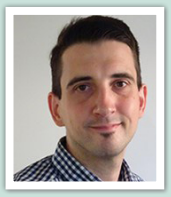

Mr Rhodri N. Owen is an analytical chemist and a final-year PhD candidate at the Institute of Life Sciences (ILS) at Swansea University Medical School. He holds a BSc in chemistry from Swansea University. He is also a Member of the Royal Society of Chemistry, the British Mass Spectrometry Society and the American Society of Mass Spectrometry.
https://orcid.org/0000-0002-3109-6653
R.N.Owen@Swansea.ac.uk

Professor Steven L. Kelly is a geneticist and professor of biomedical sciences at the Institute of Life Sciences (ILS) at Swansea University Medical School. He is a Fellow of the Learned Society of Wales. He has also been awarded the George Schroepfer Medal from the American Oil Chemist's Society for distinguished research on sterols. He holds a BSc in genetics, a PhD in yeast genetics and a DSc from Swansea University. He also worked at Sheffield and Aberystwyth Universities.
https://orcid.org/0000-0001-7991-5040
s.l.kelly@swansea.ac.uk

Professor Gareth Brenton is an emeritus professor of mass spectrometry at Swansea University Medical School. He is also the first ever recipient of the International Mass Spectrometry Society Curt Brunnée Award, and the British Mass Spectrometry Society Medal. He holds a first class Hons BSc in physics and a PhD from Swansea University. He was elected as a Fellow of the Learned Society of Wales in 2012.
https://orcid.org/0000-0003-2600-2082
G.Brenton@Swansea.ac.uk